

INSTITUTE FOR POLYMER RESEARCH
CELEBRATING 21 YEARS OF OFFICIAL INSTITUTE STATUS
TWENTY-SEVENTH ANNUAL SYMPOSIUM
ON POLYMER SCIENCE/ENGINEERING 2005

<p>Li Liu, Chemical Engineering, Waterloo (2004 IPR Scholarship Winner) VOCs separation from nitrogen stream by Poly(ether block amide) composite membranes</p>	<p>Howard Siu, Chemistry, Waterloo (2004 IPR Scholarship Winner) Characterization of the aggregation made by short PEO chains labeled at one end by the fluorophore</p>	<p>Sofia Vega, Universidad Autonoma de San Luis Potosí, Mexico winner joint SPM-CICY Prize for the Best Thesis on Polymers (MA) and IPRUW/MSED scholarship Crystallization and melting mechanisms of nylon 6-nanoclay hybrids</p>
<p>Jose Ramon Leiza, Professor, University of the Basque Country San Sebastian, Spain On Sabbatical at Queen's University Monitoring of emulsion polymerization reactors: calorimetry vs Raman spectroscopy</p>	<p>Rodolfo Salgado, Instituto Tecnologico de Tijuana, Mexico winner joint SPM-CICY Prize for the Best Thesis on Polymers (PhD) and IPRUW/MSED scholarship New temperature- and pH-sensitive smart polymers containing methacrylic derivatives with hydrophobic spacers</p>	<p>Fred Pries, Institute for Innovation Research The Changing World of Industrial Innovation</p>
<p>Francisco Lopez-Serrano, Universidad Nacional Autonoma de Mexico (UNAM) winner joint SPM-CICY Prize for the Best Thesis on Polymers (PhD) and IPRUW/MSED scholarship Determination of styrene-methyl methacrylate reactivity ratios dependencies on feed composition</p>	<p>Steven J. Teertstra, Chemistry, Waterloo Viscoelastic properties of arborescent polystyrene-graft-poly isoprenes</p>	<p>Costas Tzoganakis, Professor, Chemical Engineering, Waterloo Processing of polymers with supercritical CO₂</p>
<p>Kerry Li, Chemical Engineering, Waterloo Extrusion and fiber spinning of nylon-6,6/supercritical CO₂ mixtures</p>	<p>Mark Ingratta, Chemistry, Waterloo Fluorescence study of the effect of side-chain length on the side-chain dynamics of alpha-helical polypeptides</p>	<p>Deborah Sarzotti, Chemical Engineering, Waterloo Ethylene and propylene copolymerization with non-conjugated dienes: synthesis and characterization</p>
<p>Emma Daly, Chemical Engineering, Waterloo Reactivity ratio estimation: statistical issues and solutions</p>		

Posters

Joy Cheng Chem Eng Waterloo	Correlation of molecular properties with mechanical behaviour for high density polyethylene
Narges Ghadi Chem Eng, Ryerson Univ.	Optimization and modelling of an emulsion polymerization reactor
Pegah K. Karimi Fard Chem Eng, Ryerson Univ.	Modeling and optimization of an emulsion polymerization system
Francisco Lopez-Serrano UNAM, Mexico	Modeling discrimination in microemulsion polymerization
Gabriel Njikang Chemistry, Waterloo	Sustainable drug release from PS-g-PsVP arborescent copolymer micelles
Cristina Quinn Chemistry, Waterloo	Luminescence study of polymer chain dynamics using long-lived ruthenium complexes
Rodolfo Salgado Inst. Tecn. De Tijuana, Mexico	pH-tunable temperature sensitive materials from NIP AAm-methacrylic acid copolymers with hydrophobic spacers
Yu Shen Chemistry, Waterloo	Structure-property study of oil soluble dispersants
Sofia Vega Un. Autonoma de San Luis Potosí, Mexico	Temperature and time effects on crystallization of Nylon 6-nanoclay hybrids
Shuihan Zhu Chem Eng, Waterloo	Grafting of ethylene-ethyl acrylate-maleic anhydride terpolymer with amino-terminated polydimethylsiloxane during reacting processing

Institute for Polymer Research
27th Annual Symposium

Symposium documents for

Lui Li

Abstract

Presentation

VOCs separation from N₂ by poly(ether block amide) membranes

Li Liu, Xianshe Feng and Amit Chakma

(Dept. of Chemical Engineering, University of Waterloo, Waterloo, Ontario N2L 3G1)

Introduction

The vent streams from many manufacturing processes in chemical, petrochemical and pharmaceutical industries, fuel storage and painting operations often contain a large amount of volatile organic compounds (VOCs). Separation processes are needed to recover the VOCs and minimize their emissions into air. Most traditional methods, such as adsorption and low temperature condensation, have so far been found to be unsatisfactory. It has been shown that membrane processes are favorable over other processes for relatively small feed gas flow rates when the VOC concentrations in the vent streams are not too low.

Membrane based gas or vapor separation is a pressure driven process, and the membrane selectivity determines the recovery (i.e. process efficiency) directly. For VOCs separations, membranes are required to have a much higher permeability to VOCs than to nitrogen or air. In this work, rubbery poly(ether block amide) (PEBA) (type 2533) membranes were studied for VOCs separation from N₂. PEBA has micro-biphasic structure; the rubbery polyether segments offer high permeability to organic vapors, while the glassy polyamide domain restricts membrane swelling. Therefore, it is expected that PEBA membranes will yield a better permselectivity than silicone rubber-based membranes, which are the representative membranes for this application. The organic vapors studied include pentane, hexane, cyclohexane, heptane, methanol, ethanol, n-propanol, n-butanol, acetone, dimethyl carbonate (DMC) and methyl *tert*-butyl ether (MTBE).

Experimental

Ultra-thin PEBA membranes were prepared by the liquid surface spreading method developed recently in our lab. The ultrathin PEBA layer was laminated on porous polysulfone substrates to form a thin film composite membrane. This structure was found to have less resistance from the substrate for fast VOCs permeation than the traditional composite membrane prepared by the dip coating method.

Figure 1 is the experimental set-up for VOCs/N₂ separation. During the experiments, the feed mixture was kept at atmospheric pressure, and vacuum (< 1 kPa abs.) was applied to the permeate side. The VOC concentration in the feed stream was controlled by adjusting the pressure of the solvent bubbling tank. The VOCs permeated through the membranes were collected in a cold trap to determine the permeation rate. The flow rates and concentrations of the feed and permeate streams were measured, and the membrane performance is characterized in terms of permeance (defined as the permeation flux normalized by the partial pressure difference across the membrane) and selectivity (i.e. the permeance ratio of VOCs over nitrogen).

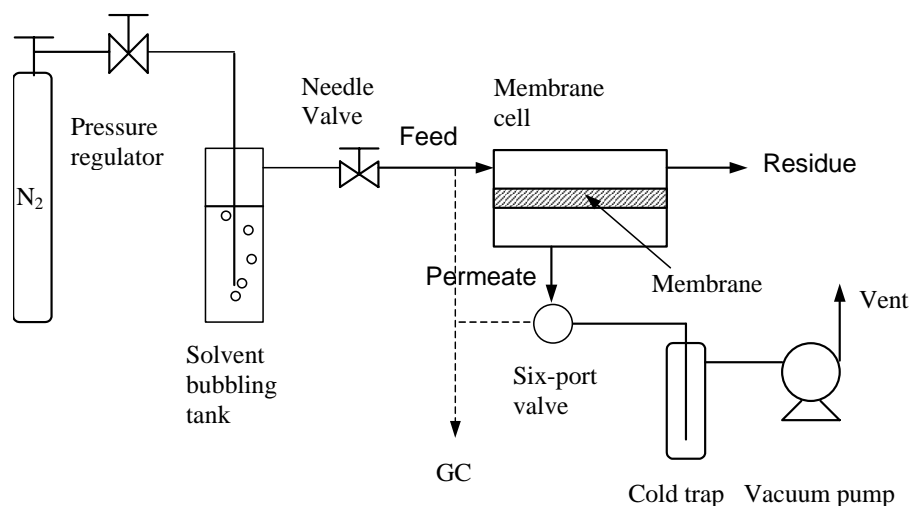


Fig.1 Schematic diagram of VOCs/N₂ separation system

A very low stage cut was used in the experiments to maintain constant concentration of VOCs along membrane surface at the feed side so that the membrane performance at a given feed concentration can be evaluated. The feed flow rate was as high as 400 cm³ (STP)/min to reduce the effect of the boundary layer.

Results and discussion

The permeation of VOCs/N₂ through the membranes at different feed concentrations was investigated. The membranes had much higher permeability to VOCs than to nitrogen. At a given feed concentration, the permeance of the four paraffin compounds tested follows the order of heptane > cyclohexane > hexane > pentane. For the other VOCs, the magnitude of the permeance is n-butanol > n-propanol > DMC > ethanol > methanol > acetone > MTBE. Generally, gas permeation through rubbery membranes is controlled by sorption. The sorption

behavior, mainly determined by the condensability of the permeant, contributes significantly to the selective permeation. Therefore, for the paraffin and the alcohol compounds, condensable vapors tend to have high permeabilities.

Figure 2 shows the permeance of the four paraffin vapors as a function of feed pressure. Because of membrane swelling caused by the organic vapor molecules, the permeance of VOCs increase with an increase in the feed VOC concentration. As VOC condensability increases the concentration dependency of VOC permeance becomes significant. The permeation of other VOCs exhibits similar behavior. The permeance of N₂ also increases with an increase in feed VOC concentration, which is mainly attributed to the membrane swelling at high feed concentrations. Furthermore, for different VOC/N₂ mixtures, the N₂ permeance tends to be higher when a high permeability VOC is present, indicating that the permeance of N₂ is significantly affected by the presence of VOC. Moreover, the VOC/N₂ selectivity increases with an increase in feed VOC concentration. This shows that increasing VOC concentration will increase the VOC permeance more significantly than the N₂ permeance. Therefore, the membrane is more selective at higher VOC concentrations. A selectivity of 40 to 180 was obtained for paraffin/N₂ separation, which are higher than the selectivities reported for silicone rubber membranes. At a given feed concentration, alcohol compounds were found to have higher VOC permeance and selectivity than hydrocarbon vapors, presumably due to the stronger affinity of polar alcohol molecules with the polyether linkage. That PEBA 2533 can be dissolved in propanol and butanol demonstrates the high affinity of the solvents and the polymer. Table 1 shows the permeance and selectivity of VOCs/N₂ at 23 °C when the feed gas is 80 % saturated with the organic compounds. The effect of temperature on membrane permeability was investigated, and the permeance of both VOC and N₂ was found to follow the Arrhenius type relation.

As shown in Figure 3, the permeate concentration was found to increase significantly with an increase in the feed VOC concentration. Generally, when the feed VOC concentration is over 5%, a permeate VOC concentration of 90 mol% can be achieved readily. This also demonstrates that the membrane is efficient for the separation of VOCs from N₂ at relatively high feed VOC concentrations.

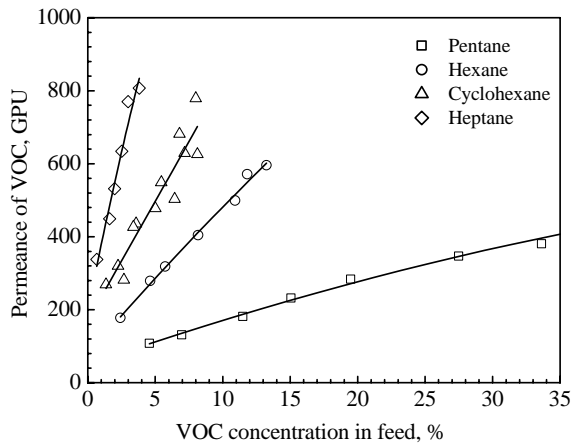


Fig 2. Permeance of VOC as a function of feed concentration

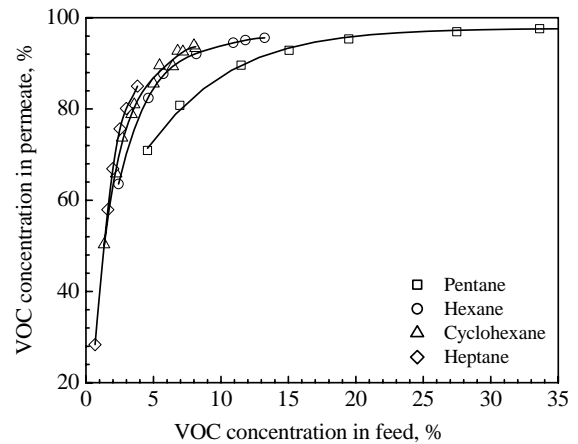


Fig 3. VOC concentration in permeate as a function of feed concentration

The effect of membrane thickness on the separation performance was studied by using two membranes with different thickness of the PEBA layer. The thinner membrane showed a lower selectivity than the thicker one, especially at high feed concentrations, though the thinner had a higher VOC permeance. This can be attributed to the boundary layer effect or the resistance of the substrate layer due to the high permeation rate of VOC. Therefore, the optimization of the flow pattern and the membrane structure are important in order to maximize the membrane performance.

Table 1 Permeance and selectivity of VOCs/N₂ at 23 °C (the feed 80% saturated with VOCs)

Mixtures	Permeance, GPU		Selectivity of VOC/N ₂
	VOC	N ₂	
Pentane/N ₂	380.7	4.76	80
Hexane/N ₂	596.1	4.21	142
Cyclohexane/N ₂	626.3	3.97	158
Heptane/N ₂	807.0	5.64	143
Methanol/N ₂	1178.3	3.77	313
Ethanol/N ₂	913.8	4.23	216
n-Propanol/N ₂	551.9	4.41	125
n-Butanol/N ₂	389.4	5.63	69
Acetone/N ₂	929.4	4.99	186
DMC	1186.0	7.23	164
MTBE	602.5	6.21	97

At a given feed concentration, the separation performance at different stage cuts was also studied for hexane/N₂ mixture. At a feed concentration of 12 mol%, more than 90 % hexane could be recovered at a stage cut of 0.16, for which the permeate hexane is about 70 mol%. Therefore, the PEBA/polysulfone composite membranes could be used to recover gasoline vapors efficiently to control the emission of gasoline vapors into the air.

Conclusions

The separation of VOC/N₂ mixtures by PEBA 2533 composite membranes were studied; it is relevant to the recovery and separation of gasoline vapor and other organic vapors from air. The membranes show good permselectivity for VOC/N₂ separation. The permeance of VOC and N₂ increases with an increase in the feed VOC concentration. The permeance of N₂ is affected by the presence of VOC significantly. Generally, more than 90 mol% VOC in permeate can be achieved when the feed concentration of VOC is over than 5 mol%. Because of the high permeability of the VOCs in the membranes, the resistance of the support layer and boundary layer effect were found to be significant. Further studies on optimizing the membrane structure and minimizing the boundary layer effect are needed to improve the separation performance of the membrane.

VOCs/N₂ separation by poly(ether block amide) composite membranes

L. Liu, X. Feng and A. Chakma

Department of Chemical Engineering
University of Waterloo
May 17, 2005

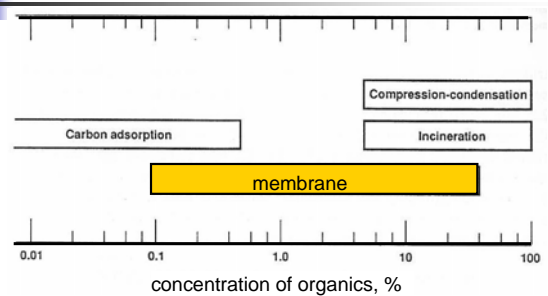
Outline

- Introduction
- Experimental
 - Membrane preparation
 - Separation process
- Results and discussion
 - VOCs/N₂ separation
 - Resistance of support layer
- Conclusions

Introduction

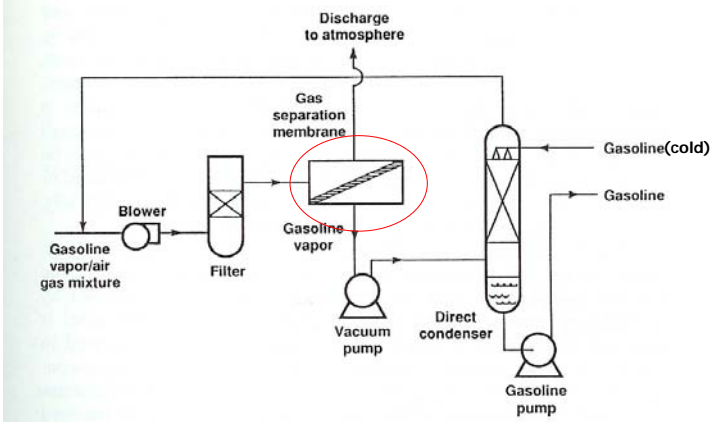
- Many industrial processes release Air/N₂ streams containing volatile organic compounds (VOCs)
 - Petrochemical & chemical industries
 - fuel storage, loading & unloading
 - coating & painting operations
- Environmental problem
- Economic loss

VOCs treatment technology



- Membrane separation
 - Energy efficient
 - Reuse of recovered solvents

VOC recovery by membrane

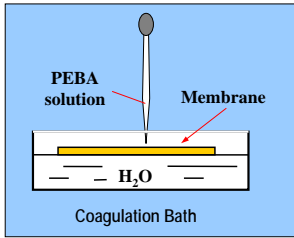


Membrane material

- Rubbery polymer: high solubility for VOCs
 - Silicone rubber: selectivity 10-100
- Poly(ether block amide) (PEBA) 2533
 - An alternative rubbery polymer to silicone rubber
 - Copolymer
 - 20 wt% polyamide: mechanical strength, chemical resistance
 - 80 wt% polyether: high chain mobility, high free volume
 - Good membrane formation characteristics
 - Good permeation performance
 - CO₂/N₂ separation, pervaporation

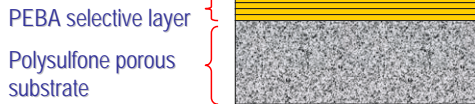
Membrane preparation

Thin skin membrane: water surface spreading

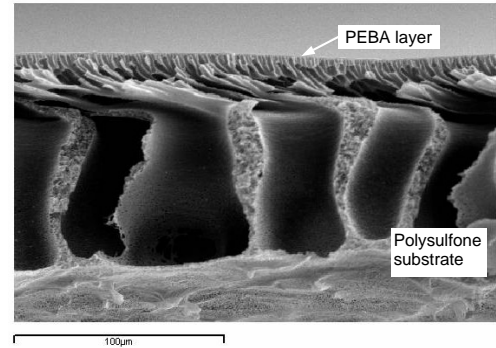


L. Liu, A. Chakma, X. Feng, J. Membr. Sci., 235 (2004) 43-52

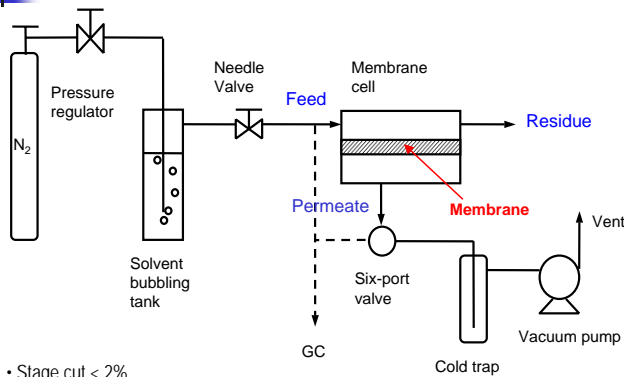
Composite membrane:
Multi-layer lamination



PEBA/polysulfone composite membrane



VOCs separation set-up



- Stage cut < 2%
- @ room temp.

Permselectivity

■ Permeance
$$J_i = \frac{Q \cdot y_i}{A \cdot (p_h \cdot x_i - p_l \cdot y_i)}$$

■ Selectivity
$$\alpha_{i/j} \equiv \frac{y_i / y_j}{x_i / x_j} = \frac{J_i}{J_j}$$

J : permeance, GPU (1 GPU = 10^{-6} cm³(STP)/cm²·s·cmHg)

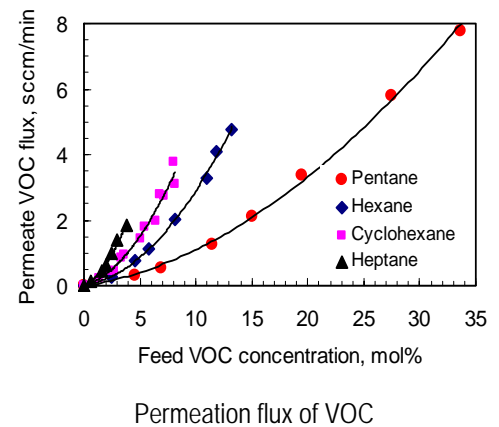
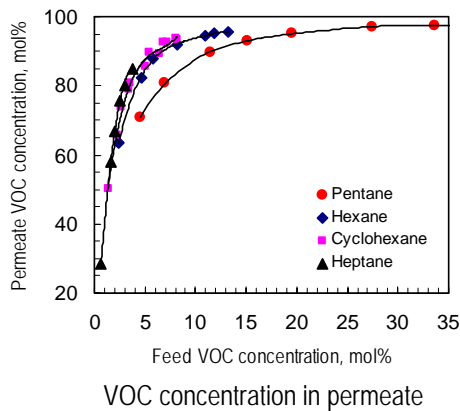
Q : permeate flow rate, cm³(STP)/s

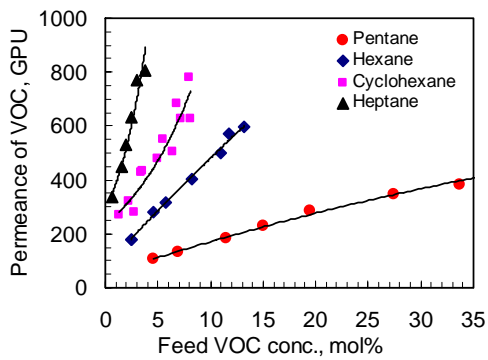
x_i, y_i : mol frac of VOC in feed & permeate

p_h, p_l : pressure in feed & permeate, cmHg

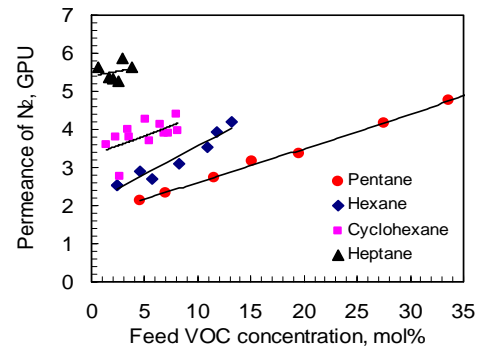
A : effective membrane area, cm²

VOC separation from nitrogen

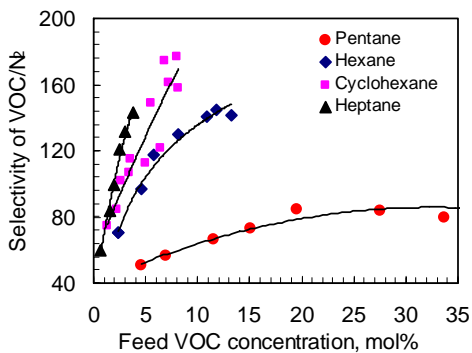




Permeance of VOC vs. feed VOC concentration



Permeance of N₂ vs. feed VOC concentration



Selectivity of VOC/N₂ vs. feed VOC concentration

Permeance of VOCs

- Hydrocarbons (main components of gasoline)
 - heptane > cyclohexane > hexane > propane
- Others
 - n-butanol > n-propanol > dimethyl carbonate > ethanol > methanol > acetone > methyl tert butyl ether
- alcohol > hydrocarbon

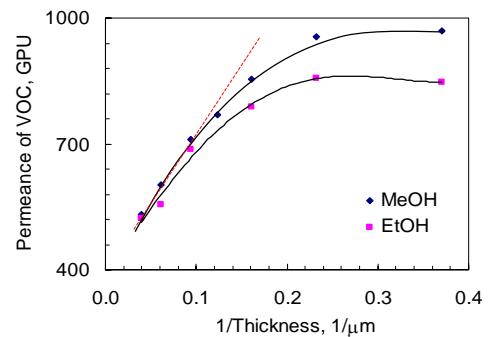
- condensibility → solubility → permeability
- interaction

VOCs/N₂ separation performance (80% feed saturated)

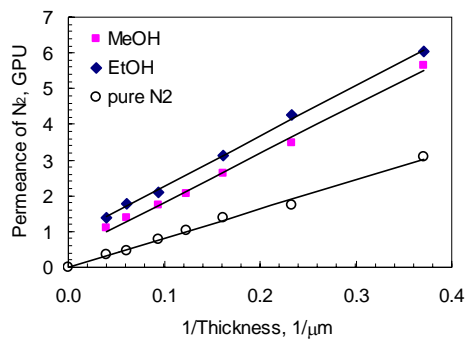
Mixtures	Permeance, GPU		Selectivity VOC/N ₂	Silicone rubber Selectivity*
	VOC	N ₂		
Pentane/N ₂	381	4.76	80	66.8
Hexane/N ₂	596	4.21	142	25.7
Cyclohexane/N ₂	626	3.97	158	
Heptane/N ₂	807	5.64	143	
Methanol/N ₂	1180	3.77	313	38.0
Ethanol/N ₂	914	4.23	216	
n-Propanol/N ₂	552	4.41	125	
n-Butanol/N ₂	389	5.63	69	
Acetone/N ₂	929	4.99	186	16.1
DMC	1190	7.23	164	
MTBE	603	6.21	97	

* Literature data

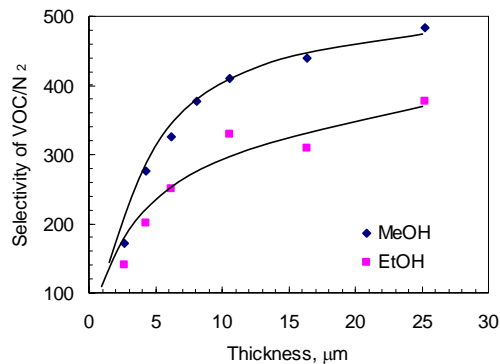
Effect of membrane thickness



VOC permeance vs. reciprocal of PEBA layer thickness
(feed methanol conc. 7.4%, ethanol conc. 3.4%)

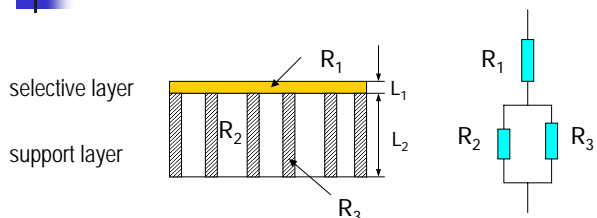


N₂ permeance vs. reciprocal of membrane thickness
(feed methanol conc. 7.4%, ethanol conc. 3.4%)



VOC/N₂ selectivity vs. membrane thickness
(feed methanol conc. 7.4%, ethanol conc. 3.4%)

Resistance of support layer



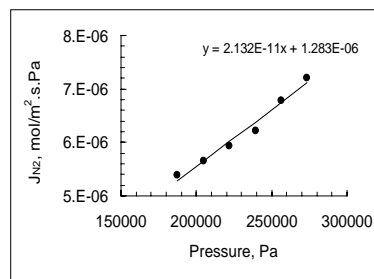
$$R_t = R_1 + \frac{R_2 R_3}{R_2 + R_3} \cong R_1 + R_2 \quad (R_2 \ll R_3) \quad J = \frac{1}{R_t A}$$

$$R_1 = \frac{L_1}{P_1 A} = \frac{1}{J_1 A} \quad R_3 = \frac{L_2}{A \epsilon r} \left(\frac{9 \pi M R T}{32} \right)^{1/2} \quad (\text{Knudsen flow})$$

Structural parameter of substrate

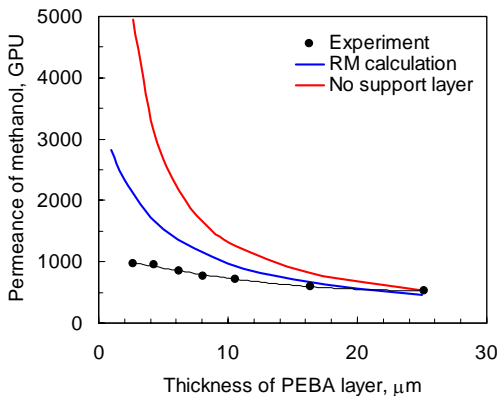
Gas permeation method: $J = \frac{\epsilon r^2}{8 \eta R T L_2} p + \frac{4}{3} \sqrt{\frac{2}{\pi M R T}} \cdot \frac{\epsilon}{L_2} \cdot r$

Viscous flow Knudsen flow



$$r = 2.3 \times 10^{-8} \text{ m}$$

$$\frac{\epsilon}{L_2} = 1.4 \times 10^4 \text{ m}^{-1}$$



Effect of membrane thickness on methanol permeance
(feed conc. 7.4%)

Conclusions

- PEBA 2533 membranes exhibited good permselectivity for VOC separation from nitrogen.
- A permeate VOC concentration of 95% can be achieved.
- Both VOC permeance and VOC/N₂ selectivity increased with an increase in the feed VOC concentration.
- The permeation of N₂ was affected by the coupling permeation of VOC due to penetrant interaction & membrane swelling.
- The membrane permselectivity was lowered by the resistance of the porous substrate.



Thank you!

Institute for Polymer Research
27th Annual Symposium

Symposium documents for

Howard Siu

Abstract

Presentation

Characterization of the Aggregation Made by Short PEO Chains Labeled at One End by the Fluorophore Pyrene

Howard Siu, Department of Chemistry, University of Waterloo

Associative polymers are an important group of polymers used in industry. In particular, two families of associative polymers, HASE and HEUR polymers (Figure 1a), are the main types of viscosity modifiers used in the paints and coatings industries. The peculiar viscoelasticities of these polymer families are rooted in the hydrophobic interactions of the hydrophobically end-capped poly(ethylene oxide) (hyd-PEO) groups which are common to both types of associative polymers. Thus, characterization studies of the aggregation properties of hyd-PEO are likely to yield important information on the associations of the HASE and HEUR polymers.

One technique that is often employed in characterizing HASE and HEUR systems is fluorescence. To gain direct information on the hydrophobic interactions, the hydrophobe can be replaced by a hydrophobic fluorophore. Pyrene is a common choice since it has the ability to complex with itself to create different fluorescence species called excimers. By monitoring the fluorescence of the various pyrene species, an idea of the amount of association between hydrophobes can be gained.

This seminar will focus on the characterization of the aggregation properties of a short poly(ethylene oxide) chain of 53 units in length capped at one end by the fluorophore pyrene (Py-PEO) (see Figure 1b). Several features of the associations of Py-PEO in water will be characterized such as the onset concentration of aggregation of Py-PEO and the sizes of these aggregates using fluorescence as well as other techniques such as surface tensiometry and light scattering.

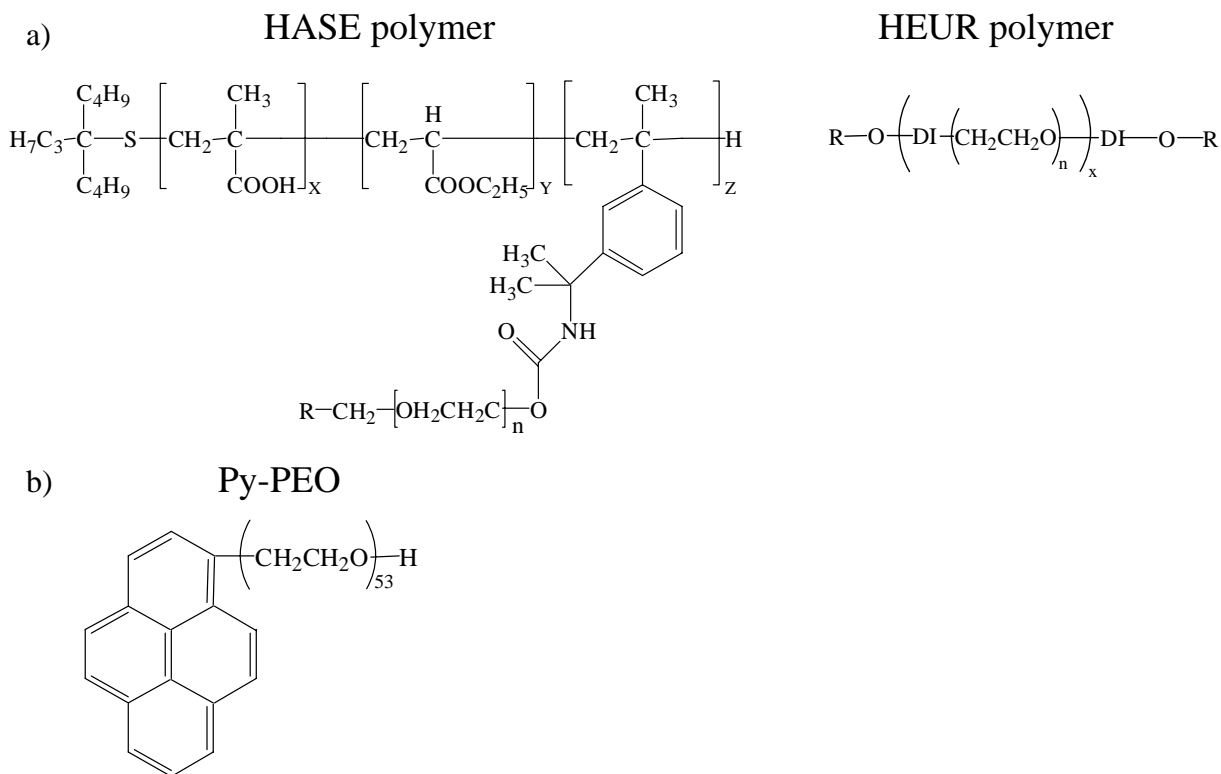


Figure 1: a) HASE and HEUR polymer structures with R and DI representing the hydrophobic group and diisocyanate linker, respectively; b) Structure of Py-PEO.

Since Py-PEO has a structure similar to that of many non-ionic surfactants, surface tensiometry should be capable of determining the critical micelle concentration (CMC) in water. For Py-PEO, the surface tension is shown in Figure 2 to drop at 0.001 g/L, from which concentration it steadily decreases upon further addition of Py-PEO until reaching a plateau at 10 g/L. Simple light scattering as well as excimer lifetime measurements indicate that micelles are being formed at concentrations above 0.003 g/L, implying that the CMC occurs at a concentration close to 0.001 g/L as observed from surface tensiometry. At concentrations above 10 g/L, dynamic light scattering

measurements showed a bimodal distribution indicating that larger aggregates are created. A potential scheme to describe the system would be that below a concentration of 0.003 g/L, only singular Py-PEO species exist in the bulk. At Py-PEO concentrations between 0.003 and 10 g/L, Py-PEO micelles are formed, which, at concentrations above 10 g/L, cluster to form larger aggregates (see Figure 2). From steady-state fluorescence spectroscopy experiments, it can be concluded that these larger aggregates consist of loosely associated Py-PEO micelles whose structure remains unchanged. This idea has also been proposed by the group of Jeanne François using poly(ethylene oxide) end-labeled with alkyl chains.¹

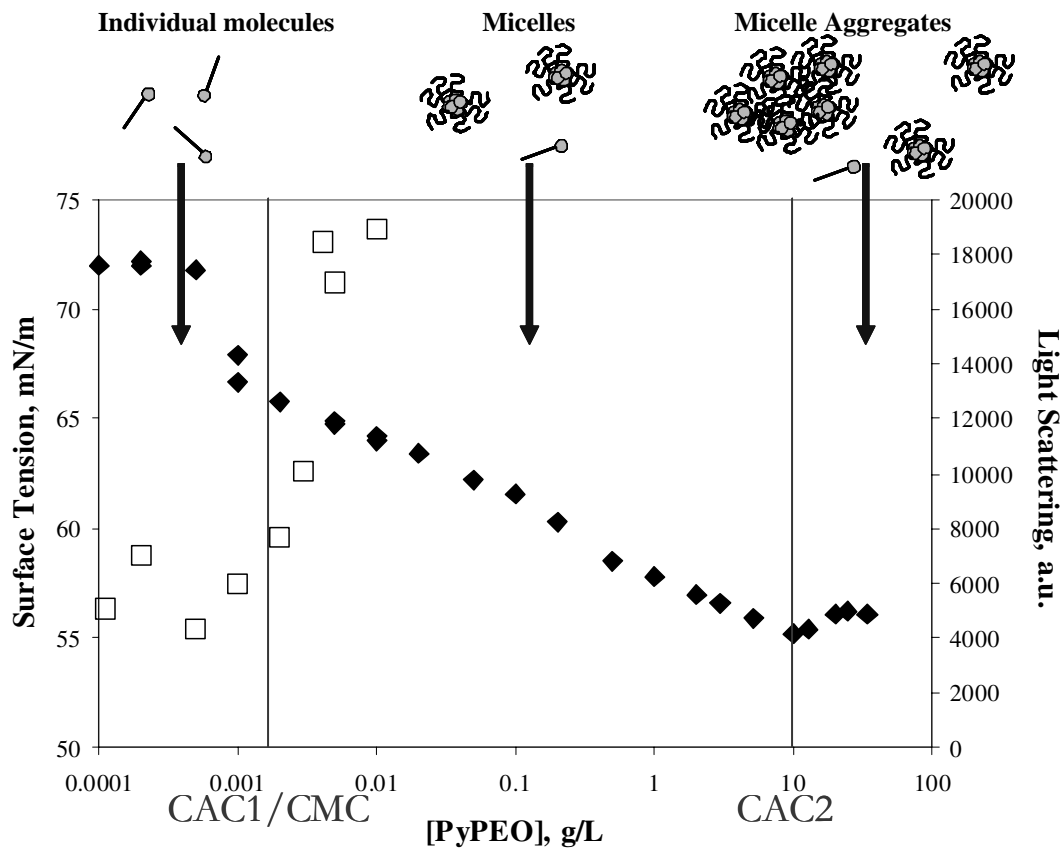


Figure 2: Py-PEO aggregation scheme in water with surface tension (◆) and light scattering (□) data.

Using Py-PEO as the surfactant, each micelle can be considered to act as a single fluorescent excimer species. Upon addition of an external hydrophobic quencher such as dodecyl pyridinium chloride (DPC), the excimer intensity is found to obey Equation 1 which was originally proposed by Turro and Yekta (see Figure 3):²

$$\ln\left(\frac{I_{E0}}{I_E}\right) = \frac{[Q]}{[M]} = \frac{[DPC] \times N_{agg}}{[Py-PEO] - CMC} \quad (1)$$

where I_E and I_{E0} are the intensities with and without quencher, respectively, and $[Q]$ and $[M]$ are the quencher and micelle concentrations, respectively. The micelle concentration for Py-PEO can be expressed as the difference between the surfactant concentration ($[Py-PEO]$) and the CMC divided by the number of surfactant molecules per micelle (N_{agg}). From this quenching study, carried out with several Py-PEO concentrations, a N_{agg} value of 20 ± 2 Py-PEO per micelle is determined. Since the micellar structure remains unchanged even after undergoing aggregation into larger structures, the Py-PEO concentrations used for this study are considered to be valid. By comparing the size of the micelles obtained by dynamic light scattering measurements with estimated sizes based on various conformations of the poly(ethylene oxide) corona, it can be concluded that the Py-PEO micelles, consisting of 20 ± 2 Py-PEO per micelle, have a pyrene core surrounded by a compact poly(ethylene oxide) corona. This conclusion differs from the extended chains proposed by the François group possibly stemming from the differences between pyrene and alkyl hydrophobic groups.

From this study, the aggregation of short poly(ethylene oxide) chains labeled at one end with pyrene (Py-PEO) has been investigated. From the results, it is found that

Py-PEO formed micelles at the very low concentration of 0.003 g/L but also undergoes a secondary aggregation into larger structures at 10 g/L. The micelles formed by Py-PEO are determined to consist of 20 ± 2 Py-PEO molecules having a PEO corona existing in a compact coiled state. It is hoped that the knowledge obtained from this study can be applied to modeling the associations of HASE and HEUR polymers to better understand those systems.

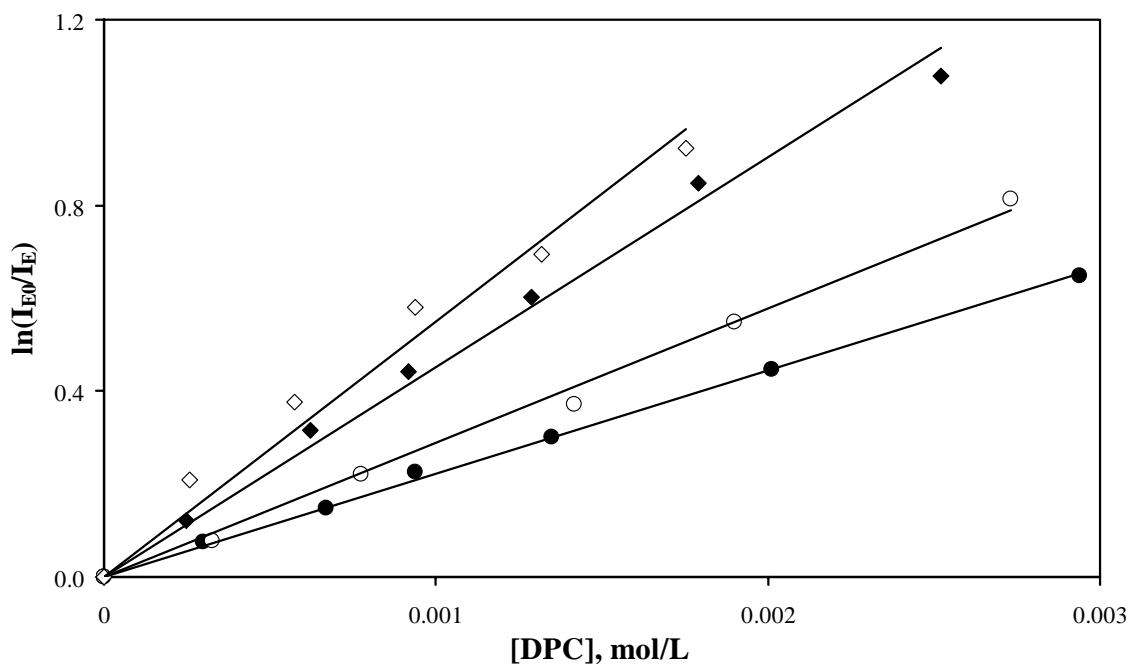


Figure 3: Quencher DPC concentration study at Py-PEO concentrations of 15 (\diamond), 44 (\blacklozenge), 100 (\circ) and 149 (\bullet) g/L.

References

1. Beaudoin, E.; Borisov, O.; Lapp, A.; Billon, L.; Hiorns, R.C.; François, J. *Macromolecules* **2002**, *35*, 7436 – 7447.
2. Turro, N.J.; Yekta, A. *J. Am. Chem. Soc.* **1978**, *100*, 5951 – 5952.

Characterization of the Aggregation Made by Short PEO Chains Labeled at One End by the Fluorophore Pyrene

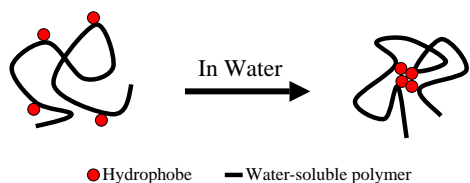
Howard Siu
 Supervisor: Jean Duhamel
 IPR Seminar
 University of Waterloo
 May 17th, 2005

Outline

- Introduction to Associative Polymers
 - HASE and HEUR polymers
 - Pyrene fluorescence and pyrene labeled HASE and HEUR polymers
- Studies of Pyrene Labeled PEO (53 units)
 - Determination the onset concentration of aggregate formation
 - Measuring the size and aggregation number of the aggregates
- Conclusions

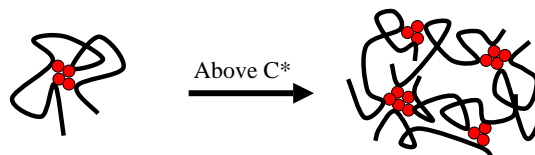
Associative Polymers

- Water-soluble polymers with a small amount (<5 mol%) of hydrophobic pendants
- In water, hydrophobes cluster to form aggregates

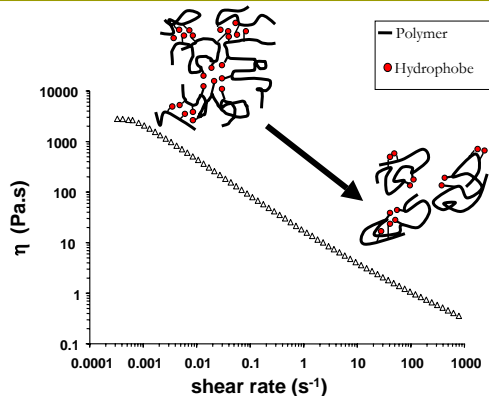


Associative Polymers

- Above C*, intermolecular bridging occurs creating a polymer network that increases the solution viscosity
- Used as viscosity modifiers for paints, coatings, dispersants and colloidal stabilizers

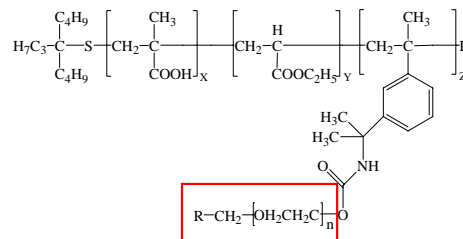


Associative Polymers in Solution



HASE Polymers

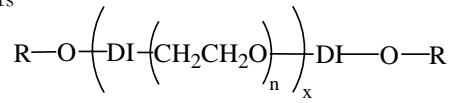
- Hydrophobically modified Alkali Swellable Emulsion (HASE) polymers



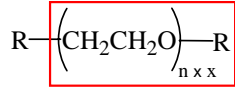
- Polymer properties can be fine-tuned by controlling the X:Y:Z ratio, PEO length n, and hydrophobe R

HEUR Polymers

- Hydrophobically modified Ethoxylated Urethane (HEUR) polymers



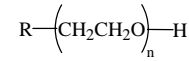
- DI represent diisocyanate linkages, effect is usually disregarded



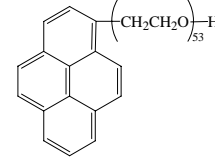
- The properties depend on the ratio of hydrophobe (R) size : hydrophilic chain (n × x) size

Proposed Model Compound (Py-PEO)

- Nature of HASE and HEUR networking based on aggregation of hydrophobically end-labeled PEO chains

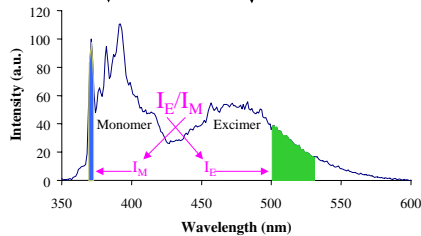
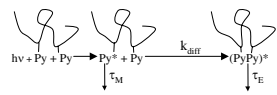


- Study of this component gives insight on HASE/HEUR aggregation

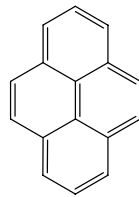


Model compound (Py-PEO) should act like a surfactant

Pyrene Fluorescence



R = Pyrene



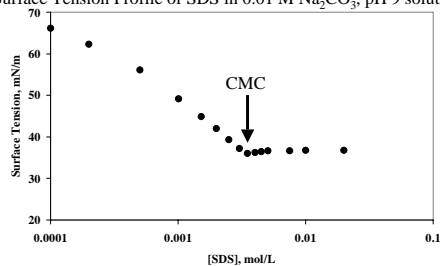
Studies of Py-PEO

- Determine the onset concentration of aggregation of Py-PEO
 - Surface tension
 - Light scattering
 - Time-resolved fluorescence of excimer
- Determine the number of Py-PEO per aggregate, N_{agg}
 - Micellar quenching studies using dodecyl pyridinium chloride (DPC)
 - Verify using dynamic light scattering (DLS)

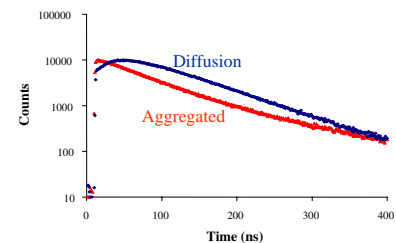
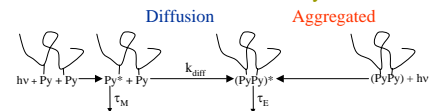
Surface Tension

- Addition of surfactants lowers the surface tension
- At critical micelle concentration (CMC), individual surfactants aggregate into structures called "micelles"

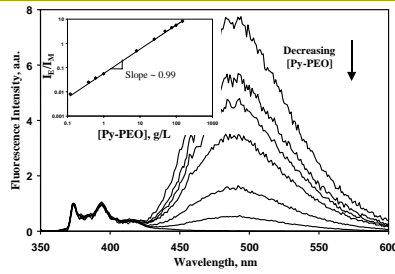
Surface Tension Profile of SDS in 0.01 M Na_2CO_3 , pH 9 solution



Fluorescence Excimer Decays

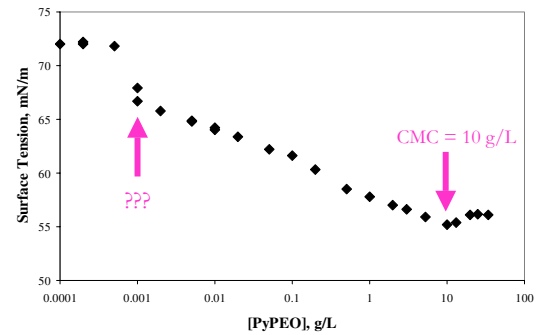


Results: Determining Onset of Aggregation

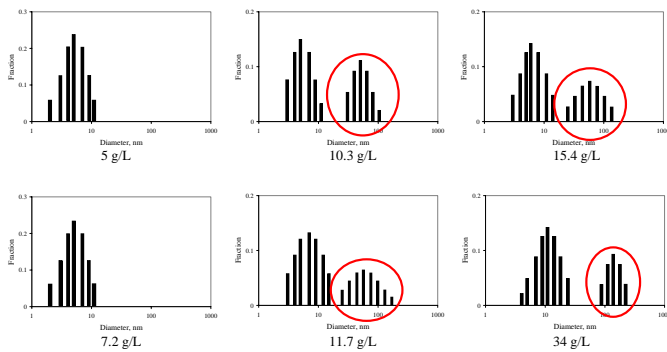


- Addition of Py-PEO (0.1 to 150 g/L) found an almost linear increase of intensity of excimer (I_E) relative to monomer (I_M) fluorescence

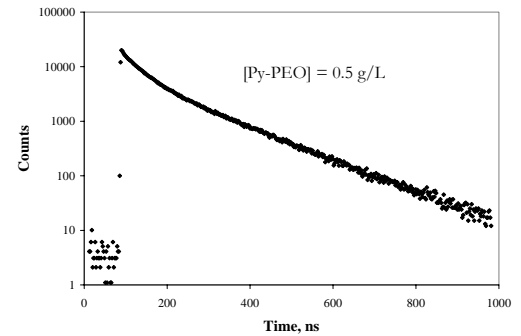
Surface Tension Measurements of Py-PEO



CONTIN Analysis of DLS of Py-PEO



Time-Resolved Excimer Decays of Py-PEO



- Lack of risetime indicates excimers formed via excited aggregates

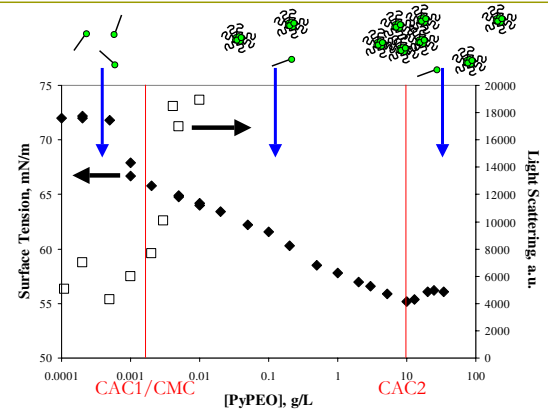
Loose Aggregation of Micelles

- Secondary aggregation occurs with micelles associating together
- Since I_E/I_M trend does not change, assume micelles stay unchanged throughout aggregation process
- The François group proposed a similar system with alkyl end-capped PEO*



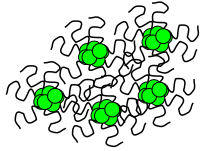
* Baudoïn, E.; Borisov, O.; Lapp, A.; Billon, L.; Hiorns, R. C.; François, J. *Macromolecules* **2002**, *35*, 7436.

Additional Light Scattering Measurements



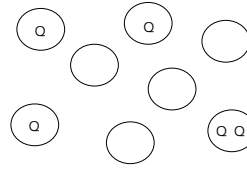
Results of Concentration Study of Py-PEO

- Determined critical micelle concentration (CMC) of Py-PEO to be 0.003 g/L
- Determined second aggregation of micelles (CAC2) of Py-PEO to be 10 g/L
 - Loose aggregates similar to those proposed by the François group



Finding the Aggregation Number, N_{agg}

- Each Py-PEO micelle acts as single excimer species
- Added hydrophobic quencher (Q), distributed amongst micelles

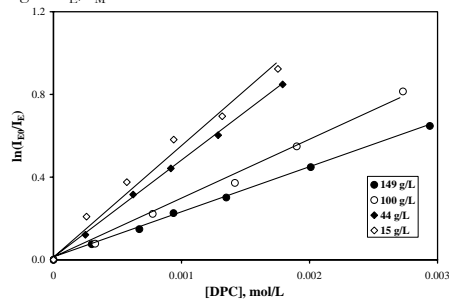


$$\ln\left(\frac{I_{E0}}{I_E}\right) = \frac{[Q]}{[M]} = \frac{[Q] \times N_{agg}}{[Py-PEO] - CMC}$$

- Micelles containing quenchers automatically quenched (i.e. do not fluoresce) reducing intensity of excimer from I_{E0} to I_E

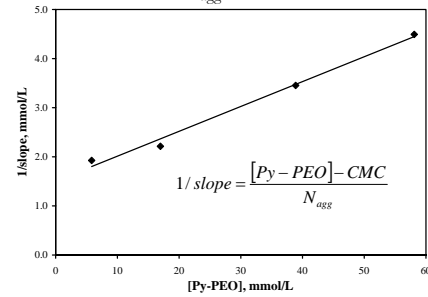
Determination of N_{agg} of Py-PEO Micelles

- Quenched Py-PEO micelles using dodecyl pyridinium chloride (DPC)
- Assumed micelle aggregation did not affect micelle structure
 - No change in I_E/I_M



Determined Value of N_{agg}

- From slopes of each Py-PEO concentration of $\ln(I_{E0}/I_E)$ vs. [DPC], one can determine N_{agg} using:



- N_{agg} determined to be 20 ± 2 Py-PEO per micelle

Comparison of Estimated vs. Measured Sizes

- Dynamic light scattering gave hydrodynamic diameters d_{H1} of 7.2 ± 3.1 nm for single micelles

- Taking into account a loosely-packed pyrene core of 20 units:

- Fully extended PEO corona has d_{H1} of 51 nm
- Unperturbed coiled PEO corona has d_{H1} of 10 nm
- Tightly packed PEO corona has d_{H1} of 6.8 nm



Conclusion:

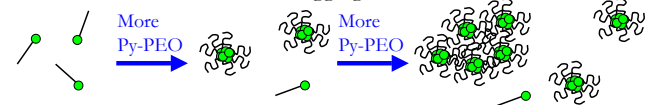
Py-PEO micelles consist of 20 ± 2 Py-PEO units with a compact PEO corona

- Contrary to extended conformation proposed by the François group!
 - François group used long PEO chains

Conclusions

- Py-PEO (53 units) forms micelles at 0.003 g/L (CMC)

- Py-PEO micelles aggregate at 10 g/L (CAC2) but individual micelle structures left intact in aggregate



- Micelles consist of 20 ± 2 Py-PEO units (N_{agg})
 - Collapsed PEO corona





Acknowledgements

- Dr. Jean Duhamel
- Telmo Prazeres
- Duhamel and Gauthier Lab Groups
- Dow Chemical
- Institute for Polymer Research
- NSERC

Institute for Polymer Research
27th Annual Symposium

Symposium documents for

Sofia Vega

Abstract

Presentation

Poster

CRYSTALLIZATION AND MELTING MECHANISMS OF NYLON 6-NANOCLAY HYBRIDS

S. M. Vega-Díaz and F. J. Medellín-Rodríguez*

Centro de Investigación y estudios de Posgrado, Facultad de Ciencias Químicas,
Universidad Autónoma de San Luis Potosí

Av. Manuel Nava N°. 6, Zona Universitaria, San Luis Potosí, S. L. P., México
Phone: 52 (444) 8 26 24 40 – 46 Ext. 531, Fax: 52 (444) 8 26 23 72,

*E-mail: francmr@uaslp.mx

Abstract

A study on the crystallization and melting mechanisms of poly (ϵ -caprolactam) [Nylon 6] nanoclay-hybrids is presented, using as a reference homopolymer Nylon 6. The effect of crystallization time was first studied, at constant crystallization temperature, in order to determine the most stable conditions before attempting melting studies after isothermal crystallization. After selecting the most stable isothermal crystallization conditions, unusual asymmetrical and truncated crystalline structures were observed in the case of the hybrids. Simulated melting diffraction patterns indicated the gradual evolution of truncated crystal structures. Optical observations under melting indicated step-like melting mechanisms in the hybrids similar to those of the reference homopolymer as an indication of similarities in both types of samples. Morphological characteristics and calculations indicated the typical evolution of Nylon 6 on melting and practically no change for the hybrids. The results allowed to conclude that nanoclay layers mainly influence crystal habits. An explanation is given for the development of truncated crystalline structures on the basis of the observed results.

Introduction

Polymeric nanocomposites are important because the introduction of nanometric particles causes a significant improvement in the overall properties of the polymer. Poly (ϵ -caprolactam) [Nylon 6] is an engineering polymer able to crystallize in at least two crystal habits, α and γ (Holmes *et al.*, 1955). It can be nanostructured with silicate layers through exchange chemical reactions, which render end-tethered polymer macromolecules to the substrate. It is therefore expected that the neat quiescent crystallization process be affected compared with the tethered system. The previous effects have both scientific and practical interests and will ultimately lead to understand and optimize the property-structure relationship in these systems.

In the present study, the crystallization and melting mechanisms of hybrid Nylon 6 were studied and compared with those of homopolymer Nylon 6. The main purpose was to understand the mechanisms involved on the crystallization and melting processes between both types of samples after isothermal crystallization under quiescent condition and linear heating.

Methodology

Nylon 6 homopolymer and Nylon 6 nanoclay-hybrids with 2 wt % (N6NCH2) and 5 wt % (N6NCH5) montmorillonite content were synthesized by Ube Industries, Japan, using ϵ -caprolactam and a modified montmorillonite. This last was prepared through cation exchange with 12-aminolauric acid (Usuki *et al.*, 1993). Nylon 6 homopolymer had an average-molecular-weight of 2.17×10^4 and the clay-hybrids N6NCH2 and N6NCH5 had average-molecular-weights of 2.22×10^4 and 1.97×10^4 respectively (Giannelis, *et al.*, 1999). All samples were originally in film form with an average thickness of 700 μm .

Differential scanning calorimetry (DSC) traces were obtained in a Perkin Elmer DSC-7 calorimeter. Calibrations were made with indium and lead standards covering all the thermal range of the studies before collecting thermal traces. Nylon 6 and the hybrids had an average weight of 8 mg. Samples were placed in aluminum sample holders, heated at 260 °C for 3 min under nitrogen atmosphere, and fast cooled at nominal cooling rate of 500 °C/min to the isothermal crystallization temperature (T_c) where they were maintained for 60 min. After this crystallization time, samples were linearly heated at 10°C /min until the equilibrium melting temperature (260 °C).

Wide Angle X-ray Diffraction (WAXD) patterns were obtained in a Siemens D-500 diffraction equipment. WAXD was used to identify crystalline structures of samples crystallized under identical conditions as in DSC, both before and after heating at specific temperatures. In this last case, samples were fast cooled after introducing the desired thermal history and some were heated up to specific temperatures before the quenching process took place.

Small Angle X-ray Scattering (SAXS) experiments were made in the in the X27C beamline at the National Synchrotron Light Source, Brookhaven National Laboratory, USA. The wavelength was 1.37 Å and a 3 pinhole collimation system was used to reduce the beam size to 0.6 mm in diameter. The 2D SAXS

patterns were taken on Fuji® imaging plates which were individually digitized. The sample to detector distance was 1400 mm.

Polarized Optic Microscopy (POM) was made in an Olympus BX60 optical microscope. This was used to register the morphology of the melting process after isothermal crystallization. The microscope was coupled with an Olympus PM-20 photographic system and two Mettler FP82HT hot stages with automatic control.

Results and Discussion

In the present study, the view is adopted that understanding melting after isothermal crystallization will lead to understanding the crystallization process of hybrids as long as there are enough complementary crystallization experiments. The DSC results in Figure 1 indicate that after isothermal crystallization at the selected temperature of 160 °C Nylon 6 and nanoclay hybrids develop different melting traces, which are affected by the crystallization time. In the homopolymer case in Figure 1(a) there is the typical multiple melting behavior. It starts with an apparent double melting and ends up with single melting after 1 hr of crystallization. The hybrid N6NCH2 in Figure 1(b) behaves different and develops a recrystallization exotherm and an almost imperceptible melting endotherm in all the range of crystallization time. As for the hybrid N6NCH5, Figure 1(c) shows a similar thermal behavior, there is the recrystallization exotherm and slightly better defined double melting behavior. Overall, the crystallization and melting process was time dependent in all three samples although it was rather similar in both hybrids. The different proportion in melting endotherms in Nylon 6 has been reported before (Medellín, *et al.*, 2004) as molecular weight dependent although in terms of crystallization temperature. The results in Figure 1 (d-f) also indicate that perfecting (higher peak intensity and truncation process (lack of a family of diffracting planes) and evolution between crystal structures (disappearance of reflections) were present, or took place, as a function of crystallization time. This was an indication of the unstable complex nature of the Nylon 6 hybrids so the highest crystallization time was selected in order to have the most stable morphology at the selected temperature to *in-situ* characterize the melting process.

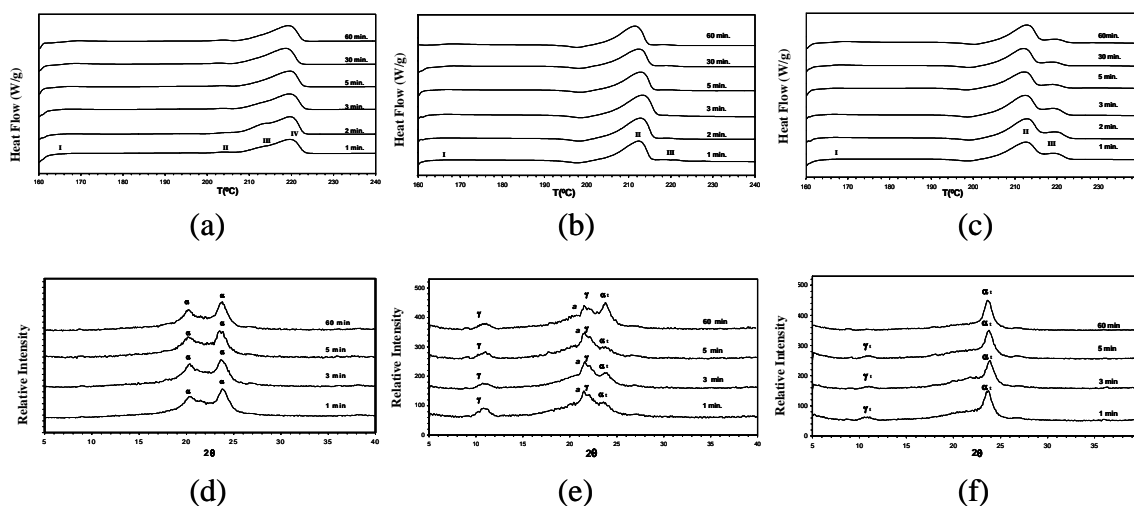


Figure 1. Melting behavior in terms of time of: (a) Nylon 6, (b) N6NCH2 and (c) N6NCH5. Diffraction patterns as a function of crystallization time of: (d) Nylon 6, (e) N6NCH2, (f) N6NCH5. The crystallization temperature was 160 °C

The *in-situ* melting process in terms of WAXD is shown in Figure 2. Other than a slight perfecting process on heating, the Nylon 6 homopolymer develops the typical α crystalline structure (Holmes, *et al.*, 1955). Both Nylon 6 hybrids on the other hand developed different behavior on heating, N6NCH2 started with a mixture of asymmetrical and a complex mixture of truncated crystal habits. These evolved with heating until the final formation of a single α_2 truncated crystal habit. N6NCH5 developed a single reflection

associated with the truncated α crystal structure which preserved characteristics on melting until the final recovery of a single truncated structure before melting, the molten state in these last two cases was highly oriented due to the presence of montmorillonite.

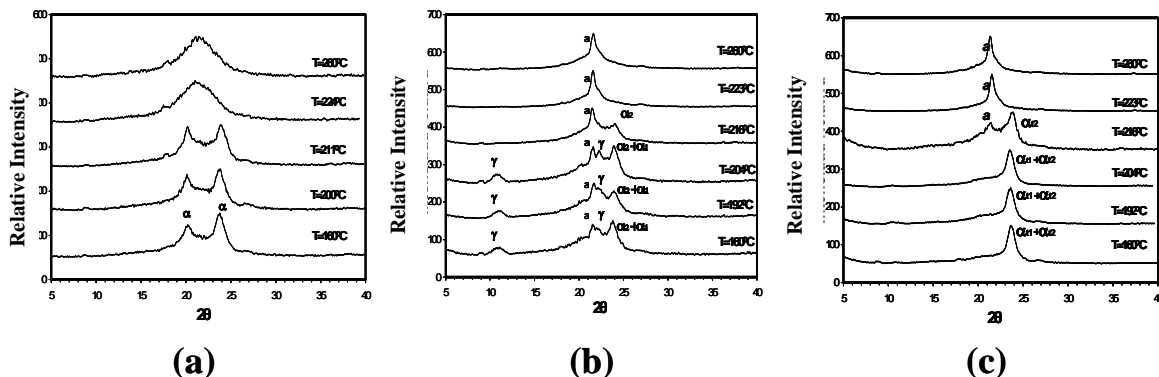


Figure 2. Diffraction patterns along the heating process of: (a)Nylon 6, (b) N6NCH2, (c)N6NCH5. The isothermal crystallization temperature and time were 160 °C and 60 min respectively.

The POM results in Figure 3 indicate that the melting process followed up step-like melting mechanisms such as in other polymeric systems (Medellín, *et al.*, 1996). This was the case both with the homopolymer and with the hybrids and was an indication that, in spite of the nanoclay presence, the crystallization process preserves the general morphological characteristics of homopolymers.

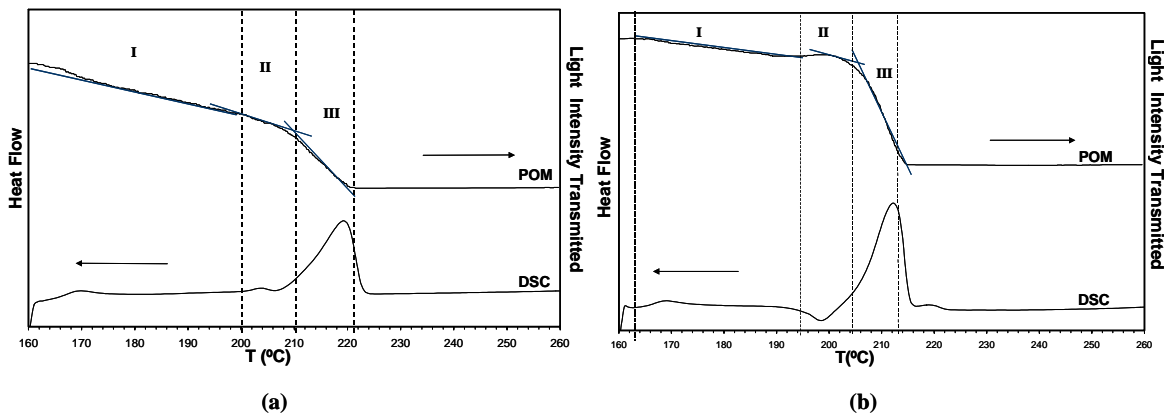


Figure 3. POM/DSC melting results after isothermal crystallization at 160 °C of: (a) Nylon 6 and (b) NCH2

The complex hybrid systems under study indicated that the observed effects could have intrinsically morphological features involved. Therefore, SAXS experiments were used in order to generate information regarding the morphological evolution on melting. It is well known (Liberti, *et al.*, 1968) that Nylon 6 is able to recrystallize to thicker crystals (and also perfect, as shown before) on heating. The recrystallization process on heating is observed as a decrease in the position of the scattering maximum and the perfecting process can be considered related to an increase of the SAXS invariant. The results in Figure 4 (a) and independent calculations, not shown here, indicated the typical evolution of Nylon 6. However, in the case of the hybrids Figures 4 (b-c) only show a decay of the scattering function as an indication of the lack of formation of periodical structures involving a correlation distance.

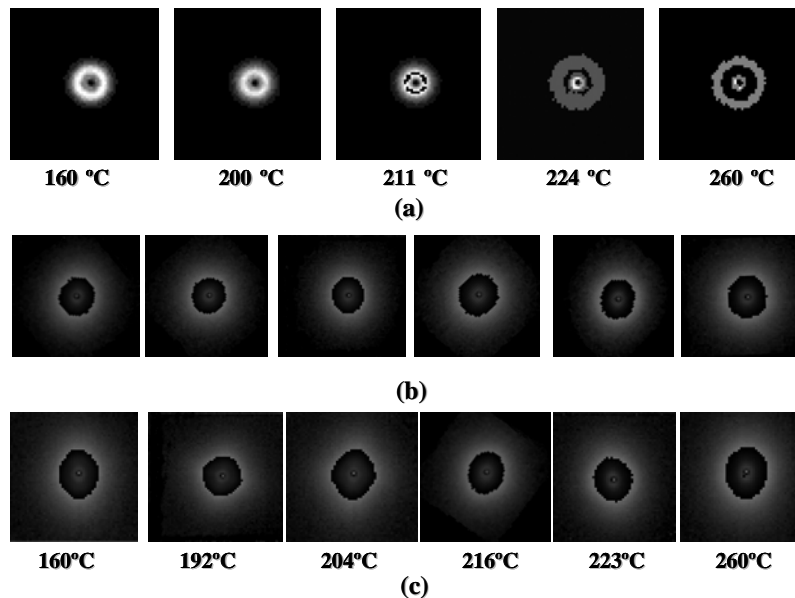


Figure 4. SAXS images corresponding to melting of: (a) Nylon 6, (b) N6NCH2 and (c)N6NCH5, isothermally crystallized at $T_c=160$ °C for 60 min.

On the basis of the previous results a crystallization mechanism for both hybrids can be proposed. Figure 5(a) illustrates the crystallization of hybrids with low nanoclay content. Step I shows the interaction between a montmorillonite layer and the polymeric chains. Step II indicates the beginning of the crystallization process under isothermal conditions. Step III shows the crystallization process where the formation of two crystal habits is involved asymmetrical γ , and a mixture of truncated α . The first structure must be formed by the vicinity of the polymeric chains attached to the montmorillonite layers, motivating hydrogen bonds between neighbor fully extended chains (Kyotani *et al.*, 1972). However if the crystallization time, or melting temperature, increase, the hydrogen bonds will break promoting the formation of folded-chain-like α_t crystal structures, which are thermodynamically more stable. Figure 5(b) shows the crystallization and evolution of the high montmorillonite content hybrids. In this case, the higher nanoclay content must decrease the number of tethered polymeric molecules per unit surface increasing as a consequence the space between molecules and promoting the folded-chain-like, although truncated, α crystals. Regarding the truncation process, it must be originated by the tethering process which impedes diffraction along specific planes such as the (100) of the α structure.

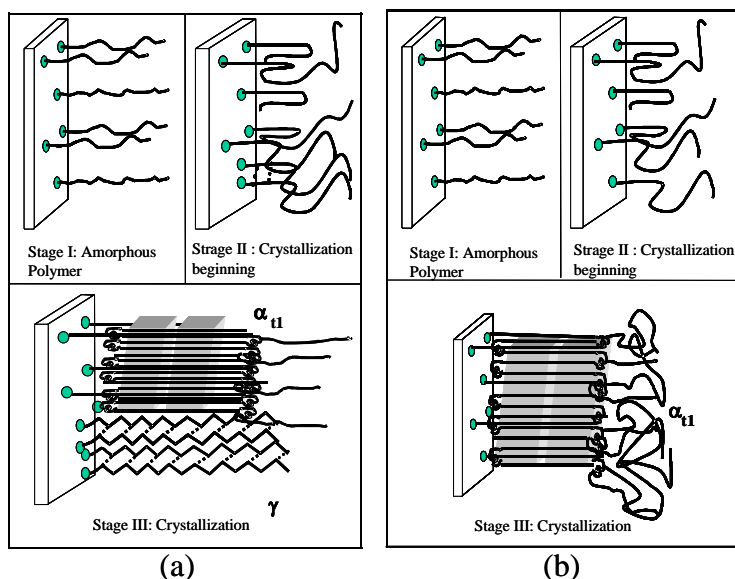


Figure 5. Crystallization Model of: (a) Nylon 6 with low and (b) Nylon 6 with high nanoclay content

Conclusions

The thermal crystallization and melting behavior of Nylon 6 homopolymers and end-tethered Nylon 6 nanoclay hybrids was modified by the nanoclay presence although only small differences were observed in thermal traces after increasing the nanoclay content.

On crystallization conditions there was the formation of atypical asymmetrical and truncated crystal structures. On melting such structures were relatively stable.

Hybrid crystals followed up step-like melting mechanisms as an indication of overall similarities with neat nylon 6 and the behavior of other macromolecules.

There was not apparent lamellar periodicity in the hybrids compared with neat Nylon 6.

The results allowed to propose a crystallization and melting mechanism for the hybrid complex systems

References

- Giza E., Ito, H., Kikutani, T., Okui, N., Journal of Polymer Engineering, Vol. 20, No. 6, 403-425 (2000)
- Giannelis, E.P., Krishnamoorti, R., Manias, E., Adv. In Polym. Sci., 138, 108(1999)
- Holmes, D.R., Bunn, C.W. y Smith, D.J., J. Polym. Sci. 17, 159-177 (1955)
- Itoh, T., Miyaji, H., Asai, K., Japanese J. Appl. Phys., 14, 206-215 (1975)
- Kyotani, M., Mitsuhashi, S, J. Polym. Sci. A-2,10,1497-1508 (1972)
- Liberti, F.N., Wunderlich, B., J. Polym. Sci.. A-2,6,833-848 (1968)
- Medellín-Rodríguez et. Macromolecules, 37, 1799-1809 (2004)
- Medellín, F.J., Chu, B., Burger, C., Hsiao, B. S., Vaia, R., S. Phillips, Polymer 42, 9015-9023 (2001)
- Medellín-Rodríguez, F.J., Phillips, P.J, Lin, J.S., Campos, R., J. Polym. Sci. Pis. Ed. 1757-1773 (1997)
- Medellín-Rodríguez, F. J., Phillips, P.J, Polym. Eng. Sci. 36, 703(1996)
- Radusch, H.J., Stolp, M., Androsh, R., Polymer, 35, 3568-3571 (1994)
- Usuki, A., Kawasumi, M., Kojima, Y., Okada, A., Kurauchi, O., J. Mater. Res., 8, 1179-1184 (1993)
- Wu, T.Z., Chen, E.C., Liao, C.S, Polymer Engineering and Science,42,6, 1141-1150 (2002)

Acknowledgements

This work was supported by CONACyT, México through grants 39638-Y and U40177-Y. S. M. Vega-Diaz thanks CONACyT for the scholarship 165314. The support of CA9/FCQ is appreciated.

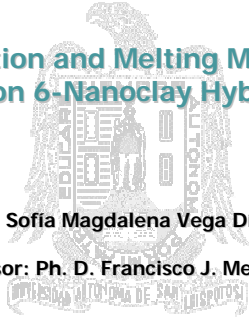
Universidad Autónoma de San Luis Potosí

Centro de Investigación y Estudios de Posgrado

“Crystallization and Melting Mechanisms of Nylon 6-Nanoclay Hybrids”

Sofía Magdalena Vega Díaz

Advisor: Ph. D. Francisco J. Medellín R.



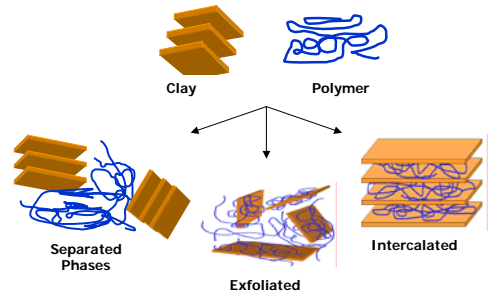
Outline

- ◆ Introduction
- ◆ Objective
- ◆ Methodology
- ◆ Results and Discussion
- ◆ Conclusions

Introduction

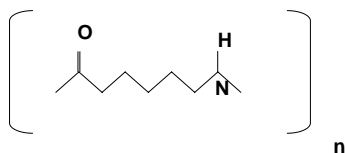
- ◆ Hybrid polymers, nanostructured materials with better physicochemical and mechanical properties
 - ◆ Reduce gas permeability (80 %)
 - ◆ Increase resistance to solvent attack
 - ◆ Decrease flame propagation (175 %)
 - ◆ Increase flexion and stress modules (110 %)
- ◆ Nanostructured polymers pose questions related to their behavior

Different Polymer-Clay Structures

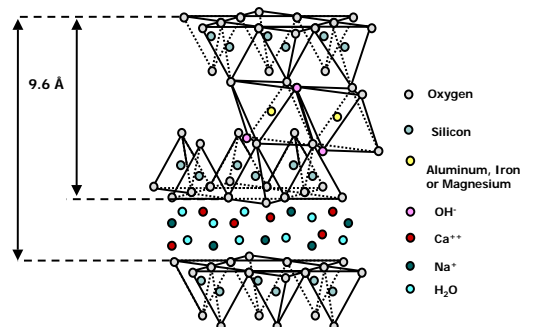


Nylon 6-Hybrid

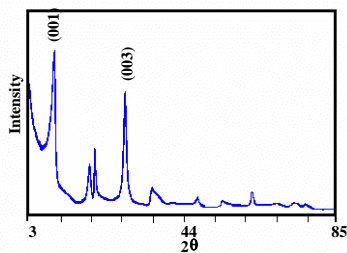
- ◆ Hybrid polymers: chemically bonded to the substrate
- ◆ Nylon 6-hybrid was developed in 1988 by Toyota
- ◆ Nylon 6 is an aliphatic polyamide which contains carboxyl and amide groups forming bifunctional monomers



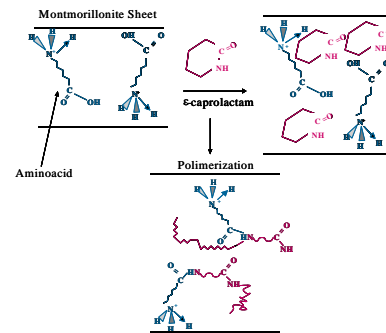
Montmorillonite Structure



Montmorillonite X-Ray Diffraction Pattern

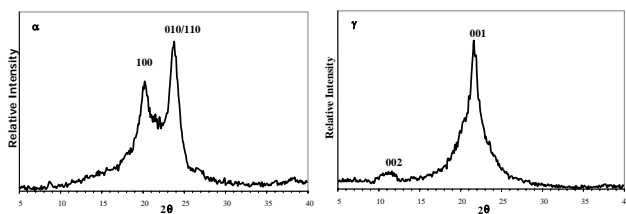


Scheme for the Nylon 6-Hybrid Polymerization Reaction



Nylon 6 Structures Without Additives

- ◆ Nylon 6 can form different crystalline structures because it has flexible chains



X-Ray diffraction patterns for the α and γ structures

Previous Results

- ◆ Kojima and Usuky (1994) determined the preferential orientation to γ form showing that the presence of anisotropic clay sheets made with silica are determinant on the orientation of Nylon 6-hybrid chains.
- ◆ Kojima (1995) proposed that the γ crystalline form has a planar orientation and this orientation increases with the clay content.

Objective

- ◆ Mathias and Davis (1999) and Medellín et al. (2001) reported that the presence of clay in Nylon tends to produce orientation in the polymer chains forming the γ crystalline structure in a preferential pathway
- ◆ Wu et al. (2002) found in Nylon 6-hybrid only one diffraction peak for the α structure in one plane

- ◆ Analyze the crystallization and melting mechanisms of Nylon 6 in the presence of nanoclay

Materials

- Materials: Nylon 6 homopolymer, Nylon 6-hybrid with 2% and 5% w/w montmorillonite content from Ube Industries, Japan

Montmorillonite content (%)	Average Molecular Weight (g/mol)	Code Name
0	2.17×10^4	Nylon 6
2	2.22×10^4	N6NCH2
5	1.97×10^4	N6NCH5

Methods

- DSC: Perkin Elmer 7 equipment
- WAXD: Siemens modelo D-500 equipment
- POM: Olympus model BX60 equipment, Hitachi digital camera model KP-D50, Mettler ZUFP82HT photomonitor, Mettler FP82HT heating platines
- SAXS: Center for Small Angle Reserch at the National Laboratory in Oak Ridge, Oak Ridge TN. USA.

Results and Discussion

Finding optimal conditions for characterization

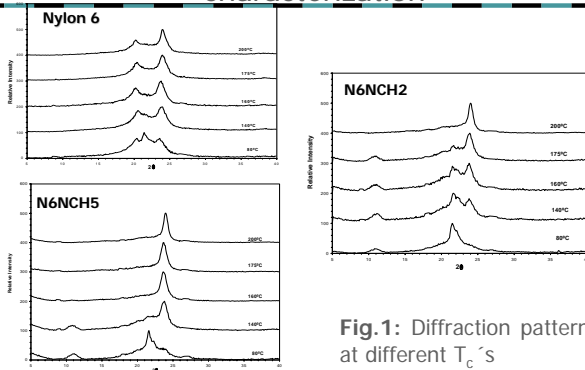


Fig. 1: Diffraction patterns at different T_c 's



N6

N6NCH2

N6NCH5

Fig. 2: Morphology for all the samples during isothermic crystallization at 160 °C

Systematic Analysis of Melting Process

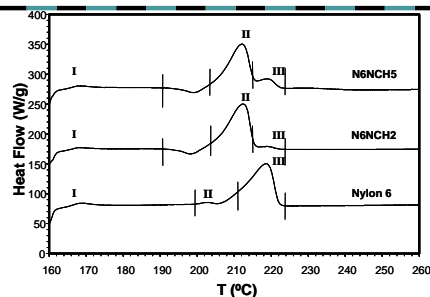


Fig. 3: Melting process for all the samples isothermally crystallized at 160 °C

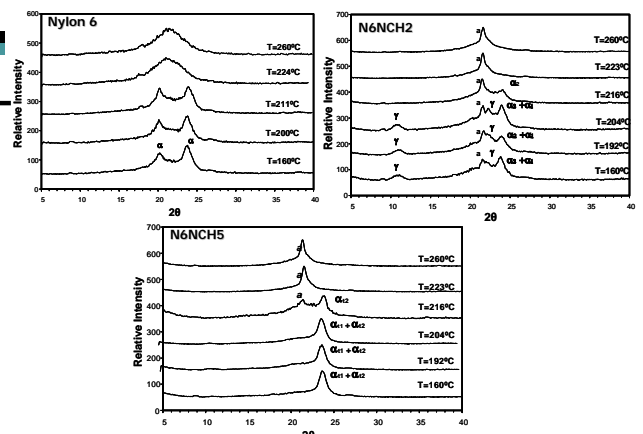


Fig. 4: Diffraction Patterns

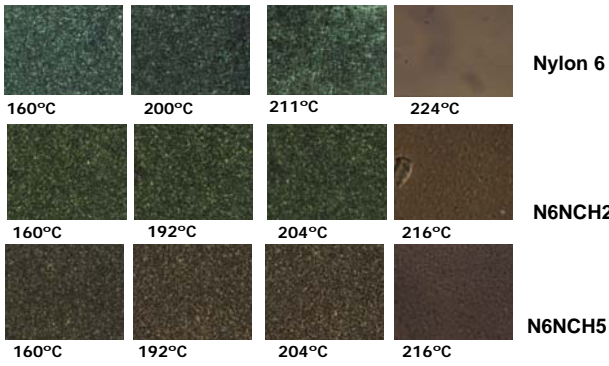


Fig. 6: Melting of the samples isothermally crystallized at 160 °C

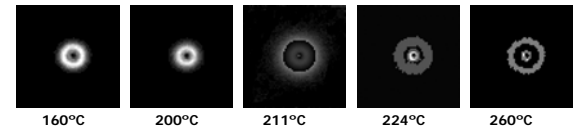
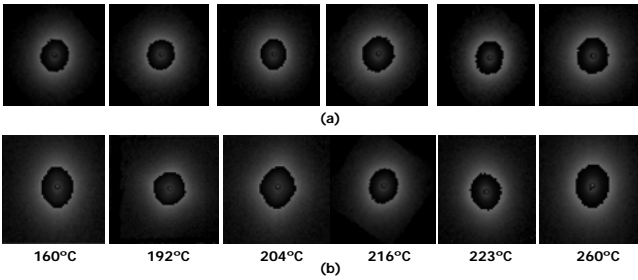


Fig. 7: SAXS images corresponding to the Nylon 6 melting after isothermic crystallization

Fig. 8: SAXS images corresponding to the (a) N6NCH2 and (b) N6NCH5 melting after isothermic crystallization at 160 °C



Recrystallization Hypothesis Analysis

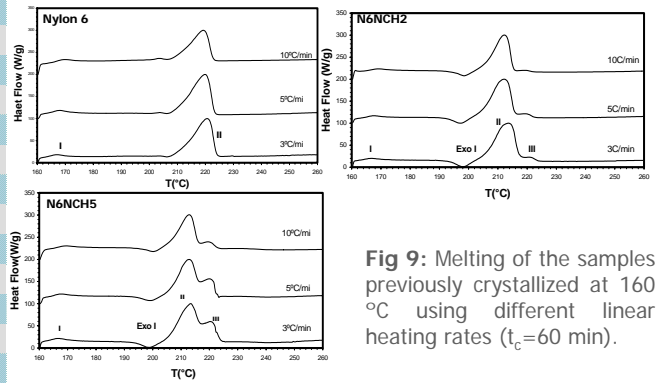


Fig 9: Melting of the samples previously crystallized at 160 °C using different linear heating rates ($t_c=60$ min).

Models

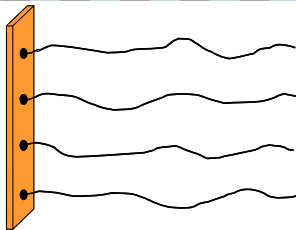


Fig 10. Schematic representation of a nanoclay sheet chemically bonded to polymer chains

Fig 11. Schematic Representation of the unit cell for the α Structure

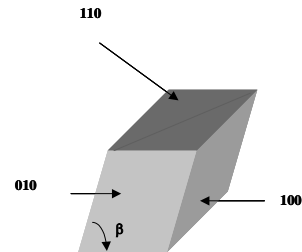


Fig. 12 Crystallization Model for N6NCH2

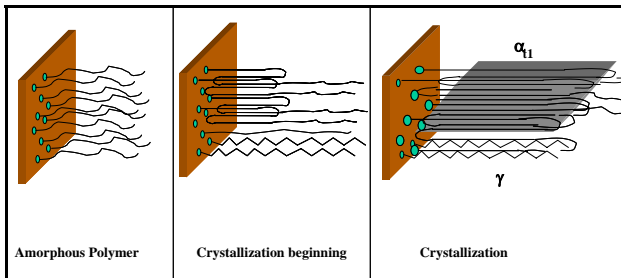


Fig. 13 N6NCH2 Melting

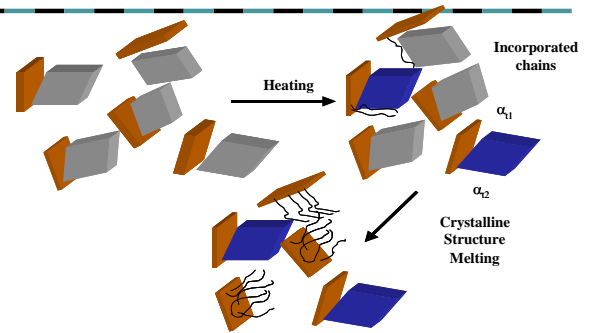


Fig. 14 Crystallization Model for N6NCH5

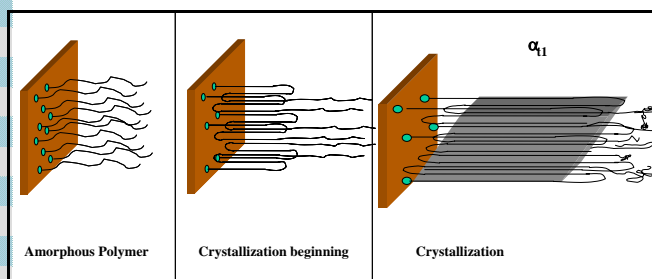
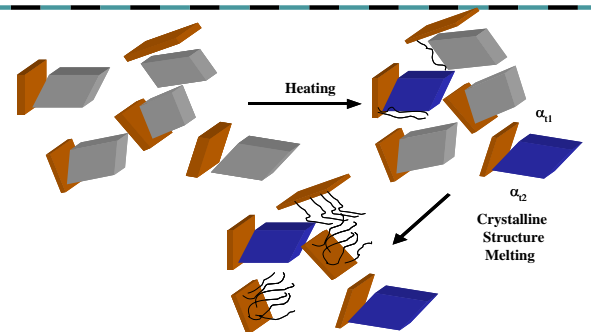


Fig. 15 N6NCH5 Melting



Conclusions

- ◆ Adding anisotropic montmorillonite modifies the crystallization and melting mechanisms
- ◆ Presence of montmorillonite promotes formation of truncated crystalline structures.
- ◆ Low clay content promotes formation of α_{t1} , α_{t2} and γ structures
- ◆ High clay content promotes formation of α_{t1} and α_{t2} structures

Conclusions

- ◆ Crystalline structure named α_{t2} may have its origin due to recrystallization processes
- ◆ The presence of clay promotes high crystallinity
- ◆ Melting process can be described as a combined mechanism involving melting and recrystallization



Acknowledgements

- ◆ **Consejo Nacional de Ciencia y Tecnología:**
project # 39638-Y and scholarship No. 165314
- ◆ **Universidad Autónoma de San Luis Potosí:**
projects CO2-FRC-08.8 and CO2-FAI-04-18.24



Temperature and Time Effects on Crystallization of Nylon 6 Nanoclay Hybrids

S.M. Vega-Díaz and F.J. Medellín-Rodríguez*

Centro de Investigación y Estudios de Posgrado, Facultad de Ciencias Químicas,
Universidad Autónoma de San Luis Potosí, Av. Manuel Nava No. 6, Zona Universitaria, San Luis Potosí, S. L. P.,
México

Abstract

Studies on the crystallization and melting mechanisms of Nylon 6 nanoclay hybrids are presented where Nylon 6 homopolymer was used as reference. Both time and temperature after isothermal crystallization were studied in terms of differential scanning calorimetry (DSC) and the results were complemented with several experimental techniques. X-ray diffraction patterns displayed unusual asymmetrical and truncated crystalline structures depending on isothermal crystallization of the hybrids. Optical microscopy showed a complex nucleated morphology when crystallization habits were in the α form. X-rays dispersion indicated diffuse scattering in the hybrids. The amount and type type of crystalline structures in the hybrids were also found to depend on crystallization time. Overall, nanoclays were determined as influencing morphological characteristics of hybrids.

Introduction

Nanostructured polymers contain nanometric size particles as fillers. The addition of such particles to a polymeric matrix strongly affects its properties and so the challenge exists of optimizing such effects. Nylon 6 nanoclay-hybrids were first developed by Toyota Inc. research laboratories and their development has motivated a number of studies. In the present, we are concerned with the thermal behavior and morphological characteristics being the main motivation to understand the evolution of a Nylon 6 when the macromolecules are end-tethered to a substrate such as montmorillonite.

Nylon 6 is a linear semi-rigid polymer with amide and carboxylic groups resulting in a polar behavior of the molecule. These characteristics allow Nylon 6 to develop two different crystalline structures, α -monoclinic and γ -pseudo-hexagonal (Holmes et al., 1955)

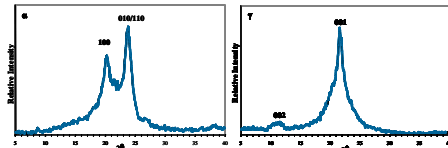


Fig. 1 X-Ray diffraction patterns of Nylon 6 crystalline structures: α and γ (Holmes et al., 1955)

Nylon 6 nanoclay hybrids are obtained end-tethering the Nylon 6 macromolecules to montmorillonite. This last is a natural clay of the smectite family with a crystallographic model proposed by Hoffman (Giannelis et al., 1999)

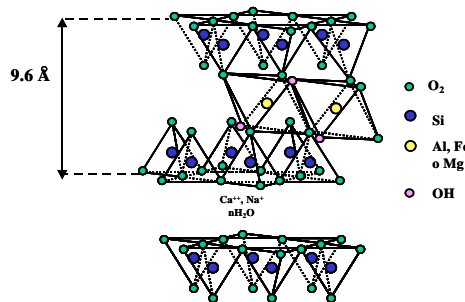


Fig. 2 Montmorillonite structure (Giannelis et al., 1999)

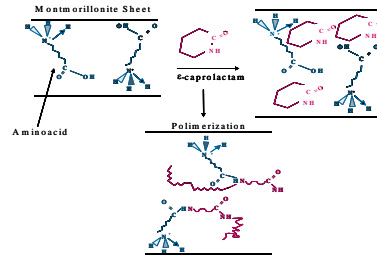


Fig. 3 Scheme for the Nylon 6 nanoclay hybrid polymerization reaction (Liang et al., 2003).

The reaction mechanism involves cations from the Montmorillonite structure which are easily exchanged by surfactants, the *in-situ* polymerization reaction follows by adding ϵ -caprolactam.

Experimental Section

Nylon 6 homopolymer and Nylon 6 nanoclay-hybrids with 2 wt % (N6NCH2) and 5 wt % (N6NCH5) montmorillonite content were synthesized by Ube Industries, Japan by *in situ* polymerization. Nylon 6 homopolymer had an average-molecular-weight of 2.17×10^4 and the clay-hybrids N6NCH2 and N6NCH5 had average-molecular-weights of 2.22×10^4 and 1.97×10^4 respectively (Krishnamoorti, et al., 1997).

Effect Of Crystallization Temperature

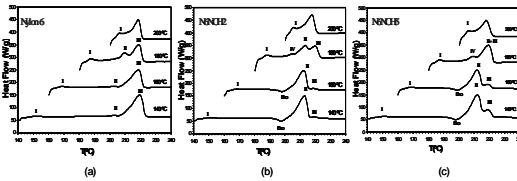


Fig. 4 Melting of (a) Nylon 6, (b) N6NCH2 and (c) N6NCH5 isothermally crystallized at different crystallization temperatures for 60 min.

The results show that all three samples have different behavior depending on crystallization temperature. However, at low crystallization temperatures the behavior is rather similar, particularly in the hybrids.

WAXD Characteristics

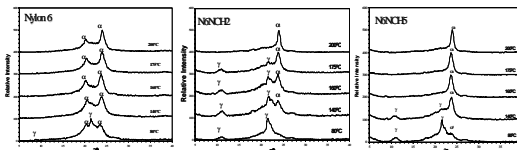


Fig. 5 X-Ray diffraction patterns of: (a) Nylon 6 homopolymer, (b) N6NCH2 and (c) N6NCH5, isothermally crystallized for 1 hr at the indicated temperatures.

At low crystallization temperatures there is asymmetrical γ in the hybrids. However, as crystallization temperature increases, there is a tendency to formation of the stable although truncated α form.

POM During Isothermal Crystallization

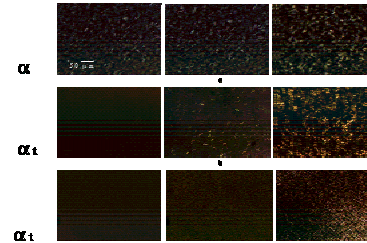


Fig. 6 Morphological evolution of: (a) Nylon 6, (b) N6NCH2, (c) N6NCH5, isothermally crystallized at 206 °C at the indicated time ($T_m^0=260$ °C).

SAXS Behavior

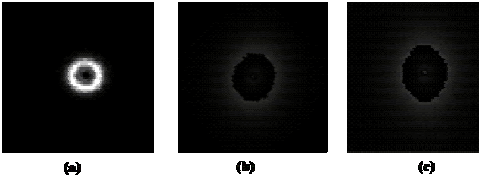


Fig. 7 SAXS images of: (a) Nylon 6, (b) N6NCH2, (c) N6NCH5 isothermally crystallized at 160 °C, for 60 min ($T_m^0=260$ °C)

Nylon 6 shows two-phase behavior whereas the hybrid materials show diffuse patterns.

Effect of Crystallization Time

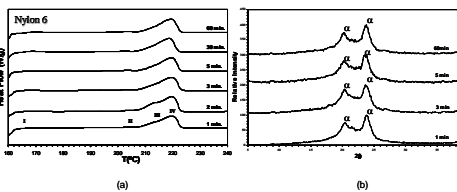


Fig. 8. (a) DSC linear heating traces after isothermal crystallization at 160 °C and different crystallization times. (b) WAXD patterns for the corresponding crystallization times.

The DSC behavior of Nylon 6 does not show important changes. The WAXD behavior indicates the formation of the stable α crystalline structure

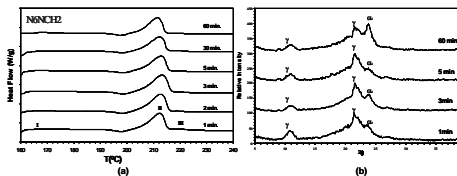


Fig. 9. Nylon 6 with 2% w/w nanoclay (N6NCH2) isothermally crystallized at 160 °C at different crystallization times (a) Melting traces and (b) Diffraction patterns

N6NCH2 shows triple melting although the first and third endotherms are only slightly defined. There is also a crystallization exotherm. The WAXD patterns start with a mixture of asymmetrical γ and not well defined α and then there is an evolution $\gamma/\alpha/\gamma$

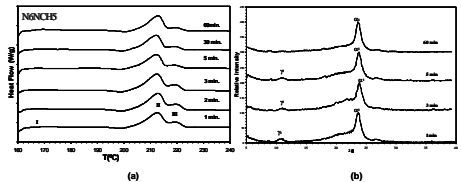


Fig. 10. Nylon 6 with 5% w/w of nanoclay (N6NCH5) isothermally crystallized at 160 °C at different crystallization times (a) Melting traces and (b) Diffraction patterns

N6NCH5 shows a better defined triple melting behavior which stays basically the same as a function of crystallization time. The WAXD behavior indicates however a mixture of truncated α/γ and the development of truncated α at high crystallization times

Conclusions

- > Nylon 6 nanoclay hybrids have complex crystallization and melting mechanisms.
- > In both hybrids, the thermal behavior is similar at low crystallization temperatures although it is very different at intermediate temperatures becoming again similar at high crystallization temperatures.
- > At low crystallization temperatures there is asymmetrical γ in the hybrids. However, as crystallization temperature increases, there is the tendency to formation of the stable although truncated α form.
- > Nylon 6 shows two-phase behavior whereas the hybrid materials show diffuse patterns.
- > In terms of time, the N6NCH2 WAXD patterns start with a mixture of asymmetrical γ and a not well defined α and then there is an evolution $\gamma/\alpha/\gamma$. As for N6NCH5 the behavior indicates however a mixture of truncated α/γ and the development of truncated α at high crystallization times

References

- >Kyotani, M., Mitsuhashi, S, J. Polym. Sci. A-2,10,1497-1508 (1972)
- >Giannelis, E.P., Krishnamoorti, R., Manias, E., Adv. In Polym. Sci., 138, 108(1999)
- >Liang, Y., Omachinski, S., Logsdon, J., Whan Cho J., Lan T., Technical information, Nanocor Inc. (2003) (www.nanocor.com)
- >Krishnamoorti, Giannelis, Macromolecules, 30,4097-4102. (1997)
- >Medellin-Rodríguez, F. J. Phillips, P.J, Polym. Eng. Sci. 36, 703(1996)
- >Usuki, A., Kawasumi, M., Kojima, Y., Okada, A., Kurauchi, O., J. Mater. Res., 8, 1179-1184 (1993)
- >Wu, T.Z., Chen, E.C., Liao, C.S, Polymer Engineering and Science,42,6, 1141-1150 (2002)

Acknowledgements

> This work was supported by CONACyT, México through grants 39638-Y and U40177-Y. S. M. Vega-Díaz thanks CONACyT the scholarship 165314. The support of CAS/FCQ is greatly appreciated.

*E-mail: francmr@uaslp.mx

Institute for Polymer Research
27th Annual Symposium

Symposium documents for

J.R. Leiza

Abstract

Presentation

Monitoring emulsion polymerization reactors: Calorimetry vs. Raman Spectroscopy

Oihana Elizalde¹, Maider Azpeitia¹, Marlon M. Reis², José M. Asua¹ and Jose R. Leiza¹

- 1- Institute for Polymer Materials (POLYMAT) and Grupo de Ingeniería Química, Departamento de Química Aplicada, The University of the Basque Country, M. Lardizabal 3, 20018 Donostia-San Sebastián, Spain
- 2- Universidade de São Paulo, Escola Politécnica, Department of Chemical Engineering, Caixa Postal 61548, CEP D5424-970, São Paulo, SP Brasil

Introduction

Emulsion polymers are *products-by-process*, which means that the final product properties and quality are defined during the polymerization. Therefore, efficient polymerization process control is needed to produce high-performance polymers. This requires the availability of on-line measurements. An adequate online sensor must be able to provide continuous (or at least frequent) measurements, must be accurate enough and has to operate over long periods of time in environments often physically and chemically aggressive.

In the last three decades significant effort has been devoted both by academic and industrial research groups to the development of suitable, accurate and robust monitoring techniques for polymerization reactors. The monitoring of emulsion polymerization reactors might a priori seem easier than the homogeneous counterpart reactors because of the lower viscosity of the reaction medium, but it turned out to be much more complex^{1,2}. Sensors for the monitoring of several properties (e.g., conversion, polymer composition, molecular weights, particle size) have been developed and assessed in polymerization reactors. Not all the reported techniques were accurate or robust enough as to be implemented in industrial environments. Excellent reviews about the development and applications of online sensors developed in the last three decades have been published³⁻⁶. The current trend is to use noninvasive techniques in order to avoid the complexity of manipulating viscous or reaction mediums prone to suffer coagulation. Reaction calorimetry and Raman spectroscopy are two of the most promising noninvasive techniques to monitoring emulsion polymerization reactors because of the advantages they have in comparison with other techniques.

In reaction calorimetry, the measurement is noninvasive, rapid, robust, relatively simple and cheap because it is based on temperature measurements. As a consequence, it is one of the techniques that most easily can be implemented in industrial environments. Among the different spectroscopies techniques that have been applied to monitor emulsion polymerization reactors, Raman spectroscopy offers several advantages in comparison with the absorption based spectroscopies: Near-Infrared (NIR) and Mid-Range Infrared (MIR). Thus, water has a very weak signal in Raman spectroscopy and functional groups that are inactive or very weak in absorption present a strong Raman scattering, i.e., carbon-carbon double bonds. Furthermore, for industrial implementation Raman spectroscopy offers the

possibility of using silica fibers (that have a low cost) with a length of up to 100 m, to transmit the radiation to and from the sample.

In this work, the performance of the noninvasive techniques (calorimetry and Raman spectroscopy) to monitoring semibatch high solids content emulsion polymerizations for two different monomer systems (vinyl acetate/butyl acrylate, VAc/BA, and butyl acrylate/ methyl methacrylate, BA/MMA) is compared. Overall and instantaneous conversions, as well as free monomer concentrations were measured. The polymerizations were carried out under starved conditions (high instantaneous conversions) for the BA/MMA system, and under non-starved conditions for the VAc/BA system.

Results and Discussion

Figure 1 shows the evolution of the instantaneous conversions (as calculated by gravimetry) for the seeded semibatch experiments carried out for each comonomer system. It can be seen that the trend was similar in both cases; namely, there was an accumulation of monomer during the first stages of the process, and then the conversions were roughly steady up to the end of the feeding period. Beyond this point, the conversions increased as the process proceeded batchwise. The conversions reached during the plateau were greater than 80% for BA/MMA and under 70% for VAc/BA. The former corresponded to starved conditions, whereas the latter did not.

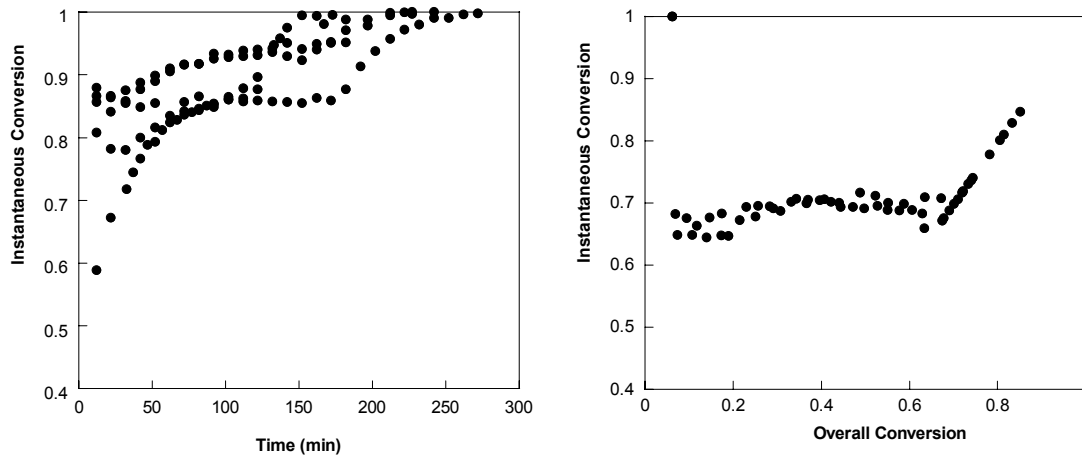


Figure 1. Instantaneous conversions for the semibatch emulsion copolymerizations used to compare Raman spectroscopy and calorimetry: (left) BA/MMA; (right) VAc/BA.

VAc/BA system (Non-starved conditions)

Figure 2 presents the comparison of the overall conversion predicted by the two monitoring techniques and by gravimetry (reference technique). It can be seen that the predictions of both Raman and calorimetry were close to the gravimetric values.

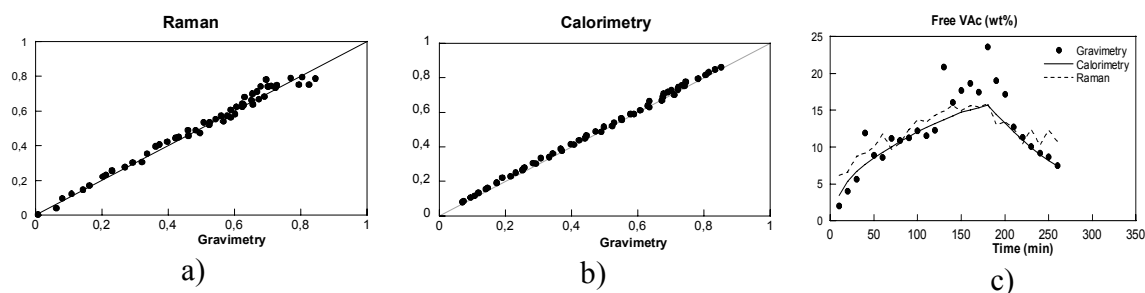


Figure 2. Overall conversion(a and b) and free VAc monomer concentration(c). Comparison of calorimetry and Raman spectroscopy with the reference techniques (gravimetry and gas chromatography).

Figure 2 also shows the unreacted VAc (weight fraction based upon the total reactor mass) as measured by the reference technique (gas chromatography), and by calorimetry and Raman spectroscopy. Both techniques provided a good prediction of the free concentration of VAc in the reactor and they were comparable to the chromatographic values. Furthermore, both techniques captured well the change in the profile when the feeding period was over and monomer concentration decreased.

BA/MMA system (Starved conditions)

As shown in Figure 1, the instantaneous conversion for this comonomer system was higher during the whole process. This means that monomer concentrations were also significantly lower than in the previous case, specially the concentration of MMA, which is the more reactive monomer in this system. Consequently, the heat released by polymerization was much lower too.

Figure 3 presents the comparison of the overall conversion measured by gravimetry and the two online techniques for the copolymerizations experiments carried out with the MMA/BA comonomer system. As it can be seen, in general there is no much difference for both techniques, and they compared well with gravimetry.

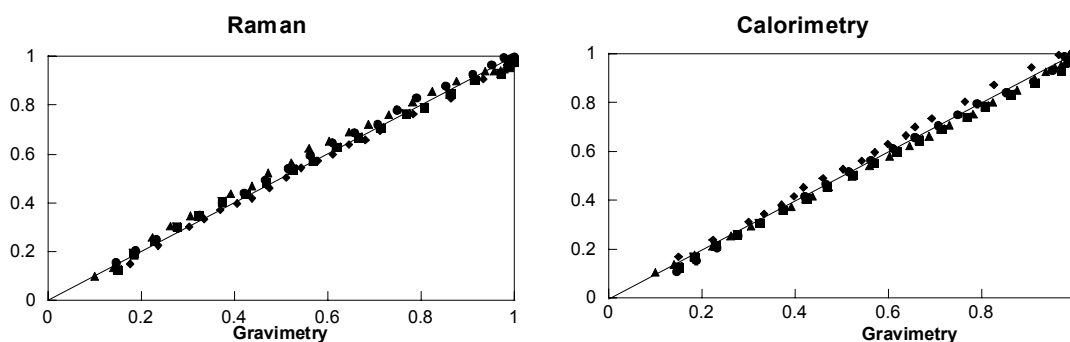


Figure 3. Comparison of the overall conversions measured by gravimetry for the BA/MMA system: Raman spectroscopy (left) and Calorimetry (right).

Figures 4 show the comparison of the instantaneous conversion and the MMA and BA monomer concentrations calculated by means of the gravimetry and by Raman spectroscopy and calorimetry for one of the experiments carried out with this comonomer system.

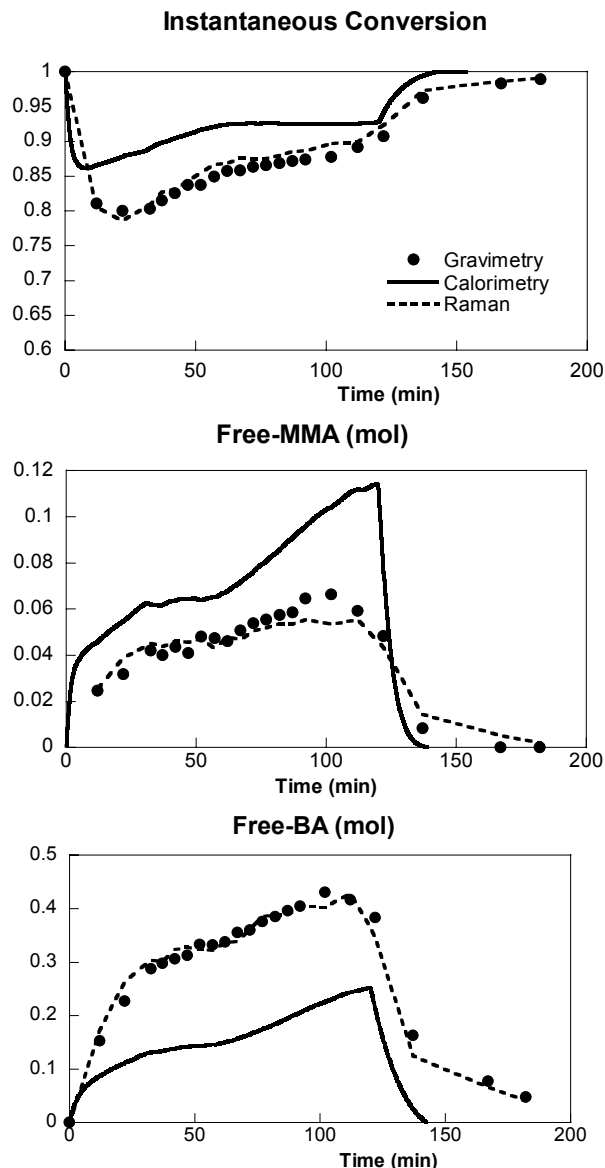


Figure 4. Comparison of the instantaneous conversion and free amounts of MMA and BA in the semibatch experiments as measured by the three techniques.

This graph shows that the prediction of the instantaneous conversion and free monomer concentrations were better for the FT-Raman spectroscopy than for reaction calorimetry. Similar results were obtained for other experiments carried out at different monomer ratios and with different feeding times for the monomer.

In conclusion the study revealed that under non-starved conditions both calorimetry and Raman spectroscopy provided comparable results. However, significant differences were found for the BA/MMA semibatch emulsion copolymerization carried out under starved conditions. The overall conversion predicted by both techniques was good, but for the instantaneous conversion and free concentrations of monomer. Raman spectroscopy was far more accurate than calorimetry.

Acknowledgements

The authors acknowledge the financial support from the University of the Basque Country (Grant UPV 0021.215-13594/2001) and CICYT (project PP02000-1185). O. Elizalde and M. Azpeitia acknowledge their scholarships from the Ministerio de Educacion y Ciencia and M. M. Reis acknowledges the FAPESP (grant number: 03/06837-8 and 01/13017-1).

References

- (1) Leiza; J.R, J.M. Asua; J.M. Asua (ed). *Polymeric Dispersions: Principles and Applications*. Kluwer Academic Publishers, 1997.
- (2) Dimitratos; J., G. Eliçabe; C. Georgakis. *AIChE J*, **1994**, 40:1993.
- (3) Chien; D.H.C., A. Penlidis. *J. Macromol. Sci., Macromol. Chem. Phys.*, **1990**, C30:1.
- (4) Embirucu; M., E.L. Lima; J.C. Pinto. *Polym. Eng. Sci.*, **1996**, 36:433.
- (5) Hergeth; W.D., J.M. Asua (ed). *Polymer Dispersions. Principles and Applications*. Kluwer Academics Publishers, 1997.
- (6) Kammona; O. E.G. Chatzi; C. Kiparissides. *Rev. Macromol. Chem. Phys.*, **1999**, C39:57.

Monitoring of Emulsion Polymerization Reactors: Calorimetry vs Raman Spectroscopy

Jose R. Leiza

O. Elizalde, M. Azpeitia, M.M. Reis, J.M. Asua
The University of the Basque Country
Donostia-San Sebastián (Spain)

POLYMAT

May 17, 2005



Outline

- Introduction
- On-line Monitoring by means of Reaction calorimetry
 - Estimation of Q_r and UA
 - Estimation of free-monomer
- On-line monitoring by means of Raman spectroscopy
 - VAc/BA and all acrylic systems
 - Calibration Models (PLS)
 - Calibration validation
- Raman spectroscopy vs. Reaction calorimetry
 - VAc/BA (non starved)
 - BA/MMA (starved)
- Conclusions

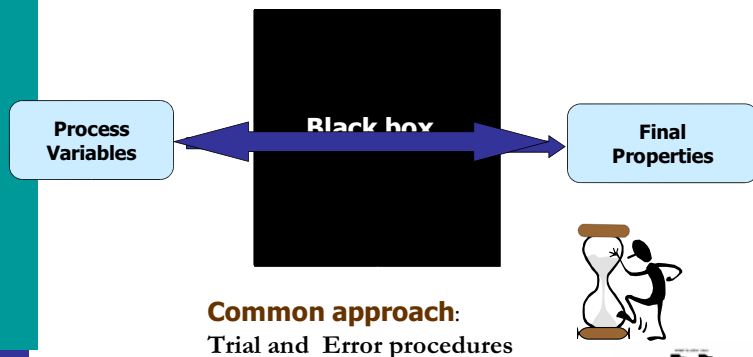
POLYMAT

May 17, 2005



Introduction

Produce materials in a consistent way with desired final properties meeting market needs

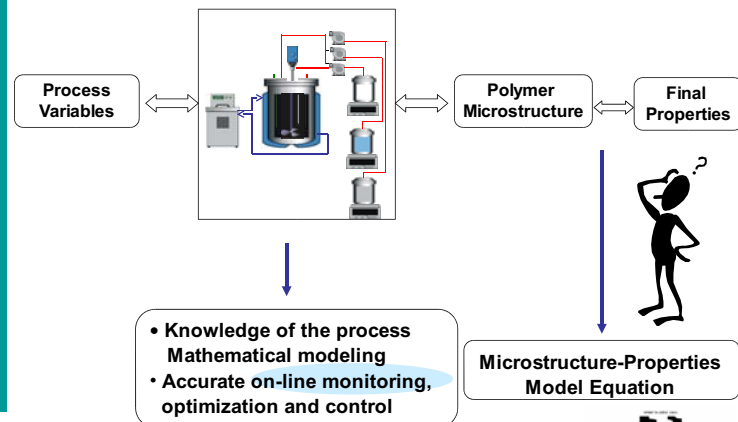


POLYMAT

May 17, 2005



Introduction

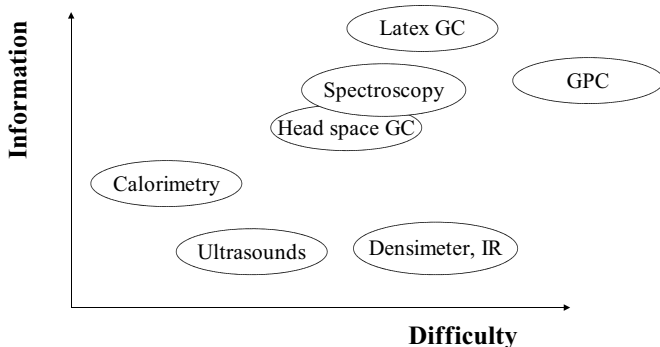


POLYMAT

May 17, 2005



Introduction



POLYMAT

May 17, 2005



Monitoring emulsion polymerizations

Reaction Calorimetry + Raman Spectroscopy



Advantages of Calorimetry

- Non-invasive technique
- Easy to implement in industrial environment and cheap
- Adequate for online control
- Provides continuous information of the heat of reaction

Advantages of Raman

- Non invasive technique
- Direct measurement of unreacted monomers, solids content
- Possible in industrial reactors

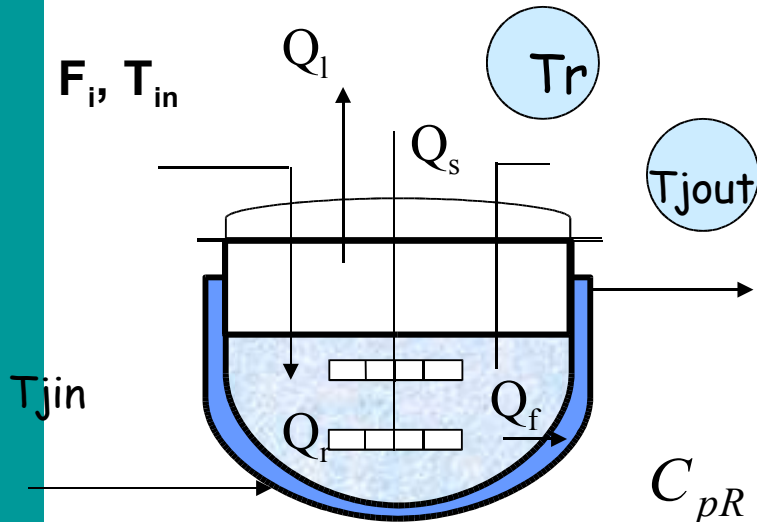
POLYMAT

May 17, 2005



Reaction Calorimetry

Heat Flow Calorimetry



Q_r = Heat of Reaction

Q_f = Heat Flow

Q_l = Heat Losses

Q_s = Heat due to Stirring

$\sum F_i c_{pi} (T_i - T_r)$ = Feed sensible Heat

$$C_{pR} \frac{dT_r}{dt} = \sum_i F_i c_{pi} (T_{in} - T_r) + Q_r + Q_f + Q_s + Q_l$$

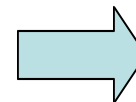
$$Q_f = UA(T_j - T_r)$$

Heat of Reaction

Parameter

$$T_{jin} \approx T_{jout} = T_j$$

High flow rates of the cooling fluid



**SMALL SIZE
REACTORS**

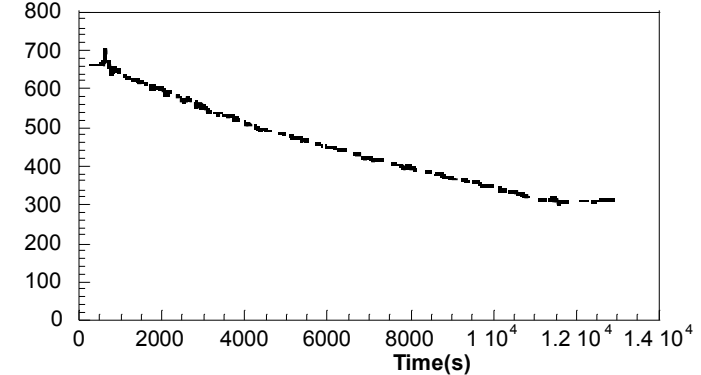
Reaction Calorimetry: Estimation of UA and Qr

Oscillation Calorimetry: Smart Calc Mettler-Toledo

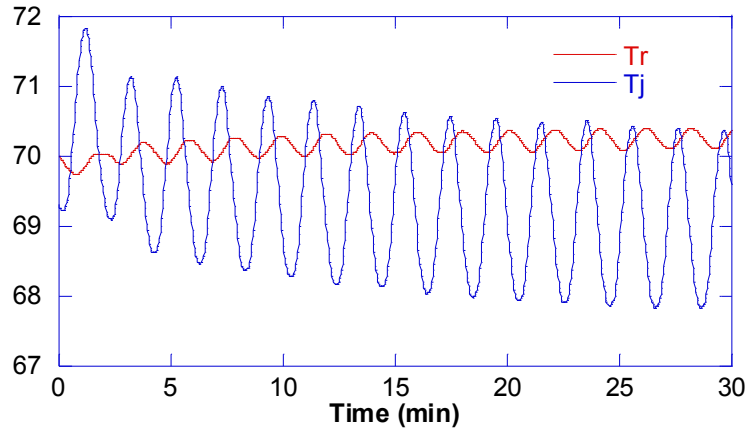
Evolution of the heat transfer monitored \longrightarrow Accurate Heat of Reaction

$$UA = \frac{C_{pr}\omega}{\tan\left(\arccos\left(\frac{\delta T_r}{\delta T_j}\right)\right)}$$

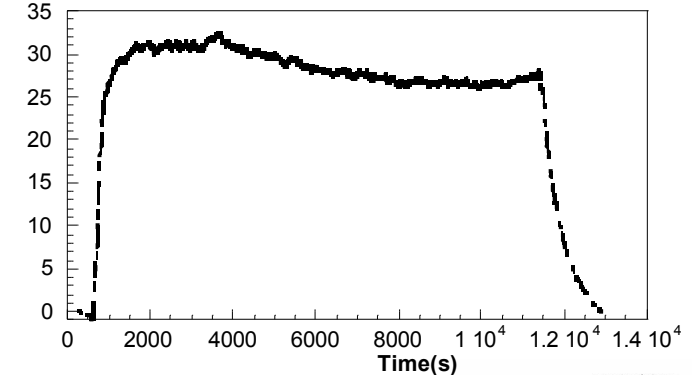
Heat Transfer Coefficient



Temperature (°C)



Heat of Reaction (W)



$$Q_r = Q_a + Q_f + Q_{feed}$$

Reaction Calorimetry: Estimation of conversion

$$\text{Overall Conversion} = \frac{\text{Polymer}(t)}{\text{Total_Monomer}(t_f)} = \frac{\int_0^t Q_r dt}{\sum M_{i,T}(t_f)(-\Delta H_i)}$$

$$\text{Instantaneous Conversion} = \frac{\text{Polymer}(t)}{\text{Monomer_Fed}(t)} = \frac{\int_0^t Q_r dt}{\sum M_{i,T}(t)(-\Delta H_i)}$$

$$\text{Polymer}(t) = \sum_i (i_0 + F_i t - i)$$

$$\text{Monomer_Fed}(t) \leq \text{TotalMonomer}(t_f)$$

Reaction Calorimetry: Estimation of free monomers

Inference of unreacted amount of monomer

$$\frac{di}{dt} = -Rp_i + F_i = - \frac{Q_r}{(-\Delta H_A) \frac{1}{D_{iA}} + (-\Delta H_B) \frac{1}{D_{iB}} + (-\Delta H_C) \frac{1}{D_{iC}}} + F_i \quad i=A, B, C$$

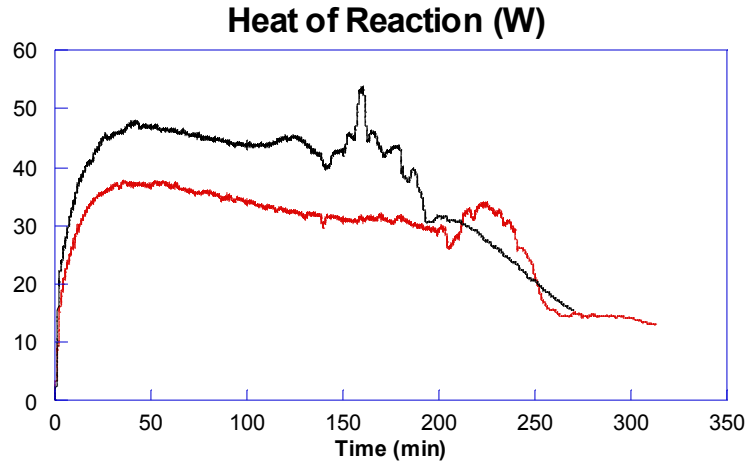
$$D_{ij} = \frac{Rp_i}{Rp_j} = \frac{r_i + [j]_p/[i]_p}{r_j([j]_p/[i]_p)^2 + [j]_p/[i]_p}$$

Accuracy of the estimation:

Reactivity ratios
Enthalpy of polymerization ($-\Delta\bar{H}$)
Partition Coefficients

Reaction Calorimetry: An example (2)

VAc/BA=50/50 Semibatch Batch 55 wt% solids content



Feeding Time:

180 min

240 min

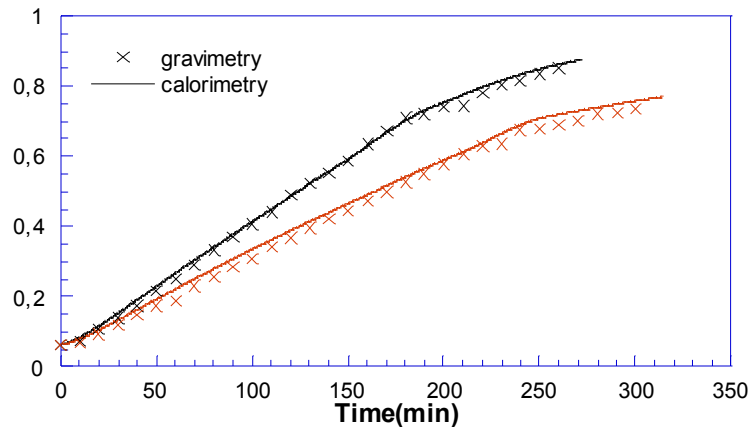
$$r_{VAc} = 0.037$$

$$r_{BA} = 6.36$$

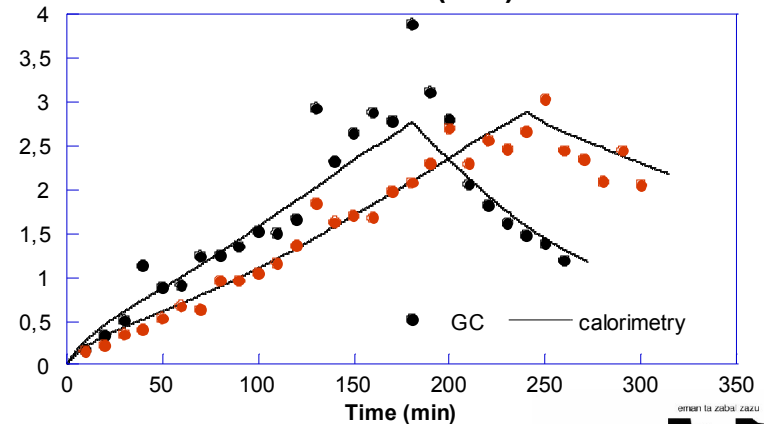
$$\Delta H_{VAc} = 89.5 \text{ kJ/mol}$$

$$\Delta H_{BA} = 78.2 \text{ kJ/mol}$$

Conversion

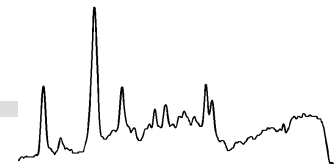


Free VAc (mol)

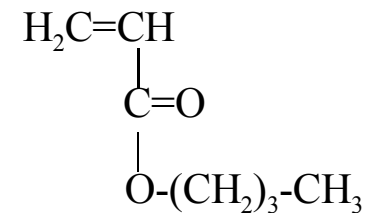
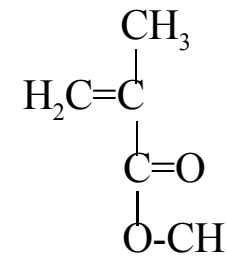
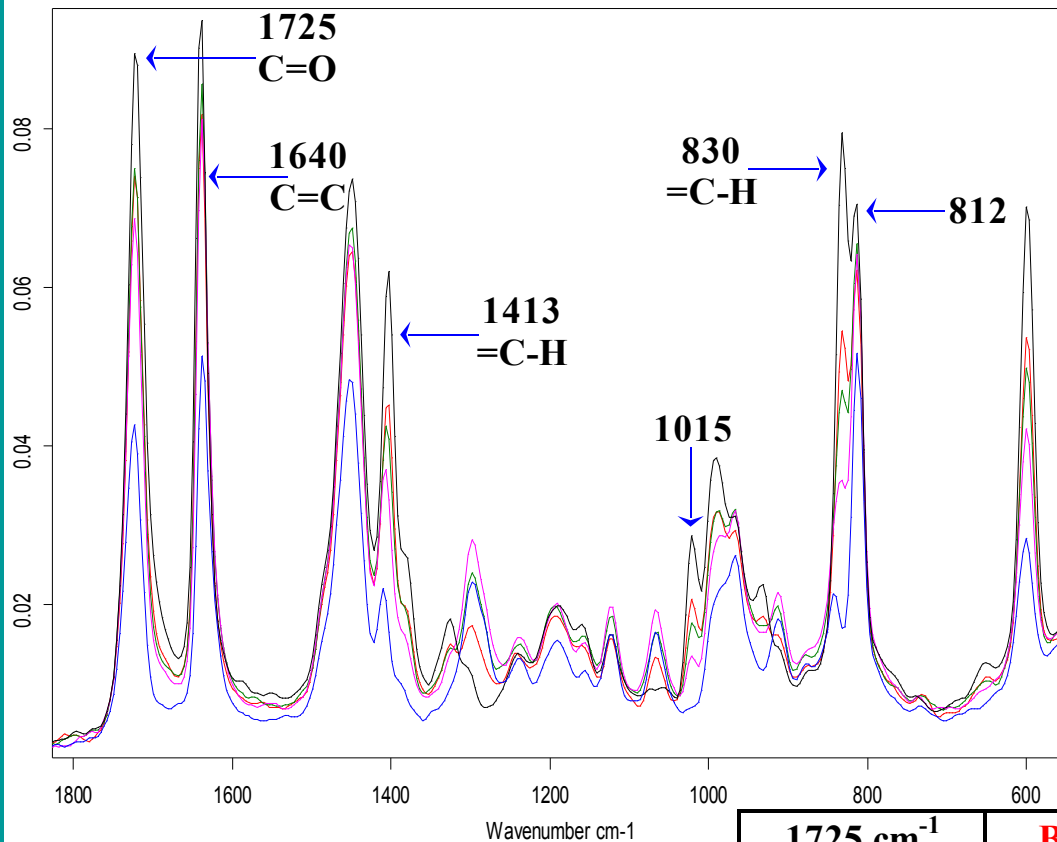


Raman spectroscopy

All-acrylic emulsion polymerizations

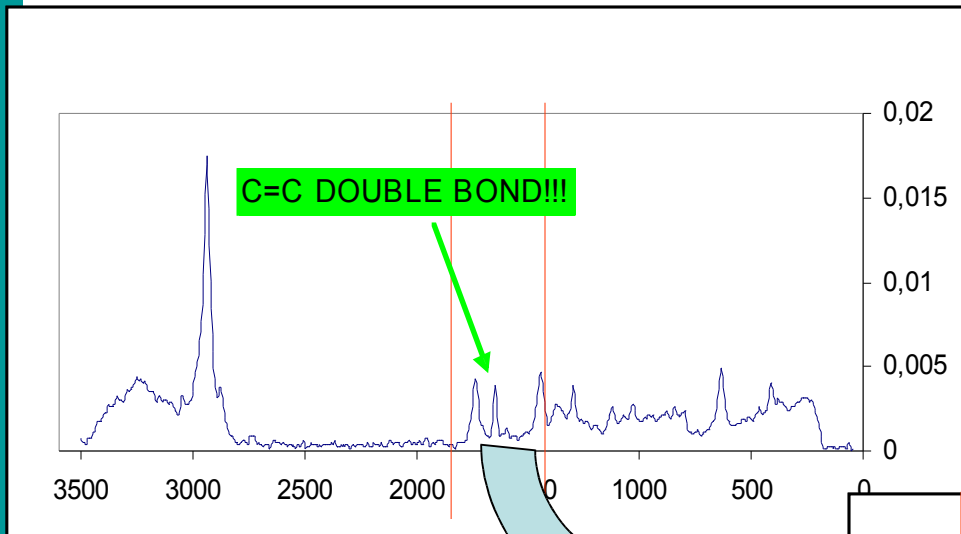
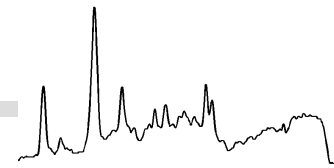


MMA/BA

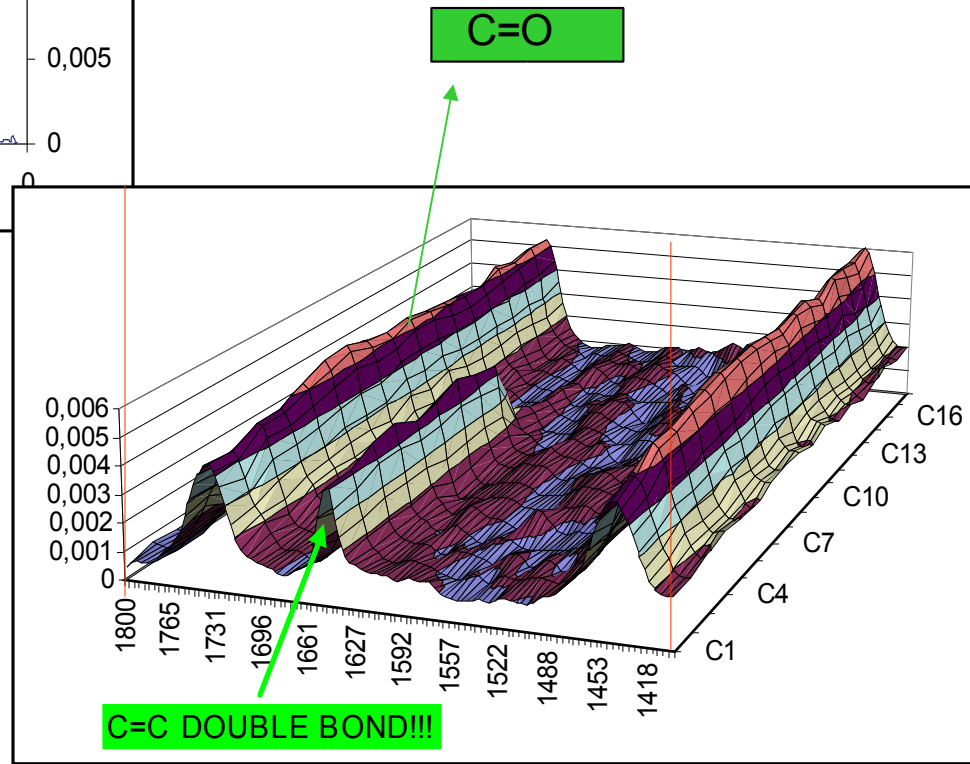


1725 cm ⁻¹	BA total + MMA total
1640 cm ⁻¹	MMA + BA
1450/1413 cm ⁻¹	MMA
1015 cm ⁻¹	MMA
830/812 cm ⁻¹	MMA
812 cm ⁻¹	PMMA

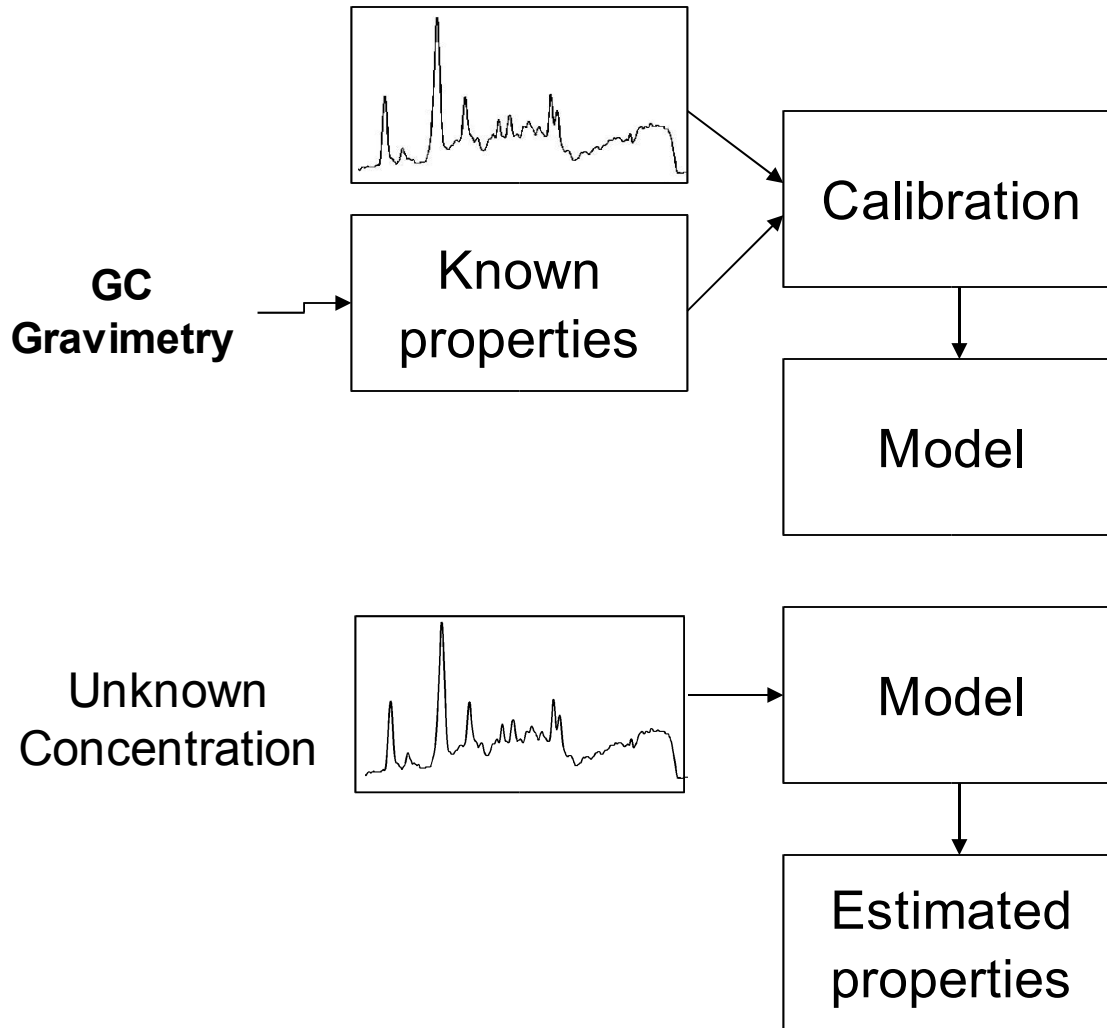
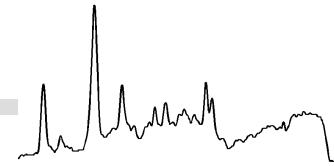
Raman Spectroscopy : Reaction monitoring



VAc/BA copolymerization



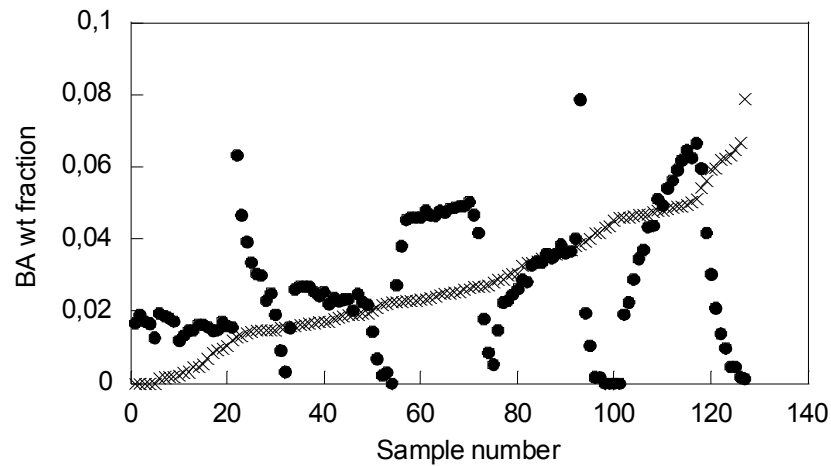
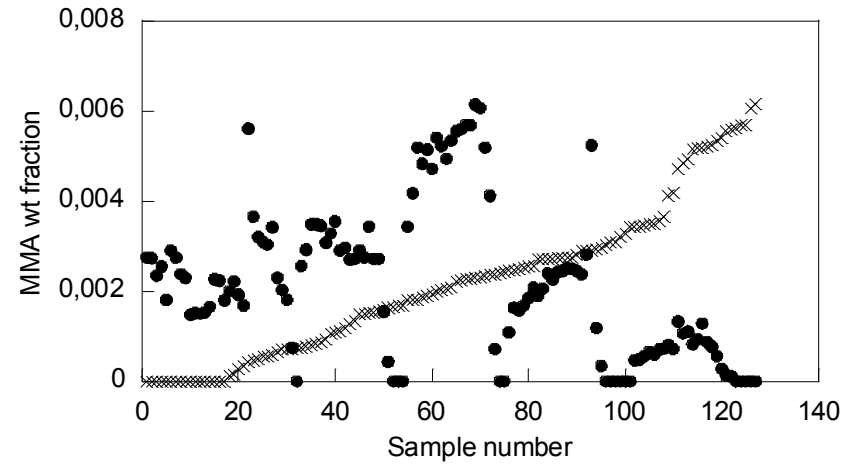
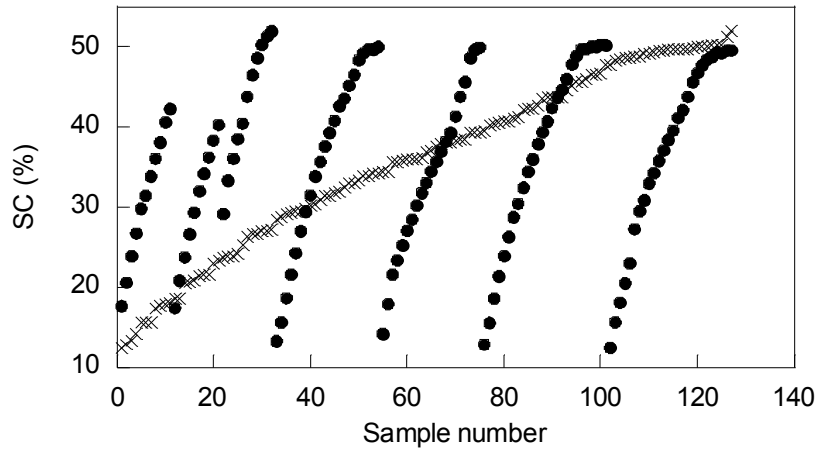
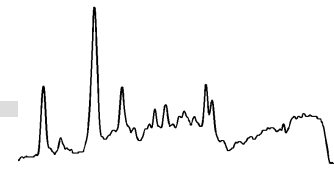
Raman Spectroscopy: Calibration



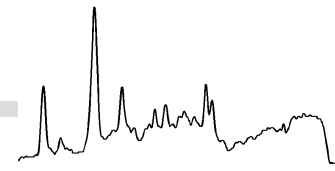
1. CALIBRATION

2. PREDICTION

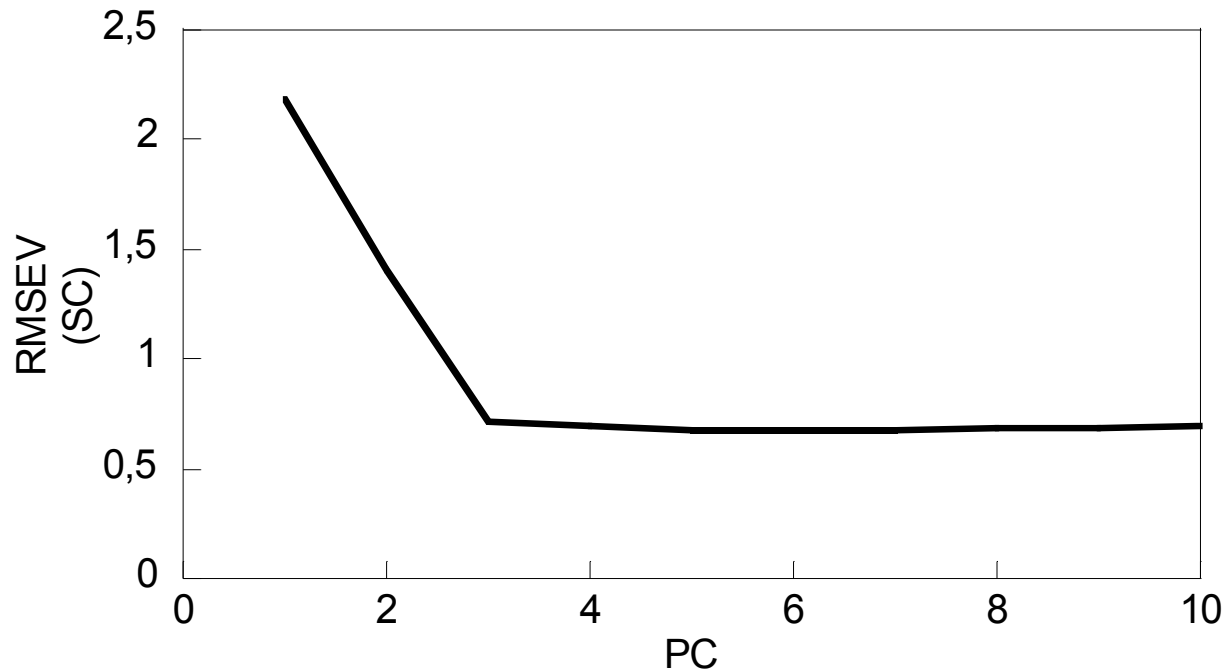
Calibration data: MMA/BA system



Example: Model for the SC (%)

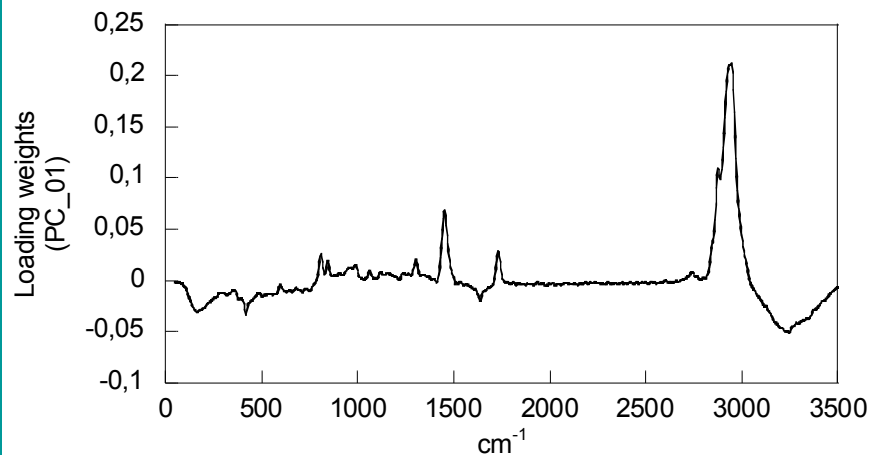


- A model using the whole normalized spectra, containing 3 PCs was considered the optimum.

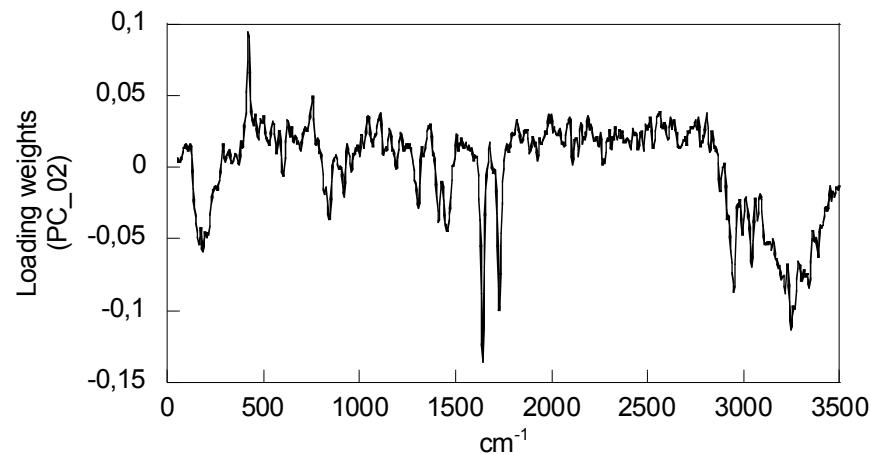


Example: Model for the SC (%)

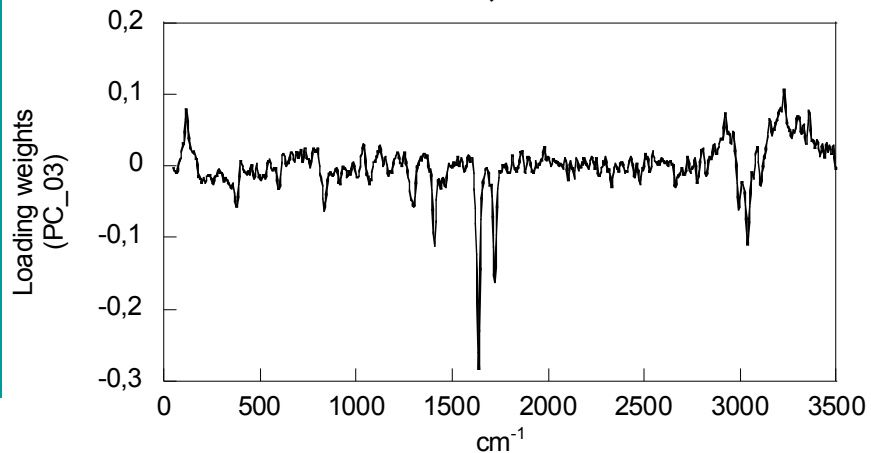
1st PC (X-expl,Y-expl):
90%, 96%



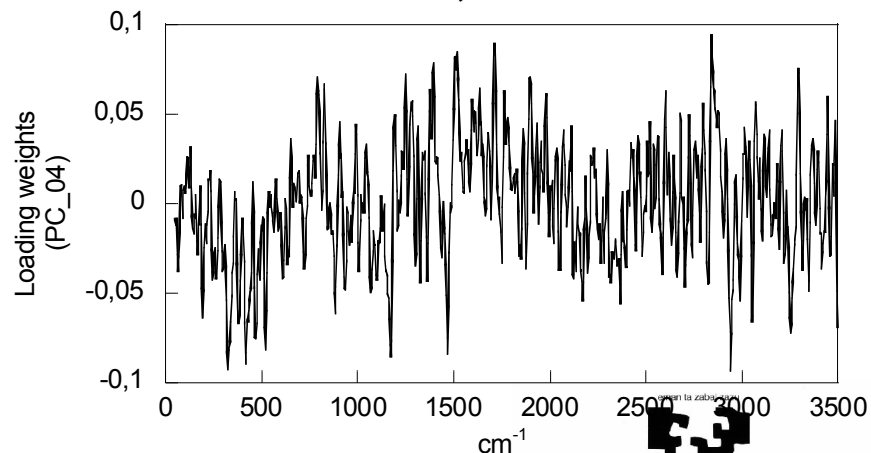
2nd PC (X-expl,Y-expl):
4%, 2%



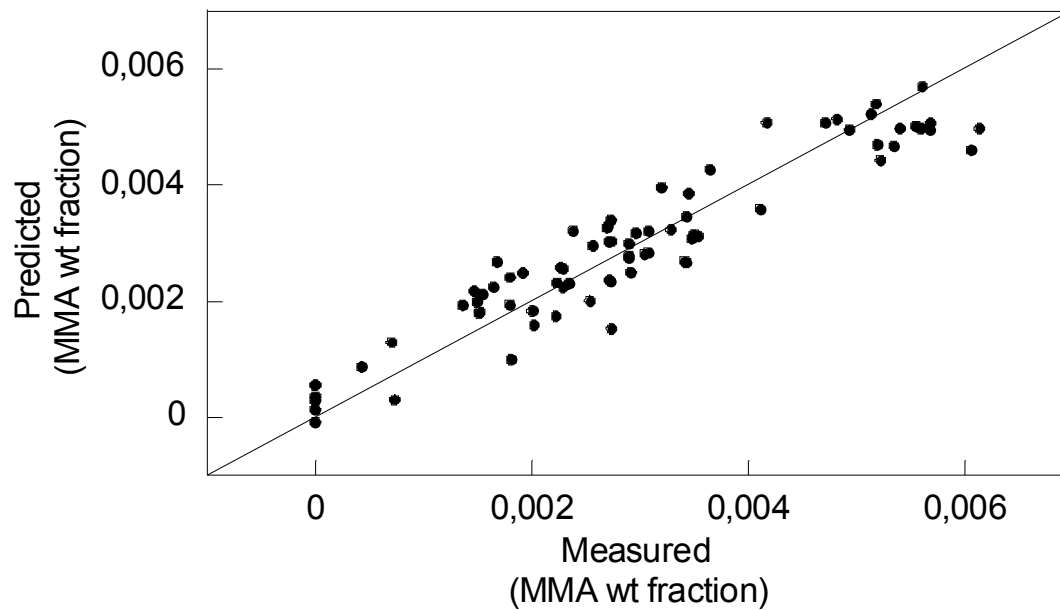
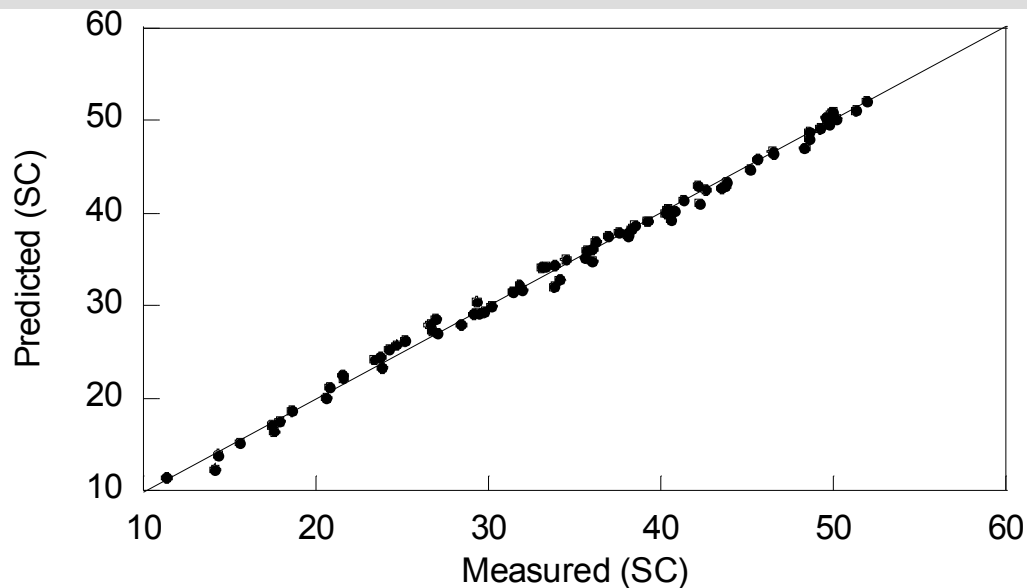
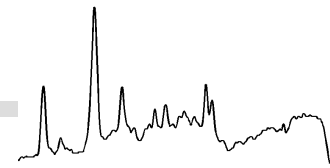
3rd PC (X-expl,Y-expl):
1%, 1%



4th PC (X-expl,Y-expl):
0%, 0%



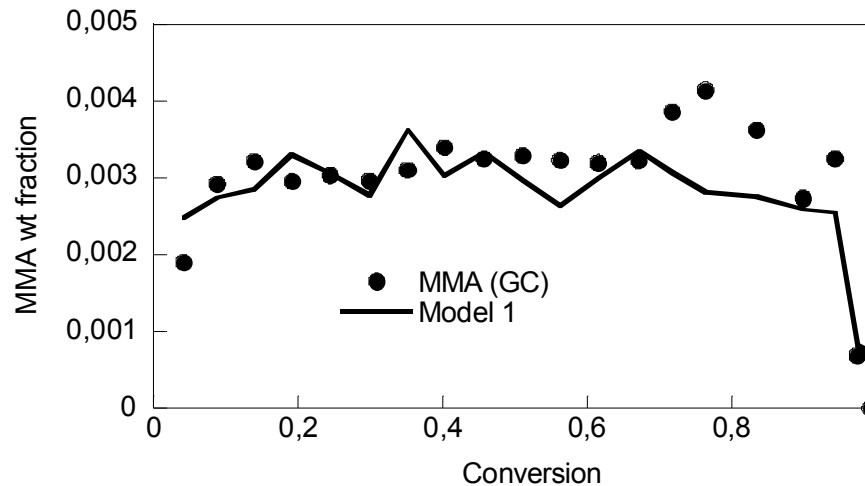
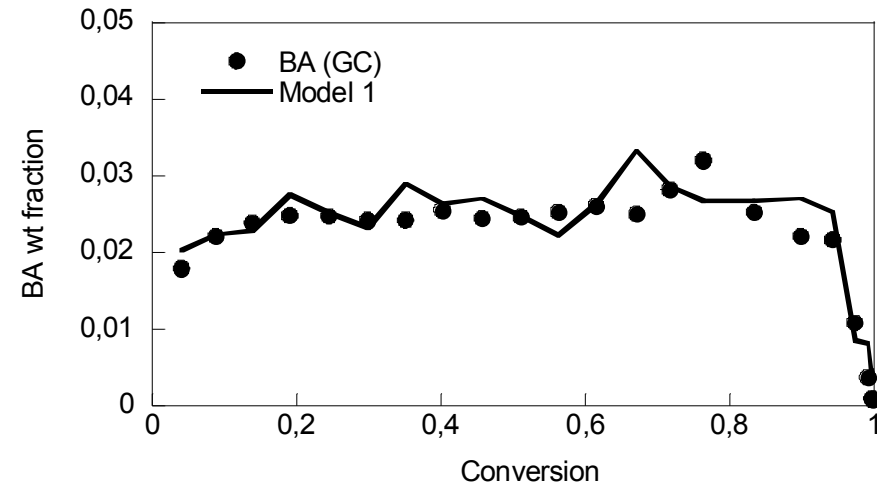
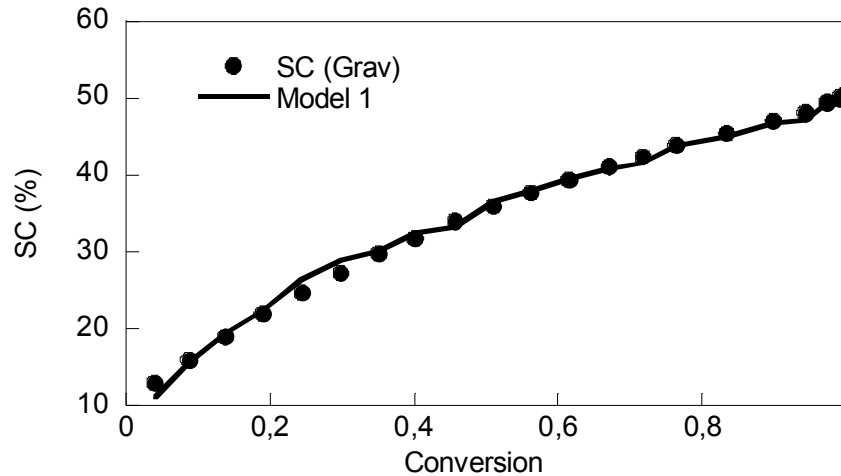
PLS Calibration models



Validation of Calibration

Oihana Elizalde Ph.D 2005

BA/MMA=50/50 composition



Calorimetry vs Raman

- **Two comonomer systems considered:
BA/MMA and VAc/BA**
- **Overall and instantaneous conversions
and Free Monomer:**

**Gravimetry and Gas Chromatography (as reference)
Reaction Calorimetry (RC1 Mettler-Toledo)
Raman Spectroscopy (RFS-100 Bruker)**

- **Semibatch reactions of high solids content**

Starved(MMA/BA) and Non-starved (VAc/BA)

Calorimetry vs Raman : Experimental Details

VAc/BA/AA

Ingredient	Initial Charge	Stream 1	Stream 2
Water	99,5	-	99,5
Alipal	6,13	-	6,13
Arkopal	6,13	-	6,13
VAc	-	600	-
n-BA	-	141,1	-
AA	-	22,9	-
K ₂ S ₂ O ₈	2,29	-	-
NaHCO ₃	2,52	-	-
Seed	527	-	-

Feeding time= 3 and 4 hours

BA/MMA

Ingredient	Initial Charge	Stream 1	Stream 2
Water	617	-	32,5
Dowfax	-	-	9,45
K ₂ S ₂ O ₈	Variable	-	-
NaHCO ₃	Variable	-	-
n-BA+MMA	-	540	-
n-BA/MMA	-	Variable	-
Seed	63	-	-

Feeding time= 2 and 3 hour

50/50(3), 70/30 and 90/10

Calorimetry vs Raman: Semibatch Operation

BA/MMA



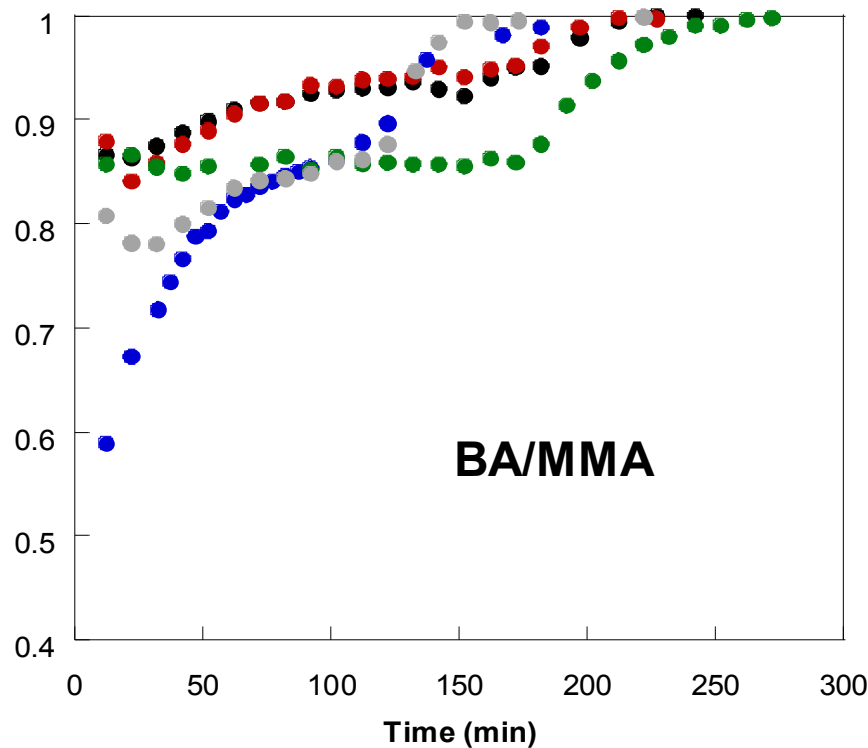
Starved Conditions 50/50 to 90/10

VAc/BA

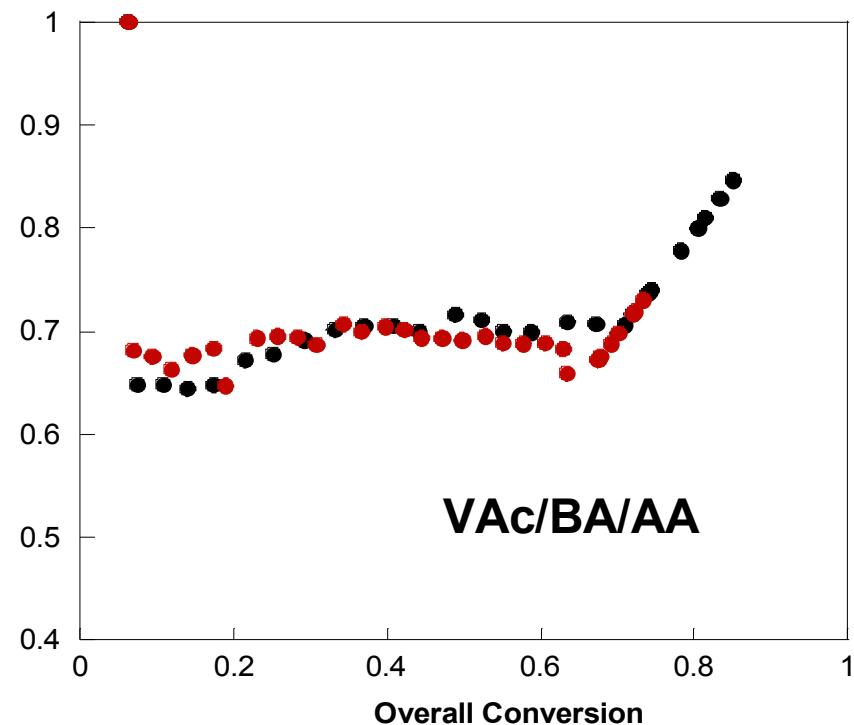


Non Starved Conditions

Instantaneous Conversion



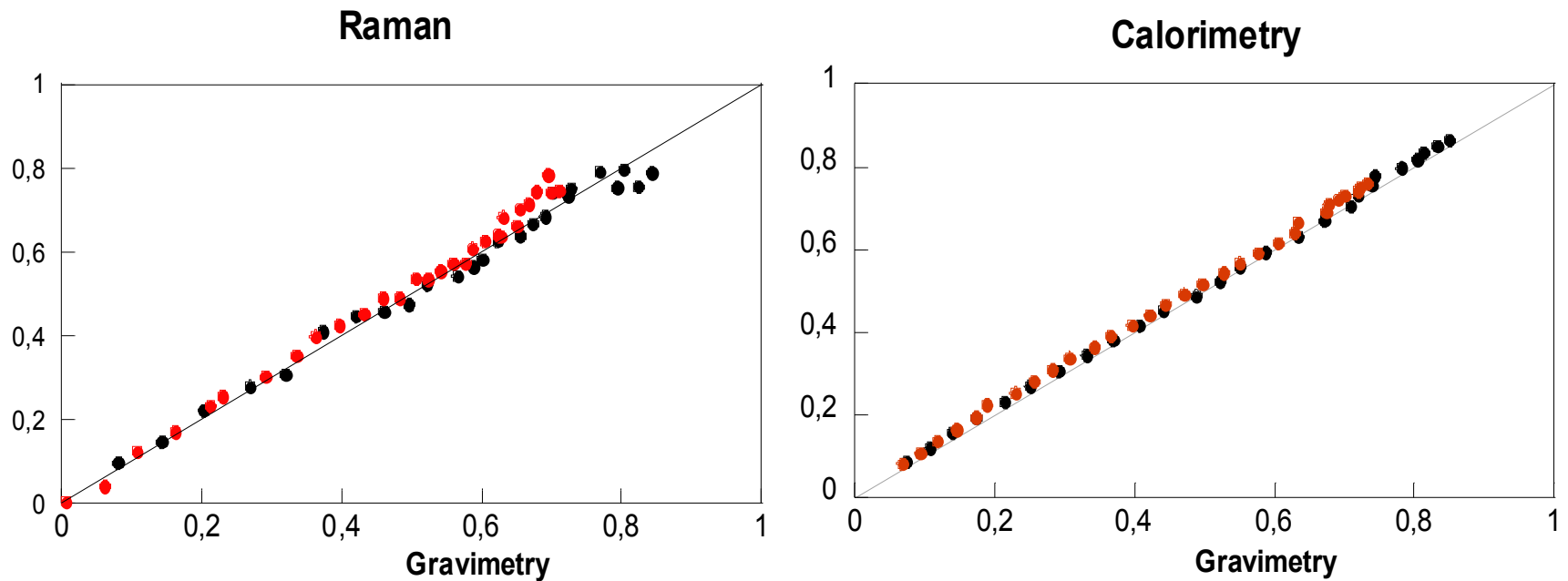
Instantaneous Conversion



Gravimetric data

Calorimetry vs Raman: Overall Conversion

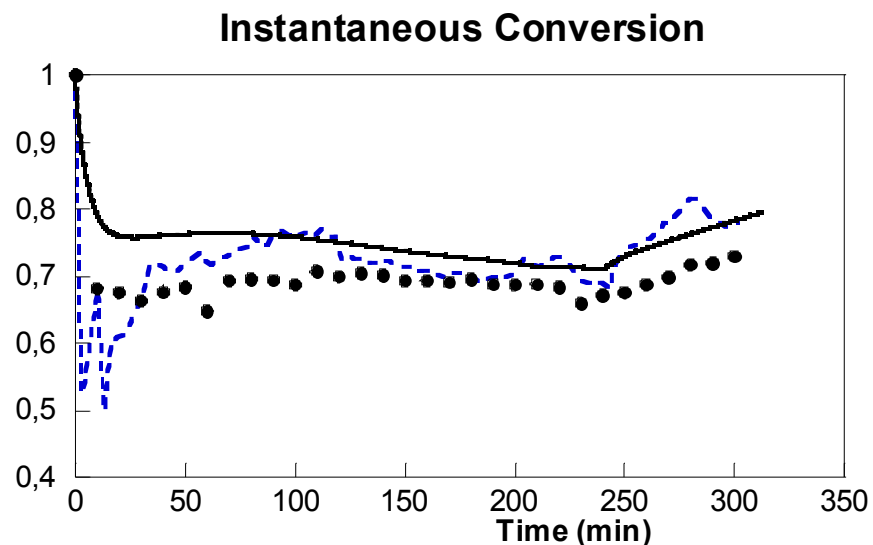
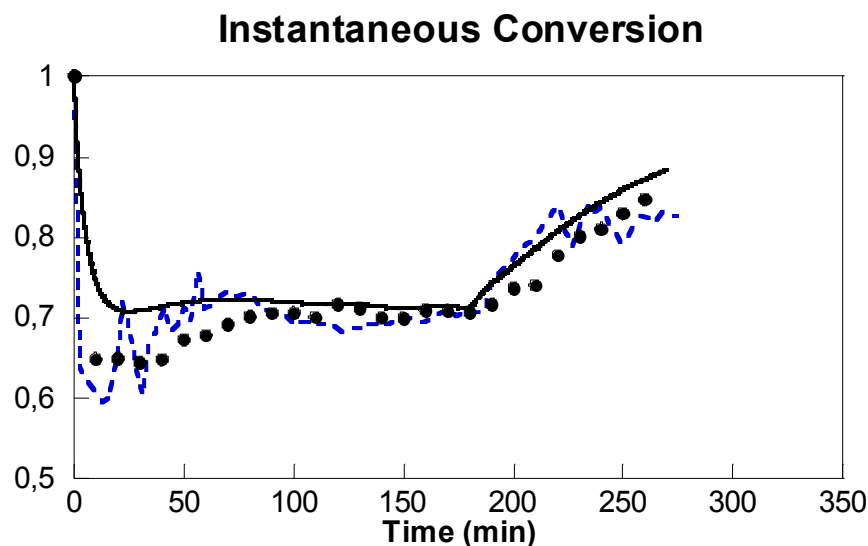
VAc/BA copolymerization. Non-starved



Raman and Calorimetry performed well

Calorimetry vs Raman: Instantaneous conversion

VAc/BA copolymerization. Non-starved

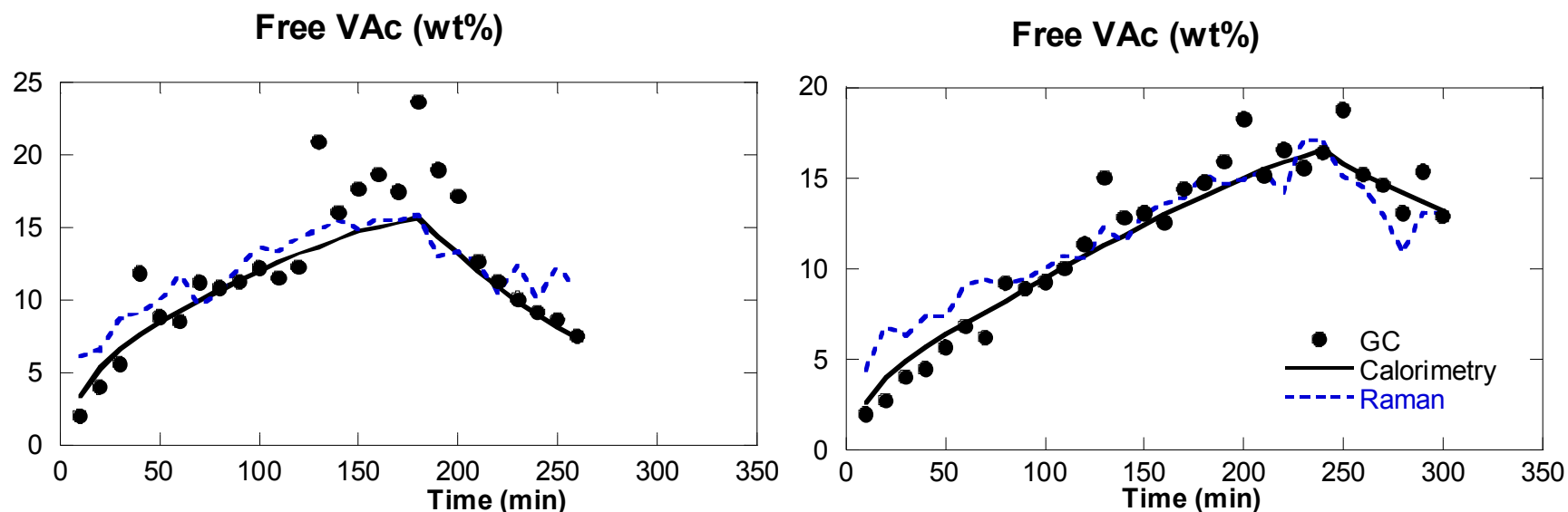


Calorimetry slightly overestimates
Raman is closer to gravimetry

In general reasonable good prediction for both

Calorimetry vs Raman: Free Monomer

VAc/BA copolymerization. Non-starved

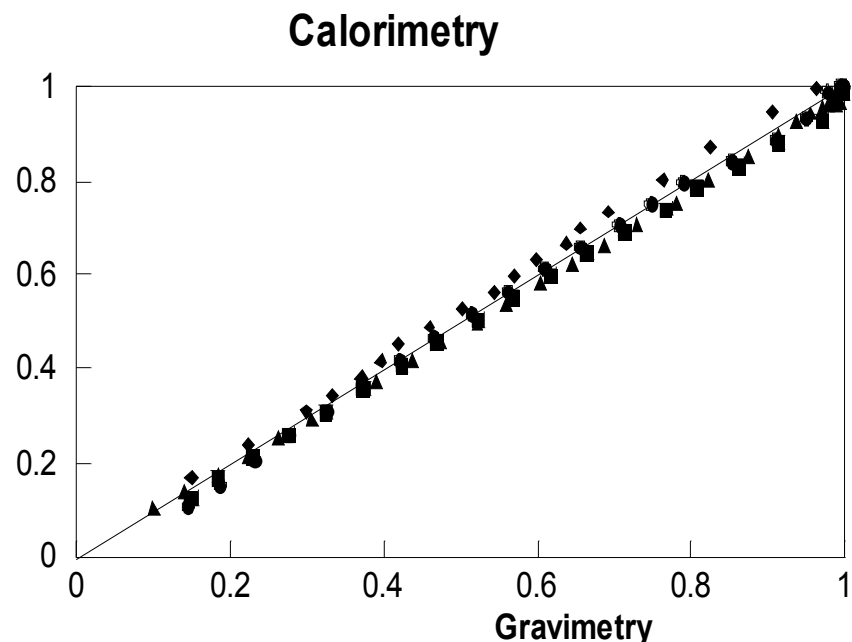
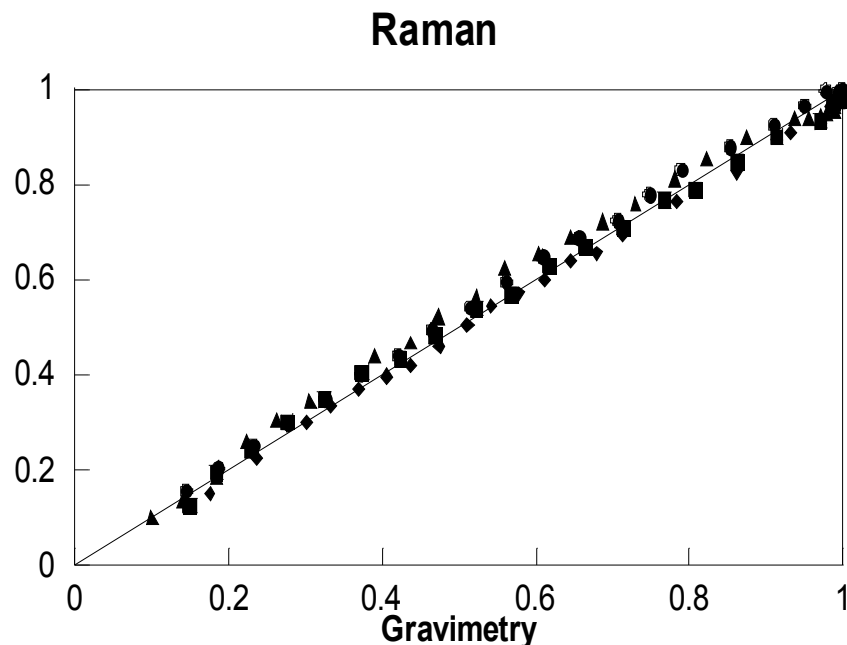


Calorimetry and Raman performed well

Chromatography (reference technique) scatters probably due to presence of droplets

Calorimetry vs Raman: Overall Conversion

BA/MMA Copolymerization: Starved Conditions

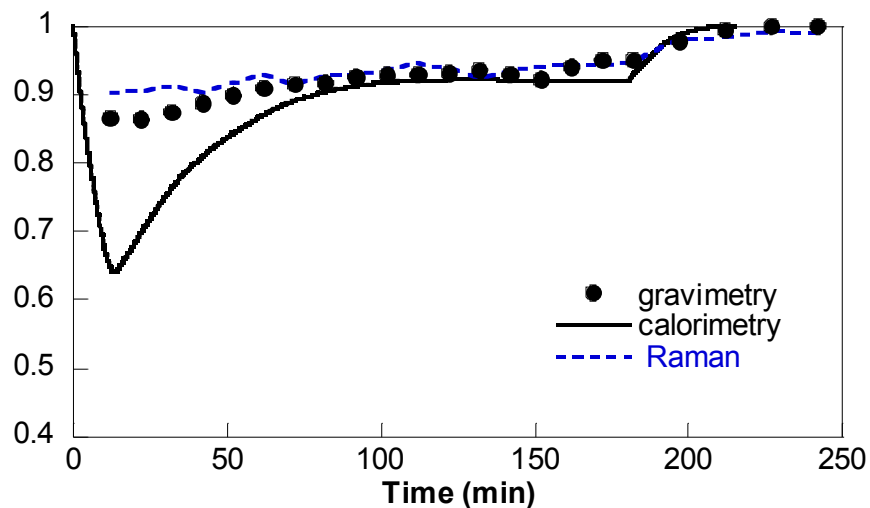


Good agreement for all techniques

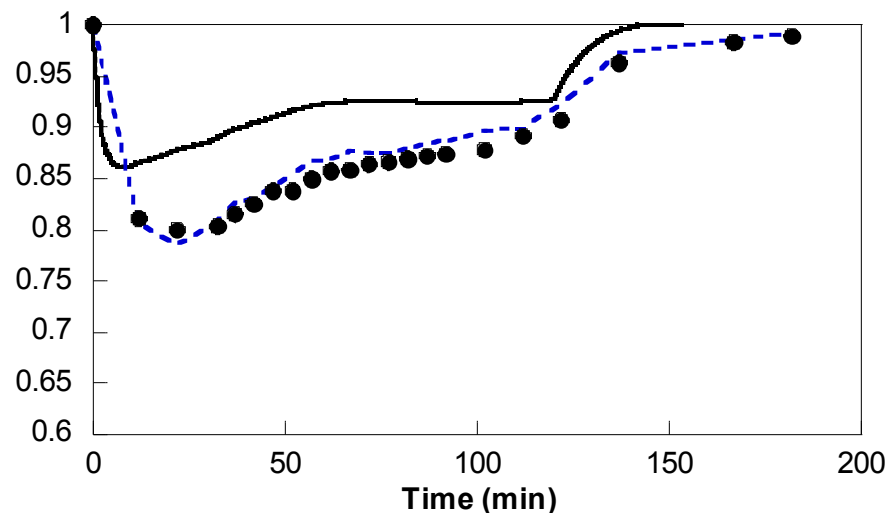
Calorimetry vs Raman: Instantaneous conversion

BA/MMA Copolymerization: Starved Conditions

Instantaneous Conversion



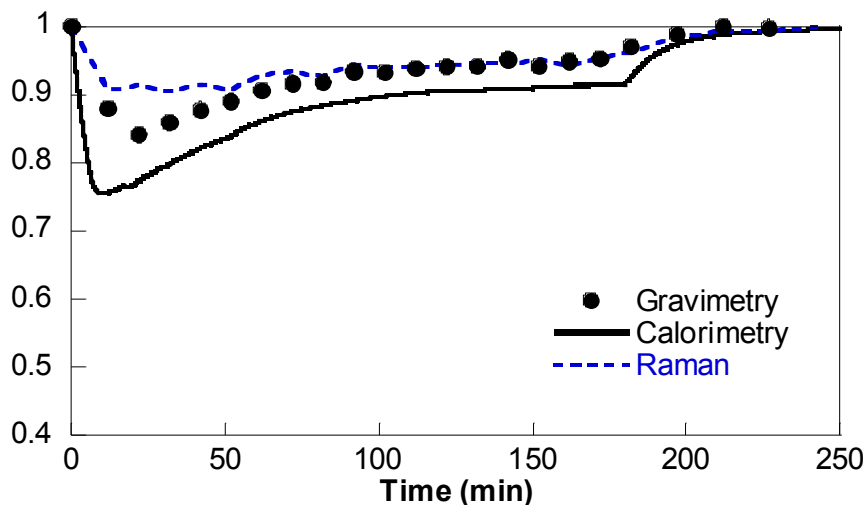
Instantaneous Conversion



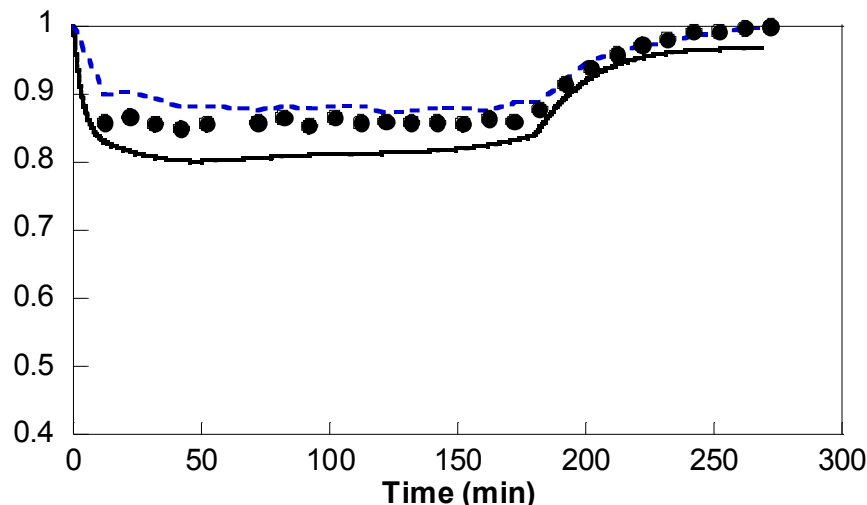
Calorimetry vs Raman: Instantaneous conversion

BA/MMA Copolymerization: Starved Conditions

Instantaneous Conversion

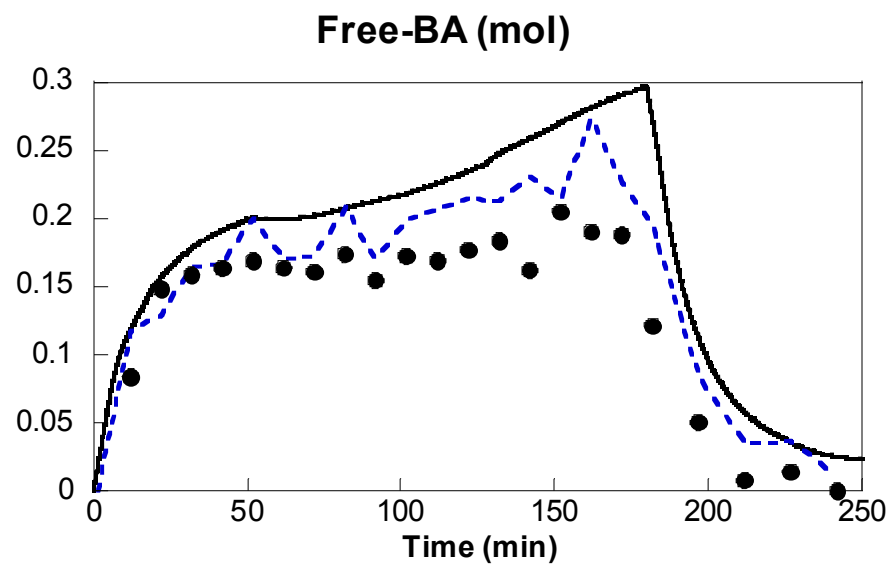
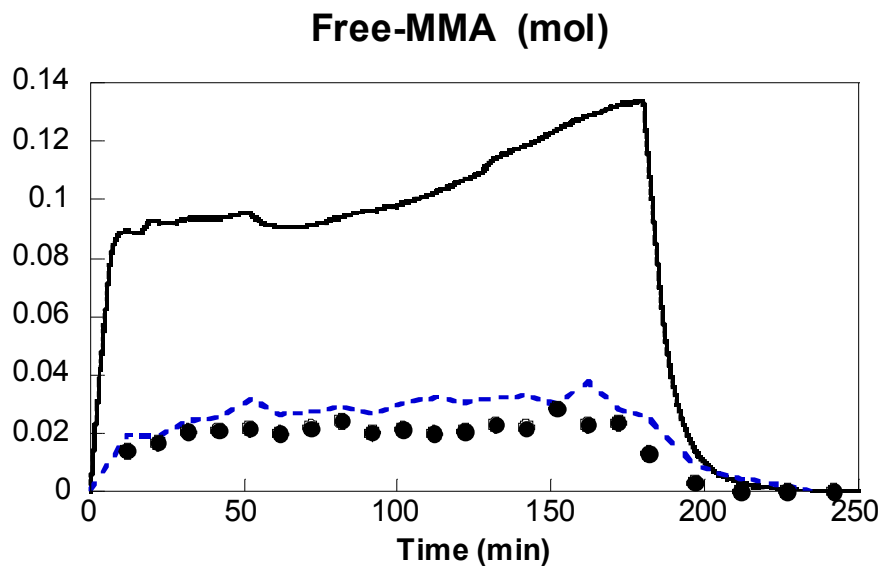


Instantaneous Conversion



**Both, Raman and Calorimetry predictions are worse
Raman is better than Calorimetry !!!**

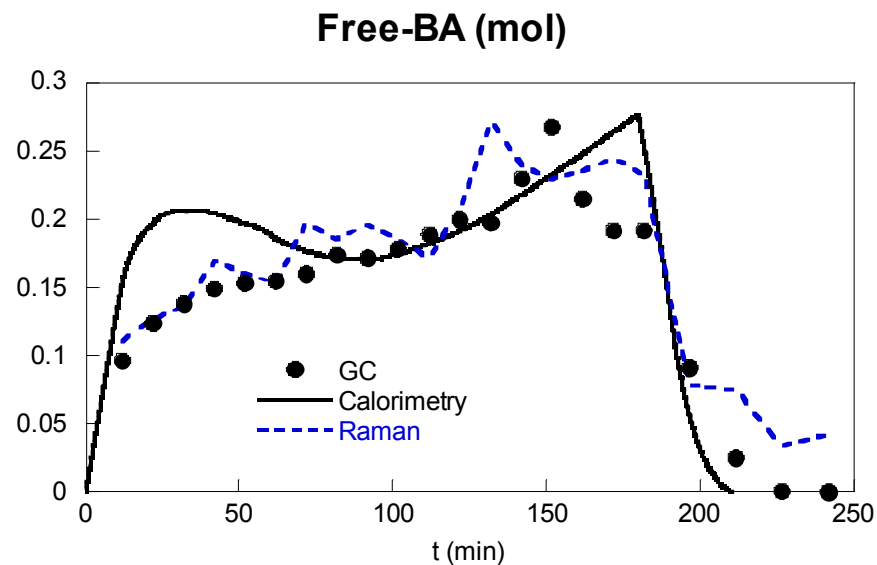
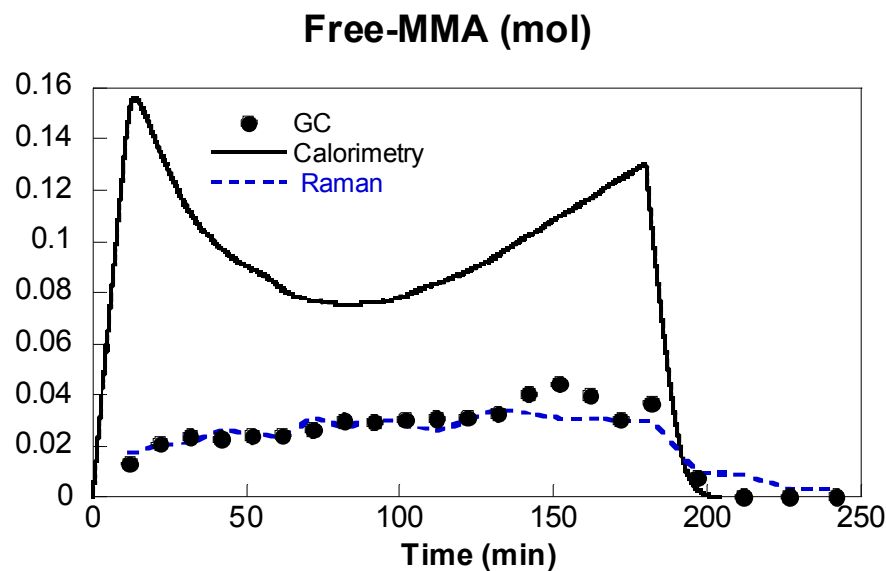
BA/MMA Copolymerization: Starved Conditions



BA/MMA=50/50

Calorimetry vs Raman: Free Monomer

BA/MMA Copolymerization: Starved Conditions

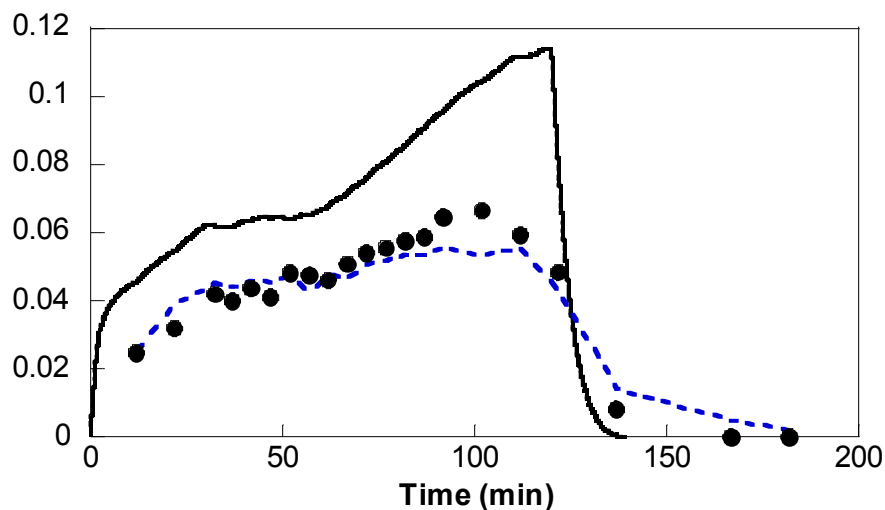


BA/MMA=50/50

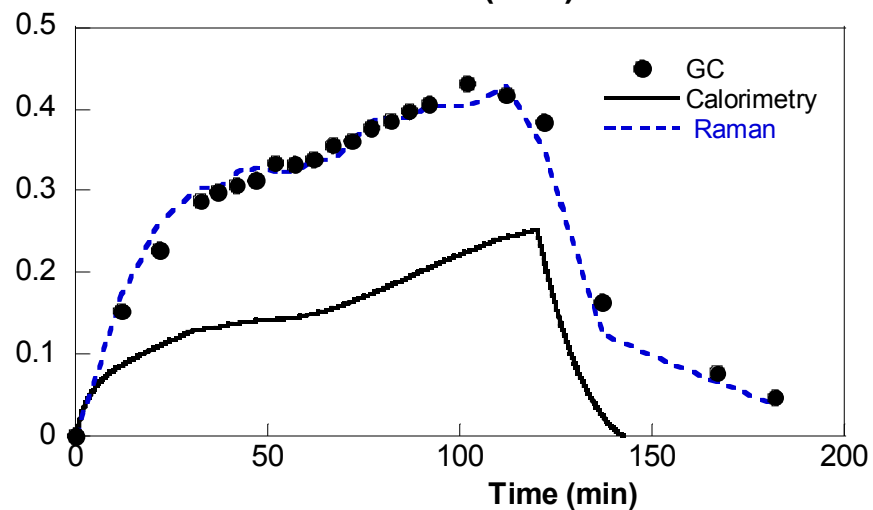
BA/MMA Copolymerization: Starved Conditions

BA/MMA=70/30

Free-MMA (mol)



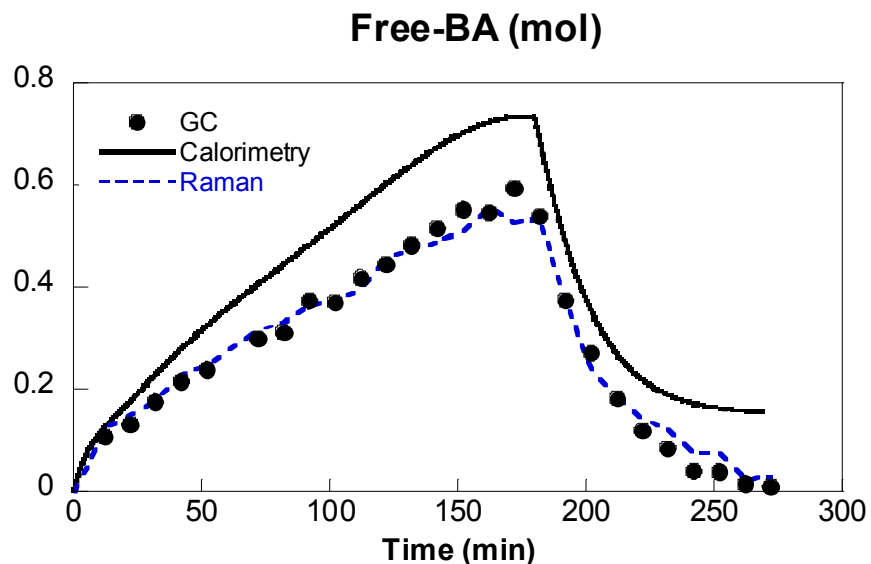
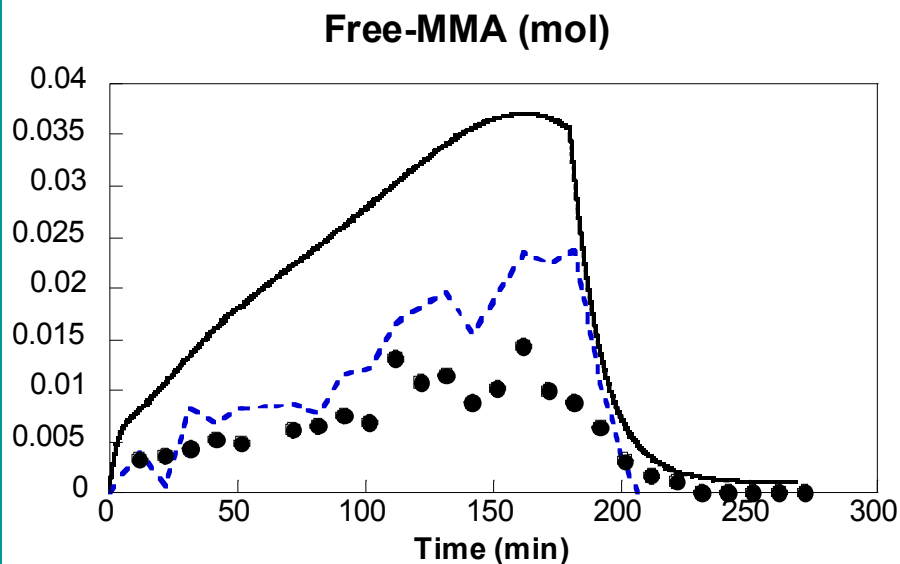
Free-BA (mol)



Calorimetry vs Raman: Free Monomer

BA/MMA Copolymerization: Starved Conditions

BA/MMA=90/10



Calorimetry predicts incorrectly free monomer, specially MMA
Raman is superior to Calorimetry
Raman suffers predicting very low concentrations!!

Error is inherent to the measurement

Example:

Estimation of unreacted monomer when there is an error of 2% :

$$x_{\text{exp}} = 60\% \rightarrow x_{\text{est}} = 61.2\%$$

$$(\text{Free monomer})_{\text{exp}} = 40\% \rightarrow (\text{Free monomer})_{\text{est}} = 38.8\%$$

2% Error

3% Error

Error is inherent to the measurement

Example:

Estimation of unreacted monomer when there is an error of 2%:

$$x_{\text{exp}} = 90\% \rightarrow x_{\text{est}} = 91.8\%$$

$$(\text{Free monomer})_{\text{exp}} = 10\% \rightarrow (\text{Free monomer})_{\text{est}} = 8.2\%$$

2% Error

18% Error

Concluding Remarks

- Raman spectroscopy in combination with chemometrics can be used to monitor high solids content reactions, even when the bands of the monomers are overlapped (all acrylic or vinyl/acrylic mixtures) and the reactions are carried out under starved conditions.
- Calorimetry and Raman predict in a similar manner overall conversion. No significant differences for starved and non starved conditions. Calorimetry is easier!
- For instantantaneous conversion and free monomer:
 - Raman and Calorimetry provide similar predictions under non-starved conditions, namely, high monomer concentrations.
 - Raman spectroscopy gave much better predictions than reaction calorimetry under starved reactions.

Acknowledgments

- Ministerio de Educación y Ciencia (Project PPQ2000-1185 and scholarships for Oihana Elizalde and Maider Azpeitia)
- The University of the Basque Country (Project 00221.215-13594/2001)
- M.M. Reis acknowledges FAPESP (grant number : 03/06837-8 and 01/13017-1)



Institute for Polymer Research
27th Annual Symposium

Symposium documents for

Rodolfo Salgado

Abstract

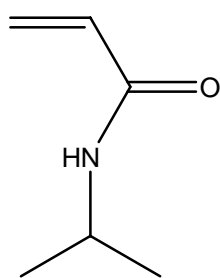
Presentation

Poster

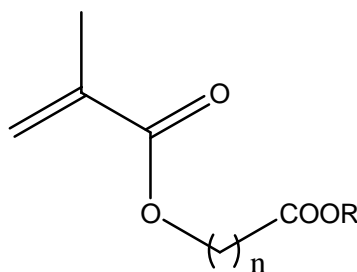
“New temperature- and pH-sensitive smart polymers containing methacrylic derivatives with hydrophobic spacers”

Rodolfo Salgado-Rodríguez, Angel Licea-Claverie
Centro de Graduados e Investigación, Instituto Tecnológico de Tijuana, A.P.1166
22000 Tijuana, B.C.; MEXICO

This work deals with temperature- and pH-sensitive materials, which have many potential applications, e.g. in controlled release of drugs or in separation processes of dissolved molecules.¹ The research was focused on the synthesis and characterization of linear and crosslinked polymers containing *N*-isopropylacrylamide^{2,3} (NIPAAm) (I) and new methacrylic acid-derivative monomers (II). These monomers have as distinctive feature a methylene chain as spacer, which varies in their length (4, 7 and 10 methylene units). The effect of the length of methylene spacer and the effect of the presence of carboxylic acid groups on phase transition temperatures, and swelling capability of the produced materials were studied as a function of temperature and pH.⁴



I



II

For R=CH₃
n=4, MOP4
n=7, MOP7
n=10, MOP10

For R=H
n=4, MOD4
n=7, MOD7
n=10, MOD10

Starting from monomers with methylester end-group, MOP4, MOP7 and MOP10, copolymers containing NIPAAm in different amounts were synthesized. Their solution behavior showed that their LCST (referred to PNIPAAm) was lower when the hydrophobic comonomer content was increased. On the other hand, copolymers containing NIPAAm were also prepared, starting from monomers

containing a carboxylic acid group, MOD4, MOD7 and MOD10. Studies in aqueous solution of all copolymers were performed in deionized water and buffer solutions at different pH values. Upon incorporation of the ionizable COOH group the range of values of LCST became wider.

Homopolymeric and copolymeric gels containing NIPAAm were prepared, starting from monomers in the form a potassium salt (M4K and M10K) (III). The swelling behavior was studied varying the temperature and using solutions with different pH values (Figure 1).

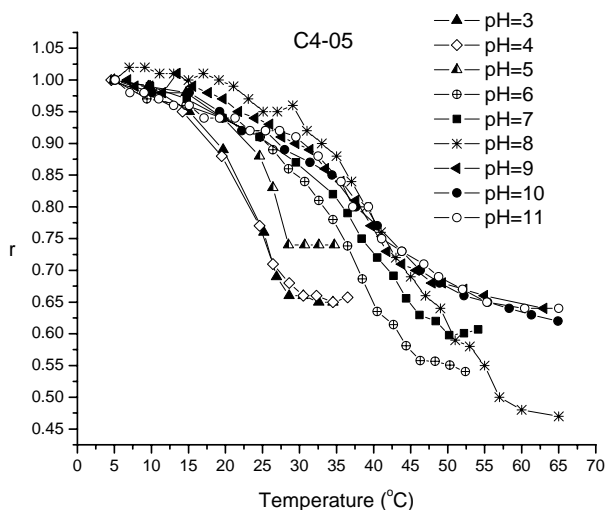
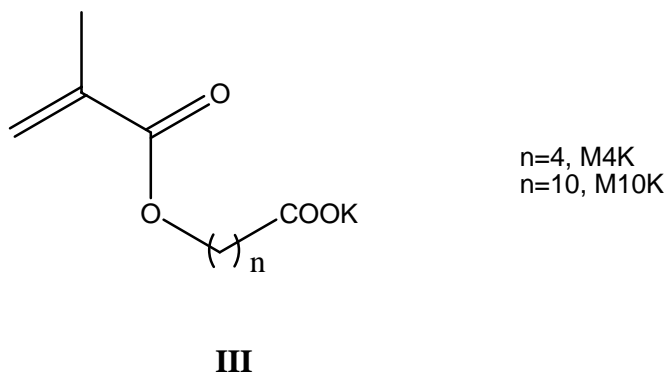


Figure 1. Temperature and pH dependence of the swelling ratio (r) for C4-05 (gel containing NIPAAm : M4K, 95:5, mol)

Phase transition temperatures (T_c) ranging from 14 to 64°C were obtained (Table 1). The effect of the pH of the swelling medium was essential to change the T_c and the amount of solution retained by the gels. Above T_c , the hydrophobic interaction becomes dominant, causing polymer to collapse and phase separate and expel water.⁵ The difference in the functional group of the comonomers used in the linear copolymers (free acid) and copolymeric gels (potassium salt) caused that the phase transition temperatures were not fully comparable. However, with pH values above 7 there are strong similarities in the behavior of these materials.

Table 1. Phase transition temperature (T_c) depending on pH

GELS	DI Water	T_c (°C)								
		pH=3	pH=4	pH=5	pH=6	pH=7	pH=8	pH=9	pH=10	pH=11
CN	33	----	----	----	----	----	----	----	----	----
C4-05	30	26	25	27	40	41	50	41	45	43
C4-10	37	19	20	24	53	48	53	47	53	50
C4-15	51	17	18	21	57	57	57	52	50	56
C4-20	N	14	17	18	64	N	N	N	N	N
C10-05	28	26	25	24	26	31	35	33	34	36
C10-10	25	21	21	22	28	32	38	37	38	41
C10-15	36	19	20	21	29	34	41	45	47	46
C10-20	29	N	N	N	24	33	44	49	49	53

ACKNOWLEDGEMENT

R. Salgado-Rodríguez thanks DAAD-Germany for financing his PhD-Sandwich program.


We are grateful to CONACYT-México (Project Nr. 28022-U) and Volkswagen Foundation-Germany (Project Nr. I/76 065) for financial support of this work.

We thank specially for valuable technical support I. Rivero (NMR), D. Scheller (NMR), I. Poitz (DSC) and C. Meissner (SLS).

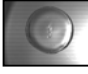
REFERENCES

1. Hoffman, A. S.; *Macromol. Symp.*, **1995**, 98, 645.
2. Heskins, M.; Guillet, J. E.; *J. Macromol. Sci. Chem.*, **1968**, A2, 1441.
3. Schild, H. G.; *Progress in Polymer Science*, **1992**, 17, 163.
4. Salgado-Rodríguez, R.; Licea-Claveríe, A.; Arndt, K. F. *European Polymer Journal* **2004**, 40, 1931.
5. Feil, H.; Bae, Y. H.; Feijen, J.; Kim, S. W.; *Macromolecules*, **1993**, 26, 2496.

1

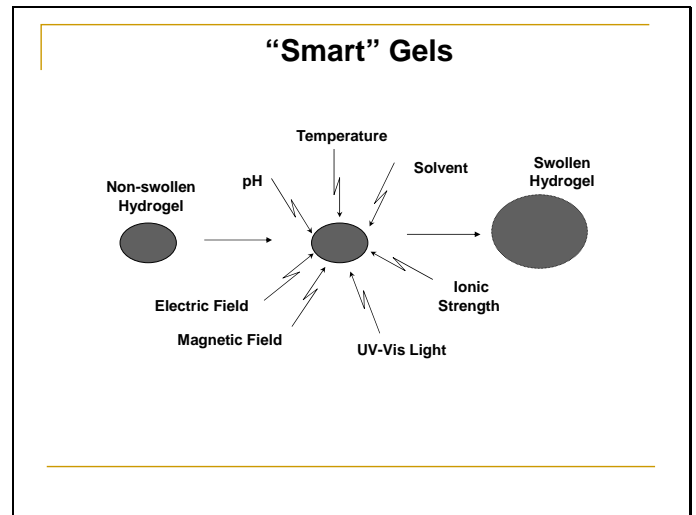

INSTITUTO TECNOLÓGICO DE TIJUANA 
 CENTRO DE GRADUADOS E INVESTIGACIÓN EN QUÍMICA

“New temperature- and pH-sensitive smart polymers containing methacrylic derivatives with hydrophobic spacers”

DR. RODOLFO SALGADO RODRÍGUEZ
DR. ANGEL LICEA CLAVERÍE

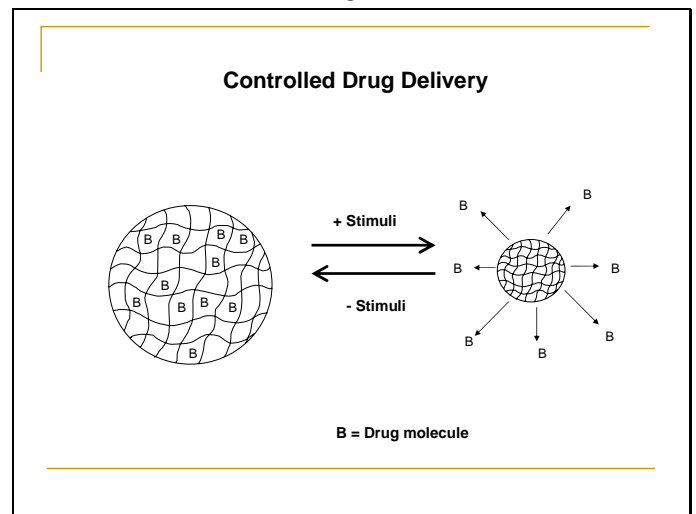
4



2

- INTRODUCTION
- GELS
- CONCLUSIONS

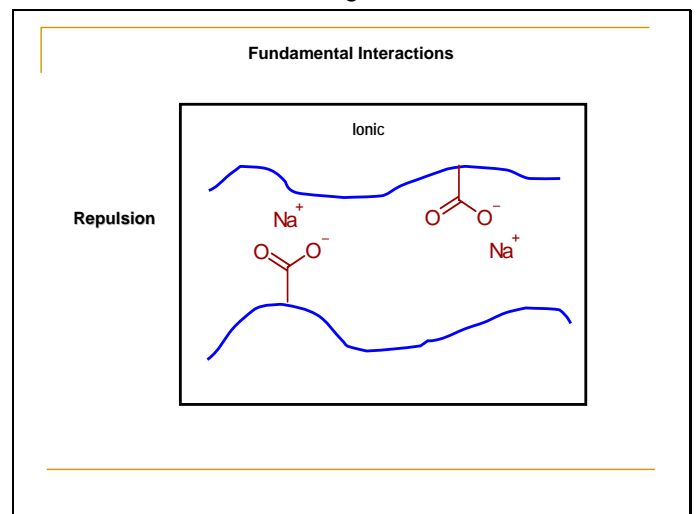
5



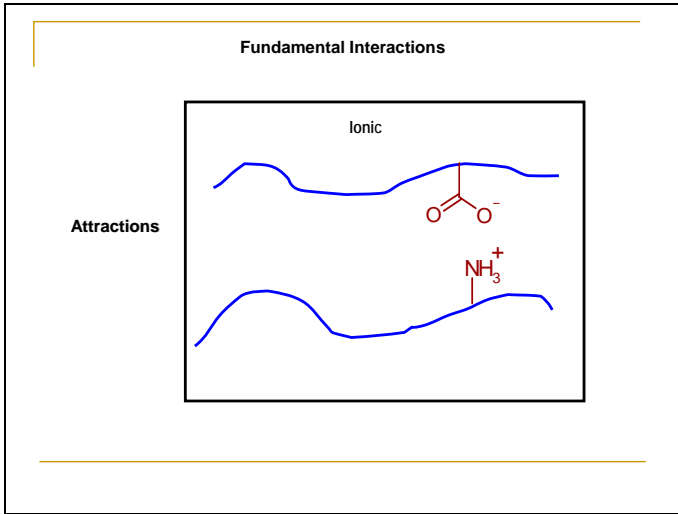
3

INTRODUCTION

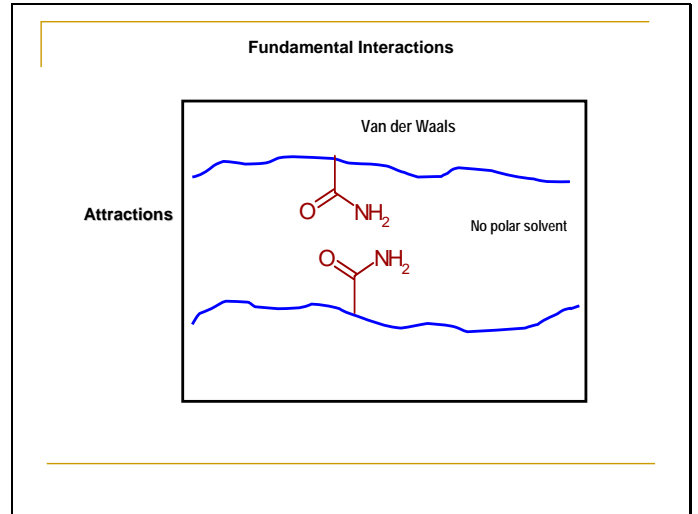
6



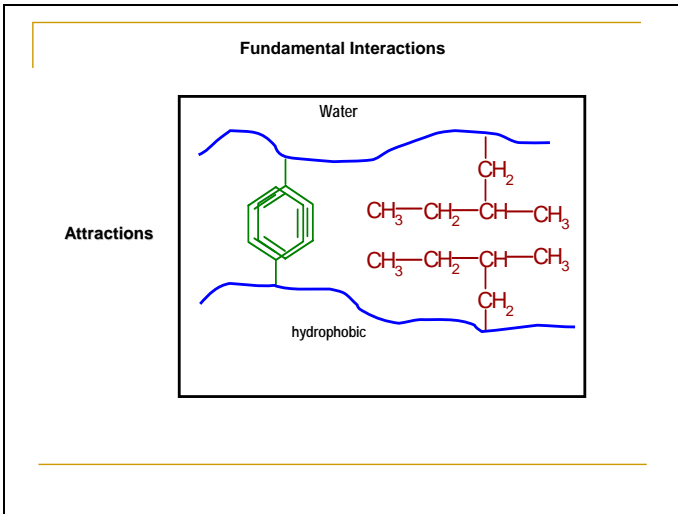
7



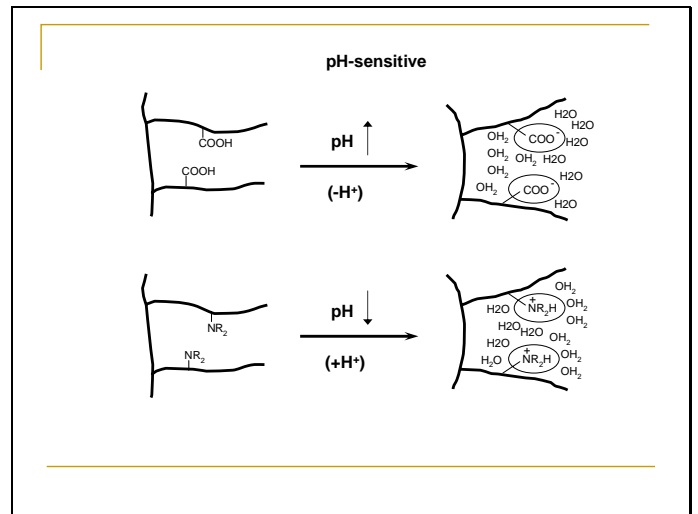
10



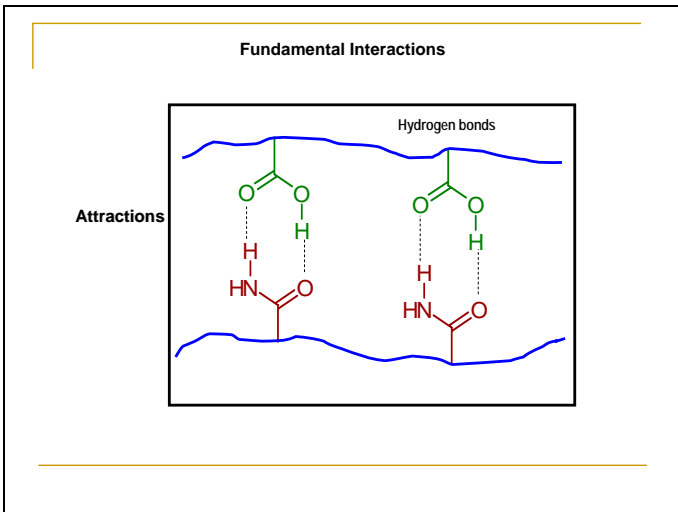
8



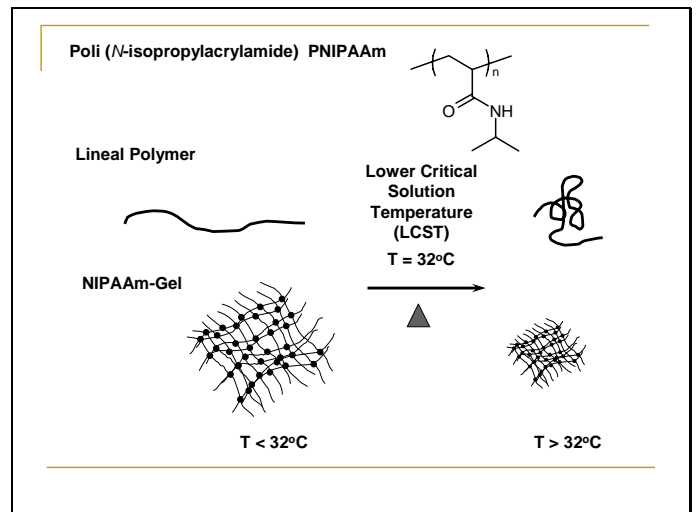
11



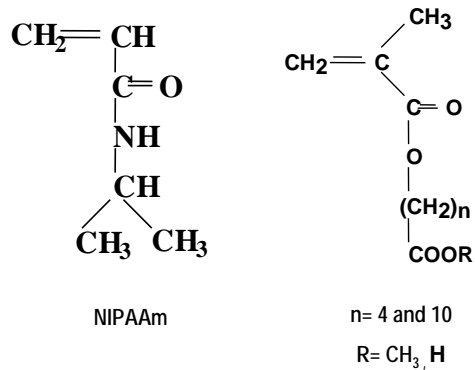
9



12

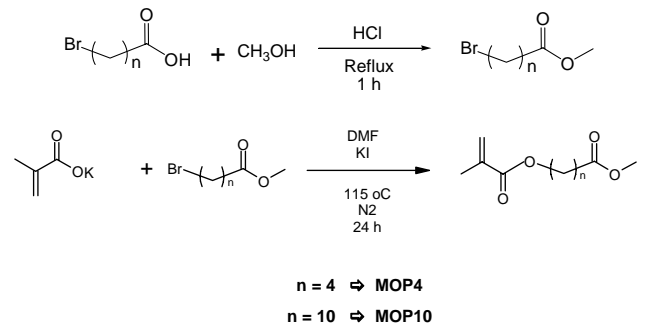


13



16

Synthesis of protected monomers

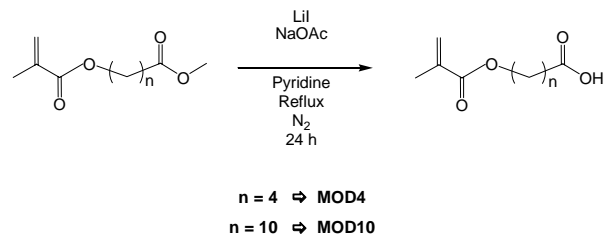


14

GELS

17

Synthesis of deprotected monomers



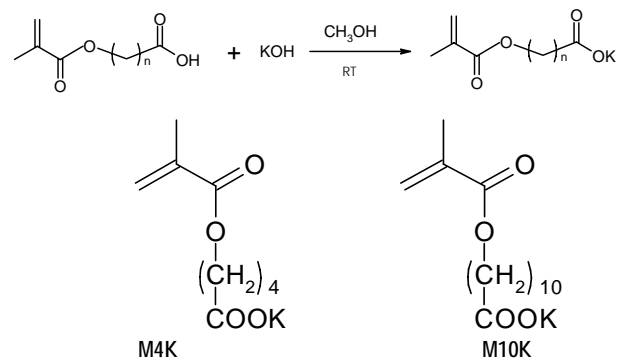
15

OBJECTIVE

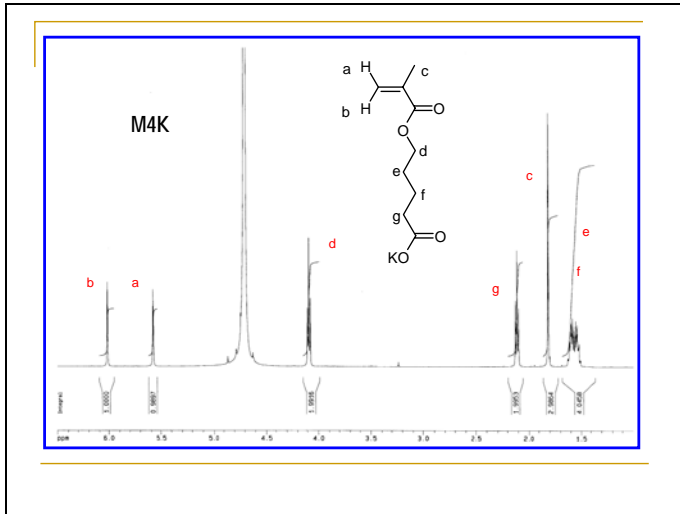
SYNTHESIS AND CHARACTERIZATION OF COPOLYMERIC GELS SENSITIVE TO TEMPERATURE AND pH CONTAINING *N*-ISOPROPYLACRYLAMIDE AND MONOMERIC DERIVATIVES FROM METHACRYLIC ACID WITH HYDROPHOBIC SPACERS.

18

Synthesis of monomers as potassium salts



19



22

Gels prepared in glass capillary tubes (Gels C)

- Open capillary tubes (both sides) of 100 x 1.0 mmØ
- Essays tubes of 100 x 16 mmØ
- Gels rinsed with deionized water
- Gels equilibrated in deionized water and in buffer solutions of pH= 3,4,5,6,7,8,9,10 and 11
- Measurement of diameter of gels at certain temperatures
- Heating of gels starting from 5 °C

$r = d/d_0$
 d_0 initial diameter
 d diameter at temperature T

20

PREPARATION OF COPOLYMERIC GELS

CC(C)NC(=O)C=C + CC(=O)OC(C)C=C

 NIPAAm + (M4K and M10K)

BIS (N,N'-Methylenebisacrylamide)
 APS (Ammonium persulfate)
 TEMED (N,N,N',N'-Tetramethylethylenediamine)

Deionized Water

5, 10, 15 and 20 % mol

23

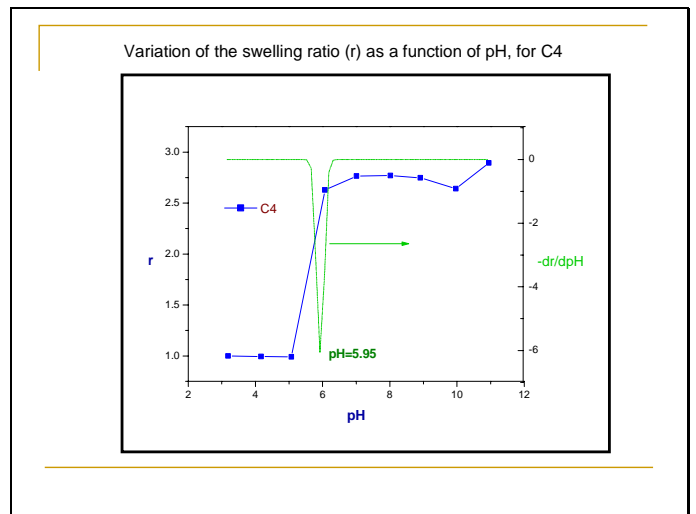
Temperature →

21

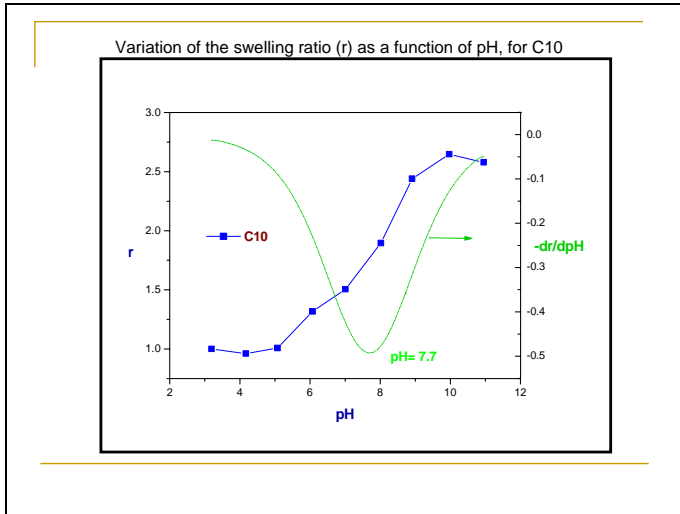
Gels prepared in glass capillary tubes and between glass plates

Molar composition	C	P
100% NIPAAm	CN	PN
100% M4K	C4	P4
100% M10K	C10	P10
5% mol M4K	C4-05	P4-05
10% mol M4K	C4-10	P4-10
15% mol M4K	C4-15	P4-15
20% mol M4K	C4-20	P4-20
5% mol M10K	C10-05	P10-05
10% mol M10K	C10-10	P10-10
15% mol M10K	C10-15	P10-15
20% mol M10K	C10-20	P10-20

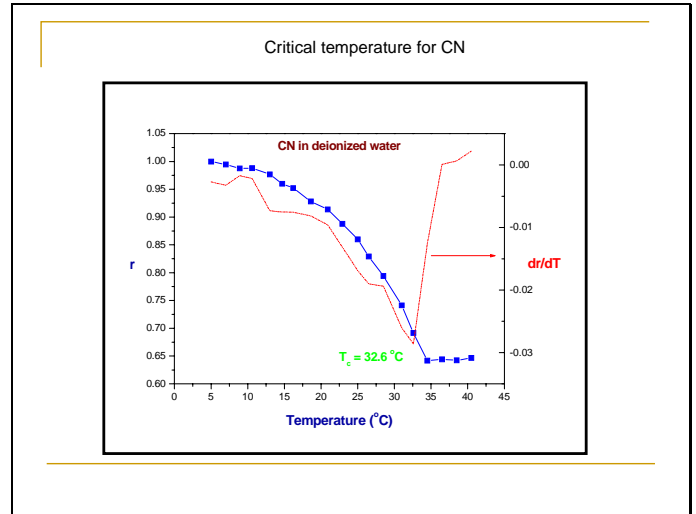
24



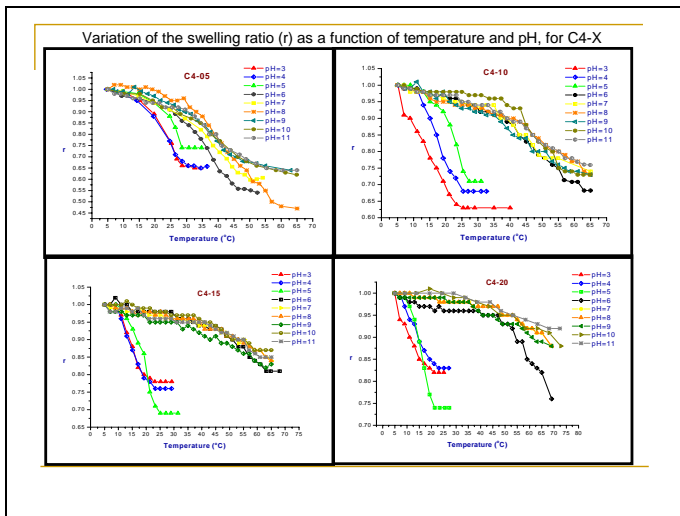
25



28



26

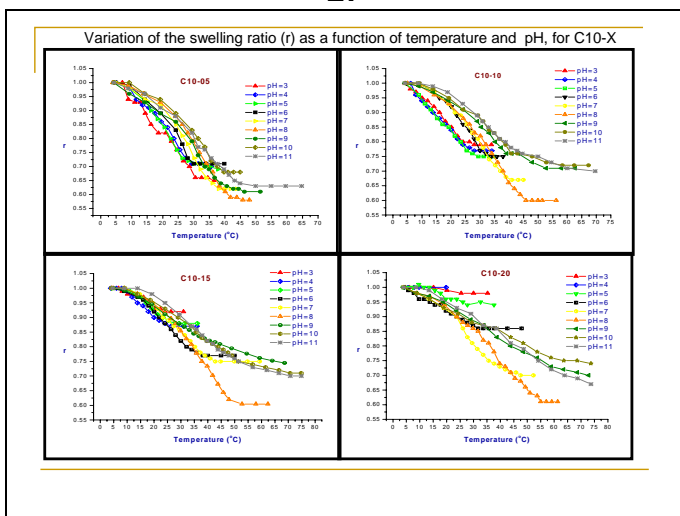


29

Critical temperature for the copolymeric gels

		Critical temperature (°C)									
GELS	Water DI	pH=3	pH=4	pH=5	pH=6	pH=7	pH=8	pH=9	pH=10	pH=11	
CN	33	----	----	----	----	----	----	----	----	----	
C4-05	30	26	25	27	40	41	50	41	45	43	
C4-10	37	19	20	24	53	48	53	47	53	50	
C4-15	51	17	18	21	57	57	57	52	50	56	
C4-20	N	14	17	18	64	N	N	N	N	N	
C10-05	28	26	25	24	26	31	35	33	34	36	
C10-10	25	21	21	22	28	32	38	37	38	41	
C10-15	36	19	20	21	29	34	41	45	47	46	
C10-20	29	N	N	N	24	33	44	49	49	53	

27



30

Gels prepared between glass plates (Gels P)

-Discs equilibrated in deionized water and in buffer solutions (pH 3 – 11)
 -Equilibrium-swelling at temperatures of: 10, 15, 20, 25, 30, 35, 40, 45, 50, 55 °C.

where:
 Q = Equilibrium swelling ratio
 W_h = Weight of the swollen gel
 W_x = Weight of the dry gel

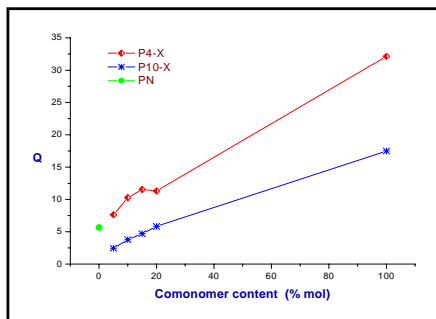
$$Q = \frac{W_h - W_x}{W_x}$$

31



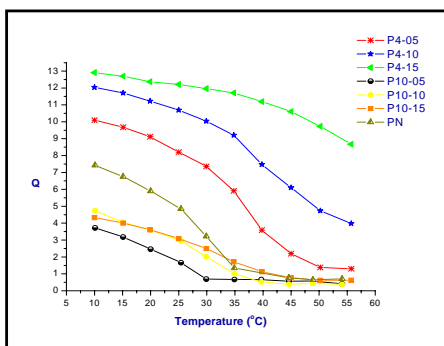
32

Variation of the equilibrium swelling ratio (Q) as a function of the comonomer content at room temperature for gels prepared between glass plates



33

Effect of the temperature and composition of the gel in the swelling ratio in deionized water



34

CONCLUSIONS

- Two new monomeric derivatives from methacrylic acid with free acid groups differing only in the spacer (chain of methylenes with $n = 4$ and 10), were prepared.
- Copolymeric gels of NIPAAm with M4K and M10K were prepared successfully and they were pH- and temperature sensitive as well. The critical temperatures values obtained for these materials ranged from 14 to 64°C.
- An hydrophobic effect due to the methylene spacer chains was observed: A higher swelling ratio for the gels containing M4K compared to M10K.
- The series of gels with M4K show a bigger swelling change at pH=5 while the gels with M10K show this change at pH=8, those values are close to the critical pH of parent homopolymers.

35

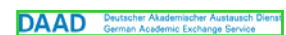
CONCLUSIONS

- The geometrical shape of the gels affects the swelling behavior: thin cylinders show more defined phase transition temperatures than discs that deswell over a wider temperature range.
- In agreement with the results obtained in this work, it is possible to design a polymeric material with an specific phase transition temperature at a certain pH using a different type and content of comonomer.
- Several materials prepared in this work could be excellent candidates for applications in controlled drug delivery as a function of pH and/or temperature changes.

36

Acknowledgements

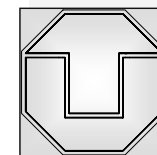
- Dr. Angel Licea Claverie
- Profr. Dr. Karl Friedrich Arndt
- CONACyT-Mexico
- DAAD-Germany
- Volkswagen Foundation- Germany
- Thanks specially for valuable technical support to : I. Rivero (NMR), D. Scheller (NMR), I. Poitz (DSC) and C. Meissner (SLS).



pH-tunable temperature sensitive materials from NIPAAm-methacrylic acid copolymers with hydrophobic spacers

R. Salgado-Rodríguez¹, A. Licea-Claveríe¹ and K.F. Arndt²

1.-Centro de Graduados e Investigación, Instituto Tecnológico de Tijuana, A.P.1166-22000 Tijuana, B.C., MEXICO
2.-Institut für Physikalische Chemie und Elektrochemie, Technische Universität Dresden, D-01062 Dresden, GERMANY



Goal

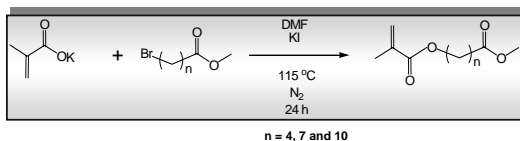
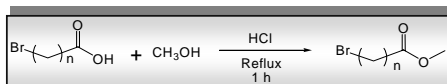
The aim of this work was to develop a series of NIPAAm-copolymers with tuning capacity for their LCST based on comonomers with hydrophobic spacers and hydrophilic ionizable groups. Furthermore, the study of the importance of intrachain hydrogen-bonding, regarding LCST of NIPAAm copolymers in pure water and in solutions with varying pH using partially hydrophobic comonomers is a further goal of this work. Finally, since linear copolymers can be easily characterized, their investigation is the basis for the better understanding of the behaviour of their corresponding polymer networks to be developed in the future.

Introduction

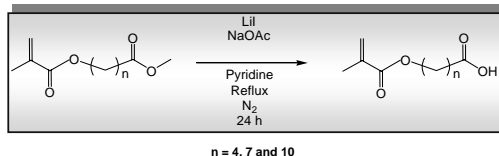
During the last years there has been a growing interest in temperature-sensitive polymers because they are potential candidates for applications as intelligent sensors, separation systems and drug release devices. It has been shown that the temperature-sensitivity of these polymers is connected with their lower critical solution temperature (LCST). There are some polymers which exhibit a LCST in aqueous solutions, the most studied polymer being the poly (*N*-isopropylacrylamide) (PNIPAAm) whose LCST lies between 30 and 35 °C. The LCST of these polymers is a result of a fine balance of hydrophilic and hydrophobic groups in their molecular structure. If the balance is slightly altered there is a possibility to vary its LCST. This can be achieved by varying the chemical composition of the polymer.

Experimental

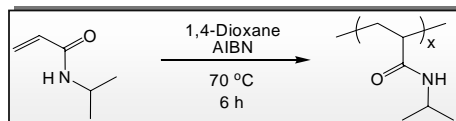
Synthesis of hydrophobic monomer derived from methacrylic acid:



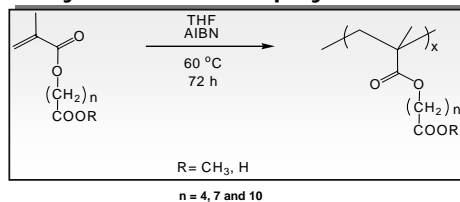
Synthesis of hydrophilic monomer derived from methacrylic acid:



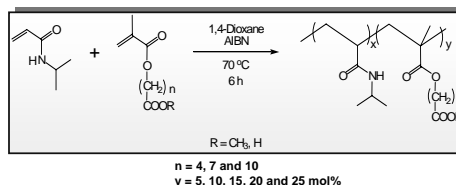
Synthesis of PNIPAAm via free radical polymerization



Synthesis of homopolymers



Synthesis of copolymers



Results

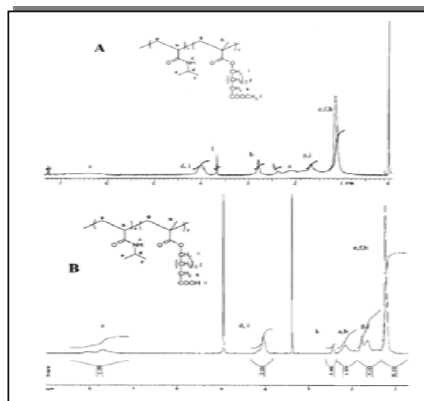


Figure 1. Selected NMR-spectra of NIPAAm-copolymers: (A) copolymers with protected acid groups, (B) copolymers with free acid groups.

Table 1. Results of protected copolymers characterization.

Polymer	Co-monomer content [mol%]	dn/dc [mL/g]	M _n [g/mol]	R _n in THF [nm]	T _g [°C]	Yield [%]
PNIPAAm	-----	0.09299	237 000	27	139	92
COPN4-05	6.2	0.09530	264 000	27	128	77
COPN4-10	9.9	0.08870	292 000	28	114	87
COPN4-15	16.8	0.08900	281 000	27	106	82
COPN4-20	20.4	0.08380	287 000	24	106	85
COPN4-25	19.6	0.09330	208 000	21	97	84
COPN7-05	7.8	0.08098	398 000	31	128	90
COPN7-10	11.6	0.07264	514 000	31	114	87
COPN7-15	15.5	0.08871	406 000	34	105	70
COPN7-20	24.6	0.04360	832 000	32	104	78
COPN7-25	29.0	0.08207	445 000	33	93	73
COPN10-05	4.8	0.09141	368 000	32	127	81
COPN10-10	8.4	0.09105	343 000	30	108	73
COPN10-15	11.3	0.08514	414 000	44	100	45
COPN10-20	23.0	0.08613	296 000	30	78	89
COPN10-25	25.6	0.07859	332 000	32	68	98

Table 2. Results of deprotected copolymers characterization.

Polymer	Co-monomer content [mol%]	dn/dc [mL/g]	M _n [g/mol]	R _n in THF [nm]	T _g [°C]	Yield [%]
CDN4-05	7.8	0.09310	291000	26	133.8	94.3
CDN4-10	12.4	0.09219	340000	23	126.7	82.0
CDN4-15	18.0	0.16856	241000	19*	121.8	87.0
CDN4-20	24	0.16912	310000	30*	117.1	95.0
CDN7-05	7.2	0.09438	354 000	29	127.9	90.9
CDN7-10	12.4	0.09497	318 000	24	118.6	86.0
CDN7-15	17.4	0.16564	275 000	19*	109.6	93.5
CDN10-05	6.6	0.09370	287 000	24	126.4	94.2
CDN10-10	12.8	0.09352	289 000	22	112.5	94.3
CDN10-15	17.3	0.17395	231 000	23*	99.7	90.3

Behaviour of linear polymer in aqueous solution

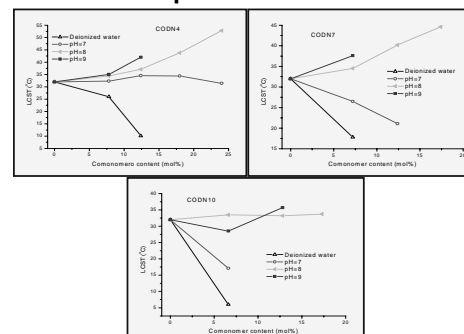


Figure 2. LCST behaviour of NIPAAm-copolymers with free acid groups in buffers of different pH as a function of comonomer content.

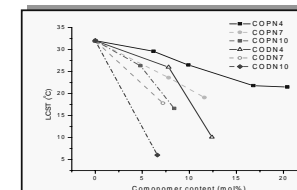


Figure 3. LCST behaviour of NIPAAm-copolymers in pure water in dependence on comonomer content.

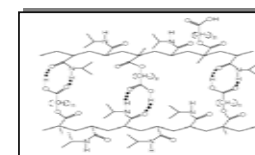


Figure 4. Proposed hydrogen-bonding interactions in the NIPAAm-copolymers.

Conclusions

- Two series of random NIPAAm-copolymers were successfully prepared using acid comonomers with aliphatic spacers (4, 7 and 10 methylene units) having the acid group either methoxy-protected or free.
- Solution free radical polymerization proved to be a good technique for their preparation since high yields (close to 90%) in 6 h were achieved. Furthermore, the copolymer composition was close to the monomer feed composition indicating a truly random distribution of the monomeric units in the copolymers.
- In the solid state, the aliphatic spacers bring side chain flexibility lowering the T_g of the copolymers while the free acid groups give the chance of interchain hydrogen-bonding increasing the T_g as a result.
- The water solubility and LCST behaviour of the prepared NIPAAm-copolymers depends on the hydrophilic/hydrophobic balance in the copolymer chain and on the hydrogen-bonding capabilities from its chemical structure. The hydrophilic/hydrophobic balance depends mainly on three elements, (a) the amount of comonomer; (b) the kind of comonomer, regarding the spacer (n = 4, 7 and 10, methylene units) and the acid group (protected or free); (c) the pH of the solution of the copolymer, which affects the extent of ionization of the carboxylic acid groups.
- Finally, our results show that both: hydrophobic interactions and hydrogen-bonding are very important for the behaviour of NIPAAm-copolymers depending strongly on the fine chemical structure of the used copolymeric units.

Acknowledgements

- R. Salgado-Rodríguez thanks to DAAD-Germany for financing his PhD-exchange program.
- We gratefully acknowledge the financial support of CONACYT-Mexico (Project Nr. 28022-U) and Volkswagen Foundation-Germany (Project Nr. I/76 065).
- We thank specially I. Rivero (NMR), D. Scheller (NMR), I. Poltz (DSC) and C. Meissner (SLS) for valuable technical support.

Institute for Polymer Research
27th Annual Symposium

Symposium documents for

Fred Pries

Abstract

Presentation

The Changing World of Industrial Innovation

Fred Pries

Institute for Innovation Research, University of Waterloo

Not all inventions become innovations. Invention involves the creation or discovery of a new technology while innovation involves putting the new technology into use either by introducing a new product to the market (product innovation) or by using it within a production process (process innovation). The paths from invention to innovation are risky and often lengthy processes with only a small percentage of inventions actually being put into use. For example, Sonora, a polymer platform developed by DuPont, took 60 years from initial discovery to product introduction. The 'struggle for life' of inventions to become innovations involves adaptation and change to overcome technical risks and market uncertainty.

The paths from invention to innovation are changing. In the 'old world' of closed innovation, all of the activities from initial research through technology development, product development and product launch took place within a single firm. This was the innovation process used by DuPont in the discovery and commercial production of nylon. While this 'old world' of innovation continues to exist, a 'new world' of open innovation is emerging. In the world of open innovation, inventions made by one organization are often commercialized by other organizations. The commercialization of the UNIPOL polyethylene gas phase process and metallocene catalyst technologies is an example of this world of open innovation.

As a result of these changes, more options for commercializing new technologies are becoming viable. Specifically, inventors of new technologies have opportunities to 1) Build – create a new business based on the technology, 2) Rent – ongoing development and marketing of the technology to established firms that use the technology in their businesses and 3) Sell – dispose of the technology to an established firm.

The world of innovation is changing. The simple linear process of research, development, product development and launch by a single firm no longer reflects how innovation happens. In this changing world, ideas come from many sources and many different options to commercialize exist.



The Changing World of Industrial Innovation

Fred Pries
University of Waterloo
May 2005



What is innovation?

- Invention – discovery of a new technology
- Innovation – “Technological product and process (TPP) innovations comprise *implemented* technologically new products and processes and significant technological improvements in products and processes. A TPP innovation has been implemented if it has been *introduced on the market* (product innovation) or *used within a production process* (process innovation).” OECD, Oslo Manual, January 1996

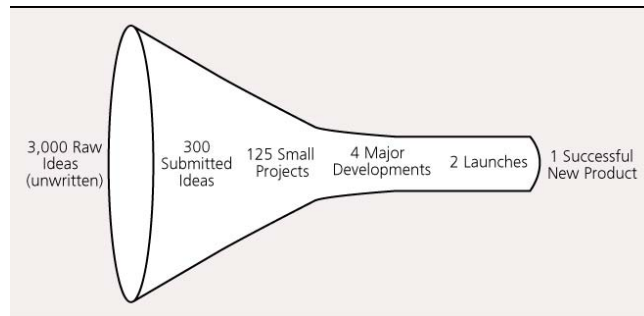


Sonora™

- Polymer platform developed by DuPont
- Early 1940s – product *invention* but cost-prohibitive to produce
- Mid 1990s – process *invention* enables cost-effective production
- Early 2000s – product availability – *innovation*
- 60 years from invention to innovation
- Major technological advances typically:
 - Require a cluster of inventions (as many as 12)
 - Take 20 years from first invention to implementation
 - Citrus fruit to cure scurvy – 200 years (Rogers, 2003)



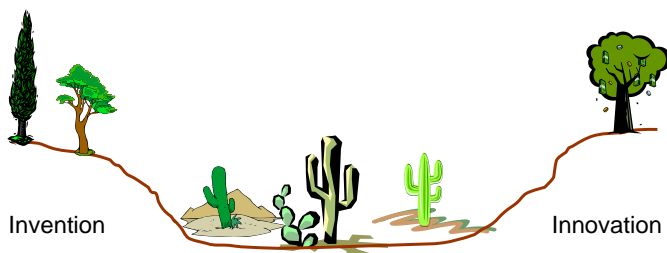
Innovation is risky



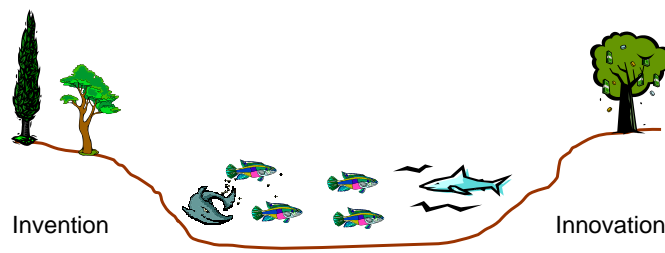
Stevens & Burley, 1997



The Valley of Death



The Darwinian Sea



“The ‘Struggle for Life’ is a sea of technical and entrepreneurship risk”



Branscomb, 2004





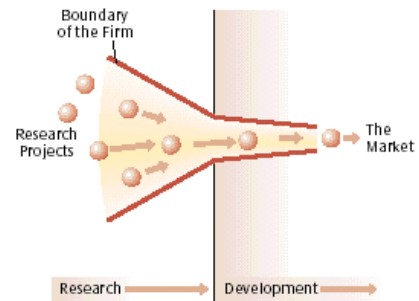
What drives innovation?

Product innovation	Replace products being phased out	3.1
	Extend product range within main product field	3.8
Product diversification	Extend product range outside main product field	2.7
Extension of local market	Increasing or maintaining market share	4.2
	Creating new markets nationally	3.4
Opening up of global markets	Creating new markets within the European Community	3.3
	Creating new markets in North America	2.0
	Creating new markets in Japan	1.7
	Creating new markets in other countries	2.3
Process innovation	Improve production flexibility	3.5
	Reducing the share of wage costs	3.4
	Reducing materials consumption	3.2
	Reducing energy consumption	2.9
	Reducing product design costs	2.3
	Reducing production lead times	3.5
	Reducing environmental damage	3.3
	Improving product quality	4.0
	Improving working conditions/safety	3.5

IR Source: Innovation in the European Chemical Industry, 1996



The 'old world' – closed innovation



Chesbrough, 2003

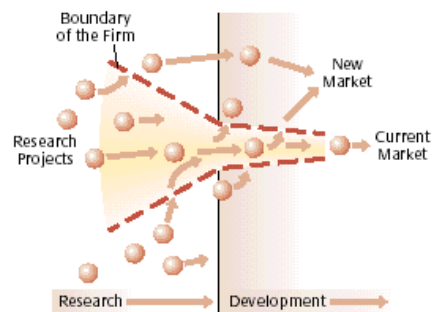


DuPont's discovery of nylon

- 1927 – DuPont sets up a fundamental research program
- 1930's – Research by Dr. Carothers and colleagues results in invention of nylon
- 1939 – DuPont begins commercial production of nylon
- Entire process in-house



The 'new world' – open innovation



Chesbrough, 2003



What is driving the transition

- Increasing availability and mobility of skilled workers
- Increasing availability of venture capital
- Emergence of external options – markets for technology
- Increasing capability of suppliers

(Chesbrough, 2003)



Univation Technologies

- UNIPOL polyethylene gas phase process – Union Carbide
- Metallocene catalyst technology – Exxon
- Univation
 - 50/50 joint venture to license the technologies
 - World's #1 licensor of PE technology with >90 reactors around the world





Sources of information for innovation

Internal sources	Internal sources within the enterprise	3.6
	Internal sources within the group of enterprises	1.9
	Patent disclosures	2.3
Science	Consultancy firms	2.0
	Universities/higher education	2.0
	Government laboratories	1.8
	Technical institutes	1.8
Other firms	Suppliers of materials and components	2.9
	Suppliers of equipment	2.9
	Clients or customers	3.4
	Competitors	2.9
	Professional conferences, meetings, journals	2.9
	Fairs/exhibitions	2.7

Source: Innovation in the European Chemical Industry, 1996



Build, rent & sell

- Open innovation allows different paths to commercialization – beyond ‘use’
- Three primary methods
 - Build – creating a new business based on the technology
 - Rent – ongoing development and marketing of the technology to firms that use the technology in their businesses
 - Sell – disposition of the technology to an established firm



Build

- Creating a new business based on the innovation
- ‘Product market’
- New technology is source of competitive advantage
- New firm acquires or develops the complementary assets (e.g., manufacturing capabilities, distribution networks) needed to commercialize the innovation



Examples: Dalsa, OpenText, Waterloo Barriers, Certicom



Rent

- Ongoing development and marketing of the innovation to established firms that use the innovation in their businesses
- ‘Market for ideas’
- Inventor/university retains ownership of the innovation and continues to grow and harvest the innovation
- Often ‘rented’ to more than one established firm



Examples: Senesco, Waterloo Emitters™ Handshake VR, Ignis Innovation



Sell

- Disposition of the innovation to an established firm
- Established firm typically has the complementary assets needed to commercialize the innovation
- Future enhancements typically undertaken by acquiring firm
- Examples: Solid phase microextraction (SPME) to Sigma-Aldrich Corporation, many biotechnology and software start-ups



Summary

- A changing world of innovation
- Simple linear process no longer reflects how innovation happens
- Ideas come from many sources
- Multiple options to commercialize exist
- Crossing the Darwinian Sea
 - “It’s a sea full of sharks, and it’s full of little fishes. There’s all kinds of stuff happening. If you think about how you get from the research world to the innovation world, it turns out there are lots of pathways. And they’re complicated. ... It is the vibrancy of this connection that is necessary to make it possible to go from one culture to a radically different culture successfully.” (Branscomb, 2004)





So what?

- Corporations
 - Look outside for sources of innovation – NIH syndrome
 - Look outside for opportunities to commercialize – Rembrandt's in the attic
- Academic researchers and independent inventors
 - Numerous options exist – build, rent & sell
 - Choice may affect likelihood of success



Questions?



Institute for Polymer Research
27th Annual Symposium

Symposium documents for

Francisco Lopez Serrano

Abstract

Presentation

Poster

Determination of Styrene-Methyl Methacrylate Reactivity Ratios Dependencies on Feed Composition.

Francisco López-Serrano*, Jorge E. Puig[#] and Jesús Álvarez^o

*Facultad de Química. Dpto. de Ing. Química. Universidad Nacional Autónoma de México. Cdad. Universitaria. CP 04510. D.F. MEXICO (lopezserrano@correo.unam.mx). # CUCEL. Dpto. de Ing. Química. Universidad de Guadalajara. Marcelino García Barragán No. 1451, CP 44430, Guadalajara, Jalisco. MEXICO (puigje@mail.udg.mx). ^o Dpto. de Ing. Química e Hidráulica. Universidad Autónoma Metropolitana-Iztapalapa. Apdo. 55534, CP 09340, D. F. MEXICO (jac@xanum.uam.mx)

Introduction

Generally, in nonlinear regression with constant parameter fitting, the information derived from the measurement derivative is not exploited [1,2] and there are multiple fittings with some models [3, 4] and it is not clear if this is due to the model or the fitting. In standard regression, a candidate model is evaluated [5,6] where the parameters constancy is assumed, the regression is applied and the model adequacy is judged by the size of its prediction errors; the choice of the number of parameters is guided by the specific candidate model [3, 4], physical insight and some dosage of trial and error. To improve the parameter model approach, recently [7] the employment of differential estimation has been proposed to address polymerization kinetics problems. The idea is to split the problem in two parts and to exploit the measurements derivatives information, in order to improve the capability and systematization of the modeling task. In the first step, the measurements and its derivatives are used with mass balances without *a priori* kinetic assumptions to draw the parameters shape against feed composition. In the second step, based on the results of step one, and on a sound theoretical or physicochemical insight, a parameter or parameter groupings fitting versus feed composition is performed according to the standard curve fitting procedure. The differential method is a well-known tool in nonlinear estimation theory, as well as in reaction kinetics via the so-called differential method [8] in batch and continuous reactor experiments. Here this approach will be employed to assess the reactivity ratios dependency on feed composition without *a priori* kinetic assumptions and in a second step, a fit can be performed according to the functionalities of existing models. The proposed approach is tested with the ultimate model (eq 1) and data previously presented in the literature for the copolymerization of styrene and methyl methacrylate [11, 12].

Constant parameter approach

In the ultimate model [5], the copolymer equation is:

$$F_1 = \frac{r_1 f_1^2 + f_1 f_2}{r_1 f_1^2 + 2f_1 f_2 + r_2 f_2^2} \quad (1)$$

and the average propagation rate constant is:

$$\langle k_p \rangle = \frac{r_1^2 f_1^2 + 2f_1 f_2 + r_2^2 f_2^2}{r_1^2 f_1 / k_{11} + r_2^2 f_2 / k_{22}} \quad (2)$$

where F_1 and f_1 are the monomer compositions in the polymer and monomer feed, respectively, $r_i = k_{ii}/k_{ij}$ ($i = 1, 2$) are the reactivity ratios and k_{ii} and k_{ij} are the homopolymerization and cross propagation rate constants, respectively. Eqs 1 and 2 can also represent the penultimate model; in this case replace k_{ii} by k_{ii}^p and r_i by r_i^p as follows:

$$r_i^p = r_i \left(\frac{r_i f_i + f_j}{r_i f_i + f_j} \right) \quad (3)$$

$$k_{ii}^p = k_{ii} \left(\frac{r_i f_i + f_j}{r_i f_i + f_j / s_i} \right) \quad (4)$$

As it can be seen in eqs 1 and 2, four parameters appear for the ultimate model: two reactivity ratios (r_i) and two homopolymerization rate constants (k_{ii}). However, in the penultimate model, eight parameters appear: four monomer reactivity ratios ($r_i = k_{ii}/k_{ij}$), $r_i^p = k_{ii}^p/k_{ij}$), two homopolymerization rate constants (k_{ii}) and two radical reactivity ratios ($s_i = k_{ii}^p/k_{ii}$). The homopolymerization (k_{ii} , k_{ij}) rate constants can be determined from independent experiments; therefore, in the ultimate model two parameters are left to be determined and six in the penultimate model. In this last model six parameters are still too many to be determined from polymer composition (F_1) and the propagation

rate constant (k_p) versus monomer feed composition (f_1). Comparing the ultimate and the penultimate models, it can be realized that the four parameters appearing in the ultimate model, can be treated as functions. It can be seen (eq 3) that r_i^p is a function of f_i with two parameters r_i and s_i and k_{ii}^p is also a function of f_i , where r_i and s_i are the parameters. Therefore, in principle, if r_i^p are allowed to vary against monomer feed (f_i) the penultimate model (eq 3) functional form can be tested, otherwise the ratios r_i^p will remain constant indicating the ultimate model validity. The same applies to eq 4, allowing also, in principle, the determination of the corresponding parameters.

The differential estimation approach.

Let us apply the differential method and take the derivative [9, 10, 15] of F_1 with respect to f_1 in eq 1 to obtain:

$$\dot{F}_1 = \frac{1 - f_1 + 2f_1(r_1 - 1)r_2 + f_1^2(r_1 + r_2 - 2r_1r_2)}{(r_2 + f_1(2 - 2r_2 + f_1(r_1 + r_2 - 2)))^2} \quad (5)$$

Mathematically speaking, this equation is a notion of "instantaneous" or differential observability [9, 10] in the sense that r_1 and r_2 can be uniquely determined from the composition measurements and their derivatives. This corresponds to the so-called differential estimation method to determine reaction rates [8]. Eq 1 represents the mass balance and eq 5 is the rate of monomer incorporation to the polymer. To determine whether eqs 1 and 5 are independent and where, the observability matrix (Jacobian) determinant is calculated yielding [15]:

$$\det O = \frac{(f_1 - 1)^2 f_1^2}{(r_2 + f_1(2 - 2r_2 + f_1(r_1 + r_2 - 2)))^3} \quad (6)$$

Eq 6 indicates that the system has no solution only when f_1 is zero or one and that elsewhere r_1 and r_2 can be uniquely determined from the

data of F_1 and \dot{F}_1 versus f_1 . Therefore, the left hand side of eqs 1 and 5 and also f_1 are known from experimental data (fit a function to the F_1 versus f_1 data take this function derivative to obtain \dot{F}_1). This procedure yields two equations (eqs 1 and 5) with two unknowns (r_1 and r_2) that allow the calculation of each reactivity ratios at every composition as follows [15]:

$$r_1 = \frac{(f_1 - 1)(F_o - 2F_o^2 + (f_1 - 1)f_1 F_p)}{f_1(-2(F_o - 1)F_o + (f_1 - 1)f_1 F_p)} \quad (7)$$

$$r_2 = \frac{f_1((3 - 2F_o)F_o - 1 + (f_1 - 1)f_1 F_p)}{f_1(-2(F_o - 1)F_o + (f_1 - 1)f_1 F_p)} \quad (8)$$

Here, F_o is the interpolated value of F_1 , and F_p its derivative at every feed composition f_1 .

Results and discussion

Composition and propagation rate data for the copolymerization of styrene and methyl methacrylate at 40°C were taken from the literature [11, 12]. Figure 1 shows the composition data fitted with four sets of penultimate reactivity ratios (Table 1). Two of the sets have been reported previously [3] indicating multiplicity of solutions; this is corroborated in Fig. 1 where no distinction can be made from the four sets. Figures 2 and 3 present the estimation of r_1 and r_2 , for each of the four fits, respectively. In these two figures, the continuous lines represent the penultimate model fit (eq 3) and it can be seen that none of the fits accurately describes this model. Another interesting fact is that all the fits coincide for $0.2 < f_1 < 0.84$ in the case of r_1 and about $0 < f_1 < 0.8$ for the r_2 estimate. This is confirmed verifying the value of the observability matrix determinant (eq 6) and also is corroborated for the values given by Tidwell and Mortimer [13] assuming the reactivity ratios constancy.

Table 1. Multiplicity of solutions when fitting the data of Fig. 1 with the penultimate model.

	Set a (this work)	Set b (this work)	Set 1 ref. [3]	Set 2 ref. [3]
r_1	0.6475	0.829	0.646	0.727
r_2'	0.3324	10.634	0.400	4.581
r_1'	0.3264	3.848	0.386	2.886
r_2	0.4994	0.5106	0.483	0.489

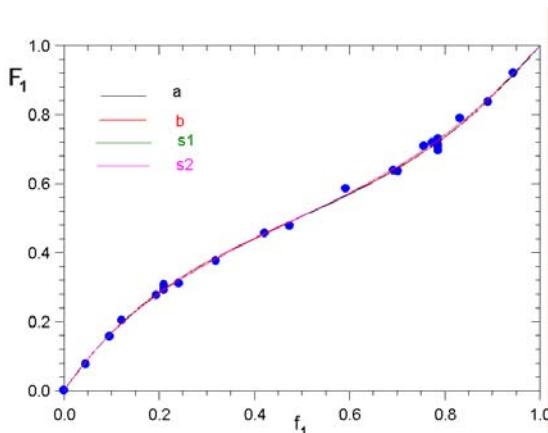


Figure 1. Composition curve, data taken from the literature [11, 12]. The continuous lines represent the fit using the penultimate model and parameters presented in Table 1.

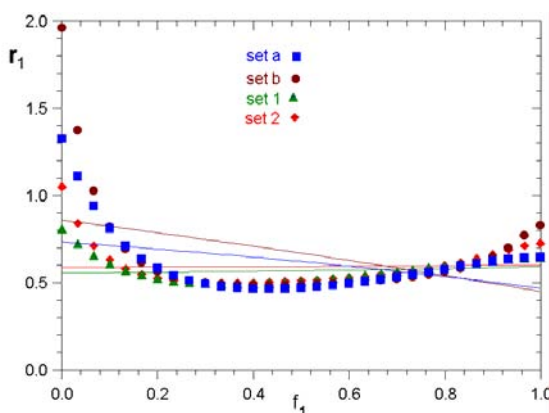


Figure 2. The symbols represent the estimation of r_1 (eq 7) using the four fits presented in Table 1. The continuous lines represent the penultimate model fit (eq 3).

An empirical fit of the estimates was applied to the four sets presented in Table 1. The fit has the following form:

$$r_1 = k_a + k_b f_1 + k_c \exp(k_d f_1) \quad (9)$$

where, k_a , k_b , k_c and k_d are fitting parameters. Eq 9, resembles the form presented previously [14]:

$$\log r_{12} = \log r_{1S} + u_2 \sigma_1 + v_2 \quad (10)$$

Here r_{1S} is the reactivity ratio of monomer 1 with styrene, u_2 represents the polarity of monomer 2, σ_1 represents the polarity of the polymer radical derived from monomer 1 and v_2 represents the intrinsic reactivity of monomer 2.

The same procedure was applied to the k_p versus f_1 data [11] and the k_{11} and k_{22} estimates using eq 2 and its derivative are presented in Figure 4. Non constant behavior is observed here.

Conclusions

A differential approach with an observability notion was applied to the styrene methyl methacrylate data finding that the penultimate model, even fitting adequately the data but with multiplicity, cannot explain the copolymerization behavior. With the differential approach presented here, where the searched

parameters were obtained with unicity, a different dependency of the reactivity ratios was found, as compared by the one postulated by the penultimate model. Also the differential approach shows a more accurate capability of model discrimination.

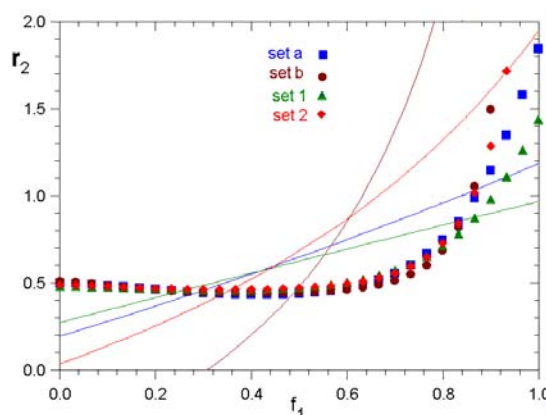


Figure 3. The symbols represent the estimation of r_2 (eq 8) using the four fits presented in Table 1. The continuous lines represent the penultimate model fit (eq 3).

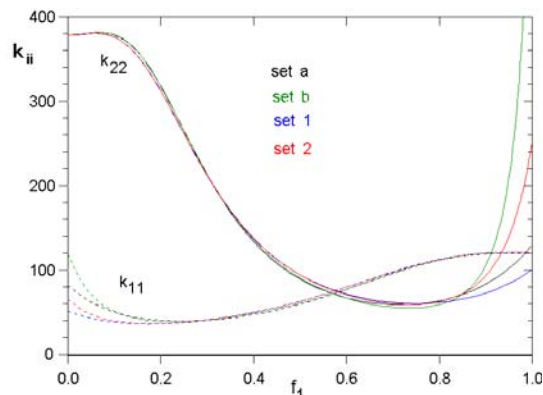


Figure 4. Estimates of k_{11} and k_{22} obtained from eq 2 and its derivative and the values of r_1 and r_2 presented in Figs. 2 and 3. The experimental k_p data was taken from the literature [11].

References

- [1] Behnken, D. W., *J. Polym. Sci., Part A*, **1964**, 2, 645
- [2] Polic, A. A., T.A. Duever, and A. Penlidis, *J. Polym. Sci., Part A: Pol. Chem.*, **1998**, 36, 813
- [3] Kaim A. and P. Oracz, *Macromol. Theory Simul.*, **1997**, 6, 565
- [4] Kaim A., *J. Polym. Sci., Part A: Pol. Chem.*, **2000**, 38, 846
- [5] Mayo, F. R., F. M. Lewis. *J. Am. Chem. Soc.* **1944**, 66, 1954.
- [6] Rossignoli, P.J. and T. A. Duever, *Polym. React. Eng. J.*, **1995**, 3, 361
- [7] López-Serrano, F., J. E. Puig and J. Alvarez. *AIChE J.* **2004**, 50, No. 9, 2246
- [8] Levenspiel, O., "Chemical Reaction Engineering" 2nd Ed. Wiley International Ed. John Wiley and Sons, New York, 1972.
- [9] Alvarez J. and T. López, *AIChE J.* **1999**, 45(1), 107-122
- [10] Alvarez, J., *J. Proc. Control*, **2000**, 10, 59-71
- [11] Fukuda, T., Y. D. Ma, H. Inagaki, *Macromolecules* **1985**, 18, 17
- [12] Maxwell, I. A., A. M. Aeridts, A. L. German, *Macromolecules* **1993**, 26, 1956-1964
- [13] Tidwell P.W. and G.A. Mortimer. *J. Polym. Sci.* **1965**, A-3 (1), 369
- [14] Jenkins, A. D. and J. Jenkins, *Macromol. Symp.* **2001**, 174, 187
- [15] López-Serrano, F., J. E. Puig and J. Alvarez. *Ind. Eng. Chem. Res.* **2004**, 43, No. 23, 7361



Determination of Styrene/Methyl Methacrylate Reactivity Ratios Dependencies on Feed Composition

F. López-Serrano, J. E. Puig, and J. Álvarez
May 17th 2005.



Motivation

“The elucidation of the mechanism of free radical copolymerization remains an open problem” (Keleman and Klumperman, *Macromolecules*, 2004, 37, 9338)

“... It is concluded that the ‘explicit’ or complete penultimate model should be regarded as the base model for the majority of copolymerization reactions” (Coote and Davis, *Prog. Polym. Sci.* 1999, 24, 1217)

“In conclusion, the triad sequence distributions measured in the work for the styrene-MMA system allow us to state with more authority that there is no penultimate unit effect on polymer chain structure.” (Maxwell et al., *Macromolecules*, 1993, 26, 1956)

2



Contents

- Copolymerization
- Previous Approaches
- Differential and Integral Methods Comparison
- Integro-Differential Estimation Proposal
- Reactivity Ratios (parameters) Estimation and Modeling Assessment. Sty-MMA
- Conclusions

3



Importance of Copolymerization

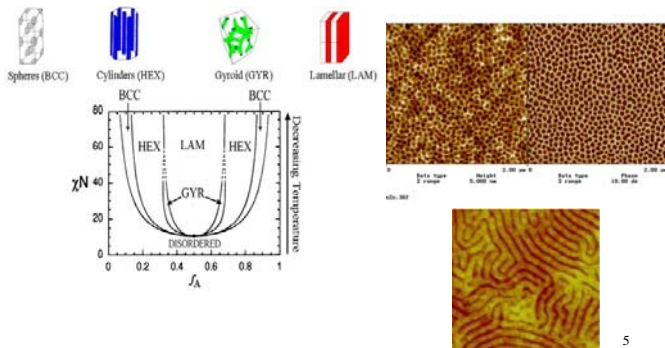
- Statistical or random
~ABAABBABAAABABB~
- Alternating
~ABABABABABABABA~
- Block
~AAAABBBBBBBBAAAA~



4



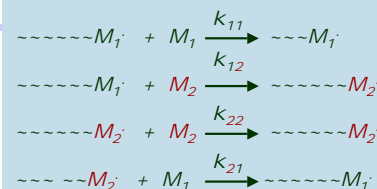
Structure and Morphology



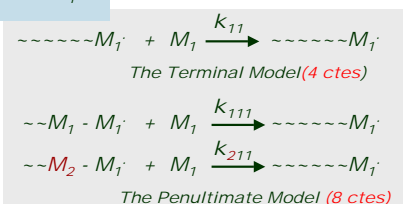
5



The Kinetics of Free Radical Copolymerization



Note that we are actually making an assumption; that the rate constants depend only on the nature of the terminal group.





The Copolymer Equation which is a differential equation; r_1 and r_2 are the reactivity ratios

$$\begin{aligned} -\frac{d[M_1]}{dt} &= k_{11}[M_1 \cdot][M_1] + k_{21}[M_2 \cdot][M_1] \\ -\frac{d[M_2]}{dt} &= k_{22}[M_2 \cdot][M_2] + k_{12}[M_1 \cdot][M_2] \end{aligned}$$

$$\frac{d[M_1]}{d[M_2]} = \frac{k_{11}[M_1] \frac{[M_1 \cdot]}{[M_2 \cdot]} + k_{21}[M_1]}{k_{22}[M_2] + k_{12}[M_2] \frac{[M_1 \cdot]}{[M_2 \cdot]}}$$

$$-\frac{d[M_1 \cdot]}{dt} = -k_{12}[M_1 \cdot][M_2] + k_{21}[M_2 \cdot][M_1] = 0$$

$$\frac{[M_1 \cdot]}{[M_2 \cdot]} = \frac{k_{21}[M_1]}{k_{12}[M_2]}$$

$$r_1 = \frac{k_{11}}{k_{12}} \quad r_2 = \frac{k_{22}}{k_{21}}$$

$$\frac{d[M_1]}{d[M_2]} = \frac{r_1 \frac{[M_1]}{[M_2]} + 1}{r_2 \frac{[M_2]}{[M_1]} + 1}$$

7



The Copolymer Equation; Alternative Forms

$$y = \frac{d[M_1]}{d[M_2]} \quad x = \frac{[M_1]}{[M_2]}$$

$$y = \frac{1 + r_1 x}{1 + \frac{r_2}{x}}$$

$$f_1 = \frac{[M_1]}{[M_1] + [M_2]}$$

$$F_1 = \frac{d[M_1]}{d[M_1] + d[M_2]}$$

$$F_1 = \frac{(r_1 - 1)f_1^2 + f_1}{(r_1 + r_2 - 2)f_1^2 + 2(1 - r_2)f_1 + r_2}$$

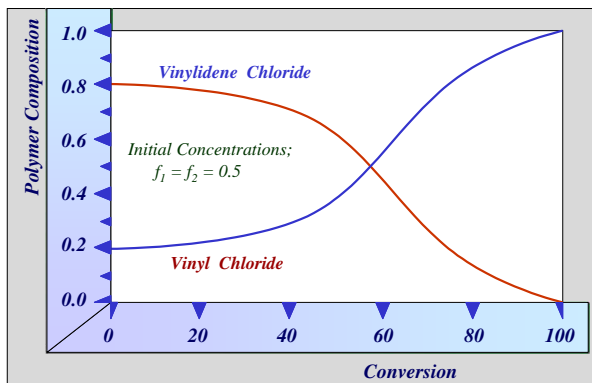
Instantaneous compositions

 f_1 is the monomer composition in the feed F_1 is the monomer composition in the copolymer

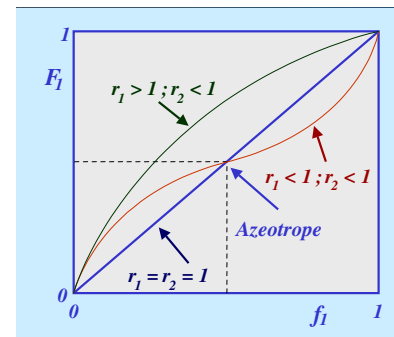
8



Composition Drift



The Instantaneous Copolymer Composition



10



Reactivity Ratios Determination

$$\frac{d[M_1]}{d[M_2]} = \frac{r_1 \frac{[M_1]}{[M_2]} + 1}{r_2 \frac{[M_2]}{[M_1]} + 1}$$

$$y = \frac{d[M_1]}{d[M_2]} \quad x = \frac{[M_1]}{[M_2]}$$

$$y = \frac{1 + r_1 x}{1 + \frac{r_2}{x}}$$

Older Methodologies

- Prepare a number of copolymers as a function of monomer composition.
- Measure the resulting copolymer composition and obtain the reactivity ratios using various plots.

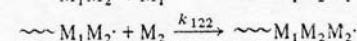
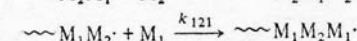
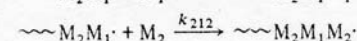
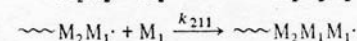
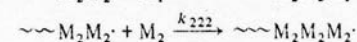
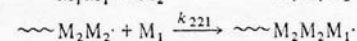
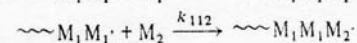
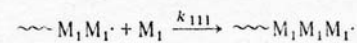
Newer Methodologies

- Measure sequence distributions using nmr and/or $\langle k_p \rangle$ with pulsed experiments.

11



Penultimate Effect Model



$$r_1 = \frac{k_{111}}{k_{112}} \quad r_1' = \frac{k_{211}}{k_{212}}$$

$$r_2 = \frac{k_{222}}{k_{221}} \quad r_2' = \frac{k_{122}}{k_{121}}$$

12



Penultimate Model

(4 parameters, 8 rate constants)

$$\frac{dM_1}{dM_2} = \frac{1 + r_{21} \frac{M_1 r_{11} M_1 + M_2}{M_2 r_{21} M_1 + M_2}}{1 + r_{12} \frac{M_2 r_{22} M_2 + M_1}{M_1 r_{12} M_2 + M_1}}$$

$$r_{11} = k_{111}/k_{112}, r_{21} = k_{211}/k_{212}$$

$$r_{22} = k_{222}/k_{221} \text{ y } r_{12} = k_{122}/k_{121}$$

13



Previous Approaches with Integral Method

• Linear

- Mayo and Lewis, *J. Am. Chem. Soc.*, **1944**, 66, 1994
- Fineman and Ross, *J. Polym. Sci.*, **1950**, 5, 259)
- Kelen and Tudos, *J. Macromol. Sci. Chem.*, **1975**, A9, 1)

• Nonlinear (Error in Variables Method)

- Rossignoli, P.J. and T. A. Duever, *Polym. React. Eng. J.*, **1995**, 3, 361
- Polic *et al.*, *J. Pol. Sci., Part A. Pol. Chem.*, **1998**, 36, 813
- Hagiopol and Frangu, *J. Macromol. Sci.*, **2003**, A40, No 6, 571

All assume constant reactivity ratios !

14



Ultimate vs Penultimate Model

r_i 's in the penultimate model can be seen as functions

$$F_1 = \frac{r_1 f_1^2 + f_1 f_2}{r_1 f_1^2 + 2f_1 f_2 + r_2 f_2^2} < k_p > = \frac{r_1 f_1^2 + 2f_1 f_2 + r_2 f_2^2}{r_1 f_1 / k_{11} + r_2 f_2 / k_{22}}$$

$$r_i^p = r_i \left(\frac{r_i f_i + f_j}{r_i f_i + f_j} \right) \quad k_{iii}^p = k_{iii} \left(\frac{r_i f_i + f_j}{r_i f_i + f_j / s_i} \right)$$

Penultimate Model

- 4 monomer reactivity ratios ($r_i = k_{iii}/k_{ijj}$, $r_i' = k_{iii}/k_{ijj}$) [i, j = 1, 2]
- 2 homopolymerization constants (k_{iii}), and
- 2 radical reactividad ratios ($s_i = k_{iii}/k_{iii}$).

The homopolymerization "constants" (k_{ii} , k_{ij}) can be determined from independent experiments; therefore, the Ultimate Model has 2 parameters to be determined, 4 in the Restricted Penultimate and 6 in the Penultimate Model.



The Bootstrap Model

Harwood, H. J. *Makromol. Chem., Macromol. Symp.* **1987**, 10/11, 331

M_{it} is considered the true monomer concentration in the reaction site and M_i is the overall monomer concentration. The partition coefficient; K is defined as:

$$\frac{M_{it}}{M_{2t}} = K \frac{M_1}{M_2} \quad F_1 = \frac{r_{1p} f_1^2 + f_1 f_2}{r_{1p} f_1^2 + 2f_1 f_2 + r_{2p} f_2^2}$$

$$< k_p > = \frac{f_1 (K(2 + f_1(r_{1p} - 2)) + r_{1p}(1 - f_1)) + r_{2p} K(f_1 - 1)^2}{(1 + f_1(K - 1))(r_{1p} f_1 / k_{11} + r_{2p} K(1 - f_1) / k_{22}}$$

$r_{1p} = r_1 K$ and $r_{2p} = r_2 / K$. Notice that the composition equation is identical to the one of the Ultimate Model. If k_i are known this model has 3 parameters.

16



Facts !!!

- The Ultimate Model (2-4p) for some systems cannot predict the $<k_p>$ behavior. To remedy this problem the Penultimate (6-8p), the Restricted Penultimate (4-6p) and the Bootstrap (3-5p) Models have been used.
- The Penultimate model presents multiplicity of solutions.
- The Bootstrap model presents two feasible solutions. $\rightarrow \rightarrow$ It is not possible to discriminate between the Ultimate-Penultimate-Bootstrap models $\leftarrow \leftarrow$
- The integral method has always been used in which it is assumed that the parameters are constant.

17



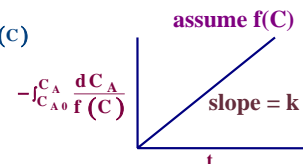
Integral and Differential Methods

I. Integral Method

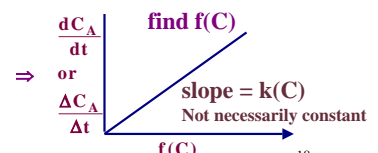
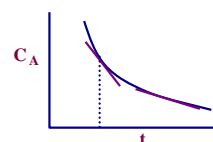
$$-r_A = -\frac{dC_A}{dt} = kf(C)$$

$$\frac{-dC_A}{f(C)} = k dt$$

$$-\int_{C_{A0}}^{C_A} \frac{dC_A}{f(C)} = kt$$



II. Differential Method



18



Integral and Differential Methods Comparison

Integral Method (IM)	Differential Method (DM)
Very robust	Less robust
Few experimental data required	Many experimental data required
Unicity verified <i>a posteriori</i>	Unicity verified <i>a priori</i> or in parallel
Observability not verified generally	Verification of observability
Requires an initial estimate of the parameters	Does not require an initial estimate of the parameters
Does not require data smoothing	Requires data smoothing
Assumes constancy in the parameters (minimizes error between model and the measurement)	Variable parameters with the independent variable (system of algebraic equations)
Contains information from past and present	Contains information at the moment

19



Methodology: Take advantage of both methods

- Fit experimental data (smoothing). Take advantage of IM robustness.
- From conservation balances write rate equations (model). DM
- Determine by means of the observability matrix the parameters to be determined (unicity) and the more robust experimental zone (less error propagation)
- Find functional dependencies of the parameters in terms of the system states. DM
----- This presentation ends here -----
- Use global regression with empirical fits for a better description (with IM)
- Based on first principles corroborate/modify the model



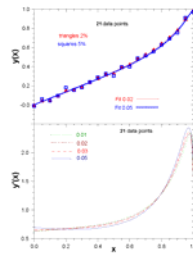
Proposed Approach: Integro-Differential Method.

Two equations (F_1, \dot{F}_1), two unknowns (r_1, r_2)

$$F_1 = \frac{r_1 f_1^2 + f_1 f_2}{r_1 f_1^2 + 2f_1 f_2 + r_2 f_2^2}$$

$$\dot{F}_1 = \frac{f_2 + 2f_1(r_1 - 1)r_2 + f_1^2(r_1 + r_2 - 2r_1 r_2)}{(r_2 + f_1(2 - 2r_2 + f_1(r_1 + r_2 - 2)))^2}$$

$$\det O = \frac{(f_1 - 1)^2 f_1^2}{(r_2 + f_1(2 - 2r_2 + f_1(r_1 + r_2 - 2)))^3}$$



Has no solution in the neighborhood of $f_1 = 0$ and $f_1 = 1$

21



Solution. Dependence of r_1 y r_2 on f_1

$$\hat{r}_1 = \frac{(f_1 - 1)(F_o - 2F_o^2 + (f_1 - 1)f_1 F_p)}{f_1(-2(F_o - 1)F_o + (f_1 - 1)f_1 F_p)}$$

$$\hat{r}_2 = \frac{f_1((3 - 2F_o)F_o - 1 + (f_1 - 1)f_1 F_p)}{f_1(-2(F_o - 1)F_o + (f_1 - 1)f_1 F_p)}$$

F_o is the experimental copolymer composition (F_1) measurement and F_p its derivative (\dot{F}_1)

22



Example MMA-STY (40°C)

Composition, triads and propagation rate constant data

Experimental data were taken from:

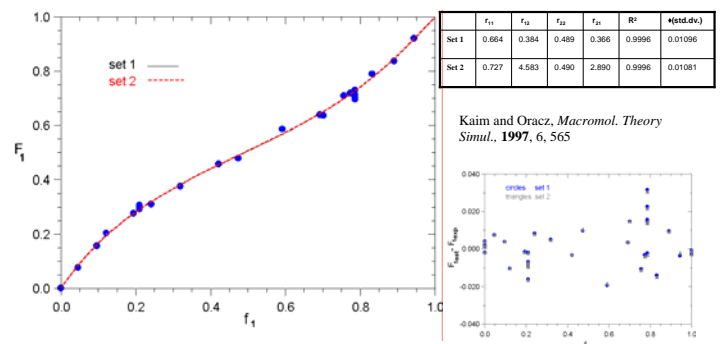
Maxwell, I. A., A. M. Aerdt and A. German. Free Radical Copolymerization: An NMR Investigation of Current Kinetic Models, *Macromolecules*, **1993**, 26, 1956

Fukuda, T., Y-D Ma and H. Inagaki, Free Radical Copolymerization. 3. Determination of Rate Constants of Propagation and Termination for the Styrene/Methyl Methacrylate System. A Critical Test of Terminal-Model Kinetics, *Macromolecules*, **1985**, 18, 17

23

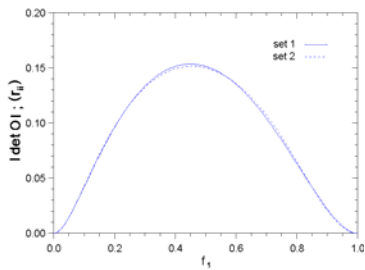


Penultimate Model Data Interpolation (Sty-MMA)





Observability Matrix Determinant



$$\det O = \frac{(f_1 - 1)^2 f_1^2}{(r_2 + f_1(2 - 2r_2 + f_1(r_1 + r_2 - 2)))^3}$$

Has no solution in the neighborhood of $f_1 = 0$ and $f_1 = 1$ 25



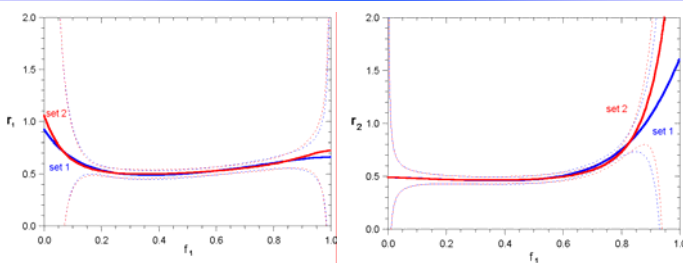
Conclusions (up to this point)

- Set 1 (with Penultimate Model), Reactivity Ratios dependencies on feed composition are more similar to the ID approach ones.
- In the Observable zone the ID approach, with either Set 1 or Set 2 (Penultimate Model used as a smoothing/fitting tool) the two RRs dependencies are not distinguishable.

27



Error Propagation Assessment. Standard Deviation σ (thin lines)

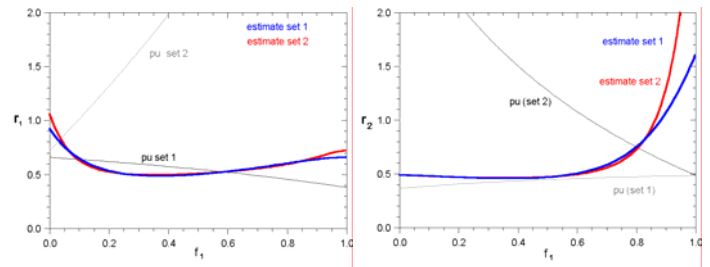


Coincides with Tidwell and Mortimer's assuming constant reactivity ratios (J. Polym. Sci., 1965, A-3, (1), 369

29



Reactivity Ratios Feed Composition Dependencies (ID Approach; thick lines, Penultimate Model; thin lines)



	r_{11}	r_{12}	r_{21}	r_{22}	R^2	$\chi^2(\text{std.dev.})$
Set 1	0.664	0.384	0.489	0.366	0.9996	0.01096
Set 2	0.727	4.583	0.490	2.890	0.9996	0.01081

26



Error Propagation Assessment. Standard Deviation σ

(Mikhail & Ackermann, Observations and Least Squares, H&R, 1976)

$$\Sigma = \mathbf{A} \mathbf{R} \mathbf{A}^T$$

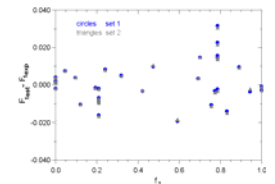
\mathbf{A} is the Observability Matrix inverse

$$\mathbf{R} = \begin{bmatrix} \sigma_{xx}^2 & 0 \\ 0 & 2\sigma_{xx}^2 \end{bmatrix}$$

\mathbf{R} contains the square of the standard deviation obtained from the F_1 vs f_1 fit

$$\Sigma = \begin{bmatrix} s_{xx} & s_{xy} \\ s_{yx} & s_{yy} \end{bmatrix}$$

Σ contains the square of the standard deviation propagated from the F_1 vs f_1 measurements and its derivative towards r_1 and r_2 .



28



Triad Predictions

Maxwell et al., Macromolecules 1993, 26, 1956

Table II
Assignments to Peak Areas (Indicated by Chemical Shift) of the Aromatic C1 Region (Styrene-Centered Triads) in the ¹³C NMR Spectra of Styrene-MMA Statistical Copolymers¹¹

X ¹¹	Y ¹¹	Z ¹¹
147.5-146.8 ppm	146.8-146.15 ppm	145.15-143.5 ppm
$(1 - \sigma_{ms})^2 F_{ms}$	$(1 - \sigma_{ms})^2 F_{ms}$	$(1 - \sigma_{ms}) \sigma_{ms} F_{ms}$
	$2\sigma_{ms}(1 - \sigma_{ms})^2 F_{ms}$	$\sigma_{ms}^2 F_{ms}$
	$\sigma_{ms}^2 F_{ms}$	$\sigma_{ms}^2 F_{ms}$
	$(1 - \sigma_{ms})(1 - \sigma_{ms}) F_{ms}$	
	$\sigma_{ms}(1 - \sigma_{ms}) F_{ms}$	
	$2\sigma_{ms}(1 - \sigma_{ms}) F_{ms}$	

Table III
Assignments to Peak Areas (Indicated by Chemical Shift) of the α -Methyl Region (MMA-Centered Triads) in the ¹³C NMR Spectra of Styrene-MMA Statistical Copolymers¹¹

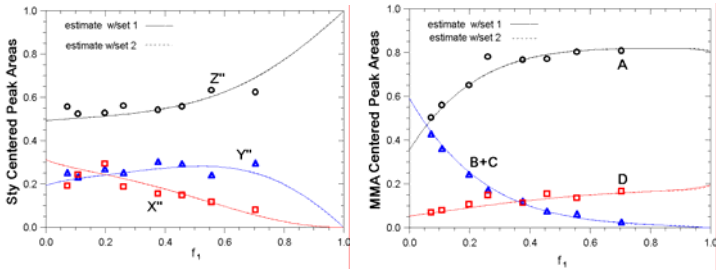
A	B	C	D
23-21.2 ppm	21.2-19.8 ppm	19.8-17.8 ppm	17.8-16.5 ppm
$\sigma_{ms}^2 F_{ms}$	$\sigma_{ms}(1 - \sigma_{ms}) F_{ms}$	$2\sigma_{ms}(1 - \sigma_{ms}) F_{ms}$	$(1 - \sigma_{ms})^2 F_{ms}$
$\sigma_{ms} \sigma_{ms} F_{ms}$	$2\sigma_{ms}(1 - \sigma_{ms}) F_{ms}$	$(1 - \sigma_{ms})(1 - \sigma_{ms}) F_{ms}$	
$\sigma_{ms}^2 F_{ms}$	$(1 - \sigma_{ms})^2 F_{ms}$	$(1 - \sigma_{ms})(1 - \sigma_{ms}) F_{ms}$	
	$(1 - \sigma_{ms})^2 F_{ms}$		

¹¹ This peak shows resonance splitting and appears in both the B and C peak areas.

30



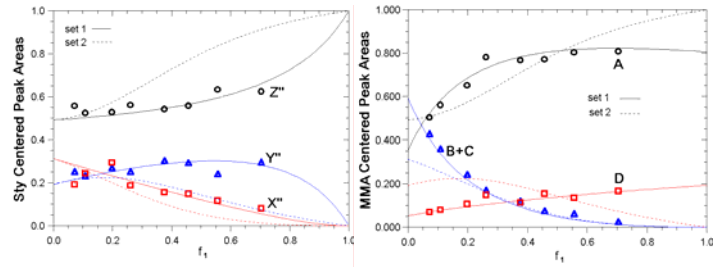
Differential Estimation Areas Prediction



31



Penultimate Model Areas Prediction



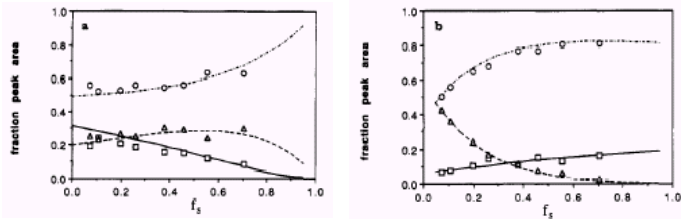
	r_{11}	r_{12}	r_{21}	r_{22}	R^2	$w(\text{std.dev.})$
Set 1	0.664	0.384	0.489	0.366	0.9996	0.01096
Set 2	0.727	4.583	0.490	2.890	0.9996	0.01081

Kaim and Oracz, *Macromol. Theory Simul.*, 1997, 6, 565

32



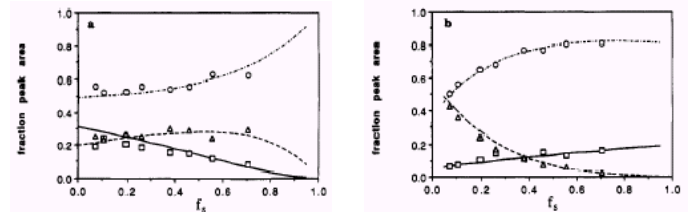
Ultimate Model Predictions ($r_s = 0.48$; $r_m = 0.42$) Maxwell et al., *Macromolecules* 1993, 26, 1956



33



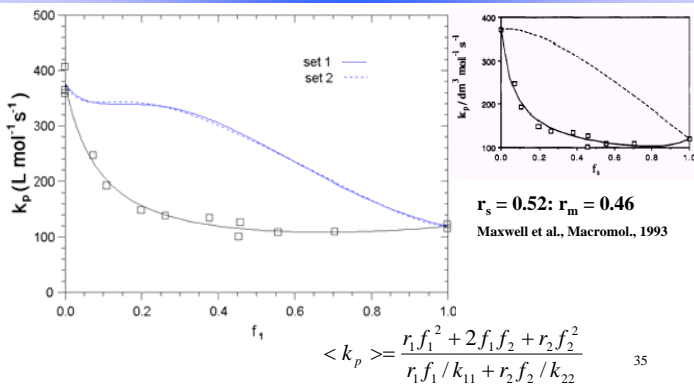
Ultimate Model Fits ($r_s = 0.51$; $r_m = 0.52$) Maxwell et al., *Macromolecules* 1993, 26, 1956



34



Terminal Model k_p Predictions

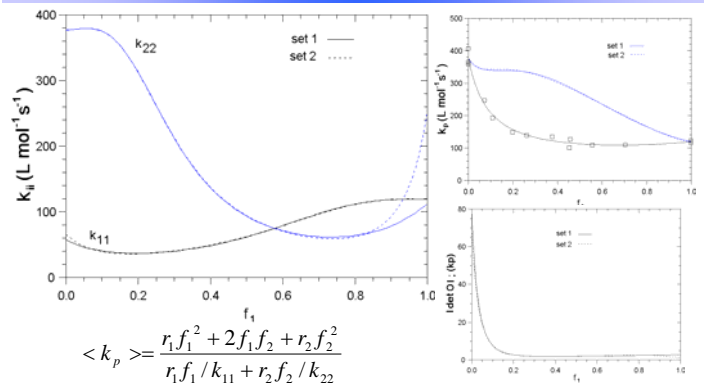


$$\langle k_p \rangle = \frac{r_1 f_1^2 + 2f_1 f_2 + r_2 f_2^2}{r_1 f_1 / k_{11} + r_2 f_2 / k_{22}}$$

35



k_{11} and k_{22} Feed Composition Dependencies. Proceed as before



$$\langle k_p \rangle = \frac{r_1 f_1^2 + 2f_1 f_2 + r_2 f_2^2}{r_1 f_1 / k_{11} + r_2 f_2 / k_{22}}$$



Error Propagation Assessment. Standard Deviation σ

(Mikhail & Ackermann, Observations and Least Squares, H&R, 1976)

$$\Sigma = \mathbf{A} \mathbf{R} \mathbf{A}^T$$

\mathbf{A} is the Observability Matrix inverse for the F_1 and F_1 vs f_1 system

$$\mathbf{Q} = \begin{bmatrix} q_{xx} & 0 \\ 0 & q_{yy} \end{bmatrix}$$

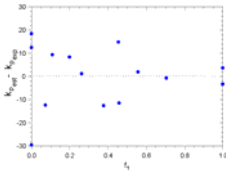
\mathbf{Q} contains the square of the standard deviation obtained from the k_p vs f_1 fit

$$\Xi = \mathbf{B} (\mathbf{Q} + \Sigma) \mathbf{B}^T$$

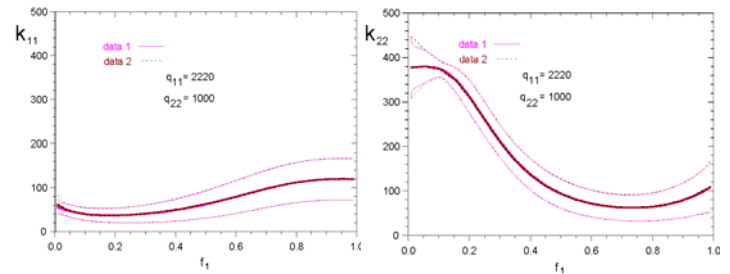
\mathbf{B} is the Observability matrix inverse for the k_p and k_p vs f_1 system

Σ contains the square of the standard deviation propagated from the F_1 vs f_1 measurements and its derivative.

37



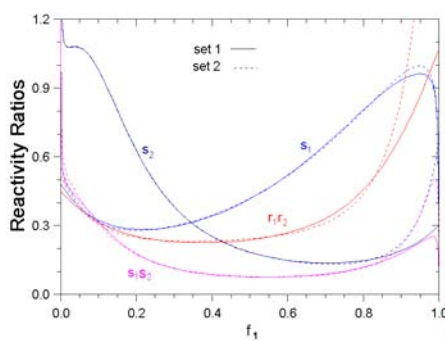
Error Propagation Assessment. Standard Deviation σ (thin lines)



38



Reactivity Ratios Feed Composition Dependencies (r_i and s_i ; $i = 1, 2$)



$$\langle k_p \rangle = \frac{r_1 f_1^2 + 2 f_1 f_2 + r_2 f_2^2}{r_1 f_1 / k_{11} + r_2 f_2 / k_{22}}$$

$$k_{ii}^p = k_{iii} \left(\frac{r_i f_i + f_j}{r_i f_i + f_j / s_i} \right)$$

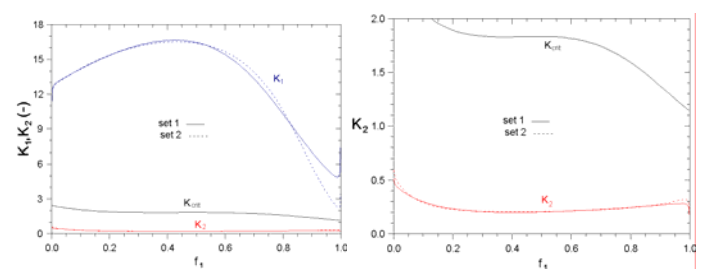
Penultimate Model
radical reactivity ratios

$$s_i = k_{ji} / k_{ii}$$

39



Bootstrap Model: Partition Coefficient (K) Feed Composition Dependency



$$\langle k_p \rangle = \frac{f_1 (K(2 + f_1(r_{1p} - 2)) + r_{1p}(1 - f_1)) + r_{2p} K (f_1 - 1)^2}{(1 + f_1(K - 1))(r_{1p} f_1 / k_{11} + r_{2p} K (1 - f_1) / k_{22})}$$

40



Conclusions

- An Integro-Differential Approach has been presented.
- No modeling *a priori* assumptions were made on reactivity ratios (i.e., constancy).
- A comonomer effect (not reported before) can be detected. A slight solvent effect on the reactivity ratios was observed (reported earlier).
- The observability notion was incorporated (unicity).
- Neither the ultimate nor the penultimate models were adequate (consistent) in terms of parameter constancy.
- One of the Bootstrap Model solutions seems to be the most consistent, based on parameter constancy.
- New experiments should be designed under a differential structure with a more dense mesh of data (more discrimination capability than integral method).
- This method allows us to obtain functional dependencies in terms of the system states.

41



Future Work

- Study the problem of individual parameter **error-propagation-estimation-robustness**
- Evaluation of several reacting systems (at present the method is being tested in other systems).
- From **First Principles** explain the **parameters evolutions**
- Apply to other polymerization systems

42



The End

Thank you for your attention!



MODEL DISCRIMINATION IN MICROEMULSION POLYMERIZATION



F. López-Serrano*, E. Mendizábal^o, J. E. Puig^o and J. Alvarez[#]
 *Universidad Nacional Autónoma de México. ^oUniversidad de Guadalajara. [#]Universidad Autónoma Metropolitana-Iztapalapa. MÉXICO

Emulsion and Micremulsion Differences

Direct Microemulsion Polymerization

- Oil soluble monomers
- Stable monodisperse microlatex
- Final Dp < 50 nm

Importance
 Micelles: 3-5 nm
 Fast reaction rates
 High Mw

Intervals in Emulsion Polymerization

Interval I: $[M] \neq N_p \neq \emptyset$
 Interval II: $[M] = N_p = \emptyset$
 Interval III: $[M] \neq N_p = \emptyset$

Kinetic Theory of Microemulsion Polymerization

Interval I: $[M] \neq N_p \neq \emptyset$
 Interval 2: $[M] \neq N_p \neq \emptyset$

Note: An interval of constant rate is not observed !!

Micremulsion Models

Model by Guo, et al. (1992). Styrene

$$\frac{dN_p}{dt} = k_p N_p (N_p - N_c) + k_{tr} N_p$$

$$\frac{dN_c}{dt} = k_{tr} N_p - k_{tr} N_c$$

$$\frac{dN_m}{dt} = -k_p N_p N_m + k_{tr} N_p N_m$$

Model by Morgan, et al. (1997). C₆MA Pseudomassic

$$\frac{d[M]}{dt} = -k_p \frac{[M] N_p}{M_0}$$

$$[M] = C_m(1-x)$$

Model by Mendizábal, et al. (1997). Styrene

$$\frac{dN_p}{dt} = k_p N_p (N_p - N_c) + k_{tr} N_p$$

$$\frac{dN_c}{dt} = k_{tr} N_p - k_{tr} N_c$$

Integrodifferential Approach

Proposal

- Take advantage of the integral method robustness and the differential one discrimination capability (López-Serrano et al., 2004, AIChE and IECR)
- First step. Smooth experimental data
- Second step verify unicity in the solution and interval zones
- Third step. Analyse constancy of the parametes and compare the with original modeling/thermodynamic hypotheses.
- Corroborate or modify model (based on first principles)

Pseudomassic Model

(de Vries et al. Macromolecules, 2001, 34, 3233)

$$\frac{dx}{dt} = k_p \frac{M_0 \rho}{M_n}$$

$$\frac{dx}{dt} = A(1-x)^b$$

Analytic solution

$$x = 1 - \left[\frac{(1-b)A t^{\frac{1}{1-b}}}{2} \right]^{\frac{1}{1-b}}$$

x = fractional conversion
 p = k_p = rate of initiation
 K_p = propagation rate constant
 M₀ = monomer conc. inside parts.
 M_n = initial monomer concentration

Integrodifferential Estimation

Provided that b ≠ 1. This Eq has two parameters; A and b, then if we have the conversion (y_i) and its derivative measurements (y_i') against time, then we have:

$$y_i = A(1-y_{o,i})^b$$

Solution:

$$A = \frac{2(1-y_{o,i})^{1+b} - 1}{(b-1)t^2}$$

$$b = \frac{\ln\left(\frac{y_i}{1-y_{o,i}}\right)}{\ln(1-y_{o,i})}$$

The solution exists always for b ≠ 1 and det O ≠ 0, t ≠ 0, y_o ≠ 1 and y_i ≠ 0

Approaches to Model Microemulsion Polymerization

	Guo et al. (1992)	Morgan et al. (1997)	Mendizábal et al. (1997)
Imp	Cell-A	Cell-A	Micellar + constant
Particle generation	N _p = N _u (exp(kt)) Micellar	N _p = K ₁ Micellar	Micellar and homogeneous (N _p , N _u) (flow = 100 km)
Capture coefficients	k ₁₀ > k ₁₁ second	k ₁₀ = k ₁₁ first	k ₁₀ > k ₁₁ second
rate of capture of particles (order)	second	first	second
rate of desorption (order)	second	second	first
System	Compartmentalized	Pseudo-hulk (neglect water phase termination)	Compartmentalized
Describes	Conversion, particle generation	Conversion	Conversion, particle generation, molecular weight

Modeling Contradictions

- Monomer inside particles
- Mass balance of monomer in droplets (micelles)
- Nucleation along the whole reaction
- First and second order capture and exit rate constants
- Pseudo-hulk vs compartmentalized systems
- Order of magnitude difference between capture coefficients particles vs droplets
- Redundant equations non steady state on N_i and N_c (Guo and Mendizábal)

Conversion

$$\frac{dx}{dt} = k_p \frac{M_0 \rho N_p}{M_n}$$

Total No. Particles

$$\frac{dN_p}{dt} = \rho_p N_p$$

Both models are analogous !

Results

Conversion Curves

Initiator V50: (▲) nC₆MA, 0.24 mM; (●) nC₇MA, 0.061 mM and (○) tC₆MA, 0.24 mM; (◐) tC₆MA, 0.061mM. (de Vries et al., 2001)

Conversion Derivative and Observability

Parameter Estimates

$A = k_p \frac{C_m \rho}{M_0}$; $M_p = C_m(1-x)^b$

Initiator V50: (▲) nC₆MA, 0.24 mM; (●) nC₇MA, 0.061 mM and (○) tC₆MA, 0.24 mM; (◐) tC₆MA, 0.061mM. b = 1.4 (de Vries et al., 2001)

Conclusions

- An Integro-Differential Approach has been presented. The observability notion was incorporated (unicity).
- With only conversion measurements it is not possible to determine if microemulsion polymerization is compartmentalized or pseudomassic.
- For tC₆MA the parameter b seemed to be higher than the one reported before (de Vries et al., 2001).
- New experiments should be designed under a differential structure with a more dense mesh of data (more discrimination capability than integral method). Study measurement propagation error on estimates.
- This method allows to obtain the parameters functional dependencies in terms of the system states and have a better model assessment.

Institute for Polymer Research
27th Annual Symposium

Symposium documents for

Steve Teertstra

Abstract

Presentation

Viscoelastic Properties of Arborescent Polystyrene-*graft*-Polyisoprenes

Steve Teertstra

Department of Chemistry, University of Waterloo

Arborescent graft polymers are highly branched, high molecular weight polymers that are constructed by coupling of linear polymer chains in a “graft-on-graft” synthetic strategy. The first examples of arborescent polymers reported in the literature were comprised entirely of polystyrene chains.¹ The initial step of the synthesis involves grafting of polystyrene chains onto a linear polystyrene backbone containing randomly-spaced reactive coupling sites, to produce a comb-branched structure termed a generation G0 arborescent polymer. The introduction of new reactive sites on the comb-branched polystyrene, followed by further grafting with polymeric chains, yields a twice-grafted G1 arborescent polystyrene. Repeated functionalization and grafting reactions yields arborescent polystyrenes up to generation G4. The arborescent polystyrenes have been investigated extensively, both in solution² and in the bulk³, to determine the influence of structural variation on the physical properties. The conclusions drawn from these studies show that arborescent polystyrenes act increasingly as rigid spheres as either the branching density is increased or the size of the grafted arms is reduced.⁴

More recently, the preparation of several different arborescent copolymers was achieved by grafting of polymer chains of a different type onto polystyrene substrates. One such copolymer was prepared by the grafting of polyisoprene chains onto polystyrene substrates of different generations to obtain arborescent polystyrene-*graft*-polyisoprenes.⁵ These arborescent isoprene copolymers possess a hard-core-soft-shell topology, of polystyrene and polyisoprene phases, respectively. This concept is illustrated in Figure 1 for a series of copolymers ranging from overall generation G0 (once grafted) to G3 (four times grafted). The synthesis of the isoprene copolymers is well established, however, there has been very little work performed to date involving physical property studies of these highly branched elastomeric materials. In the present work, the dynamic mechanical behavior of a series of well-defined arborescent polystyrene-*graft*-polyisoprenes was studied as a function of polyisoprene arm length and grafting generation.

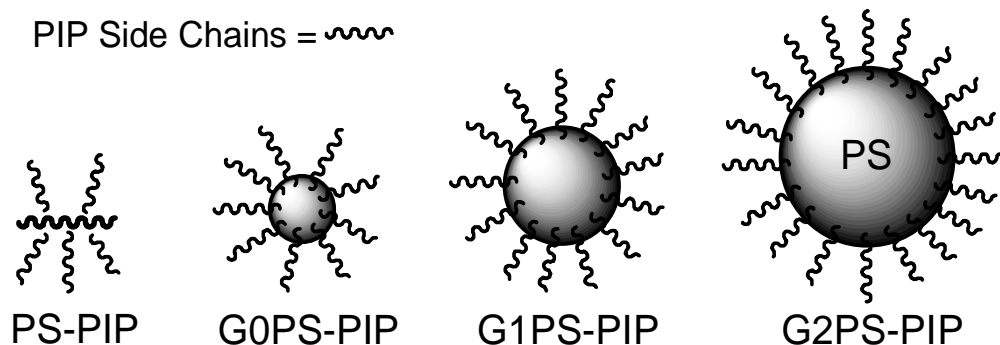


Figure 1 Hard core-soft shell topology of arborescent polystyrene-graft-polyisoprenes.

The moduli-frequency curves measured for the G0 and G1 copolymers display similar features to those found in other highly branched polymer systems, such as star and comb polymers. The G2 and G3 copolymer moduli-frequency curves displayed very different features, similar to networks or filled polymer systems. The significant change in behavior observed within the dynamic moduli-frequency curves is caused by a topological change from flexible branched structures at generation G1 or lower, to spherically shaped rigid molecules at generation G2 and higher. This change in behavior at generation G2 has been observed in previous studies involving arborescent polystyrenes.^{2(a), 3(c)} Partial failure of time-temperature superposition was observed during construction of the master moduli-frequency curves for some of the highest generation copolymers. Superposition of the low frequency data onto one single master curve could not be performed for the G2 and G3 copolymers containing short polyisoprene arms. The proportion of polystyrene within these molecules was significantly large (8 – 28 % w/w) to contribute to the overall modulus of the material, causing thermorheological complexity. The modulus shift factors required to fit the moduli-frequency data for the G2 and G3 copolymers differed significantly from those required to fit the linear polyisoprenes, G0, and G1 copolymers. This is further evidence of a change in molecular topology at generation 2, as increased structural rigidity within the G2 and G3 molecules hinders thermal expansion.

The terminal region of the moduli-frequency curves were used to determine the zero-shear viscosity η_0 , steady-state compliance J_s^0 , and terminal relaxation times. The arborescent isoprene copolymers are characterized by low zero-shear viscosities

compared to linear polyisoprenes of comparable molecular weight, as observed in Figure 2. The zero-shear viscosities measured for the G0 and G1 copolymers increased with polyisoprene arm molecular weight. The upturn observed in the zero shear viscosity η_0 versus molecular weight curves for the G0 and G1 copolymers with increasing polyisoprene arm molecular weight was evidence of viscosity enhancement by entanglement coupling of the longer polyisoprene arms of adjacent molecules. The zero-shear viscosities for the G2 copolymers, estimated by a steady-stress creep experiment, show a decrease with increasing polyisoprene arm molecular weight. This behavior reflects the change in molecular topology of the G2 copolymers to a more rigid, spherical structure. The terminal properties for G2 copolymers were more strongly influenced by the branching density rather than the molecular weight of the polyisoprene arms.

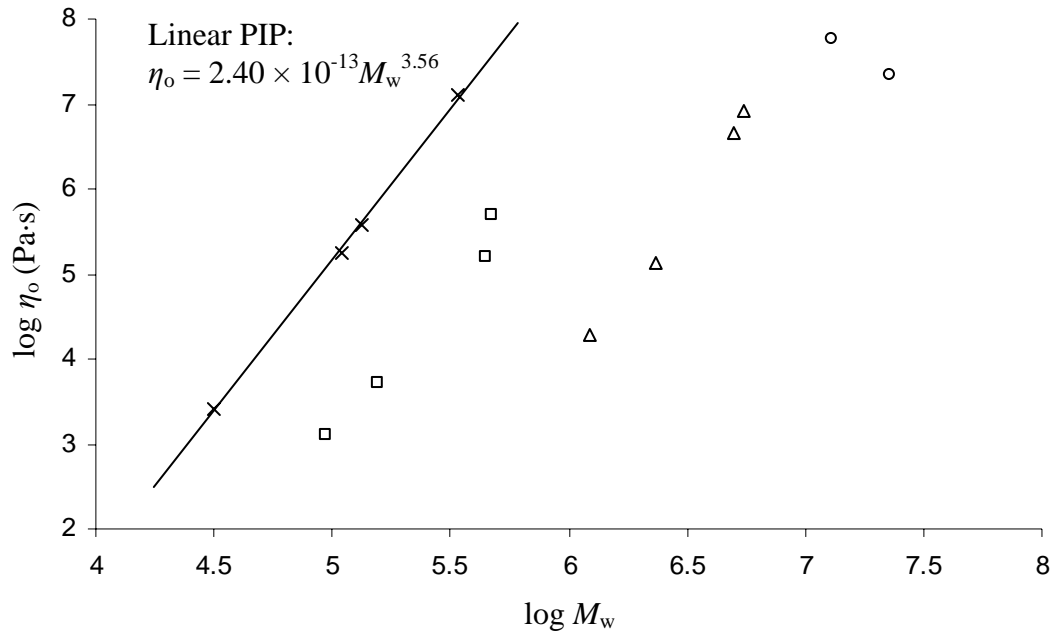


Figure 2 Zero-shear viscosity (η_0) at 20°C versus molecular weight (M_w): (×) linear polyisoprene; (□) G0 copolymers; (Δ) G1 copolymers; (○) G2 copolymers.

The higher generation copolymers (G2 and G3) were characterized by increasingly long relaxation times that could not be measured within the time scale of the rheological measurements, as configurational renewal of molecules was severely hindered by structural stiffness within the highly branched copolymers. The steady-shear compliance J_s^0 was observed to increase roughly monotonically with molecular weight

for the G0 and G1 copolymers, as observed in Figure 3. This behavior is quite different from linear polyisoprenes for which J_s^0 is usually independent of molecular weight. The highly branched arborescent isoprene copolymers are characterized by low viscosity and high elasticity, an interesting combination of properties which show the potential of these materials as rheological modifiers.

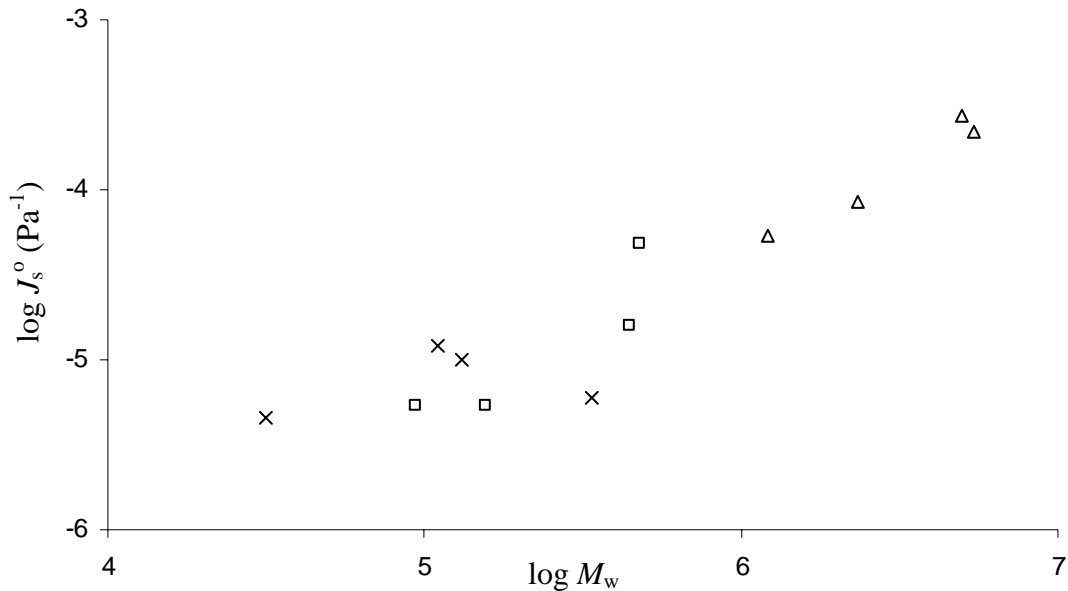


Figure 3 Steady-shear compliance J_s^0 at 20°C against M_w : (x) linear polystyrene; (□) G0 copolymers; (Δ) G1 copolymers.

1. Gauthier, M; Möller, M. *Macromolecules* **1991**, *24*, 4548.
2. (a) Gauthier, M.; Tichagwa, L. *Polymer* **1997**, *38*, 6363; (b) Choi, S.; Briber, R.M.; Bauer, B.J.; Topp, A.; Gauthier, M.; Tichagwa, L. *Macromolecules* **1999**, *32*, 7879; (c) Striolo, A; Prausnitz, J.M.; Bertuccio, A.; Kee, R.A.; Gauthier, M. *Polymer* **2001**, *42*, 2579.
3. (a) Sheiko, S.S.; Gauthier, M.; Möller, M. *Macromolecules* **1997**, *30*, 2343; (b) Choi, S.; Briber, R.M.; Bauer, B.J.; Liu, D-W.; Gauthier, M. *Macromolecules* **2000**, *33*, 6495. (c) Hempenius, M.A.; Zoetelief, W.F.; Gauthier, M.; Möller, M. *Macromolecules* **1998**, *31*, 2299.
4. Teerstra, S.J.; Gauthier, M. *Prog. Polym. Sci.* **2004**, *29*, 277
5. (a) Kee, R.A.; Gauthier, M. *Macromolecules* **1999**, *32*, 6478; (b) Li, J.; Gauthier, M.; Teertstra, S.J.; Xu, H.; Sheiko, S.S. *Macromolecules* **2004**, *37*, 795.

Viscoelastic Properties of Arborescent Polystyrene-*graft*-Polyisoprenes

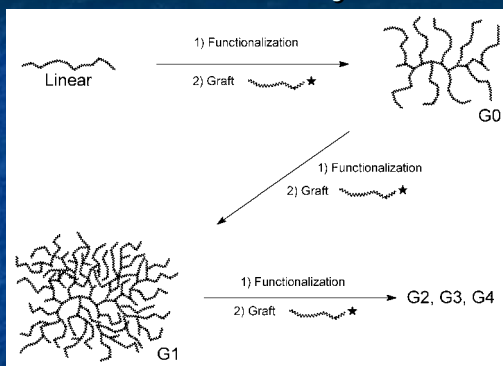
Steve Teertstra
Department of Chemistry
University of Waterloo

Institute for Polymer Research
27th Annual Symposium
May 17 2005

Outline

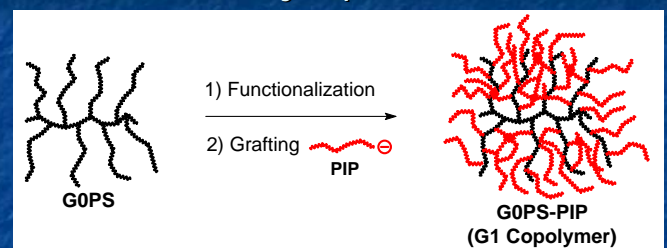
- Introduction: Arborescent Polymers
- Arborescent Polystyrene-*graft*-Polyisoprenes
- Synthesis / Characterization
- Rheological Measurements
 - Methods
 - Moduli-frequency master curves for linear PIP, arborescent isoprene copolymers
 - Zero-shear viscosity
 - Steady-state compliance
 - Relaxation modeling
 - Time-temperature superposition failure
- Conclusions

Arborescent Polymers



- Anionic polymerization and grafting techniques yield highly branched polymers with controlled structures

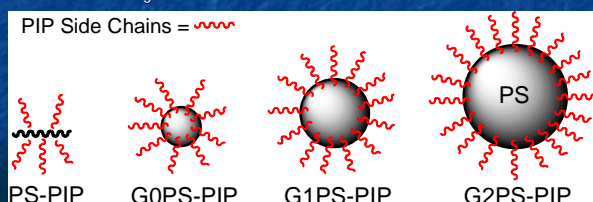
Arborescent Polystyrene-*graft*-Polyisoprenes



- Living anionic polyisoprene chains grafted onto functionalized polystyrene cores of different sizes
- Hard-core-soft-shell topology
- Composition and physical properties dominated by the shell polymer – Highly Branched Elastomer

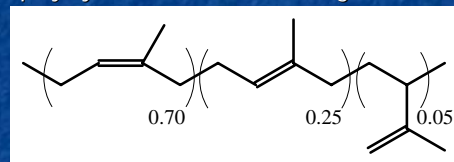
Viscoelastic Properties of Arborescent Isoprene Copolymers

- Synthesis of arborescent polystyrene-*graft*-polyisoprenes well established
- Viscoelastic properties have not been investigated
- Interesting properties due to heterogeneous morphology?
- Copolymer molecules are envisioned to resemble multi-arm stars with a rigid polystyrene core at temperatures below the T_g for PS ($\sim 100^\circ\text{C}$)



Synthesis of Arborescent *cis*-1,4-Isoprene Copolymers

- A series of arborescent copolymers prepared by coupling of *cis*-1,4- polyisoprene chains of different lengths with polystyrene cores of different generations



cPIP
 $T_g \approx -60^\circ\text{C}$ to -70°C

- Isoprene polymerized in hexanes results in a high *cis*-1,4- isoprene units content
- Elastomeric material (low softening temperature) analogous to natural rubber
- G0, G1, G2 and G3 copolymers prepared

Molecular Weight Characterization Data

	cPIP Side Chains		Graft Copolymer		
	M_w^{LS}	M_w/M_n^{SEC}	M_w^{SEC}	M_w/M_n^{SEC}	M_w^{LS}
PS-cPIP5	4860	1.08	73 000	1.08	94 200
PS-cPIP10	9370	1.06	98 000	1.06	157 000
PS-cPIP30	33 900	1.06	350 000	1.06	446 000
PS-cPIP40	40 400	1.05	410 000	1.05	477 000
G0PS-cPIP5	4950	1.09	290 000	1.07	1 120 000
G0PS-cPIP10	9830	1.07	370 000	1.05	2 040 000
G0PS-cPIP30	26 100	1.06	1 050 000	1.27*	4 990 000
G0PS-cPIP40	40 100	1.05	1 060 000	1.37*	5 450 000
G1PS-cPIP5	4800	1.07	1 330 000	1.40*	13 000 000
G1PS-cPIP30	29 800	1.06	-	-	22 600 000
G2PS-cPIP5	4810	1.07	-	-	42 700 000
G2PS-cPIP30	27 500	1.06	-	-	53 100 000

* - Band broadening effects of ultra-high molecular weight SEC columns

PIP Content and Microstructure

	PIP Content / % w/w		PIP Microstructure / mol %		
	1H NMR	M_w	cis-1,4-	trans-1,4-	3,4-
PS-cPIP5	94	93	69	24	7
PS-cPIP10	95	96	69	21	10
PS-cPIP30	>98	>98	71	23	7
PS-cPIP40	>98	>98	73	20	7
G0PS-cPIP5	93	92	69	24	7
G0PS-cPIP10	95	96	70	20	10
G0PS-cPIP30	>98	>98	71	22	7
G0PS-cPIP40	>98	>98	73	20	7
G1PS-cPIP5	94	92	68	23	9
G1PS-cPIP30	>98	95	72	22	6
G2PS-cPIP5	90	72	68	23	9
G2PS-cPIP30	90	78	71	23	6

Molecular Dimensions and Glass Transition Temperature Data

	# PIP Arms	Core Radius (nm)	Shell Thickness (nm)	Side Chain T_g (°C)	Copolymer T_g (°C)
PS-cPIP5	18	1.4	2.1	-65.7	-64.2
PS-cPIP10	16	1.4	2.7	-63.7	-61.6
PS-cPIP30	14	1.4	4.4	-64.1	-62.4
PS-cPIP40	12	1.4	4.5	-63.5	-62.5
G0PS-cPIP5	210	3.2	6.7	-65.5	-63.6
G0PS-cPIP10	200	3.2	8.1	-64.3	-62.3
G0PS-cPIP30	170	3.2	12	-64.9	-64.0
G0PS-cPIP40	130	3.2	12	-64.3	-63.1
G1PS-cPIP5	2400	7.4	16	-66.3	-63.2
G1PS-cPIP30	720	7.4	20	-65.2	-63.5
G2PS-cPIP5	6400	17	25	-66.2	-63.1
G2PS-cPIP30	1500	17	25	-64.6	-63.3

Linear Polyisoprenes

- Several linear polyisoprenes synthesized to serve as baseline materials for rheological studies
- Identical conditions used as the polymerization of PIP side chains for the copolymers

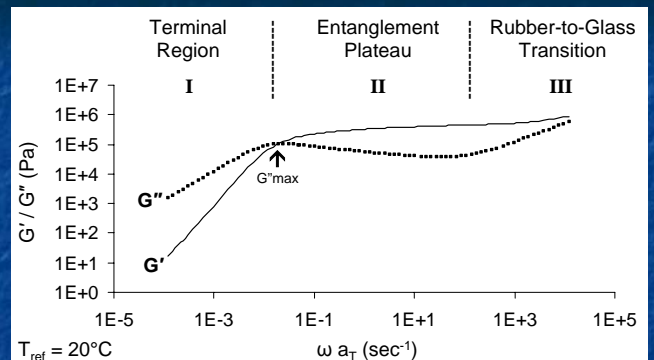
Polymer	M_w	M_w/M_n	PIP Microstructure / mol%			T_g / °C
			cis-1,4-	trans-1,4-	3,4-	
cPIP30	32 000	1.05	72	22	6	-64.2
cPIP110	110 000	1.06	75	20	5	-64.9
cPIP130	132 000	1.06	76	19	5	-65.0
cPIP340*	340 000	1.07	78	17	5	-64.7
cPIP1M*	1 150 000	1.19	78	16	6	-64.6

* - polymers prepared using a semi-bulk polymerization method

Rheology

- 0.25 % w/w *N,N'*-diphenyl-1,4-phenylene-diamine added to stabilize polyisoprene samples
- Rheometrics RDSII used for dynamic (oscillatory) measurements
 - Parallel plate geometry (25 mm diameter)
 - Plate gaps ranging from 1.5 to 3 mm
 - Strain sweeps performed to determine the linear viscoelasticity range (1 – 20%)
 - Frequency sweeps performed at set temperatures ranging from -40°C to 80°C
 - Time-temperature superposition used to build master moduli-frequency curves ($T_{REF} = 20^\circ\text{C}$)
- Paar Physica UDS200 used for steady-stress creep experiments

Linear cPIP340 Master Curve



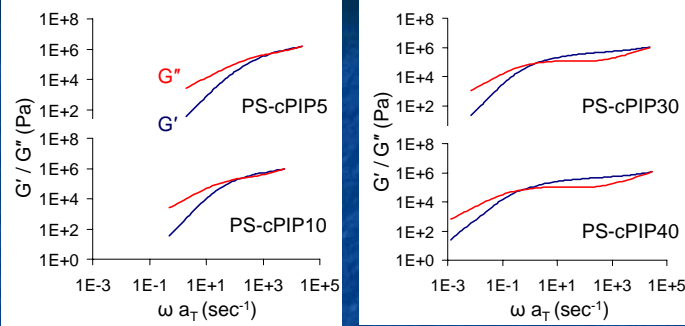
Zero-shear viscosity:

$$\eta_0 = \lim_{\omega \rightarrow 0} \frac{G''(\omega)}{\omega}$$

Zero-shear compliance:

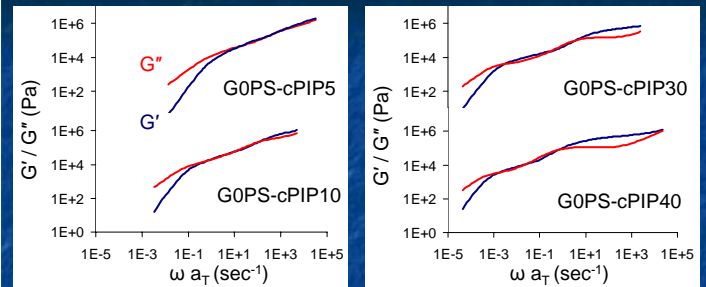
$$J_e^0 = \frac{1}{\eta_0^2} \lim_{\omega \rightarrow 0} \frac{G'(\omega)}{\omega^2}$$

G0 Copolymer Mastercurves



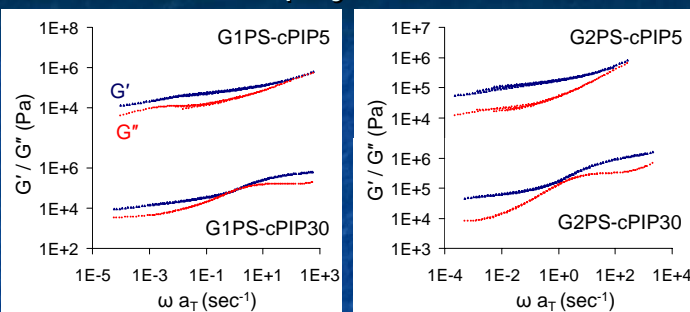
- No entanglement plateau for short PIP arms
- Moduli-frequency curves similar to star and comb-branched polymers (flexible branched polymers)
- Terminal relaxation shifted to lower frequency with increasing arm molecular weight

G1 Copolymer Mastercurves



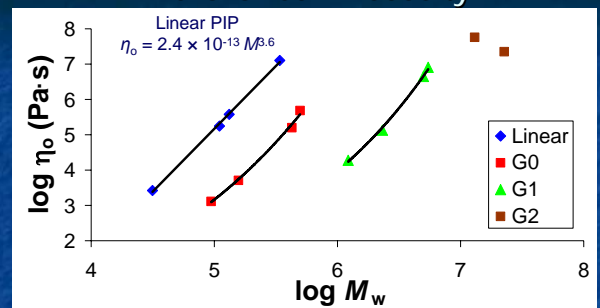
- 2 distinct maxima observed in G'' curves corresponding to arm (short time) and molecular motions (long time)
- Modulus curves similar to highly branched star polymers and G1 arborescent polystyrenes
- Terminal relaxation shifted to lower frequency with increasing arm molecular weight

G2 and G3 Copolymer Mastercurves



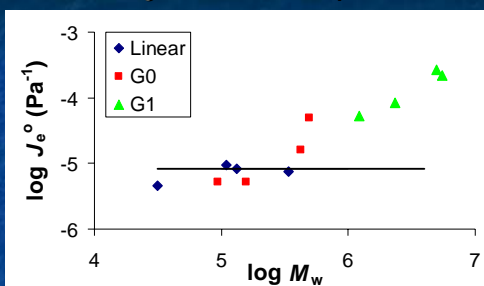
- No terminal region observed (hindered flow)
- $G' > G''$ over entire frequency range
- Modulus curves similar to networks or filled polymers
- G2 and G3 copolymers behave as more rigid spherical molecules

Zero-Shear Viscosity



- η_0 much lower for copolymers compared to linear polyisoprenes of comparable M_w due to branching
- Viscosity enhancement for copolymers with long arms due to entanglement coupling
- Branching density is the dominant factor effecting η_0 in G2 copolymers (hard sphere behavior)

Steady-state Compliance



- J_e^0 independent of M_w for linear PIP above $M_w \approx 50,000$
- Compliance increases with M_w for G0 and G1 copolymers more than 10 fold compared to linear PIP
- Interesting combination of properties: high degree of elasticity with low viscosity

Relaxation Times

Maxwell Model:

$$\eta'(\omega) = \eta_\infty' + G_m \sum_{i=1}^N \frac{\tau_{m,i}}{1 + \omega^2 \tau_{m,i}^2} + G_n \sum_{j=1}^N \frac{\tau_{n,j}}{1 + \omega^2 \tau_{n,j}^2}$$

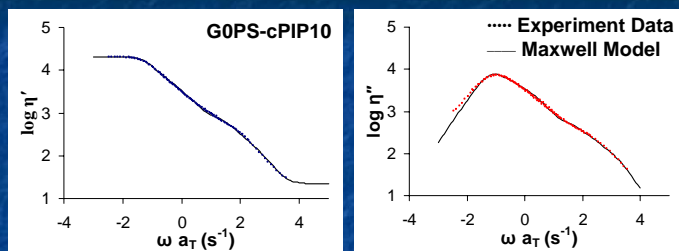
$$\eta''(\omega) = \eta_\infty'' + G_m \sum_{i=1}^N \frac{\omega \tau_{m,i}^2}{1 + \omega^2 \tau_{m,i}^2} + G_n \sum_{j=1}^N \frac{\omega \tau_{n,j}^2}{1 + \omega^2 \tau_{n,j}^2}$$

where:

$$\tau_{m,i} = \tau_{m,1} / i^2 \quad \tau_{n,j} = \tau_{n,1} / j^2$$

- Experimental dynamic viscosity curves fit with a generalized Maxwell model
- Two groups of long ($\tau_{m,i}$) and short ($\tau_{n,i}$) relaxation times with appropriate relaxation strengths (G_m and G_n) entered into the model
- Each group of times expressed relative to the longest time for each relaxation mode

Relaxation Times



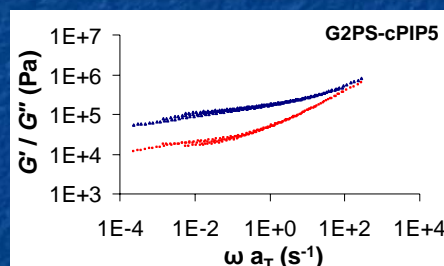
- G0 copolymers with long arms ($M_w = 30\,000, 40\,000$) and all G1 copolymers were fit with 2 groups of relaxation times
- G0 copolymers with short arms ($M_w = 5000, 10\,000$) and linear PIP fit with a single group of relaxation times

Relaxation Times

Polymer	$\tau_{G''_{max}}$ (s)	$\tau_{n,1}$ (s)	$\tau_{m,1}$ (s)
cPIP30	0.0063		0.013
cPIP110	0.25		2.1
cPIP130	0.55		4.0
cPIP340*	50		100
PS-cPIP5	0.001		0.0063
PS-cPIP10	0.0063		0.032
PS-cPIP30	0.13	0.79	0.26
PS-cPIP40	0.83	2.9	16
G0PS-cPIP5	0.001	0.0032	1.1
G0PS-cPIP10	0.0079	0.025	13
G0PS-cPIP30	0.13	1.1	1100
G0PS-cPIP40	0.78	3.4	2000

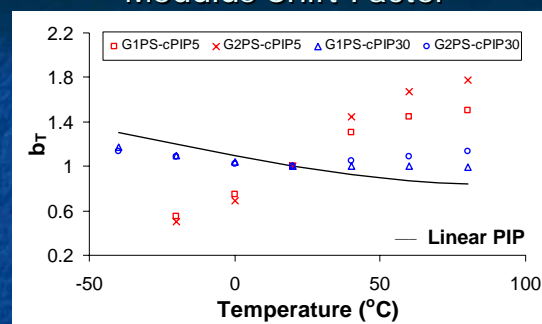
- Relaxation times estimated from G''_{max} are comparable for similar PIP arm M_w
- Short time relaxations ($\tau_{n,i}$) determined from the Maxwell model fit are comparable to G''_{max} times
- Long time relaxations ($\tau_{m,i}$) increase with PIP arm M_w

Partial Failure of Time-temperature Superposition (TTS)



- Partial failure of TTS at low frequencies ($T > 0^\circ$) for G2 and G3 copolymers with short PIP arms due to participation of polystyrene core to overall modulus of material (thermorheological complexity)
- Similar effects observed with linear polyisoprenes filled with silica or polystyrene particles

Modulus Shift Factor



Modulus shift factor:

$$b_T = \frac{\rho T}{(\rho T)_0}$$

- Modulus fitting parameters for G2 and G3 copolymers with short PIP arms display an opposite temperature dependence
- Further evidence of polystyrene core participation to the overall modulus in G2 and G3 copolymers

Conclusions: Rheology of Polystyrene-graft-Polyisoprene Copolymers

- G0 and G1 copolymers behave as flexible branched polymers
- G2 and G3 copolymers exhibit hard sphere behavior
- η_0 enhancement observed for long PIP arms
- J_e^0 increases with molecular weight (high elasticity)
- Arm relaxation times comparable for copolymers with similar molecular weight PIP arms
- Molecular (terminal) relaxation times increase with PIP arm molecular weight
- Polystyrene core acting as a filler in G2 and G3 copolymers causing thermorheological complexity
- Interesting properties: potential rheological modifiers

Acknowledgements

Mario Gauthier
Jasmin Bhatia
Matt Scora
Gauthier Group

Department of Chemistry



Institute for Polymer Research
27th Annual Symposium

Symposium documents for

Costas Tzoganakis

Abstract

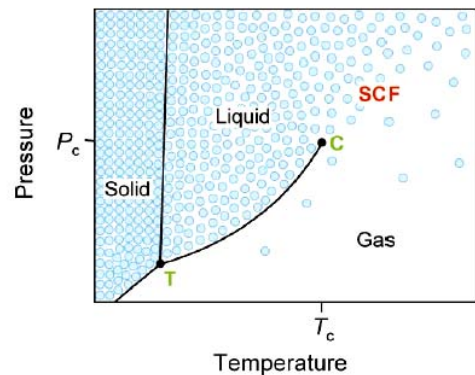
Presentation

PROCESSING OF POLYMERS WITH SUPERCRITICAL CO₂

Professor Costas Tzoganakis
Department of Chemical engineering
University of Waterloo
200 University Avenue West
Waterloo, Ontario N2L 3G1
CANADA
E-mail: ctzogan@uwaterloo.ca

ABSTRACT

Supercritical fluids (SCF) have recently achieved a widespread attention in the synthesis and processing of thermoplastic polymers. A supercritical fluid (SCF) is a substance that is compressed beyond the critical pressure and heated above the critical temperature (see figure). At these conditions, the vapour and liquid phases become indistinguishable and the substance behaves as a single phase. Although the SCF remains as a single phase, its density can be easily “tuned” from gas to liquid values merely by changing the pressure of the fluid. While the density of an SCF is liquid like, the diffusivity and viscosity are intermediate between the gas and liquid values. The motivation for using SCFs in polymer processing stems not just from the environmental impetus for their use as benign solvents. Sorption of SCFs into polymers results in their swelling and changes in mechanical and physical properties of these polymers. The higher diffusivities of SCFs provide a means of improving mass transfer characteristics, while lower viscosities assist in reduced energy for pumping. In polymer extrusion, SCFs are injected in extruders for the purpose of plasticizing a polymer, reducing the melt viscosity and increasing diffusion rates. This leads to reduced pumping requirements and thermal degradation as well as it provides interesting potential for chemical modification in reactive extrusion operations.



In this presentation, results will be presented from studies in four different areas. In the first one, the effect of supercritical CO₂ on the viscosity and elasticity of polymer melts during extrusion will be highlighted for polyethylene and polystyrene resins. In the second one, the effect of

supercritical CO₂ on the morphology of binary blends will be addressed in view of the influence of scCO₂ on the interfacial tension. In the third study, we will address the role of supercritical CO₂ in reactive extrusion processes by discussing results from grafting and reactive blending experiments. In the fourth study, the application of scCO₂ in an extrusion process for the devulcanization of rubber crumb will be presented. Finally, current research efforts on the development of a scCO₂-assisted fibre spinning processes will be highlighted.

PROCESSING OF POLYMERS WITH SUPERCRITICAL CO₂

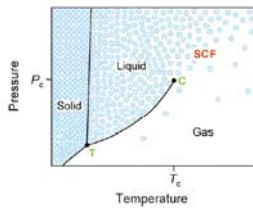
Prof. Costas Tzoganakis
 Institute for Polymer Research
 Department of Chemical Engineering
 University of Waterloo
 Waterloo, Ontario
 CANADA

OUTLINE

- Introduction
 - Supercritical Fluids (SCFs) / Applications
- Polymer Extrusion Applications
 - Plasticization / Effects on viscoelastic behavior
 - Polymer Blending / Interfacial tension and morphology
 - Reactive Extrusion
 - Rubber Devulcanization
- Closing Remarks
- Acknowledgements

INTRODUCTION

Supercritical Fluids (SCFs) / Applications



- vapour and liquid phases are indistinguishable
- SCF density can be easily “tuned” from gas to liquid values merely by changing the pressure of the fluid
- density is liquid like / diffusivity and viscosity are intermediate between the gas and liquid values

INTRODUCTION

Supercritical Fluids (SCFs) / Applications

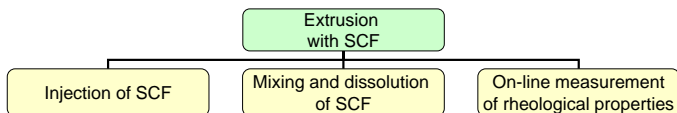
Motivation for using sc CO₂ in polymer extrusion

- Benign solvent
- Changes in mechanical and physical properties of polymers
- Higher diffusivities improve mass transfer characteristics
- Lower viscosities assist in reduced energy for pumping

References

A.I. Cooper, *J. Mat. Chem.*, **10**, 207-234 (2000).
 S.G. Kazarian, *Polymer Science, Ser. C.*, **42**, 78-101 (2000).
 P.G. Jessop and W. Leitner, “Chemical Synthesis Using Supercritical Fluids”, Weinheim, Wiley-VCH (1999).
 J.L. Kendall, D.A. Canelas, J.L. Young and J.M. DeSimone, *Chem. Rev.*, **99**, 543 (1999).
 C.A. Eckert, B.L. Knutson and P.G. Debenedetti, *Nature*, **382**, 313 (1996).

POLYMER EXTRUSION APPLICATIONS



POLYMER EXTRUSION APPLICATIONS

Plasticization / Effects on viscoelastic behavior

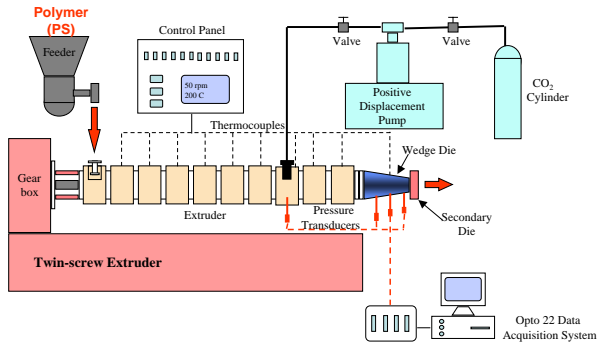
- Supercritical CO₂ (scCO₂)
- Research Studies
 - Shear Viscosity
 - Capillary, Slit, Wedge Dies
 - $\eta = \eta(\dot{\gamma}, P, T, C_{CO_2})$
 - Free Volume Scaling Model
 - Entrance Flow
 - Entrance Pressure Drop
 - Elongational Viscosity

POLYMER EXTRUSION APPLICATIONS

Plasticization / Effects on viscoelastic behavior



Viscosity of PS/CO₂ Solutions

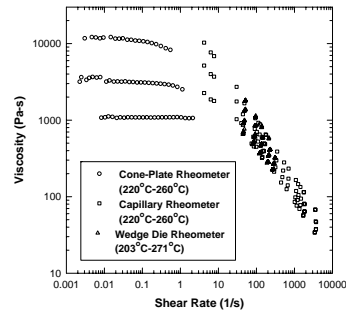


POLYMER EXTRUSION APPLICATIONS

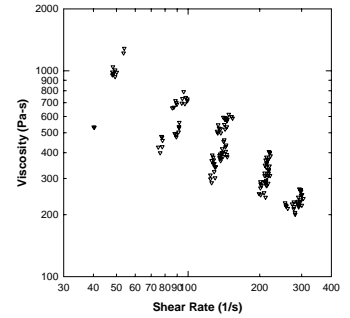
Plasticization / Effects on viscoelastic behavior



Viscosity of PS/CO₂ Solutions



PS viscosity data



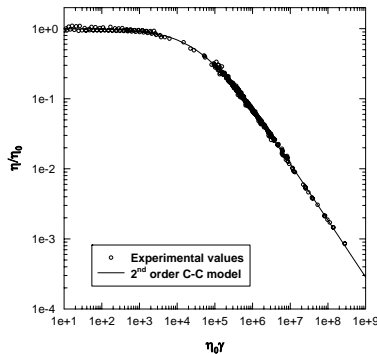
PS/CO₂ viscosity data

POLYMER EXTRUSION APPLICATIONS

Plasticization / Effects on viscoelastic behavior



Viscosity of PS/CO₂ Solutions



POLYMER EXTRUSION APPLICATIONS

Plasticization / Effects on viscoelastic behavior



Viscosity of PS/CO₂ Solutions

Increasing Temperature	Increasing CO ₂ content	Decreasing Pressure
200°C ⇒ 210°C	1.35 wt%	13.3 MPa
260°C ⇒ 270°C	0.9 wt%	8.7 MPa

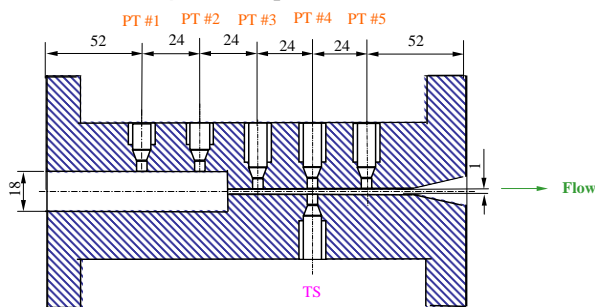
- Dissolution of 1.0 wt% of CO₂ ≈ Decreasing pressure by 9.8 MPa
- T-P and T-C interactions depend on the absolute temperature.

POLYMER EXTRUSION APPLICATIONS

Plasticization / Effects on viscoelastic behavior



Entrance Pressure Drop of PS/CO₂ Solutions



PT — Pressure Transducer
TS — Temperature Sensor

Die width is 22
All dimensions are in mm

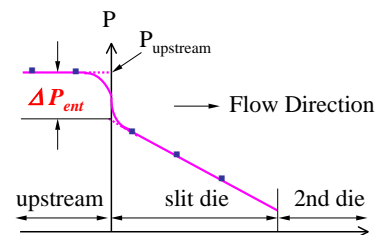
POLYMER EXTRUSION APPLICATIONS

Plasticization / Effects on viscoelastic behavior



Entrance Pressure Drop of PS/CO₂ Solutions

Pressure Profile within the Slit Die



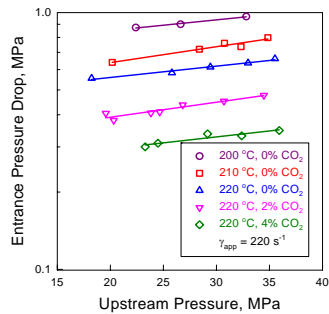
$$\Delta P_{ent} = P_{upstream} - P_{extrapolation}$$

POLYMER EXTRUSION APPLICATIONS

Plasticization / Effects on viscoelastic behavior



Entrance Pressure Drop of PS/CO₂ Solutions

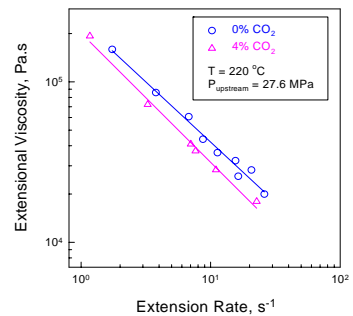


POLYMER EXTRUSION APPLICATIONS

Plasticization / Effects on viscoelastic behavior



Entrance Pressure Drop of PS/CO₂ Solutions



POLYMER EXTRUSION APPLICATIONS

Plasticization / Effects on viscoelastic behavior



Entrance Pressure Drop of PS/CO₂ Solutions

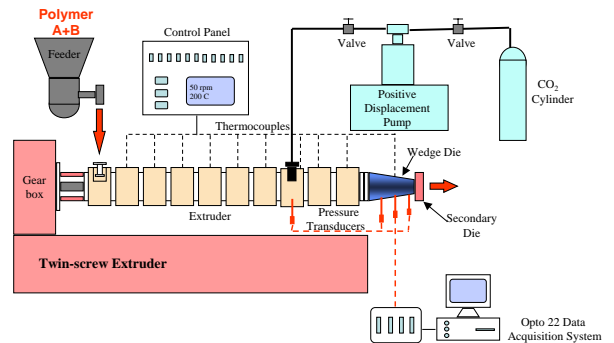
- Entrance pressure drop of PS and PS/CO₂ increases with upstream pressure
- CO₂ decreases the entrance pressure drop of PS melts. Entrance pressure drop, plotted versus wall shear stress, coincide on a master curve
- CO₂ decreases both shear and extensional viscosities of PS

POLYMER EXTRUSION APPLICATIONS

Polymer Blending / Interfacial tension and morphology



PS/LDPE Blends

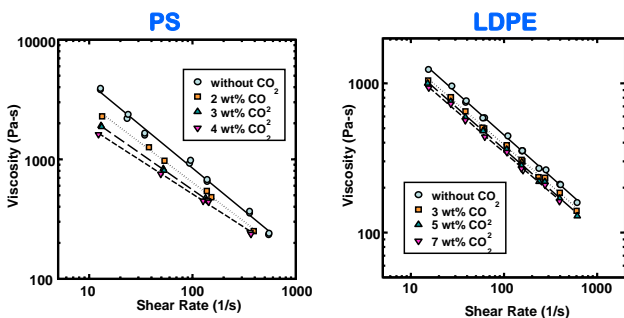


POLYMER EXTRUSION APPLICATIONS

Polymer Blending / Interfacial tension and morphology



PS/LDPE Blends



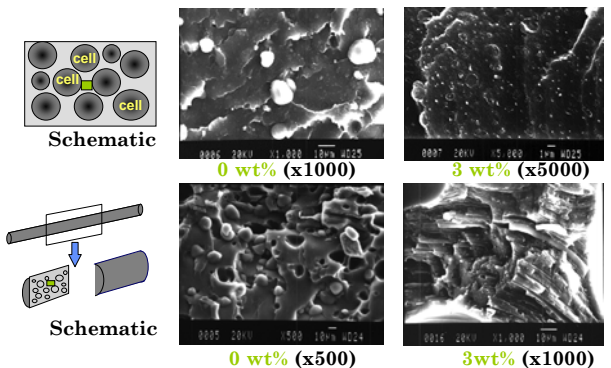
POLYMER EXTRUSION APPLICATIONS

Polymer Blending / Interfacial tension and morphology



PS/LDPE Blends

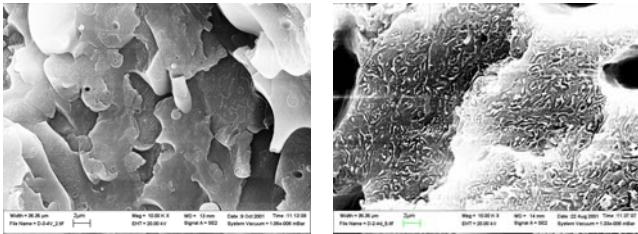
PE/PS=80/20



POLYMER EXTRUSION APPLICATIONS
Polymer Blending / Interfacial tension and morphology



PS/LDPE Blends

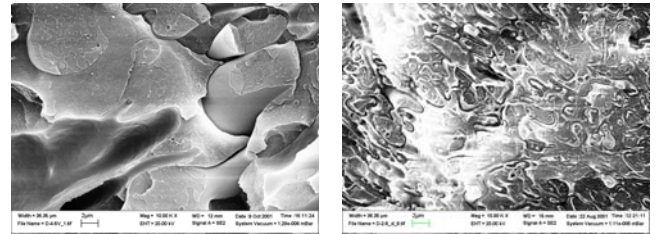


0 wt% CO₂ **PS/LDPE=60/40** 4 wt% CO₂

POLYMER EXTRUSION APPLICATIONS
Polymer Blending / Interfacial tension and morphology



PS/LDPE Blends

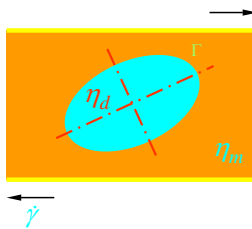


0 wt% CO₂ **PS/LDPE=50/50** 4 wt% CO₂

POLYMER EXTRUSION APPLICATIONS
Polymer Blending / Interfacial tension and morphology



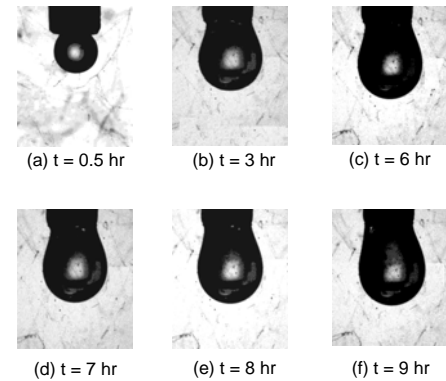
PS/LDPE Blends



POLYMER EXTRUSION APPLICATIONS
Polymer Blending / Interfacial tension and morphology



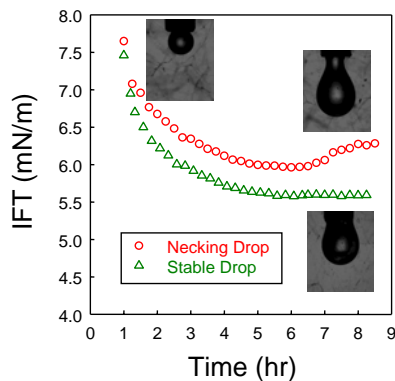
PS/LDPE Blends



POLYMER EXTRUSION APPLICATIONS
Polymer Blending / Interfacial tension and morphology



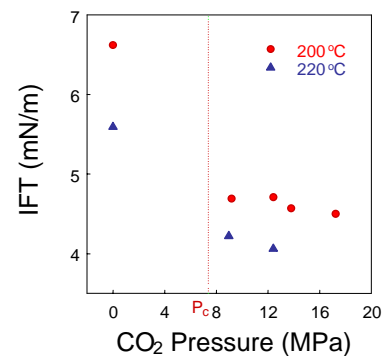
PS/LDPE Blends



POLYMER EXTRUSION APPLICATIONS
Polymer Blending / Interfacial tension and morphology



PS/LDPE Blends

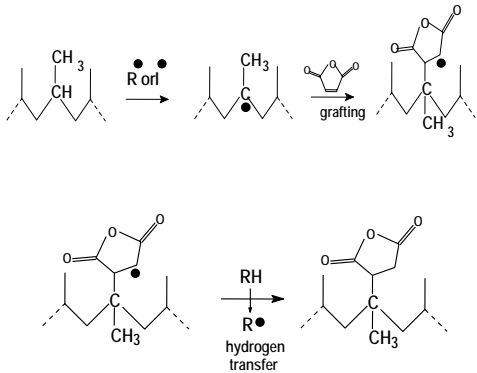


POLYMER EXTRUSION APPLICATIONS

Reactive Extrusion



Grafting of Mah on PP

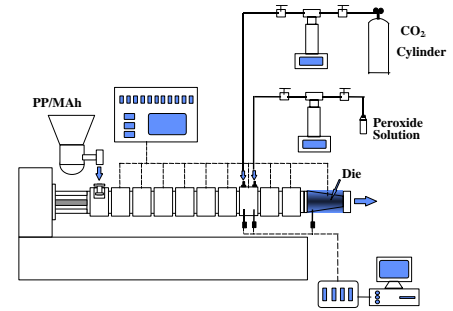


POLYMER EXTRUSION APPLICATIONS

Reactive Extrusion



Grafting of Mah on PP

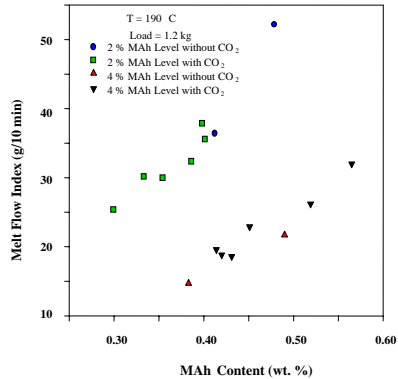


POLYMER EXTRUSION APPLICATIONS

Reactive Extrusion



Grafting of Mah on PP

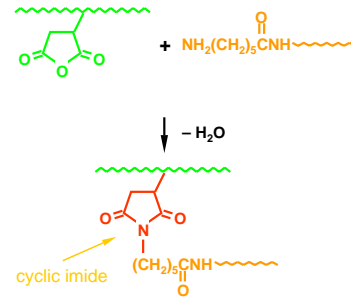


POLYMER EXTRUSION APPLICATIONS

Reactive Extrusion



Interfacial Reaction (PE-Mah / PA-6)

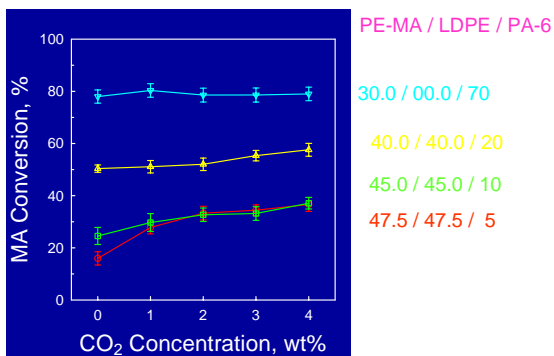


POLYMER EXTRUSION APPLICATIONS

Reactive Extrusion



Interfacial Reaction (PE-Mah / PA-6)

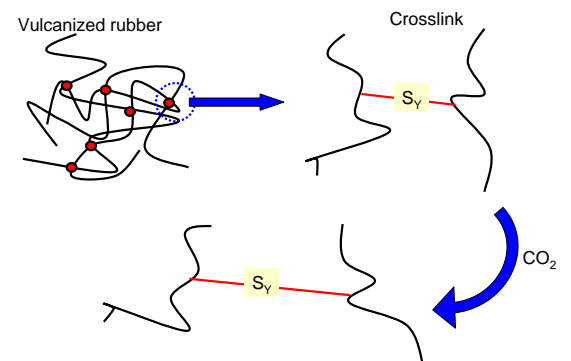


POLYMER EXTRUSION APPLICATIONS

Reactive Extrusion



Rubber Devulcanization

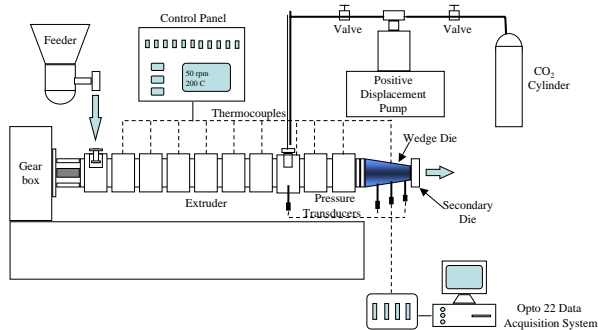


POLYMER EXTRUSION APPLICATIONS

Reactive Extrusion



Rubber Devulcanization



POLYMER EXTRUSION APPLICATIONS

Reactive Extrusion



Rubber Devulcanization

Soxhlet extraction

Two-step process to separate gel
 Acetone : Remove the low molecular weight content
 Toluene : Extract the sol content



Extrudate



Soluble



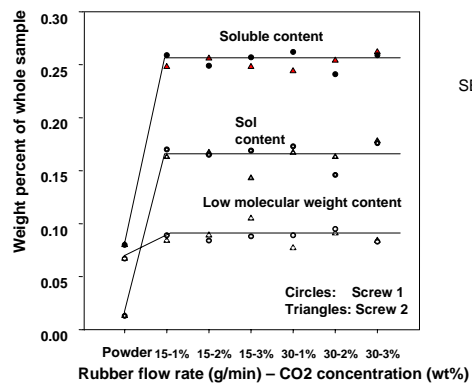
Gel

POLYMER EXTRUSION APPLICATIONS

Reactive Extrusion



Rubber Devulcanization



SBR80 / 250 °C

CLOSING REMARKS



- Highlights from our research work on polymer extrusion with supercritical CO₂ have been presented
- Potential innovative applications are numerous
- Our current efforts are focused on membrane and fiber formation as well as on block copolymer and TPV preparation

ACKNOWLEDGEMENTS



Funding

Natural Sciences and Engineering Research Council of Canada (NSERC)
 Materials Manufacturing Ontario (MMO)
 DuPont Canada Inc.

Researchers

Dr. Minhee Lee
 Dr. Anle Xue
 Dr. S. Zhu
 Ms. Beth Dorscht
 Ms. Joy Zhang

Institute for Polymer Research
27th Annual Symposium

Symposium documents for

Kerry Li

Abstract

Presentation

Extrusion and fibre spinning of Nylon-6,6 / supercritical CO₂ mixture

Kerry Li and Prof. Costas Tzoganakis
Chemical Engineering department, University of Waterloo

Abstract:

A novel technical to spin nylon fibre was developed: Addition of supercritical CO₂ to nylon melts and spinning those mixtures under different conditions were performed. CO₂ works co-ordinately with thermal to disrupt nylon-6,6 inter-chain hydrogen bond. In sequent, the intended improvement in stretching along with tensile properties of nylon fibres was evaluated.

As an elementary exploration, the rheological behaviour of nylon-6,6 / supercritical CO₂ mixture was explored through a custom extrusion. Results indicate that the CO₂ as a plasticizer reduce the bulk shear viscosity. The combined effects of temperature and hydrostatic pressure on shear viscosity were investigated accordingly.

Introduction.

Nylon-6,6 is one of semi-crystalline polymers with very polar characteristic amide groups in the symmetrical backbone chain. The amide group $-(\text{CO-NH})-$ provides high density hydrogen bonding between polyamide chains, giving nylon high strength at elevated temperatures, toughness at low temperatures, combined with its other properties, such as stiffness, wear and abrasion resistance, low friction coefficient and good chemical resistance. These properties have made nylons the strongest of all man-made fibers in common use.

Mechanical, thermal and optical properties of fibers are strongly affected by orientation and crystallinity. Basically, higher fiber orientation and crystallinity will produce better properties. In order to achieve desirable properties through molecular orientation and crystallinity, two-step melt spinning, comprised of spinning and drawing, is considered to be the conventional method to manufacture nylon filaments.

Multiple drawing stages were invented to achieve high levels of orientation. The mechanism is to obtain relaxation allow for drawing in the later stages. However, the tensile strength of nylon-6,6 produced through this technical is less than 1.0Gpa and much lower than their theoretical strength. The highest orientation and crystallinity are hard to achieve by this technical since the high density of hydrogen bond in nylon crystal stem restrict the further drawing. Therefore, disruption of the hydrogen bonds is necessary to obtain further stretching and improved tensile properties.

Lewis acid-base complexion, such as carbon dioxide interact with carbonyls, was found to be able to scission the hydrogen bond in nylon-6,6 inter-chain. Most recently, a technique to draw polymer in high pressure gases has been presented in this purpose. The drawing process has been monitor in specified temperature and pressure range. Also the gas or liquids act mostly as plasticizer in drawing process. In those attempts, the use of

scCO₂ only evaluates the ability of scCO₂ to plasticize amorphous fibres. Meanwhile, the discussion of interaction of carbon dioxide with electron donor species (e.g. carbonyls) is absent.

Ideally, if we are able to disassociate inter-chain hydrogen bond of nylon before drawing and recover them after drawing, the highest stretching may be achieved, as well as the tensile strength. In our spinning and drawing approaching, the addition of CO₂ during extrusion of nylon-6,6 melts presents complex effects attributed to both chemical structure (interact with carbonyls) and supermolecular (plasticize). The reduction of bulk shear viscosity rally with the weakness of polymer hydrogen bond may facilitate higher degree of stretching when spinning, the existing of CO₂ in subsequent drawing process function as plasticizer which promote further stretching. The CO₂ selected as a media during process leave no trace in the end, the whole process is simple and environmental benign.

In order to estimate the plasticize performance of scCO₂, a custom extrusion process designed to study the mixing and rheological behaviour in a systematic manner.

Experimental:

The viscosity behavior of nylon-6,6 / supercritical CO₂ mixture was studied in a custom extrusion process, see Diagram 2.; A wedge die was used to connected with extruder to measure shear viscosity, the following formula apply in this measurement:

$$\Delta P = \frac{K}{\tan \theta} \left(\frac{6Q}{W} \frac{2n+1}{3n} \right)^n \left[\frac{1}{2n} \left(\frac{1}{h_2^{2n}} - \frac{1}{h_0^{2n}} \right) + \frac{1}{W(2n-1)} \left(\frac{1}{h_2^{2n-1}} - \frac{1}{h_0^{2n-1}} \right) \right]$$

$$\eta = K \left(\frac{2n+1}{3n} \right) \left(\frac{6Q}{Wh^2} \right)^{n-1}$$

The spinning and drawing process show in Diagram 1. A custom high-pressure chamber will be used to avoid the foam in some instance. The design of chamber shows in Picture 1.

Results and discussion:

The pressure, gas uptake and temperature effects on bulk shear viscosity shows in plot1, 2,3 respectively:

Spinning and drawing of mixture is ongoing, some spinning results show in plot 4,5,6:

Schematic diagram of the continuous-draw apparatus

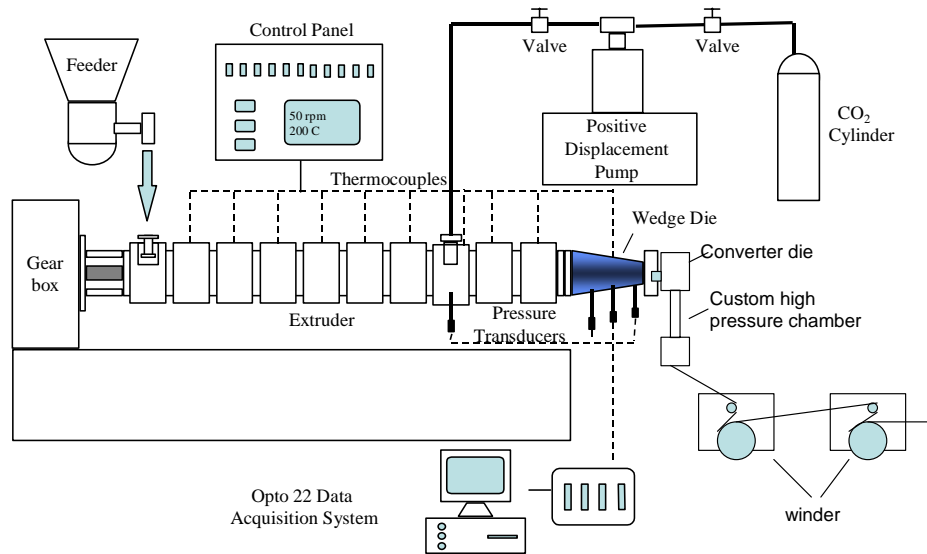
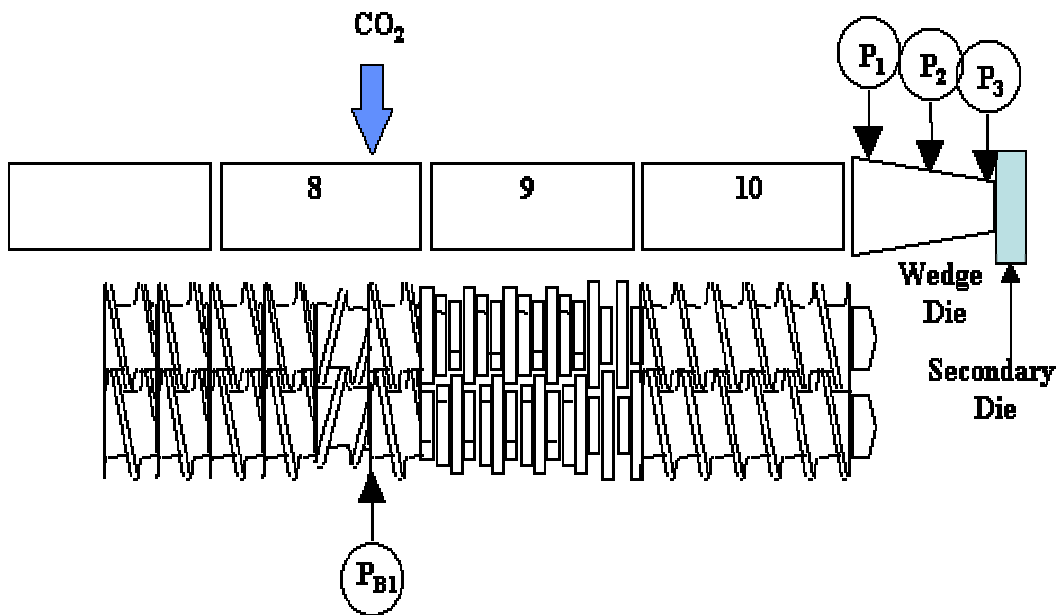
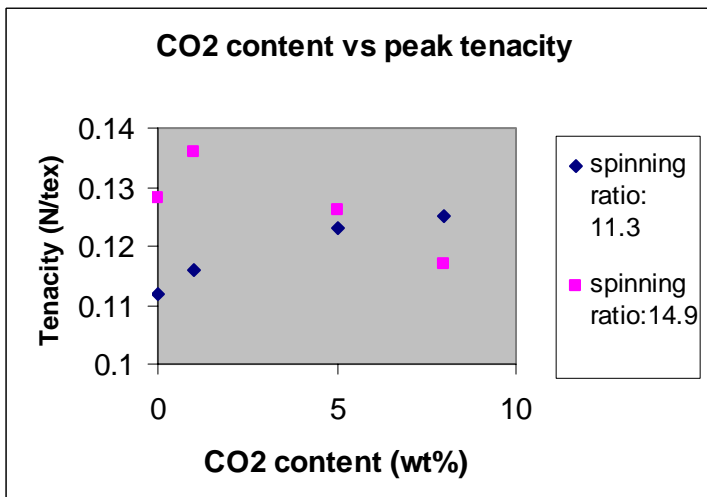
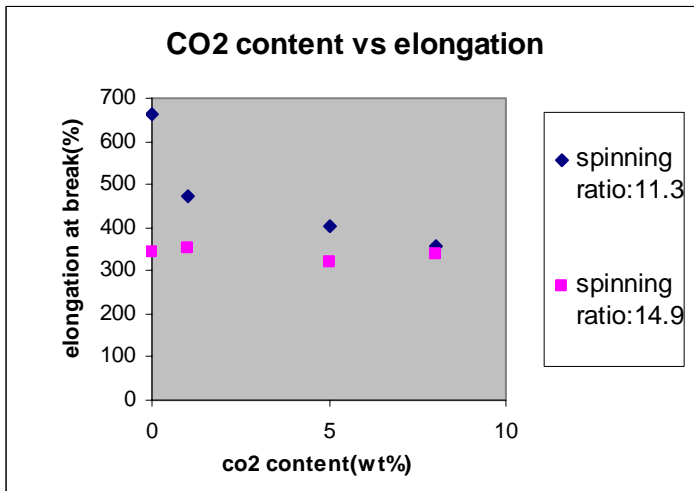
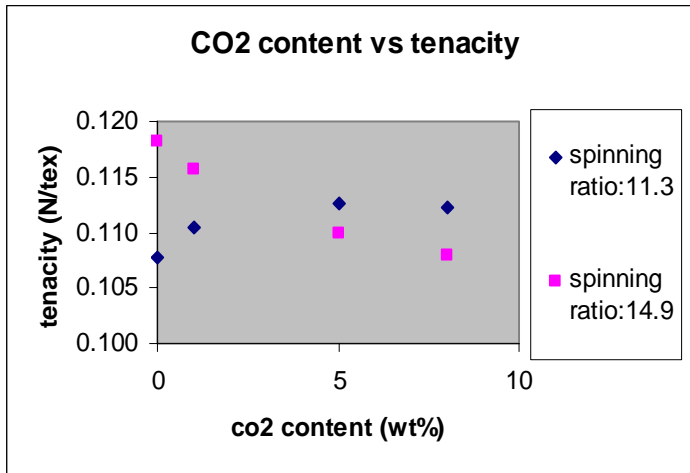


Diagram 2: Screw configuration



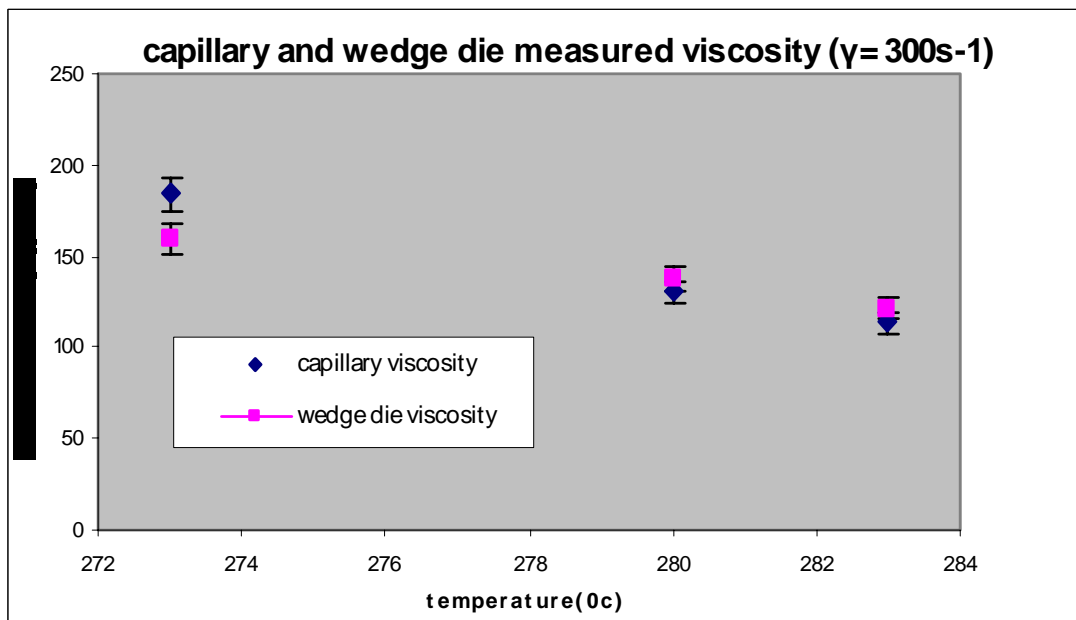
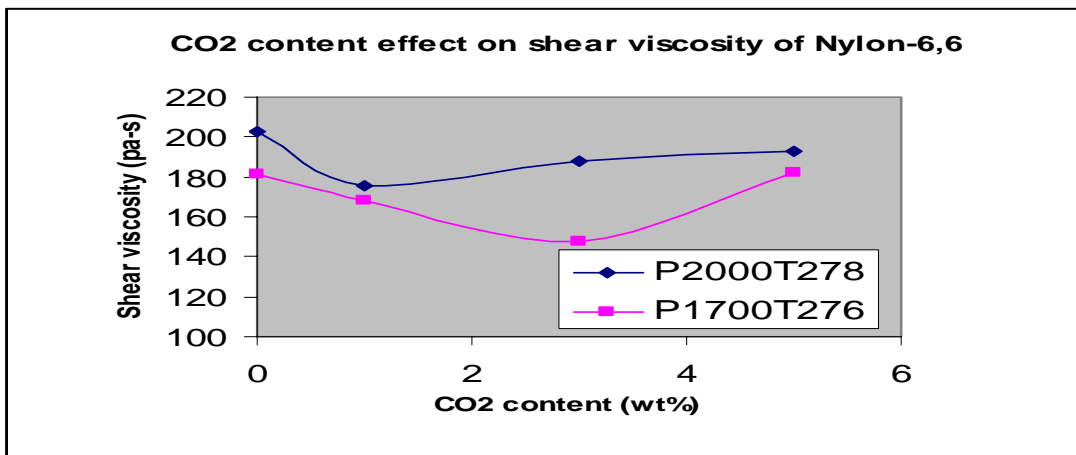
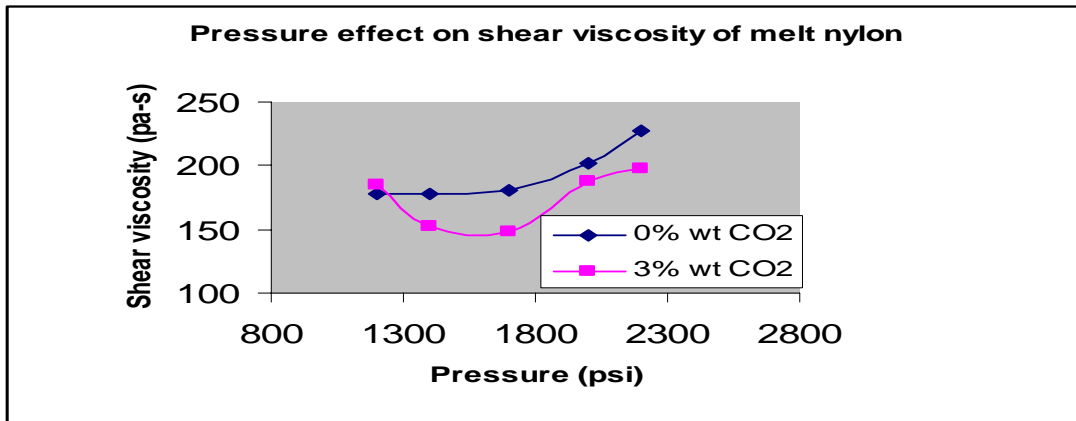
Plot 4,5,6: spinning results



Pic.1. high-pressure chamber



Plot 1,2,3: The pressure, co2 uptake and temperature effects to shear viscosity



Extrusion and fiber spinning of Nylon-6,6 / supercritical CO₂ mixtures

Presented by: Ziqiang Li
Supervisor: C. Tzoganakis

IPR Symposium: May 18, 2005

Content

- Objective
- Introduction
- Motivation and design concepts
- Preliminary experiments
- Extrusion of PA-6,6 / ScCO₂ mixture
- Filament spinning of PA-6,6 and mixture
- Conclusions
- Acknowledgement

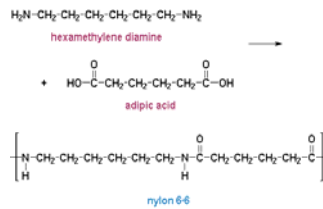
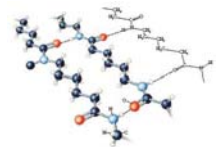
Objective

- Investigate the effects of supercritical CO₂ on nylon-6,6 viscosity:
 - Prepare the supercritical CO₂ / nylon-6,6 mixture in extruder, on-line measure the effect of T,P,CO₂ content ,shear rate to shear viscosity via connected wedge die.
- Implement the spinning and drawing of supercritical CO₂ / nylon-6,6:
 - Spinning supercritical CO₂ / nylon-6,6 mixture or / and in custom chamber.
 - Investigate the effect of uptake of CO₂ to filament's mechanic properties (tenacity, strength).

Introduction:

NYLON-6,6:

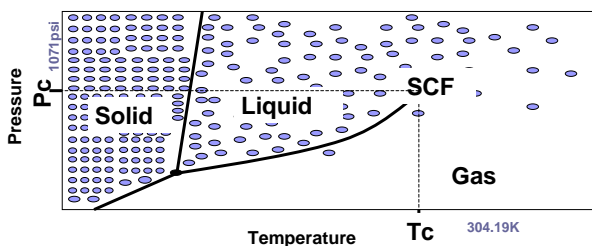
- Very polar characteristic amide groups in the symmetrical backbone chain



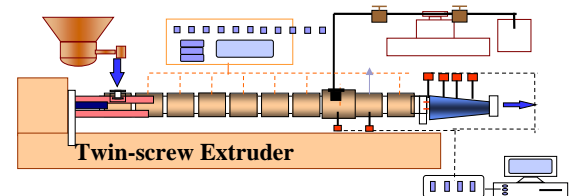
- ✓ High density of H-bond
- ✓ Semi - crystalline
- ✓ Good mechanical, thermal properties
- ✓ High DR under high temperature and moisture

Introduction:

- Supercritical Fluids
 - A fluid is supercritical when its temperature and pressure are higher than their critical point values (T_c , P_c).
- Supercritical Carbon Dioxide



Introduction: Extrusion of PA-66 / ScCO₂:

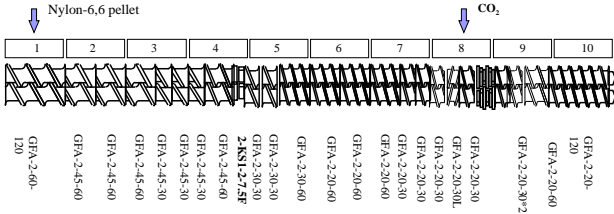


- Avoid degradation
- Maintenance high pressure
- Well mixing, avoid pressure fluctuate.
- Avoid back flow
- It is a pressure sensitive method.
- Dry and less dispersive force
- Screw arrangement
- Injection port screw arrangement
- Reverse disc applied
- Calibrate and exchange the measurement transducer

Introduction: Extrusion of PA-66 / ScCO₂



- Screw arrangement
 - Provide well mixing
 - Less degradation
 - Pressure build up
- Connect wedge die to
 - Investigate mixture viscosity under
 - Different CO₂ uptake,
 - Temperature, pressure,
 - Shear rate.



Introduction: viscosity measurement



Fiber production of GQZ

$$\Delta P = \frac{K}{\tan \theta} \left(\frac{6Q}{W} \frac{2n+1}{3n} \right)^n \left[\frac{1}{2n} \left(\frac{1}{h_2^{2n}} - \frac{1}{h_0^{2n}} \right) + \frac{1}{W(2n-1)} \left(\frac{1}{h_2^{2n-1}} - \frac{1}{h_0^{2n-1}} \right) \right]$$

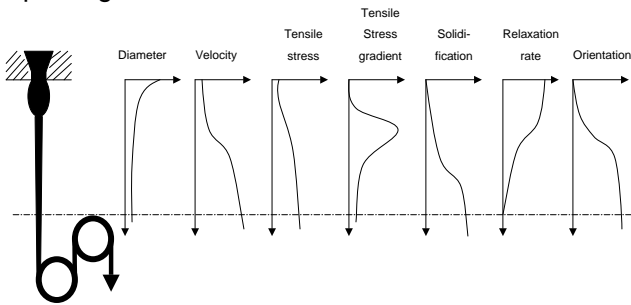
$$\eta = K \left(\frac{2n+1}{3n} \right) \left(\frac{6Q}{Wh^2} \right)^{n-1}$$

Width: 1.4 cm, $\theta: 0.9^\circ$

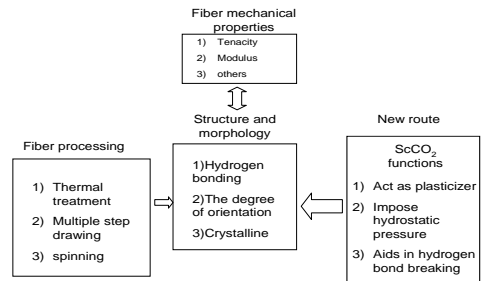
Filament spinning and drawing



■ Spinning:



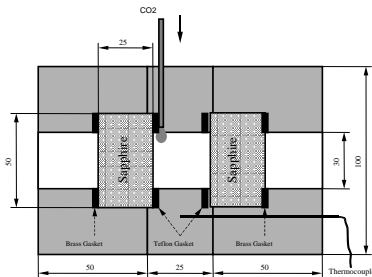
Motivation and design concepts:



Preliminary experiment - I



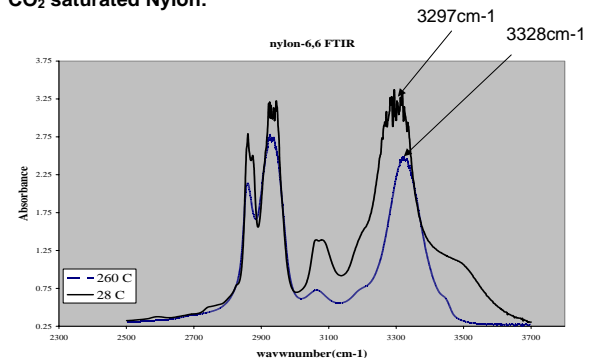
- FTIR measurement of hydrogen bond breaking process of CO₂ saturated Nylon:



Preliminary experiment - I

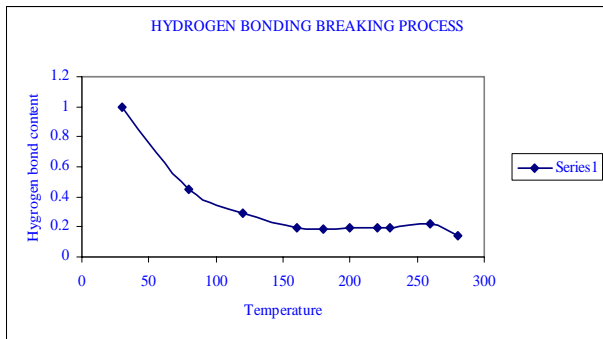


- FTIR measurement of hydrogen bond breaking process of CO₂ saturated Nylon:



Preliminary experiment - I

- FTIR measurement of hydrogen bond breaking process of CO₂ saturated Nylon:



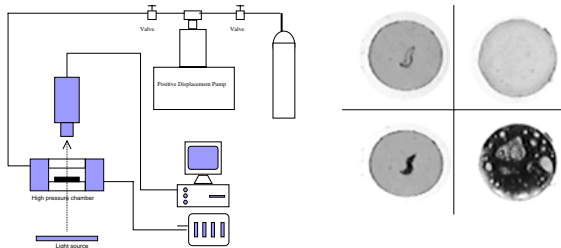
Preliminary experiment - II

Solubility of CO₂ in molten Nylon-6,6:

- Motivation:
 - Injection limits of CO₂ during extrusion.
 - Control uptake of CO₂ during fiber spinning
- Swelling image analysis...

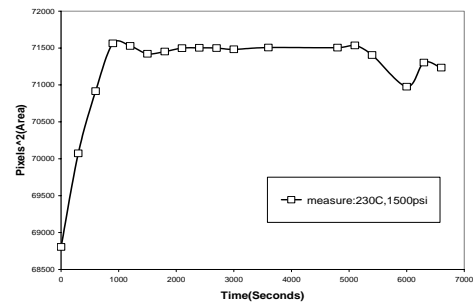
Preliminary experiment - III

Swelling of nylon-6,6 in supercritical CO₂



Preliminary experiment - III

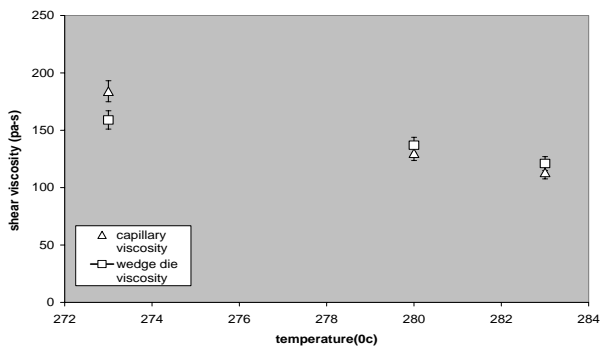
Swelling of nylon-6,6 in supercritical CO₂



The expansion of polymer volume is nonlinear till equilibrium is reached. For this to be valid, the sample has to be thermally treated to be free of strain and thermal expansion has to be excluded in this measurement.

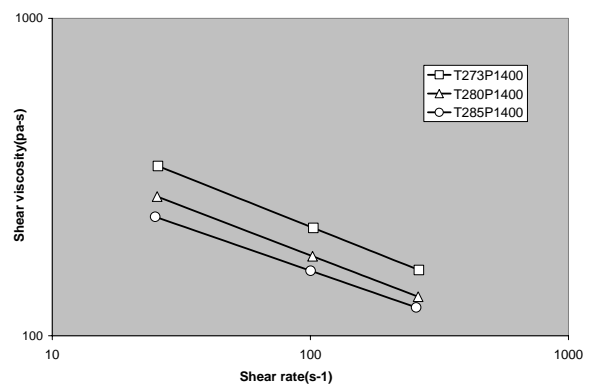
Extrusion Results:

capillary and wedge die measured viscosity ($\dot{\gamma} = 300s^{-1}$)



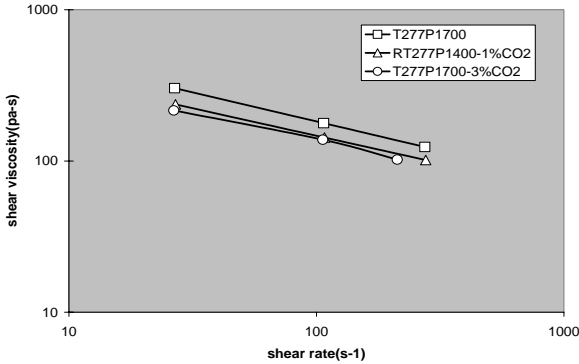
Extrusion Results:

temperature effect on nylon shear viscosity (no CO₂)



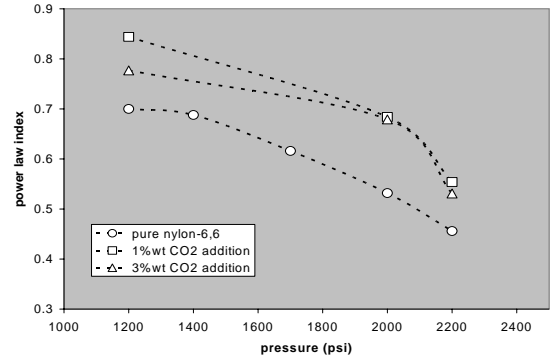
Extrusion Results:

CO₂ effect on shear viscosity of nylon-6,6

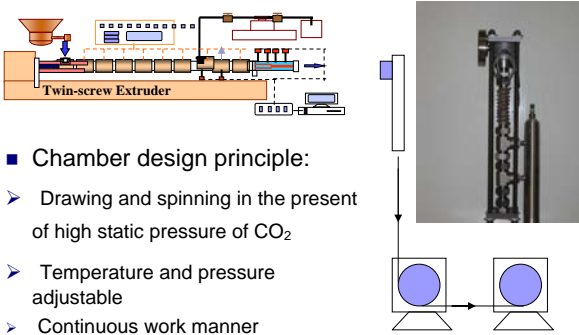


Extrusion Results:

pressure effect on power law index of nylon-6,6

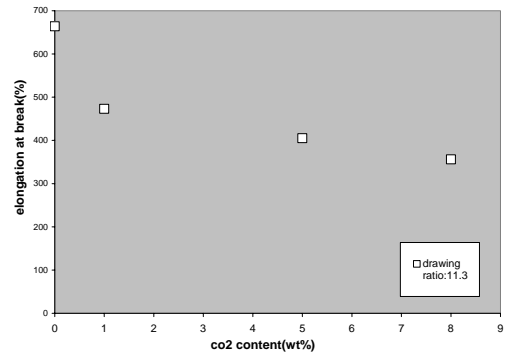


Filament spinning of PA-66 & mixtures: set up & chamber design



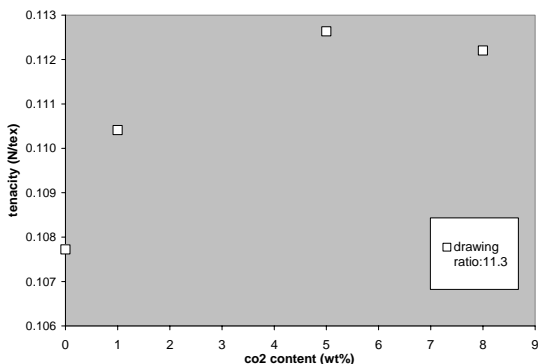
Filament spinning of PA-66 & mixtures:

CO₂ content vs elongation



Filament spinning of PA-66 & mixtures:

CO₂ content vs tenacity



Conclusions:

CO₂ function as a plasticizer to:

- Reduce nylon-6,6 melt viscosity, And mixture viscosity is the function of shear rate, temperature, pressure and CO₂ uptake.
- The solubility of CO₂ in nylon-6,6 melt is low, partially due to the high residual hydrogen bond content in nylon-6,6 melt.

Spinning and drawing process:

- Is setting up to conduct a new route to produce fibre in the present of high hydrostatic pressure CO₂
- CO₂ work to increase the fibers tenacity after post-drawing, but as a trade off, its elongation at break reduced

Future work:



- Estimate solubility of CO₂ in molten nylon-6,6 by viscosity measurement.
- Run spin experiments at high drawing ratio.
- Investigate the effect of CO₂ on fibre spinnability.

Acknowledgements:



- My sincere thanks to my supervisor, Professor Costas Tzoganakis
- Financial support from "Materials and Manufacturing Ontario" (MMO) is gratefully acknowledged.
- Donation of material from Invista is gratefully acknowledged.

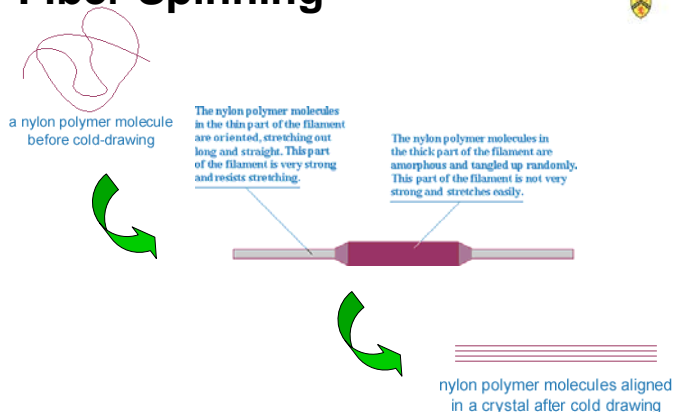
Question??



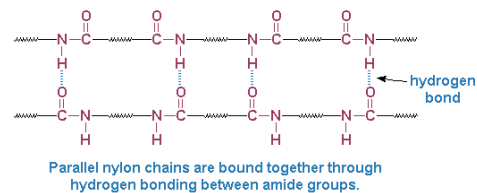
Thank you!



Fiber Spinning

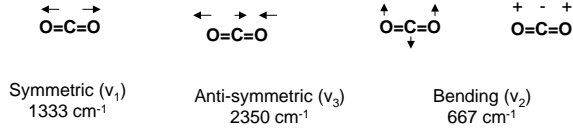


Fiber Spinning

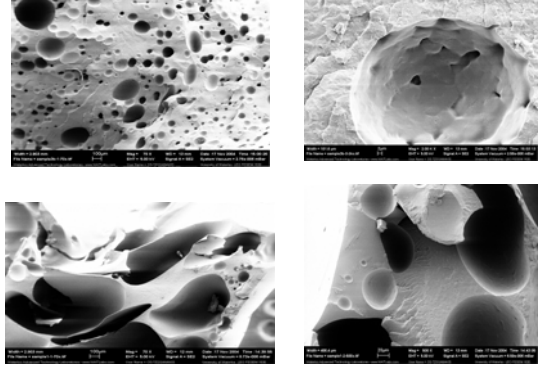


Interactions of scCO₂ with Polymers

- FTIR spectroscopic studies
- Lewis acid-base interactions between CO₂ and electron donor species (e.g. carbonyls)

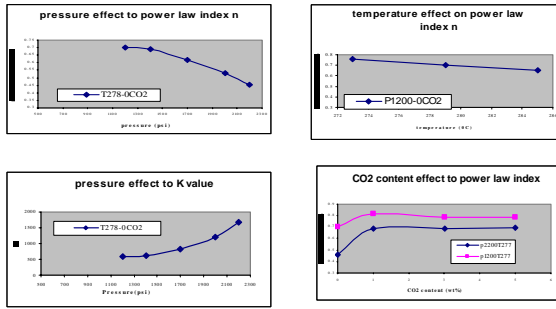


Extrusion Results: foam structure and others



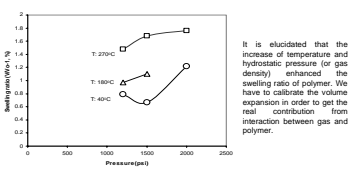
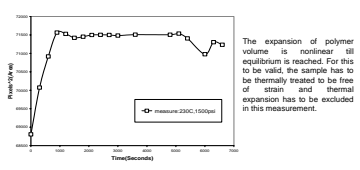
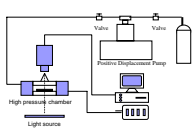
Extrusion Results:

- Power law index n and K value:



Existing technologies are either too complicated to achieve or less precise:
 FTIR; Gravimetric; Pressure decaying; Barometric, Volumetric, Quartz crystal Microbalance; Phase separation measurement;

Swelling of nylon-6,6 in supercritical CO₂



Institute for Polymer Research
27th Annual Symposium

Symposium documents for

Mark Ingratta

Abstract

Presentation

Fluorescence Study of the Effect of Side-Chain Length on the Side-Chain Dynamics of an Alpha-Helical Polypeptide

Mark Ingratta

Department of Chemistry, University of Waterloo

Developing an understanding of the physical principles that control the folding of proteins has been the focus of attention of numerous research laboratories throughout the world. The results of these studies have led to simulations that model the folding of proteins based on some fundamental assumptions. For instance, the “diffusion-collision model” assumes that secondary structure elements diffuse until they collide and adhere to form the tertiary structure of the protein.¹ The general consensus is that the tertiary structure of a protein results from interactions between the side-chains of secondary structural elements which guide the α -helices and β -sheets into their final three-dimensional arrangement that constitutes the protein structure. In view of the key role played by the side chains of secondary structures in the last steps of the protein folding pathway, experimental methods are required that can characterize the volume probed by the side chains of a secondary structure.

This study represents an attempt at achieving this goal by using fluorescence to characterize the volume probed by the tip of the side-chain of a poly(glutamic acid) (PGA) α -helix, which is used as an example of secondary structure. In these experiments, the fluorescent pyrene probe is attached randomly along the PGA α -helix via two linkers of different length. To increase the linker-length, the alkyl spacer connecting the probe with the PGA side chains is increased from a methylene to a tetramethylene linker. This increases the side chain length between the probe and the peptidic backbone from 5 to 8 atoms.

When a polymer is randomly labeled with pyrene, the dynamics of encounter between any two pyrenes is controlled by the chain length spanning and flanking them. Consequently, randomly labeled polymers exhibit a distribution of chain lengths between any two pyrenes which results in a complicated distribution of rate constants. The blob model is a tool used to circumvent this complication. It works by dividing the polymer coil into blobs, where a blob is the volume probed by an excited dye during its lifetime. In so doing, the focus of the study shifts from the whole polymer chain down to one blob and the dynamics of the chain located inside a

blob are characterized. The motions and volume probed by the side chains having different length will be characterized using the fluorescent blob model.

Pyrene was chosen as a dye to study the dynamics of polypeptides in solution by time-resolved fluorescence, because of its relatively long lifetime and high quantum yield. The natural fluorescence lifetime of pyrene when attached to a polymer is in the 200-300 ns range, depending on the solvent and polymer. Pyrene can be excited at around 340 nm, and emits in the blue region of the visible spectrum around 375 nm as a monomer. If it encounters another ground state pyrene while excited, it forms an excimer species which decays with a lifetime of about 50 ns with an emission centered in the green region of the visible spectrum (430 to 600 nm). Figure 1 displays the fluorescence spectra of pyrene labeled PGA (Py-PGA). As the pyrene content of Py-PGA increases, more excimer is being generated and the emission centered at 480 nm increases.

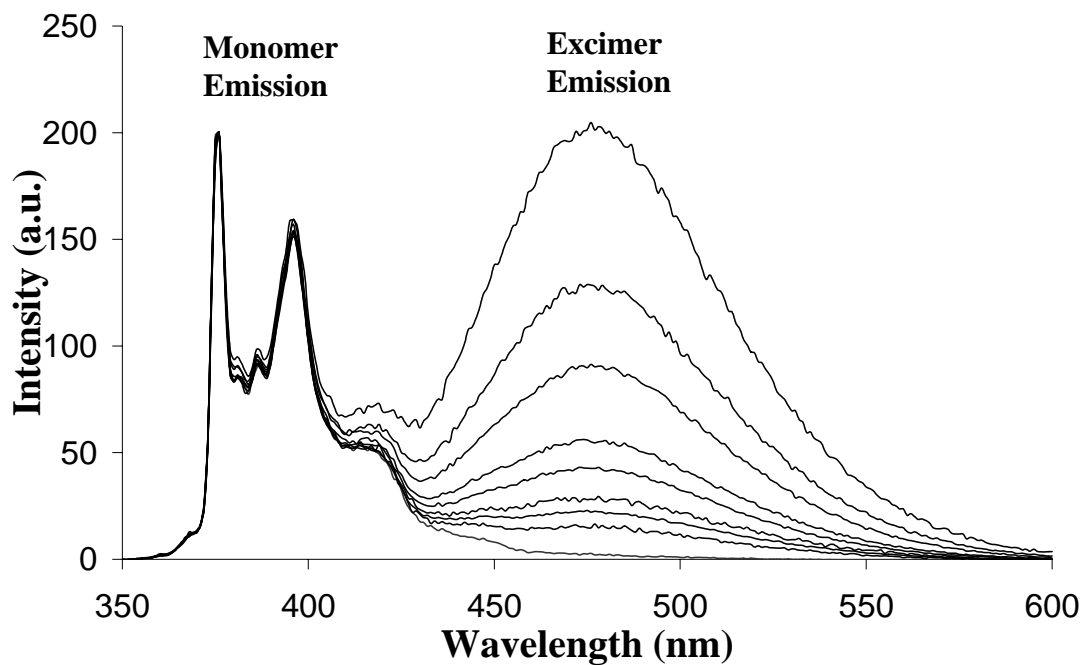


Figure 1: Fluorescence spectra of PGA labeled with increasing amounts of 1-pyrenemethylamine. Pyrene content decreases from top to bottom: 15 – 0.4 mol%.

Three parameters must be defined when using the blob model. They are k_{blob} , $\langle n \rangle$ and $k_e[blob]$. A blob is defined by the volume probed by an excited chromophore during its lifetime. For a pyrene labeled polymer, the rules set out by the blob model impose that an excited pyrene not leave a blob, but a ground state pyrene can diffuse between blobs at a certain rate. The exchange rate between blobs is k_e , while the blob concentration within the polymer coil is $[blob]$. Since the encounter between an excited pyrene and a ground state pyrene results in the formation of an excimer and the accompanying disappearance of the excited pyrene, pyrene is its own quencher. Thus, the number of quenchers per blob is equal to the number of pyrenes per blob and is referred to as $\langle n \rangle$. Finally, the rate constant for excimer formation within a blob is k_{blob} . N_{blob} represents the monomer units that an excited pyrene can probe during its lifetime. The fluorescence decays are used to obtain these characteristics about the blobs of pyrene labeled PGA. The value of N_{blob} for a series of pyrene labeled PGAs is obtained by extrapolating a plot of N_{blob} vs pyrene content to zero pyrene content as shown in Figure 2.

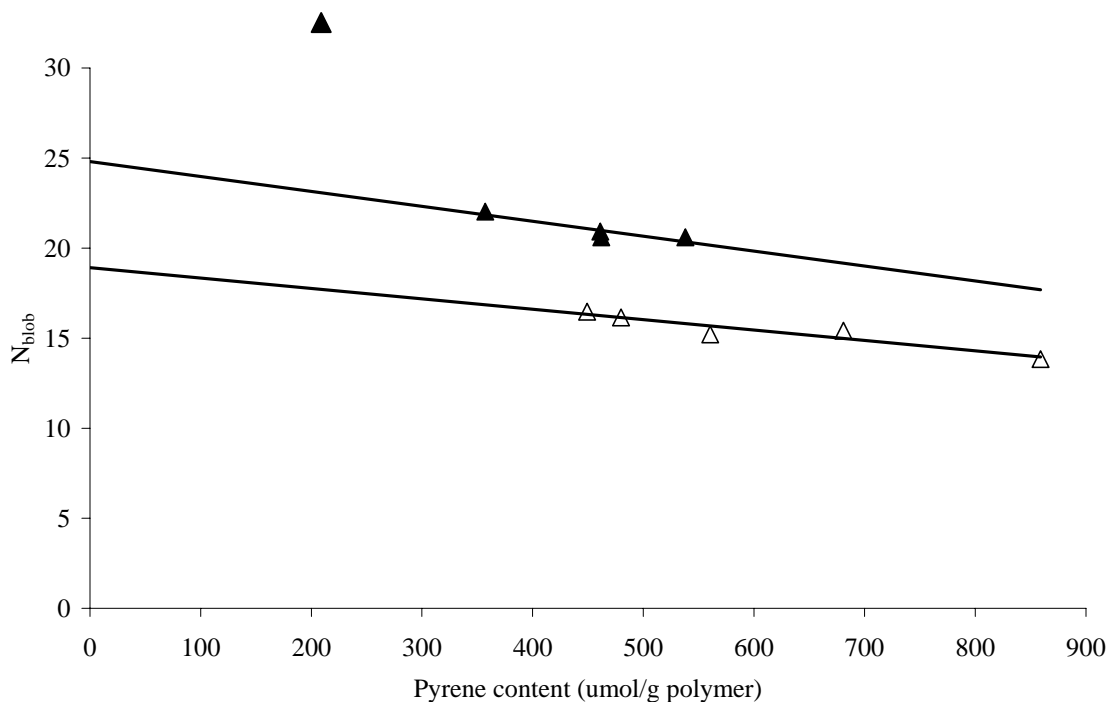


Figure 2: N_{blob} vs. Pyrene content for PGA labeled with 1-pyrenemethylamine (Δ) and 1-pyrenebutylamine (\blacktriangle) with a pyrene lifetime of 150 and 155 ns respectively.

Two of the most important characteristics obtained from the blob model are k_{blob} , and N_{blob} , which give information on the rate of encounter and volume probed by the dye within its lifetime. Since the blob size is related to the lifetime of the chromophore, a longer lived pyrene will probe a larger volume of polymer coil. For this reason, it is necessary to control the lifetime of the dye by using an external quencher. The chosen quencher is nitromethane and has been used similarly in previous work on pyrene labeled poly(*N, N*-dimethylacrylamide).² In DMF, PGA labeled with 1-pyrenemethylamine, (PGA-PMA), has a lifetime of 215 ns, while PGA labeled with 1-pyrenebutylamine, (PGA-PBA) has a lifetime of 155 ns. Thus, by adding nitromethane to a PGA-PMA solution, the lifetime of PGA-PMA can be decreased to equal that of PGA-PBA. The results are shown in Figure 2, where the fluorescence decays of PGA-PMA and PGA-PBA were acquired.

In addition to comparing PGA-PMA and PGA-PBA at 150 ns, fluorescence decays were acquired for pyrene lifetimes ranging from 50 ns up to 215 ns. The results obtained from the analysis of the decays clearly show that the longer linker is able to probe a larger PGA segment, even as the lifetime of pyrene is decreased. Within each series, N_{blob} changes little with the lifetime of pyrene as shown in Figure 3.

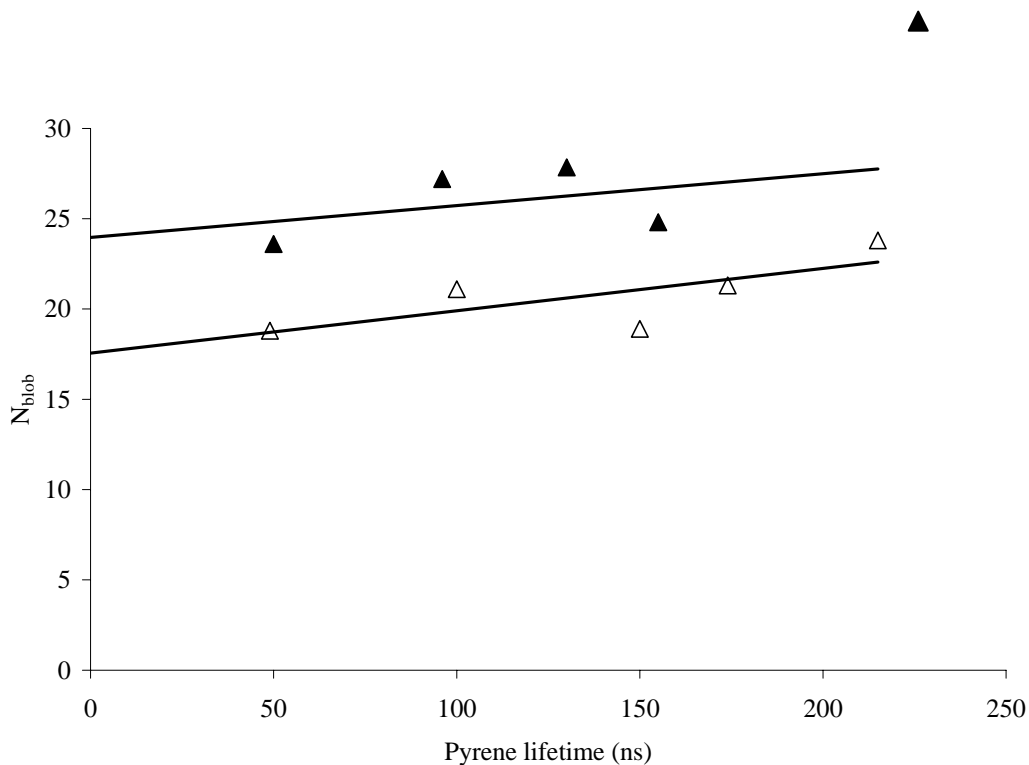


Figure 3: N_{blob} vs the lifetime of pyrene for PGA-PMA (\blacktriangle) and PGA-PBA (\triangle)

The rate constant for excimer formation, k_{blob} , can also be compared between the two PGAs. As the lifetime is decreased, k_{blob} increases. This is because the side chain is probing a smaller volume so that the encounters between pyrenes occur at a faster time scale. The physical volume probed by the side chain, V_{blob} , can be compared by looking at k_{blob}^{-1} , which is proportional to V_{blob} .² The longer side chain is shown to probe a larger volume over the range of lifetimes as expected. This is shown in Figure 4.

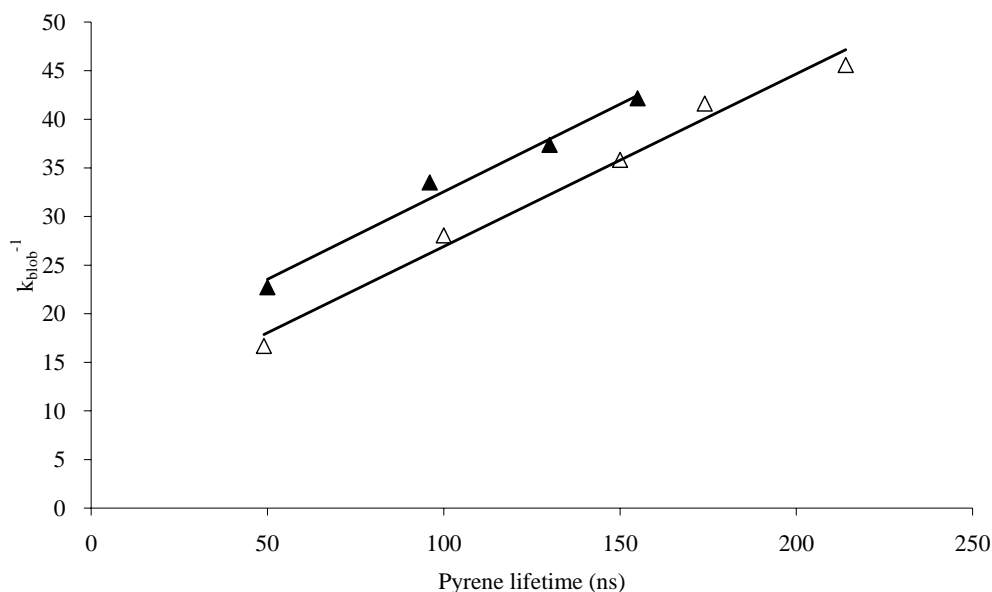


Figure 4: k_{blob}^{-1} vs. the lifetime of pyrene for PGA-PMA (Δ) and PGA-PBA (\blacktriangle)

Interestingly, although N_{blob} changes little over the time scale probed, V_{blob} increases approximately 3 times over the range studied. This implies that as pyrene is given more time to probe its surroundings, it stretches into the solvent perpendicularly to the helix axis.

Using the fluorescence blob model, an α -helical PGA with two different side chain lengths were quantitatively analyzed and compared. It was found that extending the length of the side chain leads to pyrene probing a larger volume. This is the first step illustrating that the blob model can be used to characterize the volume probed by the side chain of a structured protein or polypeptide.

¹ Karplus, M., Weaver, D.; *Protein Science* **1994**, 3, 650-668.

² Kanagalingham, S., Spartalis, J., Cao, T., Duhamel, J., *Macromolecules* **2002**, 35, 8571-8577.

A Study of Polypeptide Side-Chain Dynamics using Fluorescence

Mark Ingratta

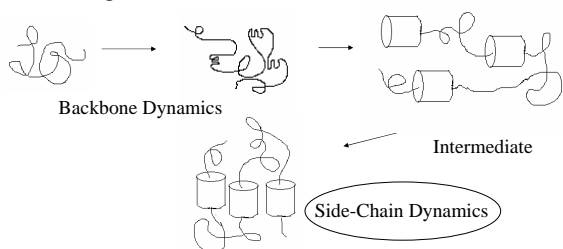
Chemistry Department
University of Waterloo
IPR Symposium
May 18, 2005

Outline

- Purpose
- Pyrene and the Fluorescence Blob Model
- Characterization of Pyrene Labeled Poly(glutamic acid)
- Results
- Future Work

Purpose

- Study dynamics of polypeptides in solution
- Contribute to a better understanding of protein folding



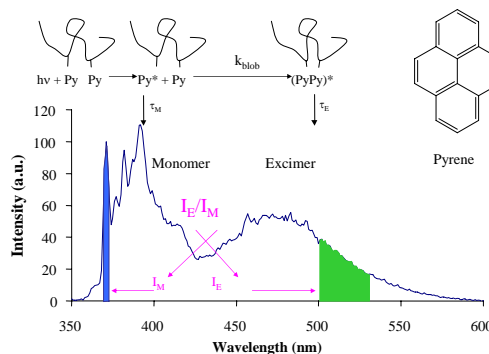
Purpose

- Study the side-chain dynamics of polypeptides in solution using fluorescence
- Side-chain interactions are thought to have an important role in protein folding

How?

- Use the Fluorescence Blob Model to analyze the time scale of diffusional motions of side-chains of different lengths
- As the side chain becomes longer, it should probe a larger volume around the backbone
- Chromophore of choice: Pyrene

Pyrene Fluorescence



Polymer → Blobs

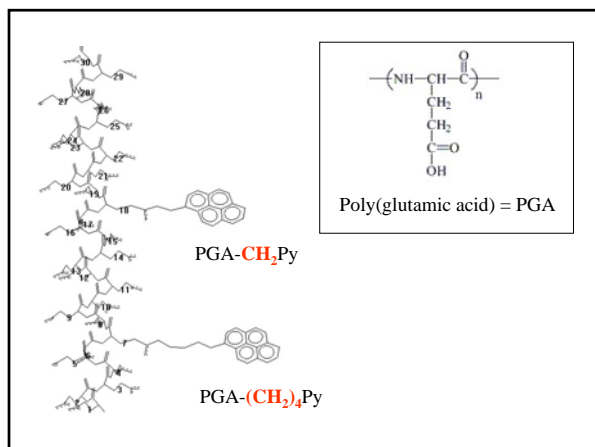
k_{blob} = rate constant for excimer formation by diffusion
 $\langle n \rangle$ = number of ground state pyrenes per blob → quenchers per blob

$k_e[blob]$ = rate of pyrene exchange between blobs × blob concentration per polymer coil
 N_{blob} = units / blob

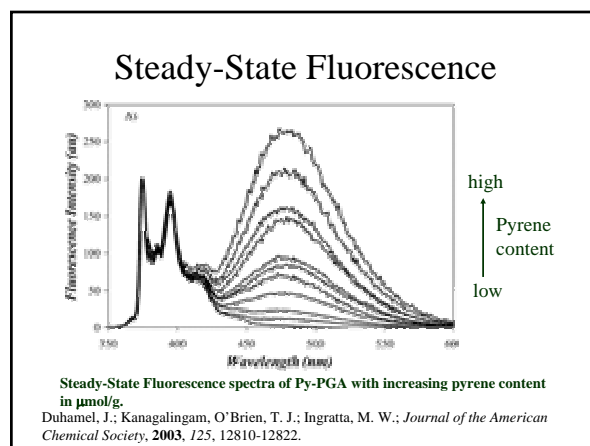
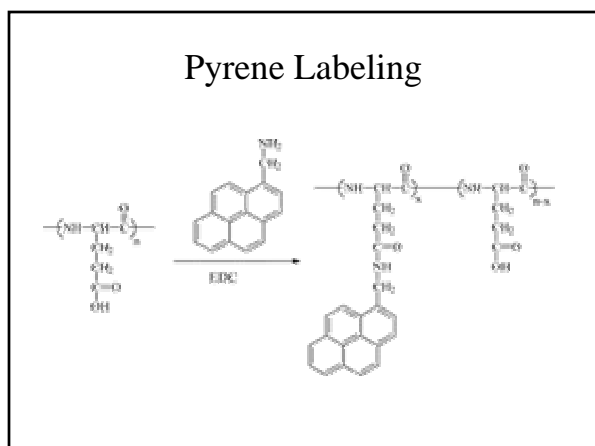
Explore the Effect of Side-Chain Length

Py-CH₂NH₂ Py(CH₂)₄NH₂ Alpha Helix

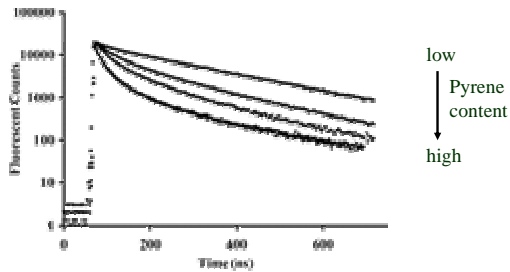
- Vary the length of the linker attached to the chromophore
- Chromophore attached to a well defined, stable structured polypeptide, poly(glutamic acid)



Characterization of Pyrene-Labeled Poly(glutamic acid)



Time-Resolved Fluorescence



Fluorescence decays of the pyrene monomer for Py-PGA.

Duhamel, J.; Kanagalingam, O'Brien, T. J.; Ingratta, M. W.; *Journal of the American Chemical Society*, **2003**, *125*, 12810-12822.

Volume Control

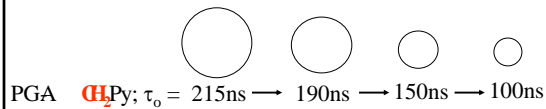
- The lifetime of Pyrene can vary depending on its connectivity to a polymer
- Because blob size is related to the lifetime of the chromophore, a longer lived pyrene will probe a larger volume.

PGA $(CH_2)_2$ Py; $\tau_0 = 215$ ns

PGA $(CH_2)_4$ Py; $\tau_0 = 155$ ns

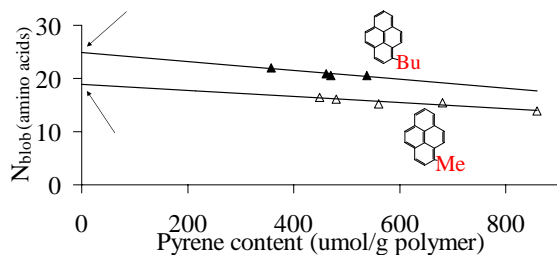
Volume Control

- Therefore, we must be able to control the lifetime of the pyrene probe.
- We do this by using Nitromethane, a well known quencher of pyrene fluorescence.
- For Example:

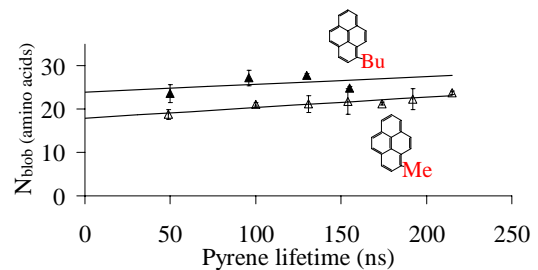


Results

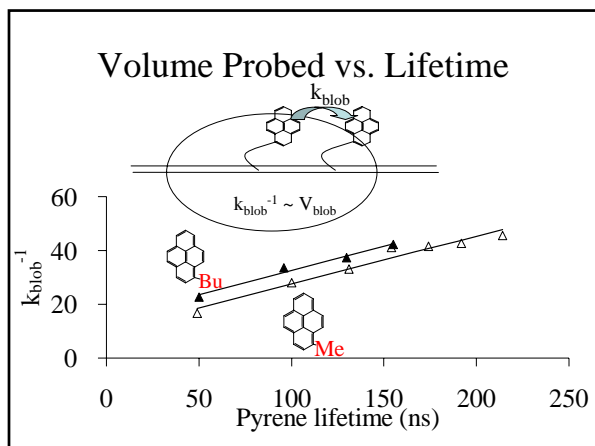
PGA $(CH_2)_2$ Py and PGA $(CH_2)_4$ Py at a Pyrene Lifetime ~ 155 ns



N_{blob} vs. Lifetime

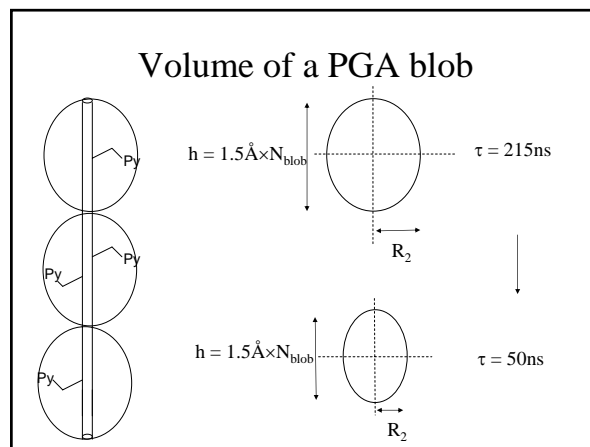
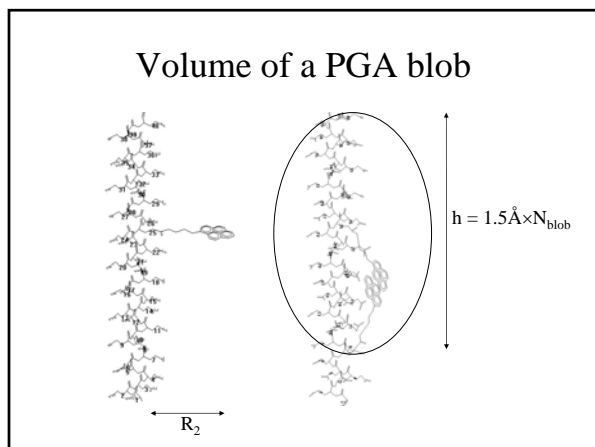


N_{blob} changes $\sim 20\%$ over the 50ns – 200ns range studied



Volume Probed

- N_{blob} decreases slowly with a decreasing lifetime, but V_{blob} decreases nearly 3 times over the same range!
- How? Why?



Finding the Volume

- Use an empirical equation derived for a pyrene labeled PEO system*, based on the diffusion of free pyrene:

$$k_{\text{blob}} = \frac{2 kT}{3 \eta} \frac{1}{V_{\text{blob}}}$$

- In this case, use

$$V_{\text{blob}} = \frac{4}{3} \pi \frac{h}{2} R_2^2 - \pi R_1^2 h$$

$V_{\text{blob}} =$ (Sphere) - (Cylinder)

*Lee, S.; Duhamel, J. *Macromolecules* **1998**, *31*, 9193-9200.

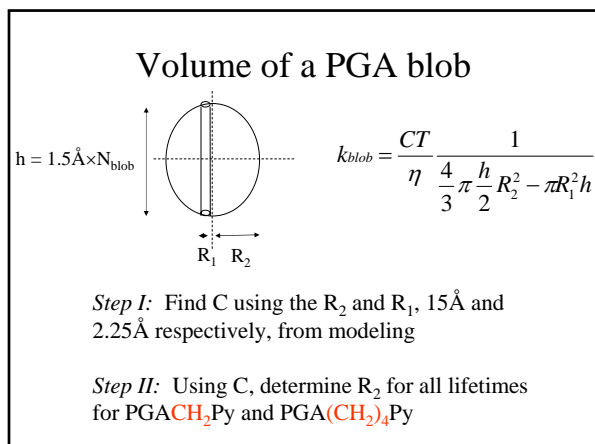
Finding the Volume

- *Complication:* The equation is based on free pyrene in solution, not attached to a chain.
- *Solution:* Use a constant to accommodate for the difference in geometry between a freely diffusing probe and a probe tethered to a rod.

$$k_{\text{blob}} = \frac{2 kT}{3 \eta} \frac{1}{V_{\text{blob}}} \longrightarrow k_{\text{blob}} = \frac{CT}{\eta} \frac{1}{V_{\text{blob}}}$$

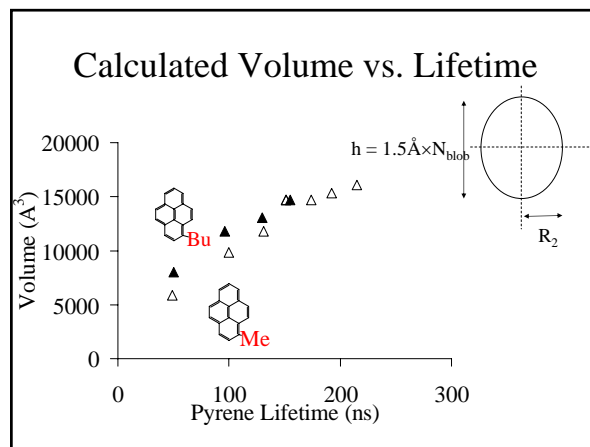
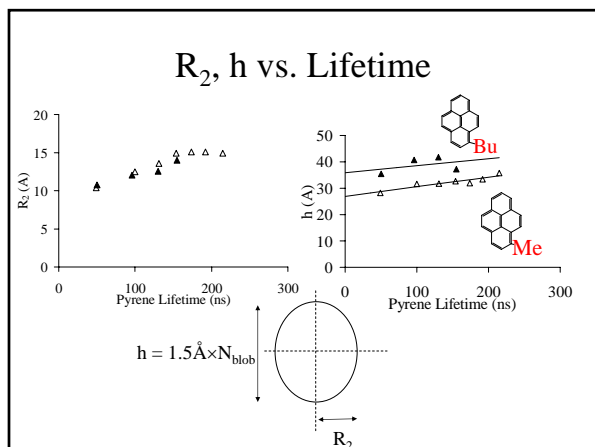
Therefore

$$k_{\text{blob}} = \frac{CT}{\eta} \frac{1}{\frac{4}{3} \pi \frac{h}{2} R_2^2 - \pi R_1^2 h}$$



Finding C using PGACH_2Py

τ (ns)	k_{blob} ($\times 10^7 \text{s}^{-1}$)	N_{blob} (a.a.)	h (\AA)	C^*T/η ($\times 10^{11} \text{JPa}^{-1}$)
215	2.2	23.8	35.7	3.6
192	2.3	22.3	33.4	3.5
174	2.4	21.3	31.95	3.5
154	2.4	21.8	32.7	3.6
131	3.0	21.2	31.8	4.3
100	3.6	21.1	31.65	5.2
49	6.0	18.8	28.2	7.7

$$k_{blob} = \frac{CT}{\eta} \frac{1}{\frac{4}{3}\pi\frac{h}{2}R_2^2 - \pi R_1^2 h}$$


- ### Summary of Results
- Value of $C \times (T/\eta)$ for free pyrene ($2/3k \times (T/\eta)$) is $3.5 \times 10^{12} \text{JPa}^{-1}$, a factor of 10 larger than the experimental value for our tethered pyrene, $3.5 \times 10^{11} \text{JPa}^{-1}$.
 - For $\text{PGA}(\text{CH}_2)_4\text{Py}$, the lifetime is too short to see the plateau; therefore at 155ns, it has not reached its full volume potential.
 - For PGACH_2Py , the length the side chain can probe into solution, R_2 , initially increases with time then becomes constant!

- ### Conclusions and Future Work
- Using the Fluorescence Blob Model, we can predict the volume probed by a side chain in a given amount of time.
 - Continue to extend the linker series, i.e. 5, 8, 11 atom linkers to establish a trend for the volume probed by a side chain.
 - These trends could be extrapolated to account for real amino acid side chains participating in protein folding.

Acknowledgements

Prof. Jean Duhamel and the
Duhamel Lab Group

The Institute for Polymer Research

Institute for Polymer Research
27th Annual Symposium

Symposium documents for

Deb Sarzotti

Abstract

Presentation

ETHYLENE AND PROPYLENE COPOLYMERIZATION WITH NON-CONJUGATED DIENES: SYNTHESIS AND CHARACTERIZATION

D.M. Sarzotti, L.C. Simon and J.B.P. Soares

Institute for Polymer Research, Department of Chemical Engineering, University of Waterloo

Introduction

Copolymerization of non-conjugated α,ω -dienes with ethylene or propylene yields functional polyolefins with unreacted vinyl groups that can be used to synthesize polyolefins with unique structures.^[1] These materials have sparked great interest because the reactive vinyl unsaturations can be used to prepare polyolefins with polar or heteroatomic (e.g., N, O) functionalities. Furthermore, polyolefin copolymerization with dienes can generate structures that act as macromonomers (very long α -olefin chains) and promote the incorporation of long chain branches (LCB) along the polymer backbone. With several coordination catalyst systems, non-conjugated dienes are also capable of undergoing cyclopolymerization resulting in polymers containing cyclic structures along the main chain.

Three types of propagation reactions are possible in the copolymerization of ethylene or propylene with linear, non-conjugated α,ω -dienes: 1,2- or 2,1-addition reactions, leaving pendant vinyl groups in the polymer; addition reactions of diene followed immediately by intramolecular cyclization, resulting in the formation of 1,3-cycloalkane structures along the polymer backbone; and reactions between a pendant double bond in the polymer chain with another propagating chain, forming a LCB or crosslinking point.^[2]

Ethylene/1,7-Octadiene Copolymerization

We have studied the copolymerization of ethylene with 1,7-octadiene (OD) using a methylaluminoxane (MAO) activated constrained geometry catalyst (dimethylsilyl(*N*-*tert*-butylamido) (tetramethylcyclopentadienyl)titanium dichloride) at 140°C in toluene. The catalyst activity as well as the molecular weights, chemical composition distributions and the number of vinyl functionalities of the resulting copolymers were determined (Table 1). Over the whole range of OD feed concentration investigated, the weight average molecular weight, M_w , and polydispersity index, M_w/M_n , increase with increasing OD in the feed. These increases are the result of the production of chains with long chain branches by the incorporation of pendant

double bonds into separate growing polymer chains. Table 1 also shows that the overall number of vinyl unsaturations increases for higher OD contents. The fact that the number of vinyl groups present in the final product increases with increasing OD content indicates that both vinyl groups have been polymerized for only a fraction of the total OD units incorporated.

Table 1 Ethylene/OD copolymerization results.

run	OD in feed ^a (mol-%)	activity (kg/mol _{Ti} ·h)	M_n^b (kg/mol)	M_w/M_n^b	T_c^c (°C)	vinyl groups ^d (/1000 C)	vinyl groups ^e (/1000 C)
1	0	15000	32	3.1	85	0.2	0.4
2	0.16	26000	35	5.6	78	1.3	1.3
3	0.31	25000	31	11	69	2.9	2.6
4	0.37	21000	27	14	64	3.5	3.1
5	0.41	16000	28	17	62	4.0	3.8
6	0.46	8000	20	17	57	3.8	4.4

^a Polymerization conditions: $T = 140$ °C; V (toluene) = 400 mL; P (C₂H₄) = 255 psig; [catalyst] = 9 μmol/L; [MAO] = 19.5 mmol/L; polymerization time = 10 min.

^b Determined by high-temperature GPC.

^c Peak crystallization temperature determined with Crystaf in TCB.

^d Number of double bonds per 1000 carbon atoms calculated from FT-IR spectra.

^e Number of double bonds per 1000 carbon atoms calculated from ¹H NMR spectra.

The distribution of unsaturated end groups was quantified by ¹H NMR and the amounts of vinylidene, vinyl and vinylene functionalities per chain were determined, revealing the relationships between of chain transfer mechanisms and OD content.

Analysis of ethylene/OD copolymers by ¹³C NMR indicates the formation of both 1,3-cycloheptane (CY₇) and 1,5-cyclononane (CY₉) structures. The relative amounts of CY₇ and CY₉ units appear to be independent of OD content with approximately 53 % of the total rings being CY₉ units. The ratio of cyclic units to vinyl groups is constant over the range of compositions analyzed, although the number of branches increases relative to both cyclic units and vinyl groups. From the results gathered, it can be concluded that the OD insertion mode is independent of OD content and is kinetically controlled at the polymerization conditions considered in this work.



Ethylene/1,7-Octadiene Copolymer Molecular Weight Fractions

An ethylene homopolymer sample (run 1) and the two ethylene/OD copolymers with the lowest OD contents (runs 2 and 3) were fractionated by molecular weight using a solvent/non-solvent

technique. Figure 1(a) shows the molecular weight distributions of a whole polymer (runs 3) and those of its fractions scaled according to the weight percentage of the total polymer that each represents. Plots of intrinsic viscosity as a function of molecular weight for an ethylene/OD copolymer (run 3) and its fractions (Figure 1(b)) clearly demonstrate that long chain branching increases with increasing molecular weight, as expected.

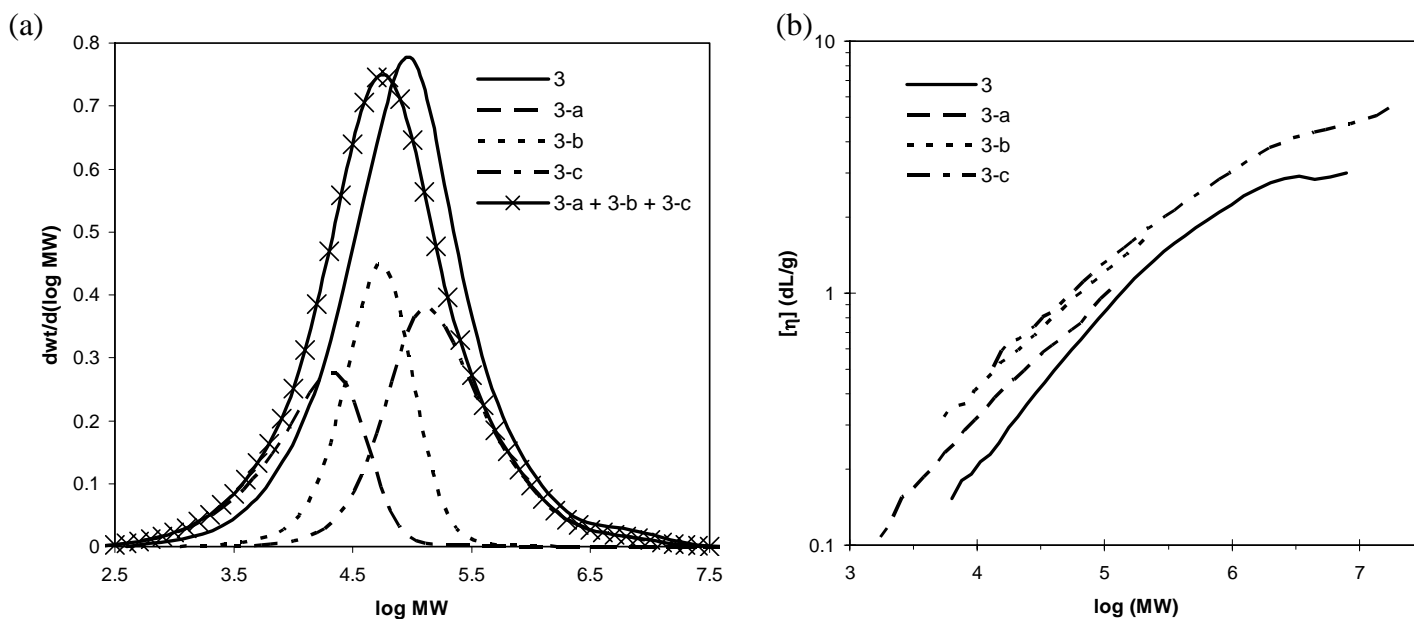


Figure 1 (a) Molecular weight distributions of ethylene/OD copolymer (run 3) and three fractions. Distributions of the fractions have been scaled by weight percentage and summed for comparison; (b) Intrinsic viscosity, $[\eta]$, of an ethylene/OD copolymer (run 3) and its fractions as a function of molecular weight measured by differential viscometry during GPC analysis.

Molecular weight fractions of the copolymer produced in run 3 were further analyzed by ^1H and ^{13}C NMR, revealing that the number of cyclic units per 1000 carbon atoms and the relative quantities of CY_7 and CY_9 units are independent of molecular weight. As molecular weight increased, the vinyl group content decreased and the number of branches per 1000 carbon atoms increased, confirming that the observed increase in molecular weight with increasing OD content is a result of the incorporation of pendant vinyl groups to form long chain branched or crosslinked structures.

Propylene/1,7-Octadiene and Propylene/1,9-Decadiene Copolymerization

The copolymerization of propylene with both OD and 1,9-decadiene (DD) using *rac*-dimethylsilanediybis(2-methyl-4-phenylindenyl)zirconium dichloride/MAO in toluene at temperatures above 100°C has been investigated. The molecular weight distributions of propylene/OD and propylene/DD copolymers synthesized at 120°C with 50 psi monomer pressure are shown in Figure 2. Preliminary results indicate that OD almost exclusively undergoes cyclization following insertion but that DD is incorporated as pendant 1-octenyl branches which are subsequently polymerized, resulting in materials with significant levels of long chain branching.

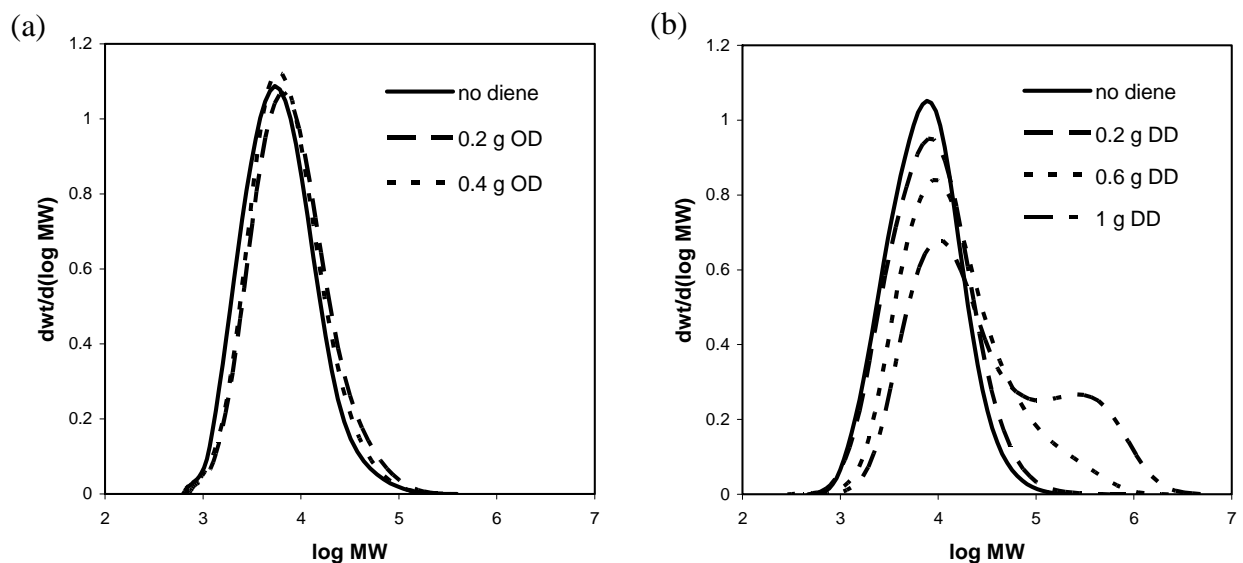


Figure 2 (a) Molecular weight distributions of propylene/OD copolymers; (b) Molecular weight distributions of propylene/DD copolymers.

References

- [1] T. Uozumi, G. Tian, C.-H. Ahn, J. Jin, S. Tsubaki, T. Sano, K. Soga, *J. Polym. Sci., Part A: Polym. Chem.* **2000**, *38*, 1844.
- [2] N. Naga, A. Toyota, *Macromol. Rapid. Commun.* **2004**, *25*, 1623.

Ethylene and propylene copolymerization with non-conjugated dienes: Synthesis and characterization

Deborah Sarzotti

Department of Chemical Engineering, University of Waterloo

May 18, 2005

Institute for Polymer Research Symposium on Polymer Science/Engineering 2005

Outline

- Introduction
- Propylene copolymerization
 - 1,7-octadiene
 - 1,9-decadiene
- Ethylene copolymerization
 - 1,7-octadiene
 - MW fractionation and compositional analysis
- Conclusions

Introduction

- Non-conjugated α,ω -dienes
- Copolymerization of dienes with ethylene (E) or propylene (P) yields polyolefins with unreacted vinyl groups that can be used to synthesize materials with unique structures
 - incorporate polar or heteroatomic functionalities
 - promote long chain branching
 - cyclic structures along main backbone

Background

- Three possible propagation reactions:
 - 1,2- or 2,1-addition \rightarrow pendant vinyl groups
 - addition followed by intramolecular cyclization \rightarrow 1,3-cycloalkane
 - addition of a pendant double bond into another propagating chain \rightarrow long chain branch or crosslinking point
- 1,5-hexadiene preferentially inserted as cyclopentane
- insertion mode of 1,7-octadiene (OD) dependent on catalyst and polymerization conditions
- little work with 1,9-decadiene (DD)

P/OD copolymers

Copolymerization of propylene and OD with metallocene/MAO:

run	P (psig)	[OD] (mol/L)	activity ^a (kg·mol ⁻¹ ·atm ⁻¹ ·h ⁻¹)	M_n^b (kg/mol)	M_w/M_n^b	$T_m,final^c$ (°C)	T_g^c (°C)	crystallinity ^d (%)
P/OD-1	50	0	10500	4.8	2.2	132	-	36
P/OD-2	50	0.012	7600	5.4	2.3	129	-12	30
P/OD-3	50	0.024	5200	5.0	2.1	114	-9	21
P/OD-4	70	0	12700	5.3	2.7	139	-	41
P/OD-5	70	0.012	10900	5.9	2.7	133	-12	37
P/OD-6	70	0.024	10100	6.3	2.8	128	-11	35
P/OD-7	70	0.036	10100	6.7	2.7	123	-9	26

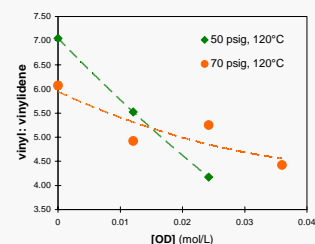
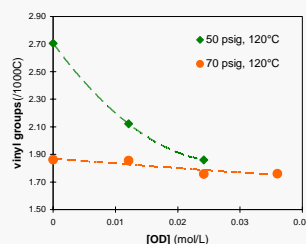
^a Polymerization conditions: $T = 120^\circ\text{C}$; V (toluene) = 150 mL; [catalyst] = 3.3 $\mu\text{mol/L}$; Al/catalyst = 500; polymerization time = 10 min.

^b Determined by high-temperature GPC.

^c Determined by DSC at a heating rate of $10^\circ\text{C}/\text{min}$ following cooling at the same rate.

^d Relative to the enthalpy of fusion of 100% crystalline PP, 209 J/g.

P/OD copolymers – ¹H NMR



P/DD copolymers

Copolymerization of propylene and DD with metallocene/MAO:

run	T (°C)	[DD] (mol/L)	activity ^a (kg/mol M-atm·h)	M _n ^b (kg/mol)	M _w /M _n ^b	T _{m,final} ^c (°C)	T _c ^c (°C)	crystallinity ^d (%)
P/DD-1	120	0	10500	4.8	2.2	132	-	36
P/DD-2	120	0.010	6300	5.5	2.3	n.m.	n.m.	n.m.
P/DD-3	120	0.029	4500	8.2	4.7	101	-5	- ^e
P/DD-4	120	0.048	2700	11.4	11.5	n.m.	n.m.	n.m.
P/DD-5	105	0	14000	9.9	2.4	148	-	43
P/DD-6	105	0.010	16900	11.1	3.4	n.m.	n.m.	n.m.
P/DD-7	105	0.029	14900	14.9	11.9	121	-4	18
P/DD-8	105	0.048	10400	17.7	21.5	111	-6	- ^e

n.m. - not measured

^a Polymerization conditions: P(C₃H₆) = 50 psi; V (toluene) = 150 mL; [catalyst] = 3.3 μmol/L; Al:catalyst = 500; polymerization time = 10 min.

^b Determined by high-temperature GPC.

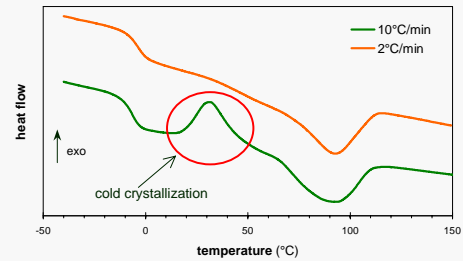
^c Determined by DSC at a heating rate of 10°C/min following cooling at the same rate.

^d Relative to the enthalpy of fusion of 100% crystalline PP, 209 J/g.

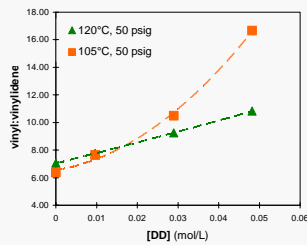
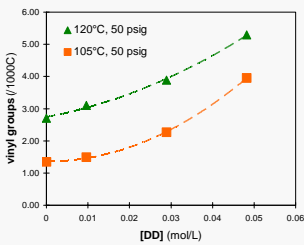
^e Not calculated due to occurrence of cold crystallization.

P/DD copolymers – DSC

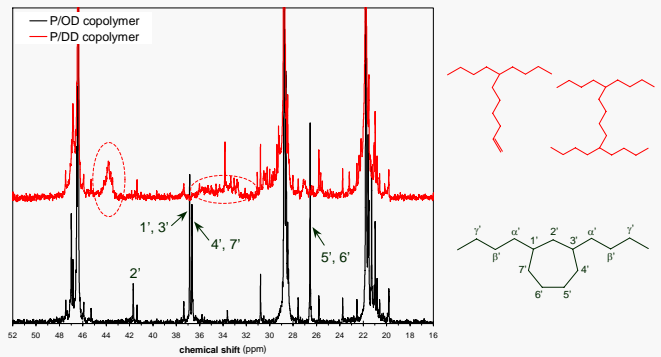
DSC analysis of P/DD-8 at different heating rates



P/DD copolymers – ¹H NMR

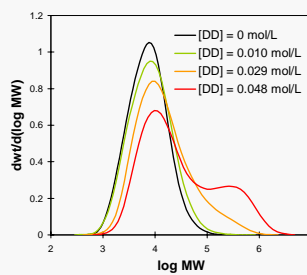
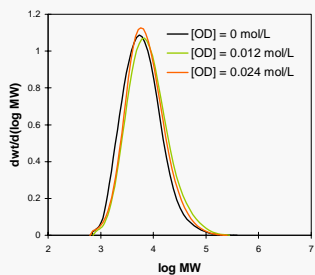


P/OD and P/DD copolymers – ¹³C NMR



OD & DD copolymers - MWD

Same polymerization conditions (T = 120°C, P(C₃H₆) = 50 psig)



E/OD copolymers

Copolymerization of ethylene and OD with CGC-Ti/MAO [1]:

run	OD in feed ^a (mol-%)	activity (kg/mol·h)	M _n ^b (kg/mol)	M _w /M _n ^b	T _c ^c (°C)	vinyl groups ^d (/1000 C)	rings ^e (/1000 C)	CY ₇ /CY ₉ ^{f,g}
1	0	15000	32	3.1	85	0.4	-	-
2	0.16	26000	35	5.6	78	1.3	2.08	0.95
3	0.31	25000	31	11	69	2.6	4.98	0.96
4	0.37	21000	27	14	64	3.1	-	-
5	0.41	16000	28	17	62	3.8	7.70	0.92
6	0.46	8000	20	17	57	4.4	-	-

^a Polymerization conditions: T = 140 °C; V (toluene) = 400 mL; P(C₂H₄) = 255 psig; [catalyst] = 9 μmol/L; [MAO] = 19.5 mmol/L; polymerization time = 10 min.

^b Determined by high-temperature GPC.

^c Peak crystallization temperature determined with Crystaf in TCB.

^d Number of double bonds per 1000 carbon atoms calculated from ¹H NMR spectra.

^e Determined by ¹³C NMR.

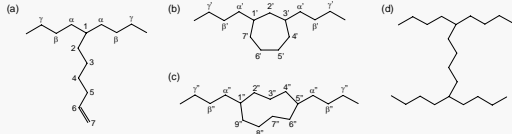
^{f,g} Number of cycloheptane units (CY₇) divided by number of cyclononane units (CY₉).

[1] D.M. Sarzotti, L.C. Simon, J.B.P. Soares, *Macromol. Mater. Eng.* **2005**, in press.

E/OD copolymers

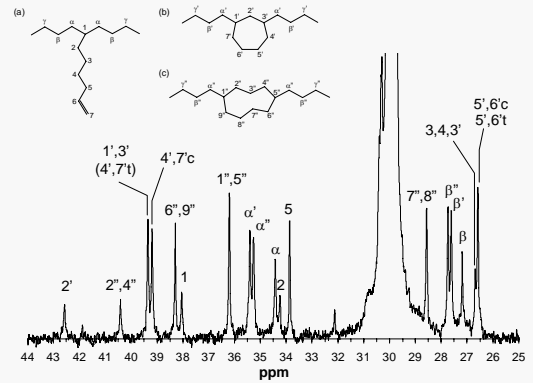
Four propagation reactions:

- 1,2- or 2,1-addition insertion
- intramolecular cyclization following addition
- intramolecular cyclization in the penultimate position [2]
- addition of pendant double bond (macromonomer)

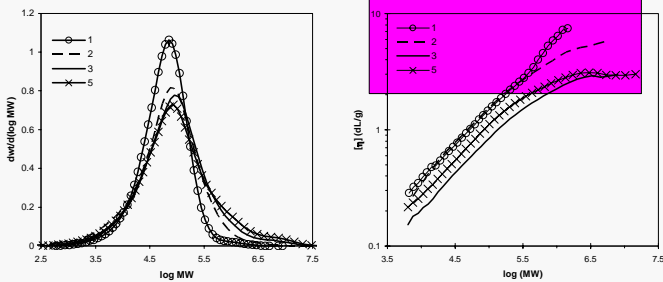


[2] N. Naga, A. Toyota, *Macromol. Rapid. Commun.* **2004**, *25*, 1623.

E/OD copolymers



E/OD copolymers -

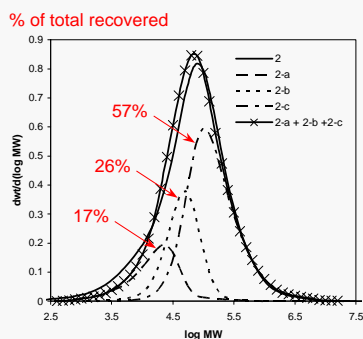


MW Fractionation

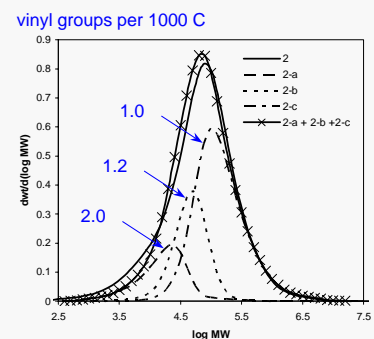
- Investigate compositional uniformity
 - distribution of structures resulting from different modes of diene incorporation
- Pietikäinen *et al.* [3] used thermal analysis and the segregation fractionation technique
 - no physical separation
- Samples fractionated by molecular weight
 - Solvent/non-solvent technique
 - low, medium and high MW fractions with 50, 58 and 100% solvent

[3] P. Pietikäinen, P. Starck, J. V. Seppälä, *J. Polym. Sci., Part A: Polym. Chem.* **1999**, *37*, 2379.

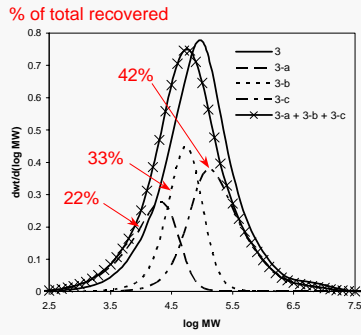
Fractions of E/OD copolymer



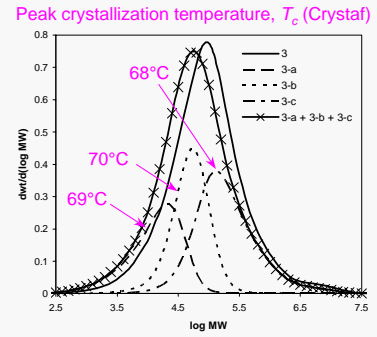
Fractions of E/OD copolymer



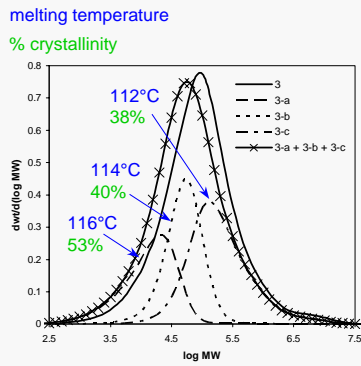
Fractions of E/OD copolymer



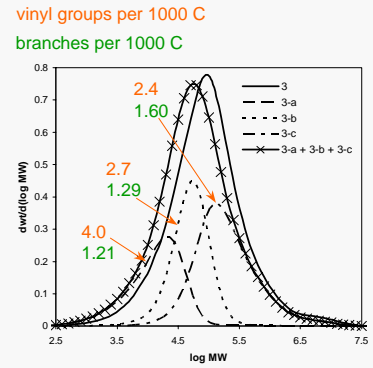
Fractions of E/OD copolymer



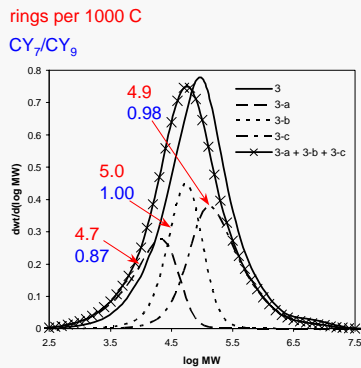
Fractions of E/OD copolymer



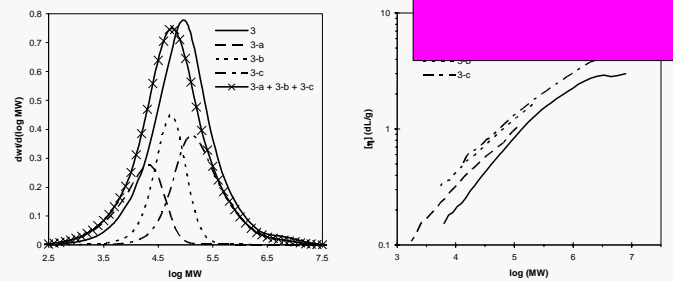
Fractions of E/OD copolymer



Fractions of E/OD copolymer



Fractions of E/OD copolymer



Conclusions

- Propylene copolymerization by metallocene/MAO
 - 1,7-octadiene incorporated as cycloheptane units
 - 1,9-decadiene incorporated as 1-octenyl branches and pendant vinyls incorporated to form long chain branches
 - Ethylene copolymerization by CGC-Ti/MAO
 - 1,7-octadiene incorporated as cycloheptane and cyclononane units as well as 1-hexenyl branches
 - fractionation by MW indicates that distribution of structures due to OD incorporation is uniform
-

Institute for Polymer Research
27th Annual Symposium

Symposium documents for

Emma Daly

Abstract

Presentation

Reactivity Ratio Estimation: Statistical Issues and Solutions

E.K. Daly, T.A. Duever, A. Penlidis

Institute for Polymer Research, Department of Chemical Engineering, University of Waterloo

Reactivity ratio estimation is a nonlinear multiresponse problem which has been discussed extensively in the literature, due to its application to both academia and industry (Polic, 1998). Typically, reactivity ratios are estimated using the instantaneous copolymer composition equation, based on low conversion (<5%) copolymer composition data, otherwise known as the Mayo-Lewis Model. The estimation method used to determine the reactivity ratios from the Mayo-Lewis model however varies from linear techniques to non-linear, such as the error in variables model (EVM) approach. Recently sequence length distribution information, such as triad fraction data, has become of greater interest in the parameter estimation research, due to the greater number of response variables and thus potentially better estimates of the reactivity ratios. In this research the EVM parameter estimation technique is compared to the results obtained when using the standard Box Draper Determinant Criterion approach for triad fraction data. Furthermore, the potential improvement in reactivity ratio estimation using triad fraction data in place of and in addition to composition data is considered.

Equations for either composition or triad fraction data can be derived for both the terminal and penultimate models. These equations can also be further classified into either instantaneous or cumulative models. The most widely used copolymerization model is the Mayo-Lewis model (1944), which expresses the terminal model using instantaneous composition data. The terminal model assumes that only the last monomer unit on the growing chain influences the subsequent monomer addition. The Mayo-Lewis model relates the instantaneous mole fraction of monomer 1 bound in the copolymer, F_1 , with the mole fractions of free monomer 1 and 2 (f_1 and f_2 respectively) via the reactivity ratios r_1 and r_2 .

Whilst copolymer composition data is easily obtained and thus has been discussed extensively in the literature, the use of triad fraction data is minimal due to the experimental complications involved in obtaining this type of data in the past. However, there has been an increase in efforts to use sequence length (triad fraction) data for estimation of the reactivity ratios, given the triad fraction equations by Koenig (1980). The triad fraction equations reported by Koenig (1980) relate the instantaneous monomer 1 centered or monomer 2 centered triads to the mole fractions of free monomer 1 and 2, f_1 and f_2 , via the reactivity ratios r_1 and r_2 .

The parameter estimation techniques used to obtain reactivity ratio values, have been studied by many authors over the years including Kelen-Tudos, Fineman-Ross and Tidwell Mortimer. These authors used general linear estimation techniques and applied them to various forms of the Mayo-Lewis model using certain assumptions and manipulation of equations. However, as Rossignoli and Duever (1995) discussed, forcing the copolymerization problem into a linear form breaks the inherent assumptions of linear estimation techniques and thus the methods are statistically invalid.

Another well known estimation technique is the Box Draper Determinant Criterion (1965), which is the most popular method for multiresponse problems. However, it does require that the independent variable has insignificant error compared to the dependent variable which poses issues in the reactivity ratio estimation problem (Rossignoli and Duever, 1995). The error in variables model (EVM) is a somewhat more recent estimation technique, which does not require as many assumptions and appears to be a more suitable method for reactivity ratio estimation.

It is reasonable then to suggest that analysis of the variables of a model and their error structure is an important stage to the parameter estimation problem. Error structure refers to: the size of the error associated with each measured variable; the errors relation to the variable; and the distribution of the error. The sizes of the measurement errors in the following case studies were assumed to be 5% for feed composition and triad fraction data and 10% for copolymer composition. The errors relation to the variable is typically defined as being either additive or multiplicative. In this research we used a multiplicative error structure for composition data, as this has been reported in the literature to be a structure most applicable to the data. However, triad fraction error structure has not been studied to any great extent and thus in this research the data set is analyzed and discussed with both error structures, to illustrate the importance of understanding the error structure of the data. Lastly, the distribution assumed for this research, where error limits are only indicated, is that of uniform.

EVM versus Box Draper Determinant Criterion using Triad Fraction Data

Burke et al (1994) provided experimental NMR triad peak data for the styrene/methyl methacrylate system in bulk at 60°C. The reactivity ratio parameter estimation problem was completed for two cases; the multiresponse determinant criterion and the error in variables model.

In the first case using the determinant criterion, the parameter estimation is a multi-response problem, where triad fractions are responses and the monomer feed fraction, f_1 , is an independent variable. As discussed by Burke (1994), if all the data is used in the parameter estimation problem then issues involving co-linearity will be present, due to the triads summing to equal one. Co-linearity problems cause the solution to be very unstable and the variance of the parameter estimates to be quite large. Consequently, in order to avoid these problems two redundant variables were eliminated arbitrarily from the system.

The parameter estimation was carried out using both the multiresponse determinant criterion and the EVM approach coded in MATLAB. Comparison of the two parameter estimation methods and the effect of the error structure can be seen when the point estimates and the exact 95% confidence region for the cases are plotted (refer to Figure 1).

As can be seen the determinant criterion estimate falls outside the 95% confidence region of both the additive error and the multiplicative error EVM cases. There are two possible explanations for this behavior, the first is that the determinant criterion does not include the feed composition to be a random variable with error, but rather assumes that the error associated with the feed is negligible compared to the error in the triad fraction measurements. Furthermore, it has been shown by Oxby et al (2003) that the Box Draper Determinant Criteria method for parameter estimation is highly dependent on the data sample size.

In order to determine if the sample size was indeed the cause of the estimates not being in agreement, simulated data was used to increase the amount of data used in the analysis. Eight simulated points were used in conjunction with the experimental data provided by Burke to create a sixteen point data set. The analysis was redone using both the EVM and Box Draper Determinant Criteria methods and the resulting joint confidence regions can be seen in Figure 1 as the grey points. It can be seen that the simulated data combined with the experimental Burke (1994) data results in the estimates of the reactivity ratios being in agreement. The determinant criteria estimate using the sixteen data points falls within the JCR of both the purely experimental Burke data EVM (additive error) contour and the Simulated Burke data EVM (additive error) contour. Therefore, this shows that the Determinant Criteria estimate is highly dependent on the size of the data set, while

the EVM method (additive error) point estimate is not. As expected, the confidence region of the EVM method is reduced as the amount of data for analysis increased. Further analysis of the diagram shows that the error structure of the data greatly influences the parameter point estimates and their respective exact shaped 95% probability confidence contours.

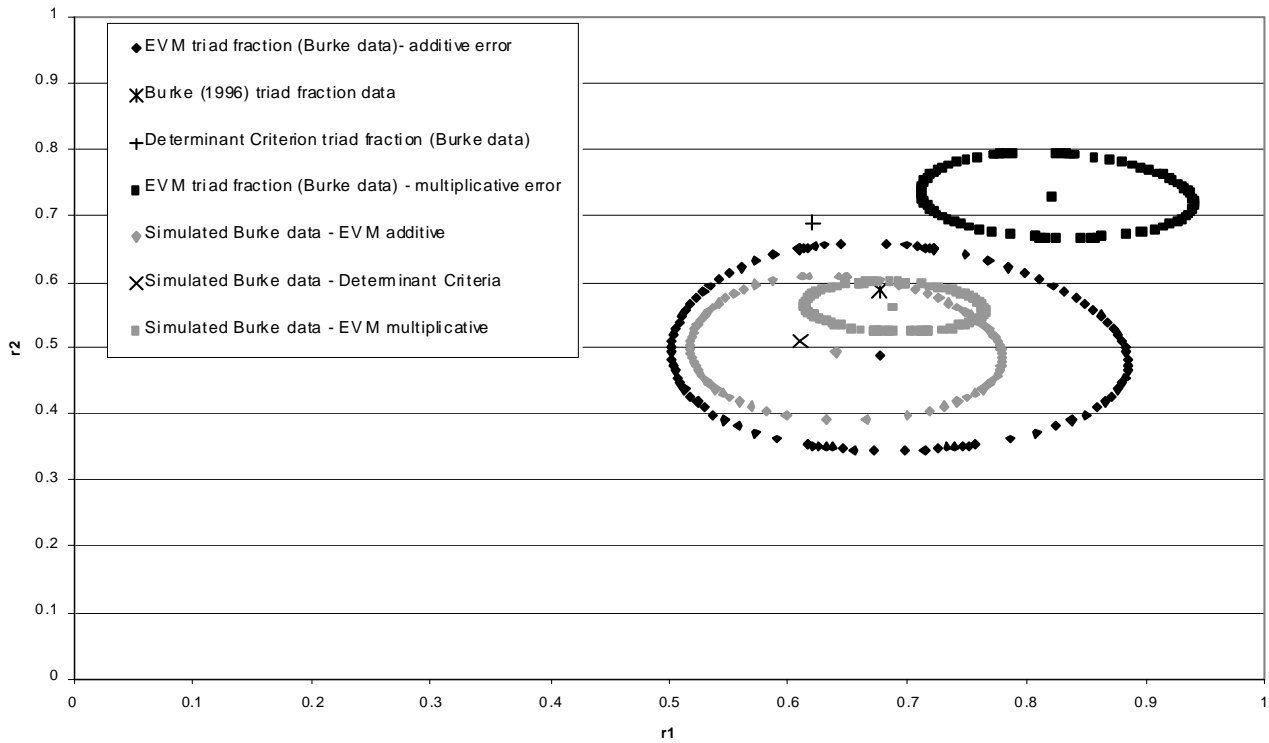


Figure 1: 95% Joint Confidence Region for EVM analysis of triad fraction data

Triad Fraction versus Composition Data using the EVM parameter estimation technique

Maxwell et al. (1993) studied the copolymerization of styrene and methyl methacrylate at 40°C in bulk and presented extensive experimental data on both copolymer composition and triad fractions. Therefore, both data types were analyzed in this research in order to: determine whether the point estimates were influenced by the data type used; determine if one data type resulted in a smaller confidence region (less uncertainty); and evaluate the potential improvement of using both data types combined. The point estimates obtained from the different data sets along with the point estimates published by Maxwell et al (1993), can be seen in Table 1.

Table 1: Point estimates obtained using either triad fraction or composition data and the literature values published by Maxwell et al (1993).

	Data Source	Estimation Method	Error Structure	r1	r2
Maxwell (1993)	Triad fraction	NLLS		0.51	0.52
Maxwell (1993)	Composition	NLLS		0.48	0.42
Daly (2005)	Maxwell triad fraction	EVM	Additive	0.526	0.5078
Daly (2005)	Maxwell triad fraction	EVM	Multiplicative	0.6512	0.3683
Daly (2005)	Maxwell composition	EVM	Additive	0.479	0.4182
Daly (2005)	Maxwell composition	EVM	Multiplicative	0.4787	0.418
Daly (2005)	Maxwell triad and composition combined	EVM	Additive	0.5427	0.4846
Daly (2005)	Maxwell triad and composition combined	EVM	Multiplicative	0.6143	0.3683

The exact shaped 95% probability joint confidence regions of the triad fraction and the copolymer composition (refer to Figure 2) demonstrate the following:

- i) The use of triad fraction data results in less uncertainty in the parameter estimates (reactivity ratios) than using the conventional copolymer composition data.
- ii) The use of either multiplicative or additive error structure to copolymer composition data does not significantly affect the point estimate obtained; however the uncertainty in the parameter estimates is greatly reduced when using a multiplicative error structure.
- iii) The use of either multiplicative or additive error structure to the triad fraction/NMR peak data does significantly affect the point estimates and the confidence region (uncertainty) of the parameters.

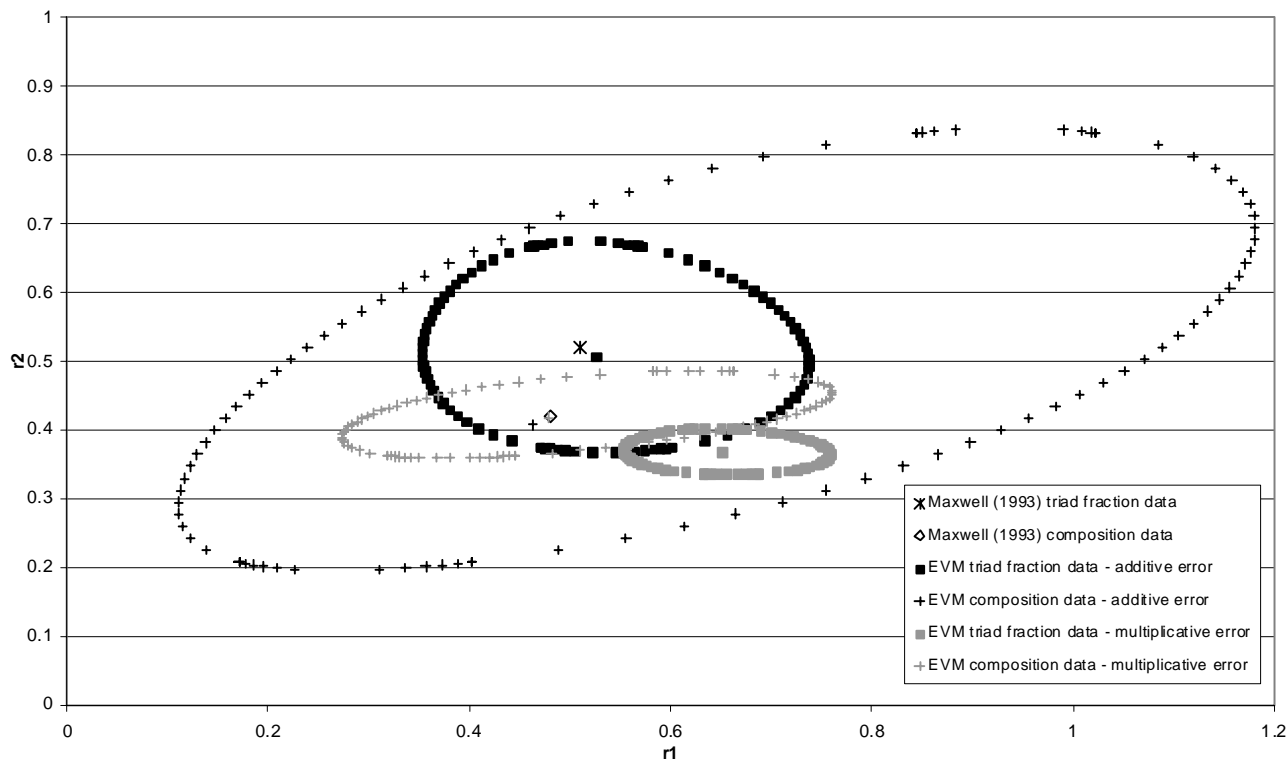


Figure 2: 95% Joint Confidence Region for EVM analysis of Maxwell et al (1993) triad data and composition data cases (additive and multiplicative error)

The question then becomes, is multiplicative error structure the incorrect structure for triad fraction/NMR normalized peak area data, or is the point estimates published in the literature incorrect due to statistically invalid parameter estimation techniques (i.e. non linear least square - NLLS)?

The next stage of analysis was to determine whether using all the available composition and triad fraction data results in a significant improvement in the degree of uncertainty of the reactivity ratio estimates compared to the confidence when using only triad fraction data (refer to Figure 3). The additional use of the copolymer composition data with the triad fraction data does not appear to have a significant increase in confidence, compared to that obtained when using only triad fraction data. That is, the slight decrease in area of the joint confidence region when both data sets are used does not seem sufficiently significant to warrant the need for conducting the measurement of the copolymer composition, regardless of which error structure is implemented.

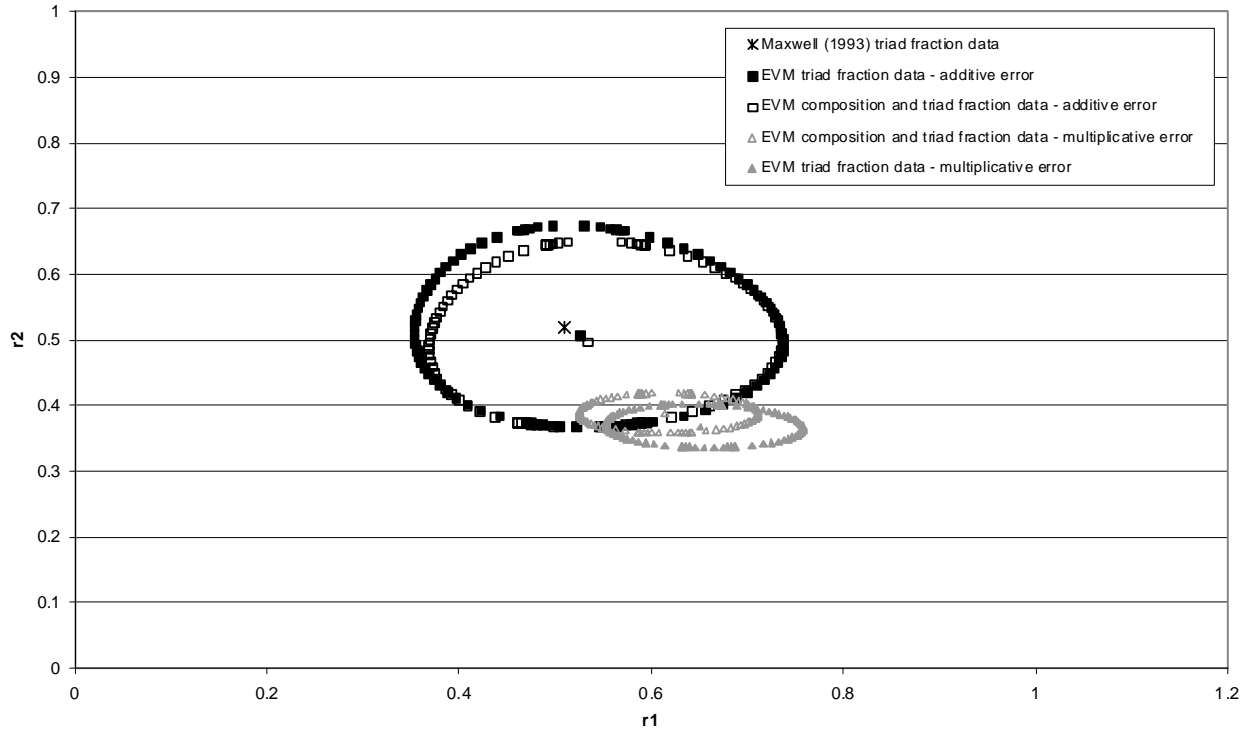


Figure 3: 95% Joint Confidence Region for EVM analysis of Maxwell et al (1994) triad and composition data combined vs. only triad fraction data



Reactivity Ratio Estimation: Statistical Issues and Solutions

Research Seminar

Emma Daly
May 18, 2005

Department of Chemical Engineering
University of Waterloo

Outline

- Introduction and objectives
- Background
 - Basic Models
 - Parameter Estimation Methods
- Results and Discussion
 - Point estimates and 95% Probability exact shaped joint confidence regions (JCR)
- Conclusions
- Future work

Introduction and Objectives

- Reactivity ratio estimation – a nonlinear parameter estimation problem.
- MATLAB program based on the EVM parameter estimation algorithm (Reilly, 1993).
- Triad fraction or composition data - which gives better estimates?
- Combining the data sets – any improvement?

Basic Models

- Terminal or Penultimate?
- Research based on Terminal Model

	Composition data		Triad Fraction data
Instantaneous Model	Mayo – Lewis Equation		Koenig Equations
Cumulative Integral Model	Analytical Solution (Meyer Lowry Model)	Numerical Solution	Numerical solution

Basic Models

	Composition data		Triad Fraction data
Instantaneous Model	Mayo – Lewis Equation		Koenig Equations
Cumulative Integral Model	Meyer Lowry Model	Numerical Solution	Numerical solution

$$F_1 = \frac{r_1 f_1^2 + f_1 f_2}{r_1 f_1^2 + 2 f_1 f_2 + r_2 f_2^2}$$

Basic Models

	Composition data		Triad Fraction data
Instantaneous Model	Mayo – Lewis Equation		Koenig Equations
Cumulative Integral Model	Meyer Lowry Model	Numerical Solution	Numerical solution

$$A_{111} = \frac{r_1^2 f_1^2}{r_1^2 f_1^2 + 2r_1 f_1 f_2 + f_2^2}, \quad A_{212} = \frac{f_2^2}{r_1^2 f_1^2 + 2r_1 f_1 f_2 + f_2^2}$$

$$A_{211} = A_{112} = \frac{r_1 f_1 f_2}{r_1^2 f_1^2 + 2r_1 f_1 f_2 + f_2^2}, \quad \text{thus, } A_{211+112} = \frac{2r_1 f_1 f_2}{r_1^2 f_1^2 + 2r_1 f_1 f_2 + f_2^2}$$

Basic Models

- Triad fraction data obtained from NMR peak data (Aerdts, 1993).

$$\begin{bmatrix} X \\ Y \\ Z \end{bmatrix} = \begin{bmatrix} 0 & 0 & (1-\sigma_{12})^2 \\ 1 & (1-\sigma_{12}) & 2\sigma_{12}(1-\sigma_{12}) \\ 0 & \sigma_{12} & \sigma_{12}^2 \end{bmatrix} \begin{bmatrix} A_{111} \\ A_{112+211} \\ A_{212} \end{bmatrix}$$

$$\begin{bmatrix} A \\ BC \\ D \end{bmatrix} = \begin{bmatrix} \sigma_{22} & \sigma_{22}\sigma_{12} & \sigma_{12}^2 \\ 2\sigma_{22}(1-\sigma_{22}) & (1-\sigma_{12}\sigma_{22}) & (1-\sigma_{12}^2) \\ (1-\sigma_{22})^2 & 0 & 0 \end{bmatrix} \begin{bmatrix} A_{222} \\ A_{122+221} \\ A_{121} \end{bmatrix}$$

- Where σ_{22} is tacticity parameter, σ_{12} is the coisotacticity parameter (Aerdts, 1993).

Review of Estimation Methods

- Linear(ized) methods
 - Fineman-Ross (FR)
 - Kelen-Tudos (KT)
 - Extended KT
 - Inverted FR
- Nonlinear Methods
 - Nonlinear Least Squares (NLLS): Copolymer Comp. data
 - Box Draper Determinant Criterion: Triad fraction data
 - Error in Variables Model (EVM): BOTH

Review of Estimation Methods: Linear Models

- Estimates of reactivity ratios (rr) using linear models are well known to be statistically incorrect due to violation of linear regression assumptions, namely;
 - The error in the independent variable is negligible.
 - The error associated with the dependent variable is assumed independent and identically Normally distributed for the purpose of making statistical inferences.
- Linear estimates are however good initial values for NL parameter estimation problems.

Review of Estimation Methods: Nonlinear Models

- NLLS minimizes sum of squared differences between observed and fitted values of the dependent variable.
 - E.g. Mayo Lewis model: dependent variable = copolymer comp.
- Determinant Criterion minimizes determinant of the estimate of the covariance matrix.
 - Multi response problems: Multi dependent variables = triads.
- Determinant + NLLS: Negligible error in the independent variables.
 - I.e. Feed composition has insignificant error.
- EVM: Compares measured and fitted values, but it does so for all measured variables.
 - Assigns relative weights to measured quantities according to their precision.

Error Structure

- Error structure refers to:
 - size of the error associated with each measured variable.
 - errors relation to the variable (additive or multiplicative).
 - distribution of the error.
- In this work:
 - Size = 5% for feed composition & triad fraction data, 10% for copolymer composition.
 - Distribution = uniform.
 - Relation to variable = multiplicative for copolymer composition; analyzed both for triad fraction data.

Review of Estimation Methods: EVM

- EVM consists of two statements:
 - 1) Equating the vector of measurements X to the vector of true values ξ .
For an additive error vector ϵ ,
$$X = \xi + \epsilon$$
while for a multiplicative error vector ϵ ,
$$X = \xi (1 + \epsilon)$$
 - 2) Relates the true values of the parameters (θ^*) and variables with a model represented by;

$$f(\xi, \theta^*) = 0$$

$$f(\xi, \theta^*) = F_1^* - \frac{r_1^* f_1^{*2} + f_1^* (1 - f_1^*)}{r_1^* f_1^{*2} + 2f_1^* (1 - f_1^*) + r_2^* (1 - f_1^*)^2}$$

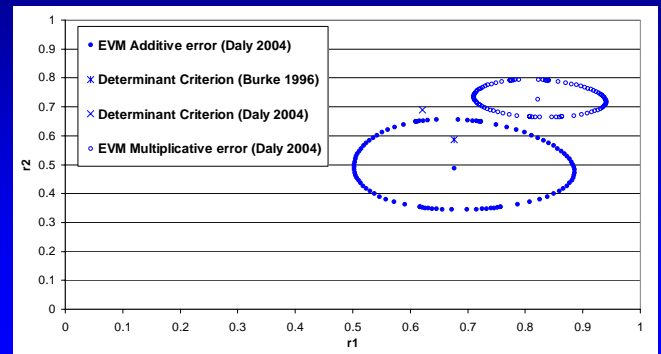
- EVM is a nested-iterative scheme (Rossignoli, 1995 or Reilly, 1993).

Triad Fraction Data: EVM vs. Determinant Criterion

- To ensure EVM program worked with triad fraction data, performed analysis on same data set using Box Draper Determinant Criterion.
- Compared the two methods performance at reactivity ratio estimation.

Results: Triad fraction data

STY-MMA: 95% Probability exact shaped Joint Confidence Regions (JCR);



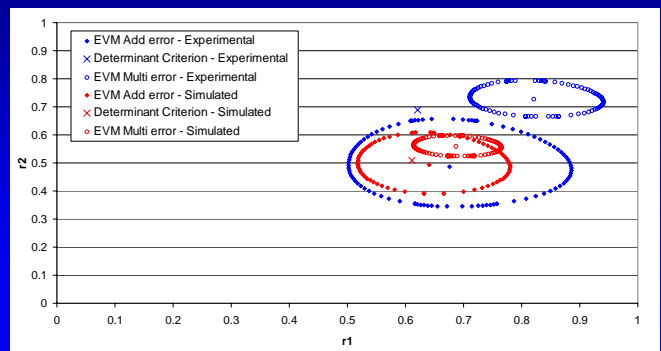
Data set provided by Burke (1997)

Discussion: EVM vs. Box Draper

- Determinant Criterion \neq EVM
- Explanation??
 - Determinant Criterion assumes error in feed composition to be insignificant.
 - Determinant Criterion method is highly dependent on the data sample size (Oxby et al., 2003).

Results: Simulated data set

- STY-MMA: 95% Exact shaped Joint Confidence Regions (JCR)



Data set provided by Burke (1997)

Discussion

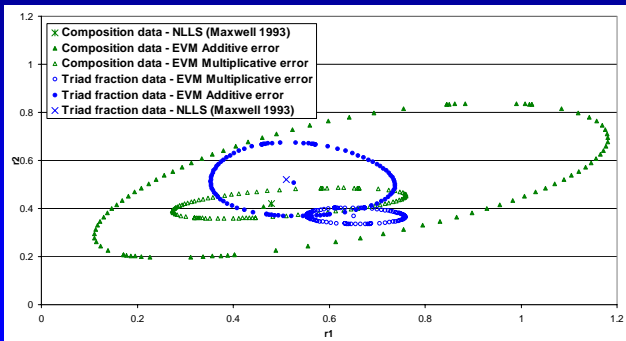
- Determinant Criterion point estimate shifts significantly when data set increased. Thus, the estimate is highly dependent on the size of the data set.
- EVM JCR area decreased as data set increased.
- Error structure influences location of the parameter point estimates.

EVM: Triad Fraction vs. Composition data

- Are triad fractions a better statistical data set for reactivity ratio parameter estimation?

EVM: Triad Fraction vs. Composition data set

- STY-MMA: 95% Exact shaped Joint Confidence Regions (JCR)



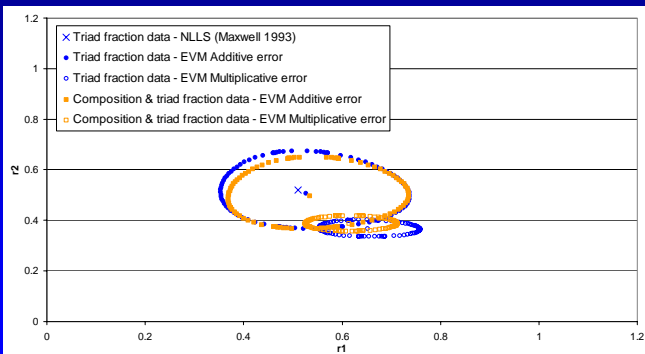
Data set provided by Maxwell et al. (1993)

Discussion

- The 95% exact shaped JCR's demonstrate the following:
 - Use of triad fraction data results in less uncertainty than using the conventional copolymer composition data.
 - Use of either error structures to copolymer composition data **does not** significantly affect the location of point estimates; however multiplicative structure greatly reduces uncertainty.
 - Use of either error structures to triad fraction data **does** significantly affect the location and confidence of the point estimates.
 - Literature value not contained in JCR of triad fraction data with a multiplicative error structure.
- Thus the question becomes: Is multiplicative error the incorrect structure for triad fraction data, or are literature point estimates incorrect?

EVM: Triad Fraction vs. Combined data set

- STY-MMA: 95% Exact shaped Joint Confidence Regions (JCR)



Data set provided by Maxwell et al. (1993)

Discussion

- Slight decrease in JCR area when both data sets are used = slight increase in confidence in the point estimates.
- Change in JCR area not sufficiently significant to warrant need for conducting the extra measurement (regardless of error structure implemented).

Conclusions

- EVM is a better statistical parameter estimation method than other conventional NL methods.
- Using triad fraction data results in less uncertainty in parameter estimates. However, NMR peak assignment and thus triad fraction data may be difficult to obtain.
- If obtaining triads are possible then no need to obtain copolymer composition data.
- Multiplicative error for triad fraction data is either incorrect structure or the literature point estimates are incorrect.

Future work

- Cumulative Composition Integral Model in EVM MATLAB program, both the analytical and numerical solution.
 - To account for feed composition drift in high conversion copolymerization.
- Terpolymer composition model in EVM MATLAB program.

Acknowledgements

- Prof. Tom Duever and Prof. Alex Penlidis
- Ontario Graduate Scholarship
- Anil Dalvi, 4th yr student who begun transfer of Fortran EVM coding to MATLAB.

Questions?

Ethylene and propylene copolymerization with non-conjugated dienes: Synthesis and characterization

Deborah Sarzotti

Department of Chemical Engineering, University of Waterloo

May 18, 2005

Institute for Polymer Research Symposium on Polymer Science/Engineering 2005

Outline

- Introduction
 - Propylene copolymerization
 - 1,7-octadiene
 - 1,9-decadiene
 - Ethylene copolymerization
 - 1,7-octadiene
 - MW fractionation and compositional analysis
 - Conclusions
-

Introduction

- Non-conjugated α,ω -dienes
- Copolymerization of dienes with ethylene (E) or propylene (P) yields polyolefins with unreacted vinyl groups that can be used to synthesize materials with unique structures
 - incorporate polar or heteroatomic functionalities
 - promote long chain branching
 - cyclic structures along main backbone

Background

- Three possible propagation reactions:
 - 1,2- or 2,1-addition → pendant vinyl groups
 - addition followed by intramolecular cyclization → 1,3-cycloalkane
 - addition of a pendant double bond into another propagating chain → long chain branch or crosslinking point
- 1,5-hexadiene preferentially inserted as cyclopentane
- insertion mode of 1,7-octadiene (OD) dependent on catalyst and polymerization conditions
- little work with 1,9-decadiene (DD)

P/OD copolymers

Copolymerization of propylene and OD with metallocene/MAO:

run	<i>P</i> (psig)	[OD] (mol/L)	activity ^a (kg·mol M ⁻¹ ·atm ⁻¹ ·h ⁻¹)	<i>M_n</i> ^b (kg/mol)	<i>M_w</i> / <i>M_n</i> ^b	<i>T_{m,final}</i> ^c (°C)	<i>T_g</i> ^c (°C)	crystallinity ^d (%)
P/OD-1	50	0	10500	4.8	2.2	132	-	36
P/OD-2	50	0.012	7600	5.4	2.3	129	-12	30
P/OD-3	50	0.024	5200	5.0	2.1	114	-9	21
P/OD-4	70	0	12700	5.3	2.7	139	-	41
P/OD-5	70	0.012	10900	5.9	2.7	133	-12	37
P/OD-6	70	0.024	10100	6.3	2.8	128	-11	35
P/OD-7	70	0.036	10100	6.7	2.7	123	-9	26

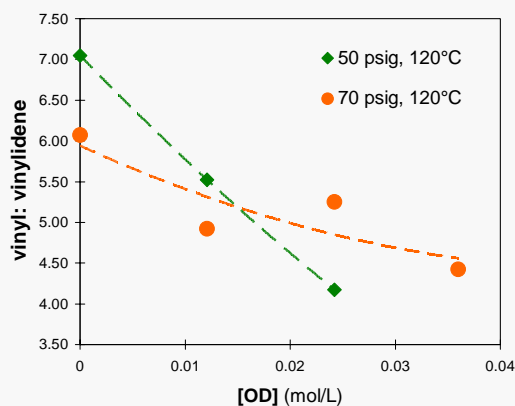
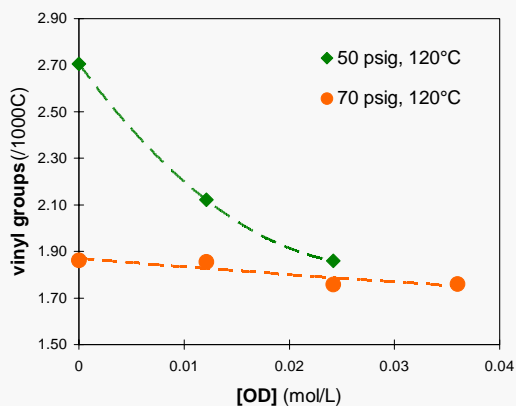
^a Polymerization conditions: *T* = 120°C; *V* (toluene) = 150 mL; [catalyst] = 3.3 μmol/L; Al:catalyst = 500; polymerization time = 10 min.

^b Determined by high-temperature GPC.

^c Determined by DSC at a heating rate of 10°C/min following cooling at the same rate.

^d Relative to the enthalpy of fusion of 100% crystalline PP, 209 J/g.

P/OD copolymers – ¹H NMR



P/DD copolymers

Copolymerization of propylene and DD with metallocene/MAO:

run	T (°C)	[DD] (mol/L)	activity ^a (kg/mol M·atm·h)	M_n^b (kg/mol)	M_w/M_n^b	$T_{m,final}^c$ (°C)	T_g^c (°C)	crystallinity ^d (%)
P/DD-1	120	0	10500	4.8	2.2	132	-	36
P/DD-2	120	0.010	6300	5.5	2.3	n.m.	n.m.	n.m.
P/DD-3	120	0.029	4500	8.2	4.7	101	-5	- ^e
P/DD-4	120	0.048	2700	11.4	11.5	n.m.	n.m.	n.m.
P/DD-5	105	0	14000	9.9	2.4	148	-	43
P/DD-6	105	0.010	16900	11.1	3.4	n.m.	n.m.	n.m.
P/DD-7	105	0.029	14900	14.9	11.9	121	-4	18
P/DD-8	105	0.048	10400	17.7	21.5	111	-6	- ^e

n.m. – not measured

^a Polymerization conditions: $P(C_3H_6) = 50$ psi; V (toluene) = 150 mL; [catalyst] = 3.3 μ mol/L; Al:catalyst = 500; polymerization time = 10 min.

^b Determined by high-temperature GPC.

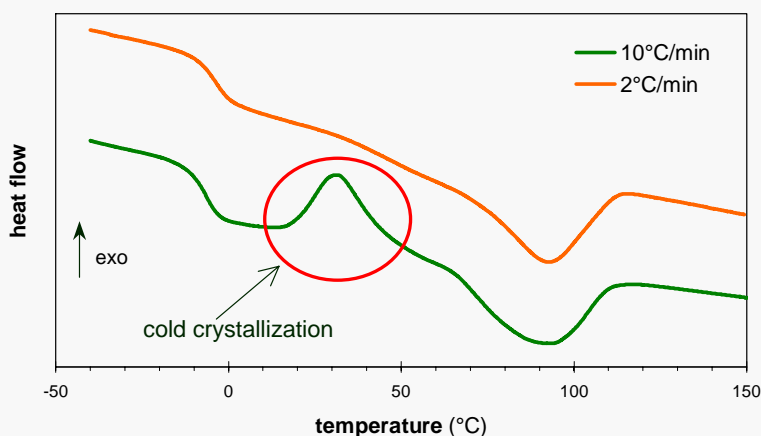
^c Determined by DSC at a heating rate of 10°C/min following cooling at the same rate.

^d Relative to the enthalpy of fusion of 100% crystalline PP, 209 J/g.

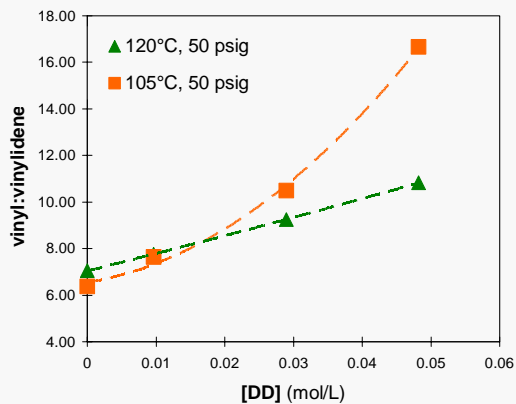
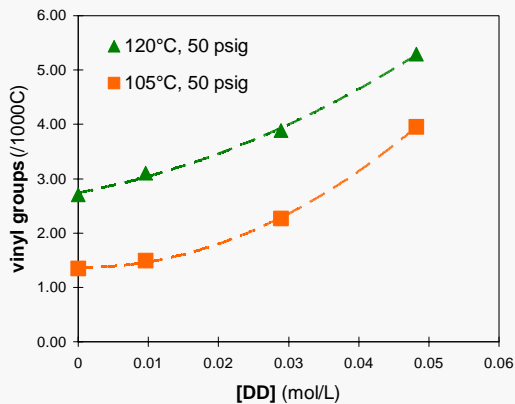
^e Not calculated due to occurrence of cold crystallization.

P/DD copolymers – DSC

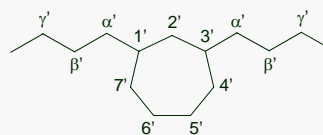
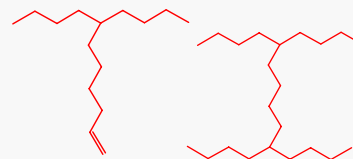
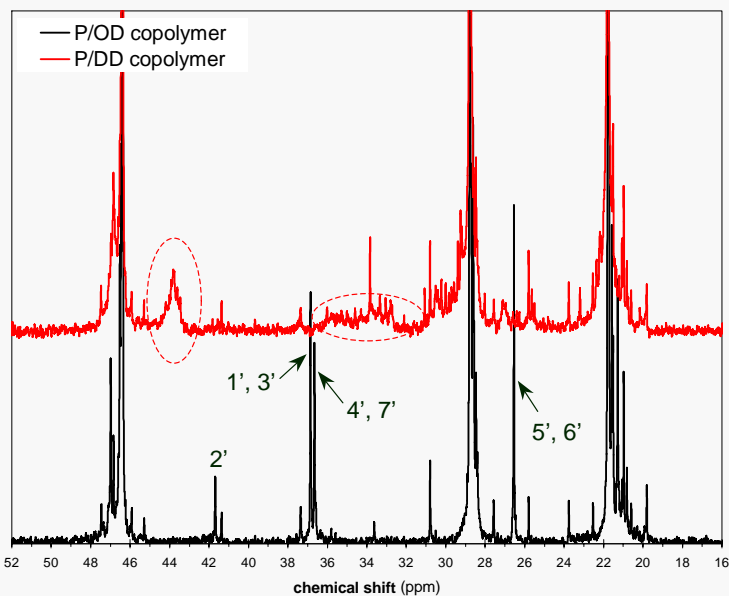
DSC analysis of P/DD-8 at different heating rates



P/DD copolymers – ^1H NMR

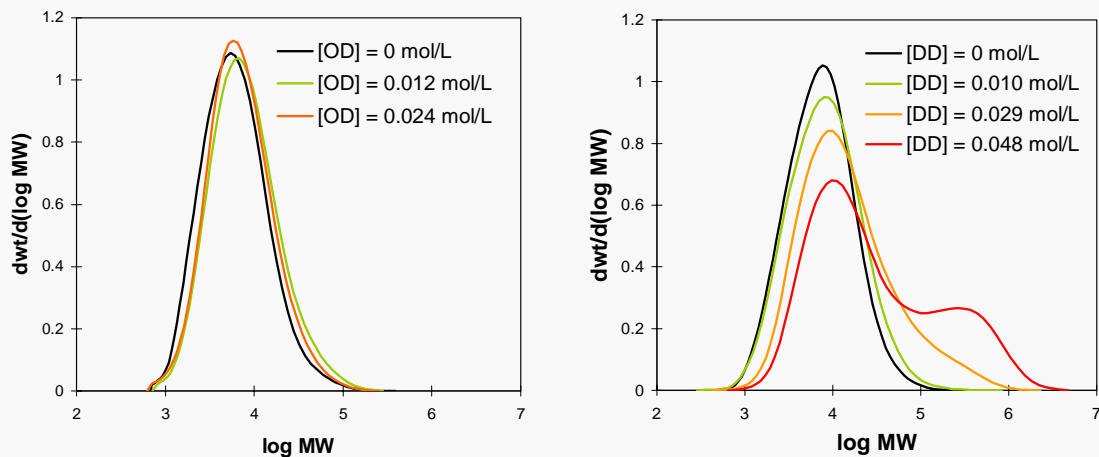


P/OD and P/DD copolymers – ^{13}C NMR



OD & DD copolymers - MWD

Same polymerization conditions ($T = 120^\circ\text{C}$, $P(\text{C}_3\text{H}_6) = 50$ psig)



E/OD copolymers

Copolymerization of ethylene and OD with CGC-Ti/MAO [1]:

run	OD in feed ^a (mol-%)	activity (kg/mol _{Ti} ·h)	M_n^b (kg/mol)	M_w/M_n^b	T_c^c (°C)	vinyl groups ^d (/1000 C)	rings ^e (/1000 C)	CY ₇ /CY ₉ ^{e,f}
1	0	15000	32	3.1	85	0.4	-	-
2	0.16	26000	35	5.6	78	1.3	2.08	0.95
3	0.31	25000	31	11	69	2.6	4.98	0.96
4	0.37	21000	27	14	64	3.1	-	-
5	0.41	16000	28	17	62	3.8	7.70	0.92
6	0.46	8000	20	17	57	4.4	-	-

^a Polymerization conditions: $T = 140$ °C; V (toluene) = 400 mL; P (C_2H_4) = 255 psig; [catalyst] = 9 $\mu\text{mol/L}$; [MAO] = 19.5 mmol/L; polymerization time = 10 min.

^b Determined by high-temperature GPC.

^c Peak crystallization temperature determined with Crystaf in TCB.

^d Number of double bonds per 1000 carbon atoms calculated from ^1H NMR spectra.

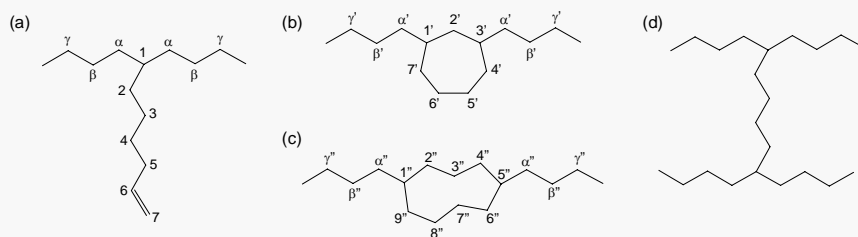
^e Determined by ^{13}C NMR.

^f Number of cycloheptane units (CY₇) divided by number of cyclononane units (CY₉).

E/OD copolymers

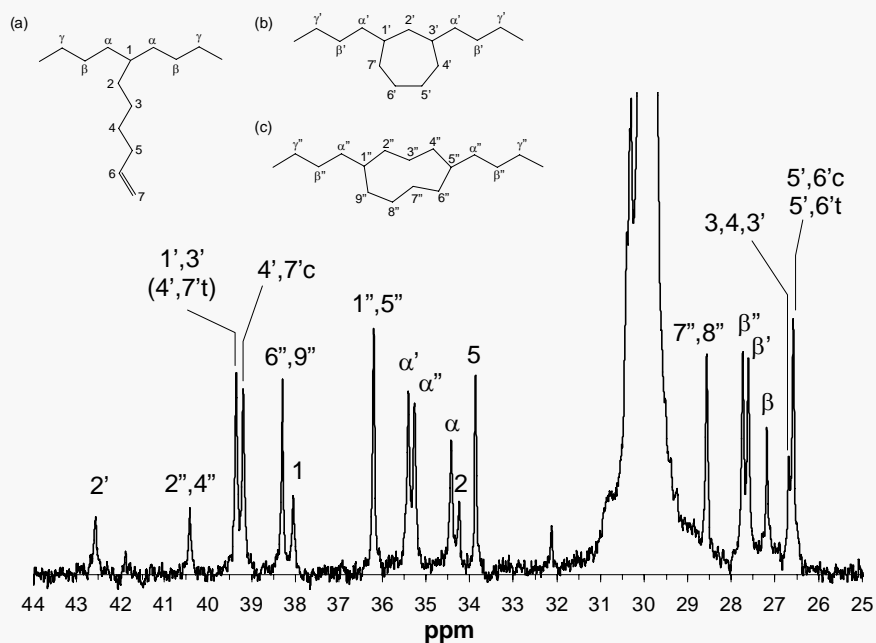
Four propagation reactions:

- (a) 1,2- or 2,1-addition insertion
- (b) intramolecular cyclization following addition
- (c) intramolecular cyclization in the penultimate position [2]
- (d) addition of pendant double bond (macromonomer)

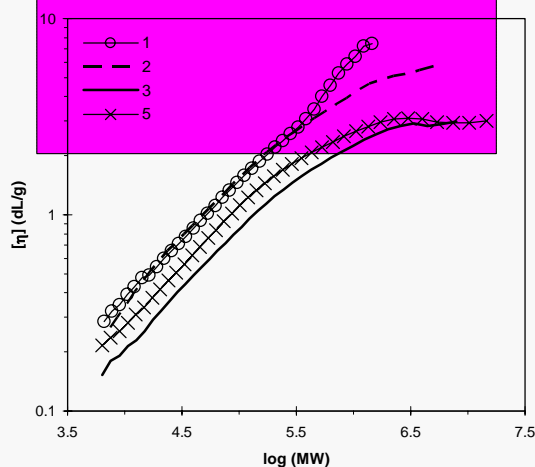
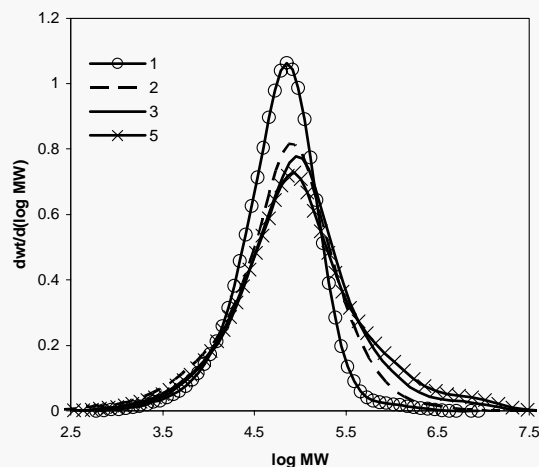


[2] N. Naga, A. Toyota, *Macromol. Rapid. Commun.* **2004**, 25, 1623.

E/OD copolymers



E/OD copolymers -

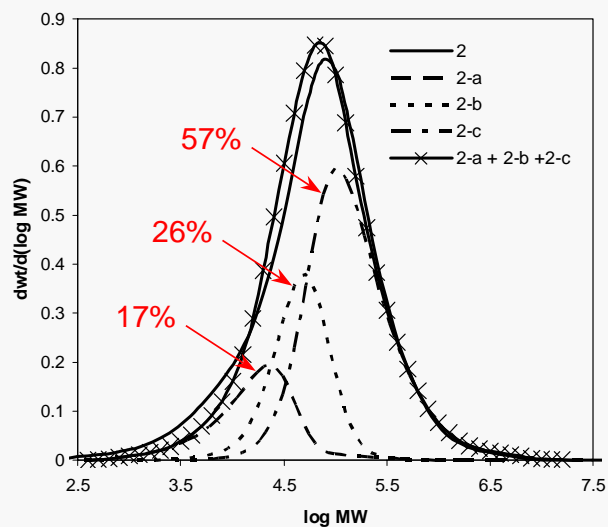


MW Fractionation

- Investigate compositional uniformity
 - distribution of structures resulting from different modes of diene incorporation
- Pietikäinen *et al.*^[3] used thermal analysis and the segregation fractionation technique
 - no physical separation
- Samples fractionated by molecular weight
 - Solvent/non-solvent technique
 - low, medium and high MW fractions with 50, 58 and 100% solvent

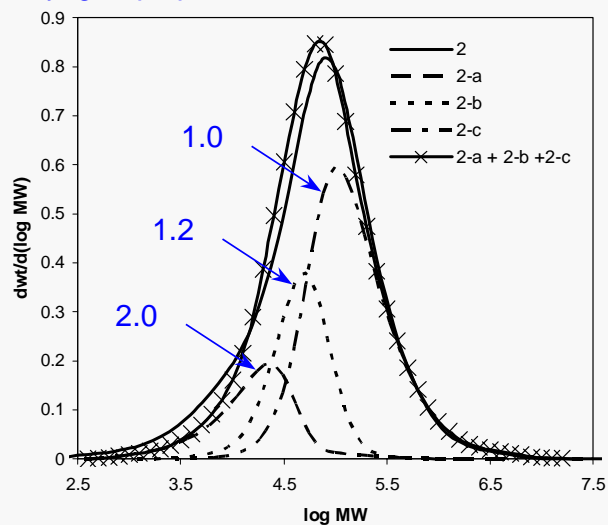
Fractions of E/OD copolymer

% of total recovered

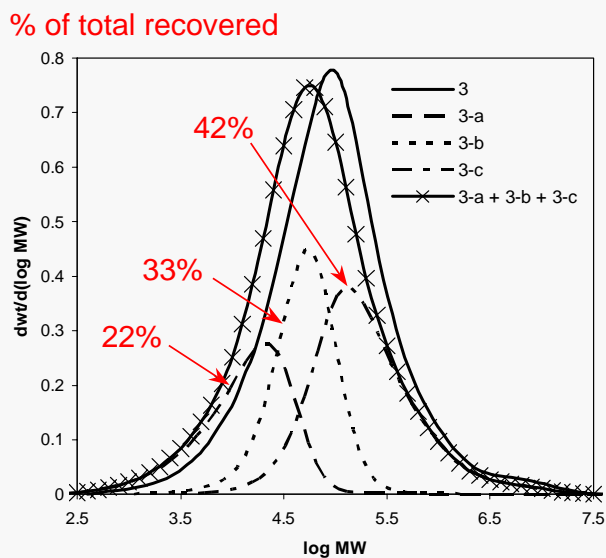


Fractions of E/OD copolymer

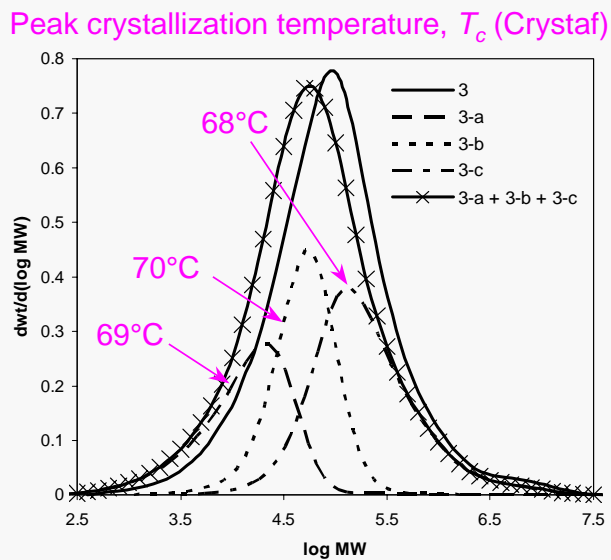
vinyl groups per 1000 C



Fractions of E/OD copolymer



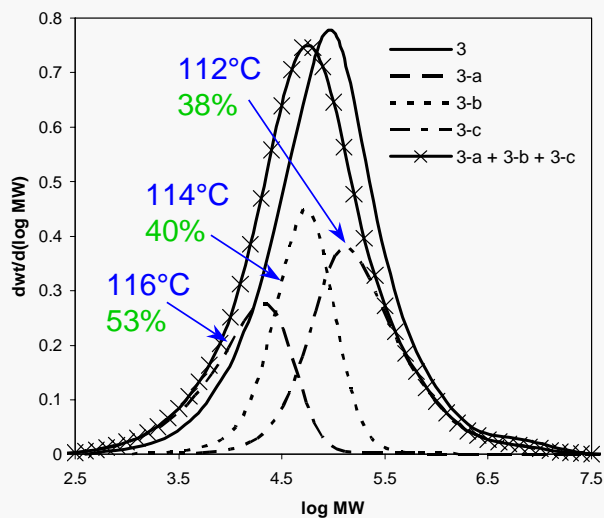
Fractions of E/OD copolymer



Fractions of E/OD copolymer

melting temperature

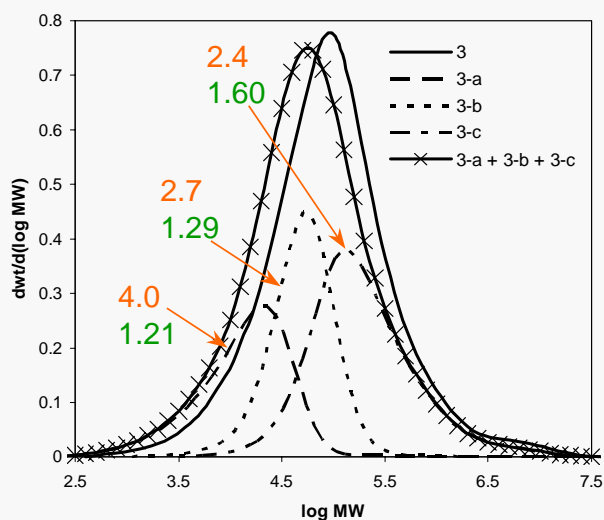
% crystallinity



Fractions of E/OD copolymer

vinyl groups per 1000 C

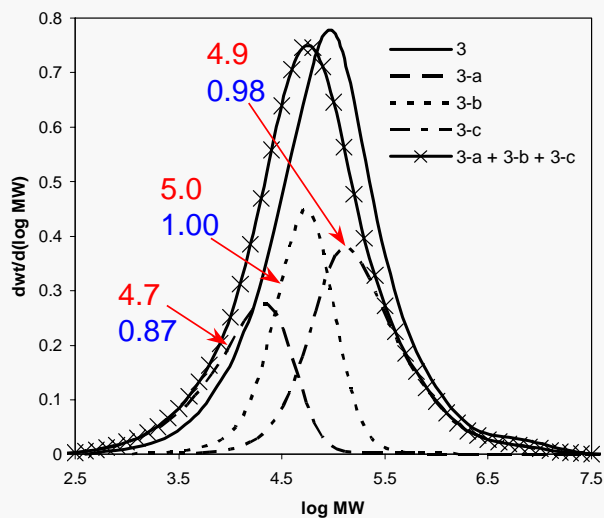
branches per 1000 C



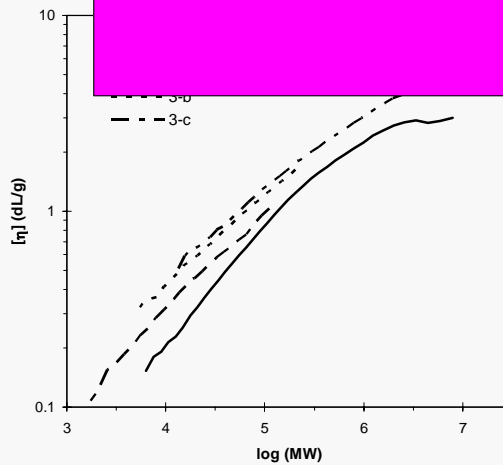
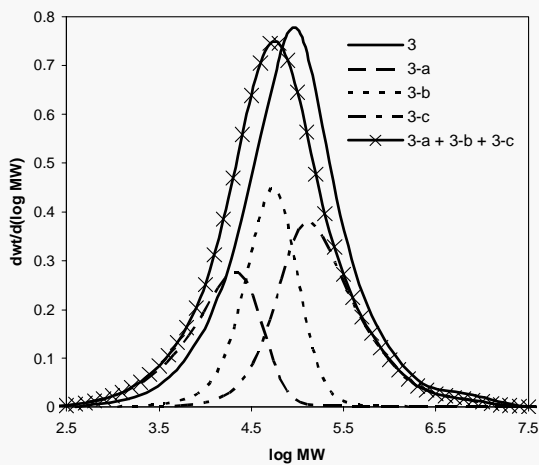
Fractions of E/OD copolymer

rings per 1000 C

CY₇/CY₉



Fractions of E/OD copolymer



Conclusions

- Propylene copolymerization by metallocene/MAO
 - 1,7-octadiene incorporated as cycloheptane units
 - 1,9-decadiene incorporated as 1-octenyl branches and pendant vinyls incorporated to form long chain branches
 - Ethylene copolymerization by CGC-Ti/MAO
 - 1,7-octadiene incorporated as cycloheptane and cyclononane units as well as 1-hexenyl branches
 - fractionation by MW indicates that distribution of structures due to OD incorporation is uniform
-

Correlation of Molecular Properties with Mechanical Behaviour for High Density Polyethylene

Joy Cheng, Maria Anna Polak, Alexander Penlidis

Overall research objectives

- Civil engineering:** mechanical properties such as creep are important to characterize the behavior of the polymeric material, including structural failure characteristics.
- Chemical engineering:** material properties such as molecular weight averages, molecular weight distributions and branching indicators offers insight into the molecular microstructure of polyethylene.
- Collaboration of chemical and civil engineering:** the goal of the project is to develop a theoretical model for predicting mechanical behavior of polyethylene based on its chemical properties.

Materials

- Industrial HDPE resin
 - Different mechanical properties
 - Similar chemical characteristics

Chemical Properties	PE1	PE2	PE3
Density	0.963	0.963	0.95
Melt index	0.25	0.73	0.3
Melt point (°C)	130.06	134.84	134.53
% crystallinity	53.68%	56.32%	59.81%
Mechanical Properties			
Tensile Strength at Yield (Mpa)	27	32	31
Elongation at Yield (%)	9	7	8
Elongation at Break (%)	600	35	450
Tensile Modulus (Mpa)	1,790	2,620	2,340
Flexural Modulus ³ (Mpa)	1,200	1,720	1,620
Impact Brittleness Temperature (°C)	-76	-76	-76
Environmental Stress Crack Resistance ⁴ (hours)	65	10	15

- More resins tests are planned

Experimental methods

- Tests used in this project
 - One objective of our project is to find test that are most useful in our investigations.

Chemical	Rheological	Mechanical
GPC	Capillary rheometer	Creep and relaxations
DSC	DMA -Parallel plate rheometer	Constant strain and stress rate
NMR		
CRYSTAF		

- Rheological test is very sensitive to molecular structure of the material, but it is difficult to quantify the results. Conclusion can only be drawn base on relative terms.

Preliminary results

- The question we are trying to answer is "What essential molecular quality makes these resins have all the different mechanical properties?"
- So far chemical tests could not detect any significant property differences for the three resins
- Mechanical behavior of these HDPE are very different, especially between PE1 and PE2
 - Environmental stress cracking resistance (ESCR) of PE1 is six time greater than ESCR of PE2
 - PE2 have greater tensile strength and tensile modulus than PE1

Based on DSC, PE1, PE2 and PE3 all have similar percent crystallinity. The shape of the melting heat flow curve also do not indicates any major composition differences. (Figure 1)

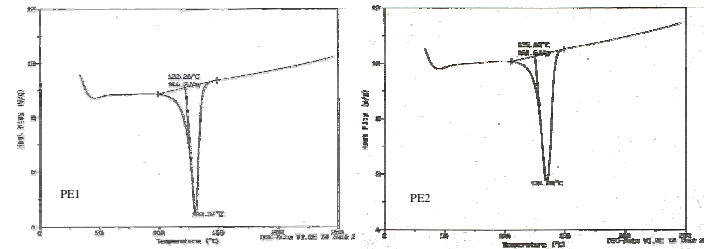


Figure 1: DSC results for PE1 and PE2

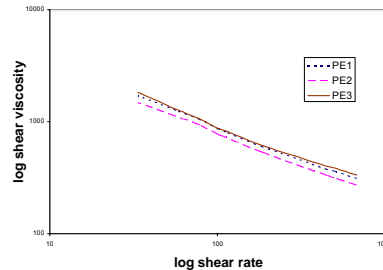


Figure 2: Capillary shear viscosity measurements at 230°C

Capillary rheometer results showed all three resins behaved similarly, even at elevated temperature (Figure 2). Further investigation was carried out using parallel plate rheometer.

Results from parallel plate rheometer indicates there is MW difference between the resins (Figure 3). Detailed information about MWD will be obtained using GPC.

Rheological test seems to be the most promising in detecting molecular property difference for our resins. More focus will be put on using DMA techniques as the primary analysis tool.

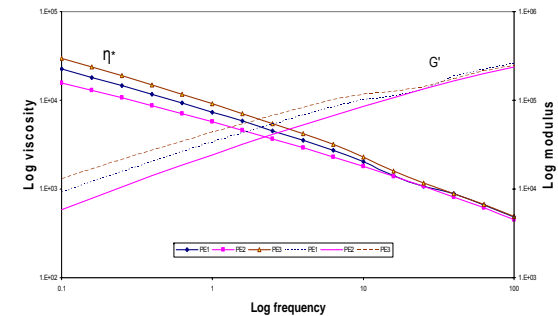


Figure 3: DMA frequency scan results at 150°C

Issues and Obstacles

- Pipe piece and resin contain fillers which interfere with chemical testing (e.g. fillers blocking GPC columns)
- Methods for filler removal is needed

Next step

- Applying statistical method to resin testing. To investigate whether the small differences observed in chemical tests are statistically significant or not.

Optimization Strategies of an Emulsion Polymerization Reactor

Narges GHADI and Ramdhane DHIB
Ryerson University, Toronto

Introduction

Emulsion polymerization (EP) is :

- An important process for manufacturing water based polymers such as rubbers, coatings and adhesives.

- A free radical polymerization carried out under the heterogeneous condition.

- A mostly used process for latex production

Advantages:

- Easy control due to the physical state of kinetics

- High average molecular weight of product

- Less thermal and viscosity problems than bulk polymerization

Objectives:

Modeling and simulation of the process to determine:

- Monomer conversion

- Size and number of generated particles

- Molecular weight averages and distributions

Investigation of the model's Prediction for

- Batch reactor

- Semi-batch reactor

- Continuous stirred tank reactor (CSTR)

Optimization of the process to:

- Enhance the monomer conversion and product quality

- Stabilize the reactor operation

Reaction Mechanism

The model focuses on the behaviour of vinyl acetate :

High water solubility and significant desorption

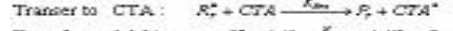
Assumptions of model

- Negligible gel effect

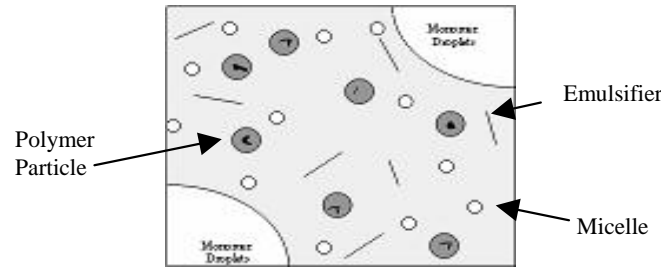
- Less dominance of termination reactions

- Importance of chain transfer reactions in controlling molecular weight averages

- Introduction of chain transfer to monomer as the first step in desorption process



Emulsion Polymerization \Rightarrow Three stages



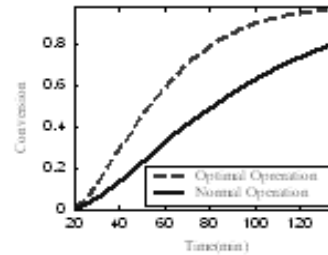
1- Optimization of Batch Reactor

- Effect of impurity on conversion

Normal Condition

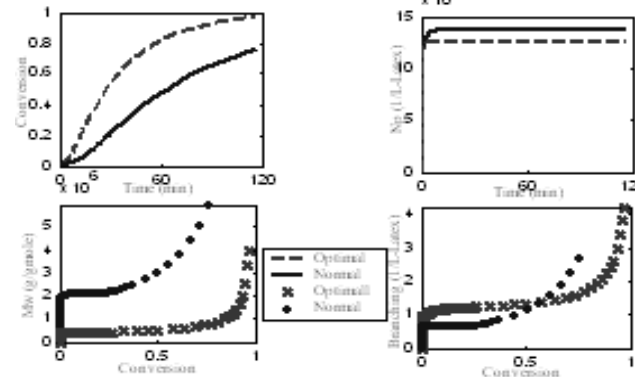
$$\begin{cases} T = 323.15 & K \\ I_f = 0.0022 & \text{mol} / L \\ S_f = 0.0417 & \text{mol} / L \\ IM = 200 & \text{ppm} \end{cases}$$

$$J_{\min} = (\text{Conversion} - 1)^2$$



- Increasing the monomer conversion and average molecular weight

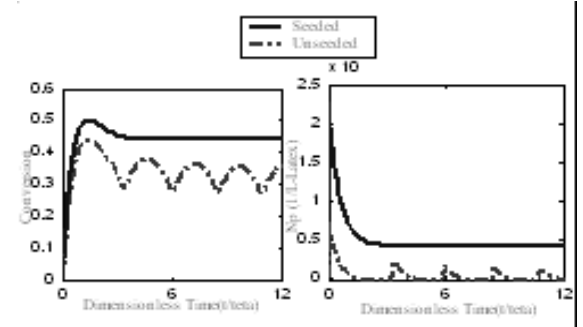
$$J_{\min} = (\bar{M}_w - 8 \times 10^6)^2 + (\text{Conversion} - 1)^2$$



2- Optimization of Continuous Reactor

- The oscillatory behavior due to periodic particle nucleation

Basic Remedy \Rightarrow Feeding a stream of seed particles



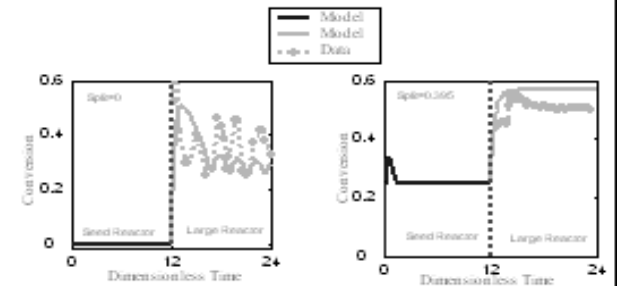
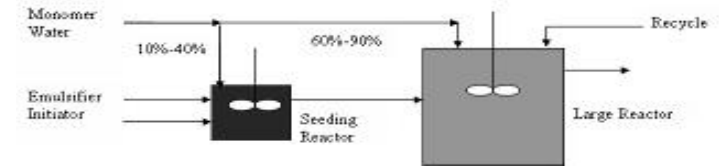
Emulsion Reactor Train Configuration

The first large reactor is preceded by a very small initial CSTR :

- Almost all of the initiator and emulsifier are fed to the first reactor

- Generation of most polymer particles can be entirely accomplished in the first reactor

- The second reactor will be used only for particle growth

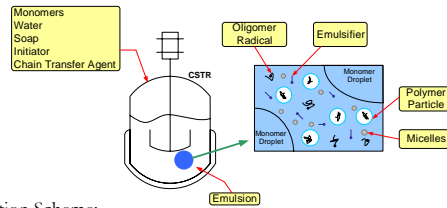


Modeling and Optimization of Emulsion Copolymerization

by: Pegah Khazraei, Chemical Engineering Dept., Ryerson University, Toronto

Emulsion polymerization process is :

- An important process for manufacturing water based polymers. It is a free radical polymerization carried out under heterogeneous conditions and it is common process for latex production
- Very interesting industrial applications (SBR rubber, latex paints & adhesives, PVC "paste" polymers, coatings):
 - ✓ Low dispersion viscosity compared to bulk polymerization:
 - ✓ Good heat transfer and easy control of the process
 - ✓ High polymerization rate and high molecular weights
 - ✓ Direct application of latex
 - ✓ High separation costs, waste water problems, emulsifier as impurity of product
- Main components in emulsion copolymerization :
 1. Monomers, slightly soluble in water
 2. The dispersion medium (water)
 3. Water soluble Initiator(persulfates) and Emulsifier (sodium dodecyl sulfate)
- Some systems are: styrene/butadiene, styrene/acrylonitrile, Ethylene/vinyl acetate, methyl methacrylate/st., acrylonitrile/butadiene, Butyl acrylate/MMA/VAc



Reaction Scheme:

Mechanism	Kinetics
Initiation: Thermal	$S_2O_8^{2-} \xrightarrow{k_d} 2SO_4^{\cdot-}$
Redox	$SO_4^{\cdot-} + M_i \xrightarrow{k_{si}} R_{i,j}^{\cdot}$
	$S_2O_8^{2-} + Fe^{2+} \xrightarrow{k_i} SO_4^{\cdot-} + Fe^{3+} + SO_4^{2-}$ $Fe^{2+} + RA \xrightarrow{k_2} Fe^{3+} + RA^{\cdot}$
Propagation	$SO_4^{\cdot-} + M_i \xrightarrow{k_{si}} R_{i,j}^{\cdot}$
Chain Transfer To Monomers	$R_{n,i}^{\cdot} + M_j \xrightarrow{k_{jm,i}} P_{n,i} + R_{j,i}^{\cdot}$
Chain Transfer To Polymer	$R_{n,i}^{\cdot} + P_{m,j} \xrightarrow{k_{pm,i}} P_{n,i} + R_{m,j}^{\cdot}$
Chain Transfer To CTA	$R_{n,i}^{\cdot} + T \xrightarrow{k_{tw,i}} P_{n,i} + T^{\cdot}$
Termination: Combination	$R_{n,i}^{\cdot} + R_{m,j}^{\cdot} \xrightarrow{k_{tm}} P_{n+m}$
Disproportionation	$R_{n,i}^{\cdot} + R_{m,j}^{\cdot} \xrightarrow{k_{td}} P_n + P_m$
Chain Transfer to Inhibitor	$R_{n,i}^{\cdot} + MSI \xrightarrow{k_{msi}} P_{n,i} + MSI^{\cdot}$
Internal and Terminal double bond reactions	$R_{n,i}^{\cdot} + P_m \xrightarrow{k_p^*} R_{m+n,i}^{\cdot}$
	$R_{n,i}^{\cdot} + P_m \xrightarrow{k_p^*} R_{m+n,i}^{\cdot}$

Mass transfer events:

Mechanism	Kinetics
Micellar Nucleation	$R_i^{\cdot} + micelle \xrightarrow{k_m} Particle$
Homogeneous Nucleation	$R_{jcr}^{\cdot} + M \xrightarrow{k_s} new\ Particle$
Absorption of Radicals	$R_{j(aq)}^{\cdot} \xrightarrow{k_{aw}} R_{j(par)}^{\cdot}$
Desorption of Radicals	$R_{j(par)}^{\cdot} \xrightarrow{k_{sw}} R_{j(aq)}^{\cdot}$

Development of Emulsion Polymerization Simulation Model :

- The goal is to develop a practical tool to predict polymer production rate and product quality. The procedure is:
 - ✓ Apply material and energy balances to determine polymerization rate, monomer conversion, temperature in the reactor
 - ✓ Apply particle population balances to determine polymer properties such as, polymer composition, the number and weight average molecular weights, the number and average size of the polymer latex particles, and branches frequency
 - ✓ The final model consists of a set of ode's describing the evolution of $x(t)$, $I(t)$, $S_p(t)$, $V_p(t)$ (material balances); of $N_p(t)$, $D_p(t)$, $A_p(t)$, $V_p(t)$ (Particle size balance); and of $\lambda_0, \lambda_1, \lambda_2$ and $B_N(t)$ and μ_0, μ_1, μ_2 molecular weight part
- The model should include the elements:
 - ✓ Molar balances for initiator, monomers and emulsifier
 - ✓ Molar balances for live radicals, including application of population balance to determine the total moments of Live Radicals
 - ✓ Molar balances for Dead polymer, including application of population balance to determine the total moments of dead polymer
 - ✓ Population balance to describe the evolution of the PSD of the latex and the MWD of the polymer based on an age distribution analysis
 - ✓ Molar balances for SCB and LCB (Branching points)
 - ✓ An energy balance for the reaction mixture
 - ✓ In the case of copolymers , **pseudo-rate constants** are defined to account for the contribution of each monomer to the overall rate of reaction:

$$\phi_A = \frac{k_{pBA} f_A}{k_{pBA} f_A + k_{pAB} f_B}, \quad \phi_B = 1 - \phi_A; \quad f_A = \frac{[M_A]_p}{[M_A]_p + [M_B]_p}, \quad f_B = 1 - f_A$$

$$k_p = \phi_A (k_{pAA} f_A + k_{pAB} f_B) + \phi_B (k_{pBA} f_A + k_{pBB} f_B)$$

$$k_{fm} = \phi_A (k_{fAA} f_A + k_{fAB} f_B) + \phi_B (k_{fBA} f_A + k_{fBB} f_B)$$

$$k_{fca} = \phi_A k_{fcaA} + \phi_B k_{fcaB}$$

$$k_{fp} = \phi_A (k_{fpaA} \bar{F}_A + k_{fpaB} \bar{F}_B) + \phi_B (k_{fpbA} \bar{F}_A + k_{fpbB} \bar{F}_B)$$

$$k_p^* = \phi_A (k_{pAA}^* \bar{F}_A + k_{pAB}^* \bar{F}_B) + \phi_B (k_{pBA}^* \bar{F}_A + k_{pBB}^* \bar{F}_B)$$

➤ Population Balance Approach :

- ✓ In emulsion polymerization systems, accounting for the change in number of droplets or particles of a given size range is required. This is an example of population balances.
- ✓ A population balance is defined as a balance on a specified set of countable or identifiable entities that accounts for the net accumulation of such entities.
- ✓ The birth time of the polymer particles, τ is set to phase coordinate. $n(t, \tau)$ shows the class of particles in the reactor at time t , which were born in time τ . The number density of particles in the phase space, $n(t, \tau) d\tau$ is the class of particles in the reactor at time t which were born between times τ and $\tau + d\tau$.
- ✓ Any physical property, $p(t, \tau)$ of polymer particles (e.g. average diameter or area of a particle) is calculated by summing up the $p(t, \tau)$ over all classes of particles in the reactor.

$$P(t) = \int p(t, \tau) n(t, \tau) d\tau$$

- ✓ Differentiating the above equation with respect to time and using Leibnitz,s rule one can obtain the evolution of $P(t)$ with time.

➤ Polymer Reaction Equations:

✓ Reactants Molar Balances:

$$\frac{d[M(t)]}{dt} = \frac{[M(t)]_F}{\theta} - \frac{[M(t)]}{\theta} - R_p(t)$$

$$\frac{d[I(t)]_w}{dt} = \frac{[I(t)]_F}{\theta} - \frac{[I(t)]_w}{\theta} - K_d [I(t)]_w \quad (\text{Thermal Decomposition})$$

$$\frac{d[S(t)]}{dt} = \frac{[S(t)]_F}{\theta} - \frac{[S(t)]}{\theta}$$

✓ Moments of Distribution (Steady state hypothesis)

$$\frac{dV_p \mu_0}{dt} = \left(\tau + \beta / 2 - \frac{C_k \mu_1}{[M]_p} - \frac{K \mu_0}{[M]_p} \right) k_p [M]_p Y_0 V_p$$

$$\frac{dV_p \mu_1}{dt} = \left(1 + C_{fm} + \frac{C_{fca} [CTA]_p}{[M]_p} - \frac{C_{fmsi} [MSI]_p}{[M]_p} \right) k_p [M]_p Y_0 V_p$$

$$\frac{dV_p \mu_2}{dt} = \left(factor + 2 \left(1 + \frac{K \mu_1 + C_k \mu_2}{[M]_p} \right) \frac{bracket}{denom} + \beta \left(\frac{bracket}{denom} \right)^2 \right) k_p [M]_p Y_0 V_p$$

$$where: \quad \tau = \frac{k_d Y_0}{k_p [M]_p} + C_{fm} + \frac{C_{fca} [CTA]_p}{[M]_p} + \frac{C_{fmsi} [MSI]_p}{[M]_p}, \quad \beta = \frac{k_t Y_0}{k_p [M]_p}$$

$$factor = 1 + C_{fm} + \frac{C_{fca} [CTA]_p}{[M]_p} + \frac{C_{fmsi} [MSI]_p}{[M]_p} \quad denom = \tau + \beta + \frac{C_{fp} \mu_1}{[M]_p}$$

$$bracket = 1 + C_{fm} + \frac{(C_{fp} + C_k) \mu_2}{[M]_p} + \frac{K \mu_1}{[M]_p} + \frac{C_{fca} [CTA]_p}{[M]_p} + \frac{C_{fmsi} [MSI]_p}{[M]_p}$$

$$\frac{dV_p \mu_0 B_{N3}}{dt} = k_p Y_0 V_p (C_{fp} \mu_1 + K \mu_0), \quad \frac{dV_p \mu_0 B_{N3}}{dt} = k_p Y_0 V_p C_k \mu_1$$

$$C_{fm} = k_{fm} / k_p, \quad C_{fca} = k_{fca} / k_p, \quad C_{fmsi} = k_{fmsi} / k_p, \quad C_{fp} = k_{fp} / k_p, \quad C_k = k_t^* / k_p, \quad K = k_p^* / k_p$$

$$\mu_i(t) = \sum_{i=1}^{\infty} r^i [P_i(t)] \quad Y_0 = \frac{\bar{n} N_p}{V_p N_A} \quad \bar{M}_w = \mu_2 / \mu_1 M_{weff} \quad \bar{M}_n = \mu_1 / \mu_0 M_{weff}$$

Optimization of Emulsion polymerization:

- The objectives in Emulsion polymerization usually are to optimize production rates and to control product quality variables, such as polymer size distribution (PSD), particle morphology, copolymer composition, molecular weights, long chain branching (LCB), crosslinking frequency and gel content

➤ Classification of control variables

- ✓ Initiator variables: number and type of Initiator, flow rate and concentration
- ✓ CTA variables: number and type of CTA, flow rate and concentration
- ✓ Emulsifier variables :number and type of Emulsifier, flow rate and concentration
- ✓ Reaction Temperature

➤ Mathematical formulation of optimization problem

- ✓ The objective function is formulated based on maximum production rate (monomer conversion) to obtain a polymer with desired molecular properties (M_{nd} , PD_d).

$$J = w_1 (y_{nd} - y_m)^2 + w_2 \left(\frac{M_{nd}}{M_{nd}} - 1 \right)^2 + w_3 \left(\frac{PD_d}{PD_d} - 1 \right)^2$$

- ✓ Numerical methods to optimize:

- Nelder-Mead Simplex Method: Local optimization
- Successive Quadratic programming: Local optimization
- Simulated Annealing (SA): Global Optimization

SA analogy with annealing process of metals :

- ✓ When molten metal is cooled, individual atoms rearrange themselves into a regular array corresponding to a minimum energy to form a crystalline structure.
- ✓ At a given temperature, there is a probability of energy leap from E_1 to higher level E_2 , the probability is expressed by Boltzman formula: $p = \exp\left(-\frac{E_2 - E_1}{kT}\right)$

- ✓ In optimization, the objective function is analogized to the energy of the system.

- ✓ Artificial temperature $\beta = -\frac{1}{kT}$ is used, which is related to Boltzman Probability distribution.

- ✓ SA is a heuristic method characterized by random walk , objective is analogized with energy of system : $\Delta f = f_2 - f_1$

- ✓ Directions that increase the value of the objective are sometimes permitted to escape local optimum

Step accepted $X = X_{new}$	$f_2 < f_1$	$f_2 > f_1$
	$p' = \text{random number}$	
$p=1$	$\exp(\beta \Delta f) > p'$	$\exp(\beta \Delta f) < p'$
	new state probabilistically accepted . $X = X_{new}$	New state probabilistically rejected $X = X_{old}$

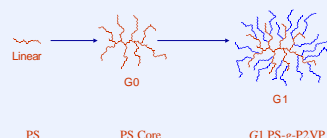
Abstract

Release properties of indomethacin and lidocaine from a dendritic copolymer consisting of a polystyrene (PS) core and poly(2-vinyl pyridine) (P2VP) shell to a 0.05 M HCl solution have been investigated and kinetically analyzed. *In vitro* release tests showed that sustained release characteristics were achieved. Release of lidocaine was greater because of its higher solubility at low pH. The release of indomethacin increased with a decrease in the generation number of the micelles and with initial concentration of probe in the micelles. This is an indication that release might be diffusion controlled. The diffusion coefficients and release rates of indomethacin were calculated by fitting experimental data to the solution of Fick's second law of diffusion. While the initial release rates decreased with generation number, the diffusion coefficients increased, indicating a more diffused structure of higher generation dendritic micelles, probably due to higher electrostatic repulsions between charged P2VP chains. The release decreased sharply at a pH of 4 as the hydrodynamic volume is reduced due to reduction in electrostatic repulsions.

Introduction

The use of polymeric micelles, especially block copolymer micelles has attracted considerable attention in the development of controlled release devices in recent years. In certain applications, the use of block copolymer micelles becomes inadequate. Their shape and stability depend on their immediate surroundings, as these assemblies are held together by weak van der Waals forces. These limitations can be overcome by using dendritic micelles which have a covalently bonded structure. We present here an investigation of the controlled release characteristics of arborescent PS-g-P2VP copolymers. The effect of generation number on release is discussed. Experimental data is analyzed by the power law model and the solution to Fick's law.

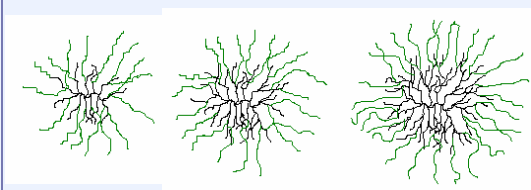
Synthesis of Arborescent PS-g-P2VP



- Linear polystyrene functionalized with coupling sites
- Living polystyryl anions reacted with substrate
- Comb-branch (G0) polystyrene core obtained
- Random functionalization of PS substrate
- Grafting of living P2VP chains on functionalized PS substrate yields PS-g-P2VP
- Polymeric chains used as building blocks and highly branched, high molecular weight dendritic polymers obtained only after few reactions cycles
- Anionic polymerization technique coupled with reaction cycles enable the synthesis of well-defined structures with low molecular weight distributions.

Materials

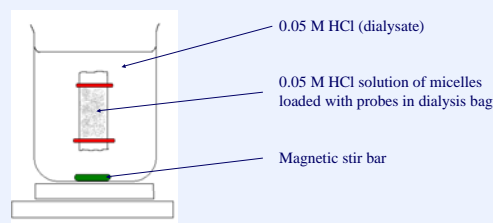
- Indomethacin
- Lidocaine
- Hydrophobic at pH < 4
- Hydrophilic at pH < 4



G1 PS-g-P2VP G2 PS-g-P2VP G3 PS-g-P2VP

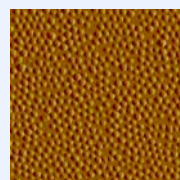
- Branching functionality increases with generation
- Core shell characteristics increase with generation

In vitro Release Studies



- At predetermined intervals 3 mL of dialysate are extracted for UV analysis
- Fresh 0.05 M HCl added to maintain constant volume and sink condition

Results



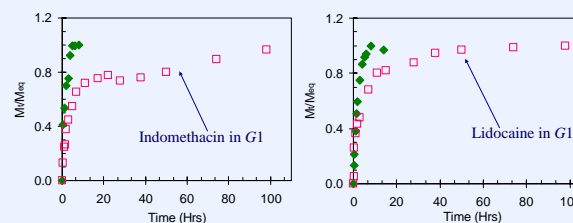
1.2 μm^2 AFM image of G2 PS-g-P2VP

- Particles are spherical and monodispersed
- Diameter of particles \approx 45 nm

Characterization of Copolymers

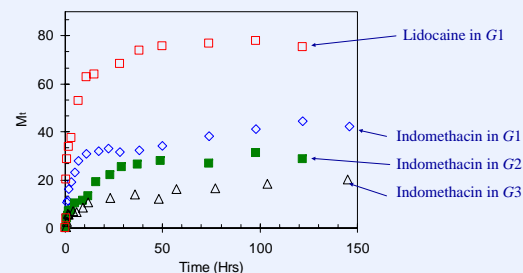
Sample	P2VP Side Chains		Graft Copolymers			
	M_w	M_w/M_n	M_w	M_w/M_n	f_w	Wt % PS
G1	5100	1.06	4.7×10^5	1.08	82	12
G2	5200	1.08	3.7×10^6	1.07	630	13
G3	5300	1.07	2.2×10^7	NA	3400	18

Sustainable Release Characteristics of G1 PS-g-P2VP



- Rapid release of free probes through dialysis bag (green boxes)
- Release of probes from dendritic micelle is slow and shows sustained character
- An initial burst release followed by a slow release to equilibrium is observed for both profiles

Effect of Probe/Micellar Structure on Release



- 80% of lidocaine released at equilibrium
- 40% of indomethacin released at equilibrium
- Amount of indomethacin released at equilibrium decreases with generation number
- A large fraction of indomethacin may be entrapped in the hydrophobic PS core

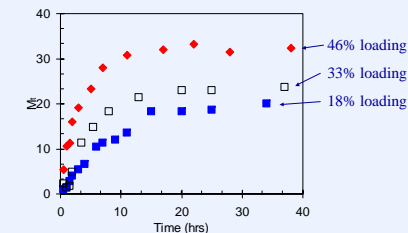
Data Analyses with the Power Law Model ($M_t/M_{eq} = kt^n$)

- n = transport mechanism
- k = interaction between probe and micelle

	Lidocaine		Indomethacin	
	G1	G2	G1	G3
n	0.34	0.60	0.48	0.39
k	0.34	0.21	0.14	0.15

- Fickian diffusion for lidocaine
- Combination of transport mechanisms for indomethacin in G1
- Lidocaine interacts more strongly with solvent molecules

Effect of Loading on Release



- Release increases with loading
- Release mechanism is diffusion controlled

Calculation of Diffusion Coefficients and Release Rates from Fick's Law

	G1	G2	G3
Diffusion Coefficient (m^2h^{-1})	4.50×10^{-19}	1.68×10^{-18}	1.56×10^{-18}
Radius (m)	12.5×10^{-9}	22.5×10^{-9}	39.5×10^{-9}
Rate (h^{-1}) time = 2 hours	0.074	0.047	0.043

- Diffusion coefficient increases with generation number
- Initial rate decreases with generation number
- Dendritic structure becomes more diffused at higher generation

Acknowledgements

ICCS and NSERC

Cristina Quinn, Jean Duhamel

ABSTRACT

Luminescence is a common technique used to characterize polymer dynamics in solution. Use of the Blob Model to analyze the luminescence data obtained with several pyrene labeled polymers has provided information on the dynamics of these polymer chains. The hydrophobicity of pyrene restricts its use in aqueous solutions because of pyrene aggregation. A water soluble dye used in place of pyrene would overcome this problem. In this study, the water-soluble dye ruthenium (II) bisbipyridine 5-amino-1,10-phenanthroline hexafluorophosphate will be synthesized, characterized, and used as a luminescent label on poly(*N,N*-dimethylacrylamide). Since the Blob Model has previously been applied to study the chain dynamics of pyrene labeled poly(*N,N*-dimethylacrylamide), comparison of the Blob Model results obtained for the same polymer but labeled with a different dye will further demonstrate the generality of the Blob Model. Furthermore, the two positive charges on the Ruthenium complex are expected to enhance the solubility of this dye in water which will enable luminescence studies of water-soluble polymers.

INTRODUCTION

There are few techniques available to study the folding dynamics of polymer chains. One method consists in labeling the ends of a monodisperse chain with a dye and its quencher and measuring the rate of encounter between the two ends using luminescence. However, this method essentially treats the bulk of the chain as being invisible.

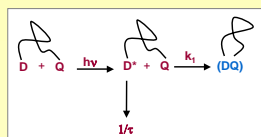


Figure 1: Illustration of Birks Scheme

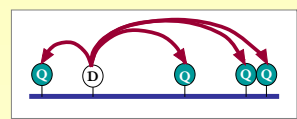


Figure 2: Schematic representation of possible encounters for a randomly labelled polymer.

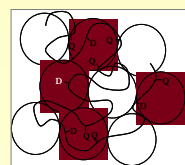


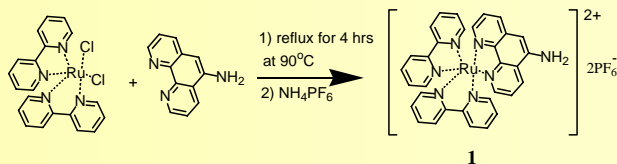
Figure 3: Schematic representation of the Blob Model approach.

PURPOSE

The goals of this project are:

- 1) To establish a set of luminescent dye and quencher which can be used to study water-soluble polymers.
- 2) To demonstrate the generality of the Blob Model concept by using a second dye/quencher system to investigate the dynamics of poly(*N,N*-dimethylacrylamide) which has previously been studied using pyrene and the Blob Model.

The water soluble luminescent dye selected for this project is ruthenium bisbipyridine 5-aminophenanthroline hexafluorophosphate **1** (Ru-bpy). The positive charges on the ruthenium atom will help solubilize the molecule in water while the primary amine group on the phenanthroline ligand will allow for the attachment of the dye onto a polymer backbone. Ru-bpy is synthesized by coupling 5-amino-1,10-phenanthroline to *cis*-bis(bipyridyl) ruthenium (II) dichloride as shown in Scheme 1.



Scheme 1: Synthesis of ruthenium (II) bisbipyridine 5-amino-1,10-phenanthroline hexafluorophosphate **1** (Ru-bpy).³

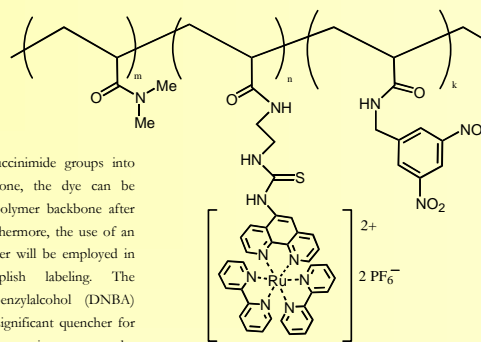


Figure 4: Proposed structure for labeled polymer

By incorporating succinimide groups into the polymer backbone, the dye can be attached onto the polymer backbone after polymerization. Furthermore, the use of an ethylenediamine linker will be employed in order to accomplish labeling. The compound dinitrobenzylalcohol (DNBA) was found to be a significant quencher for Ru-bpy. In order to incorporate the quencher into the polymer, it will be converted from an alcohol to an amine. The amine group is expected to react with the succinimide groups on the polymer. The final structure of the polymer is illustrated in Figure 4.

RESULTS

Thus far, the dye Ru-bpy has been synthesized according to the method described by Ellis et al. with an 87% yield.³ The structure of the dye was confirmed by both ¹H NMR and ESI-TOF-MS

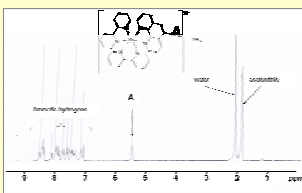


Figure 5: ¹H NMR spectra of Ru-bpy.

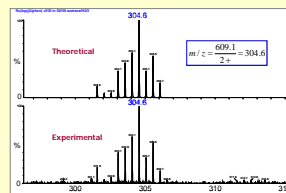


Figure 6: Electrospray ionization - time of flight - mass spectrometry spectra of Ru-bpy.

The literature reports that the extinction coefficient for Ru-bpy in 0.1 M Na₂CO₃ solution of pH 9.6 is equal to 13 800 M⁻¹cm⁻¹ at 454 nm.⁴ As Figure 7 indicates, the experimental results obtained in this study are in agreement with the reported value.

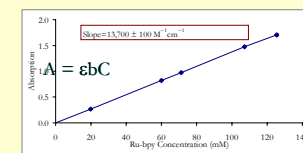


Figure 7: Plot of absorption versus dye concentration to determine the extinction coefficient of Ru-bpy in a 0.1 M Na₂CO₃ solution of pH=9.6 at 454 nm.

The strongest quencher for Ru-bpy was found to be DNBA. A Stern-Volmer plot (Figure 8) was obtained for this system and a quenching constant of $2.7 \times 10^{10} \text{ M}^{-1}\text{s}^{-1}$ was obtained. Since the theoretical maximum value is $1.0 \times 10^{10} \text{ M}^{-1}\text{s}^{-1}$, DNBA is considered to be an acceptable quencher. The extinction coefficient of DNBA in a 0.1 M Na₂CO₃ solution at pH 9.6 was found to be 15 300 M⁻¹cm⁻¹ at 246 nm. DNBA absorbs strongly at 246 nm with no overlapping absorption with the dye in the 454 nm region. Therefore, the dye and quencher content of the polymer will be determined by its UV-visible absorption.

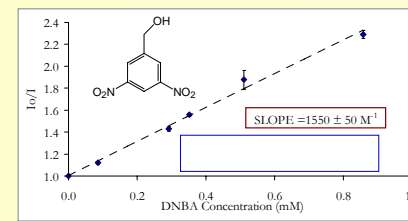


Figure 8: Stern-Volmer plot to determine quenching effects of DNBA on Ru-bpy where [Ru-bpy]=0.5mM.

FUTURE WORK

Having successfully synthesized and characterized a water-soluble dye, the first goal of the project has been fulfilled. The next step will be to synthesize the proposed labeled polymer and to carry out the Blob Model analysis. Since the lifetime of Ru-bpy is much longer than the lifetime of pyrene, Ru-bpy will be quenched such that its lifetime approaches that of pyrene. If the Blob Model holds true, then it is expected that N_{blob} will vary with lifetime according to the trend which was previously observed for the PDMAA system labelled with pyrene (Figure 8).

ACKNOWLEDGEMENTS

Funding provided by OGSST and NSERC.

REFERENCES

1. Winnik, M. A. *Acc. Chem. Res.* **1985**, *18*, 73-79.
2. Mathew, A. K.; Siu, H.; Duhamel, J. *Macromolecules*, **1999**, *32*, 7100-7108.
3. Ryan, E.; O'Kennedy, R.; Feeney, M.M.; Kelly, J.M.; Vos, J.G. *Bioconjugate Chem.* **1992**, *3*, 285-290.
4. Ellis, C.D.; Margerum, L.D.; Murray, R.W.; Meyer, T.J. *Inorg. Chem.* **1983**, *22*, 1283-1291
5. Kanagalangam, S.; Spartalis, J.; Cao, T.M.; Duhamel, J. *Macromolecules* **2002**, *35*, 8571-8577.

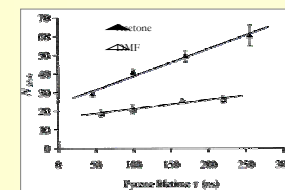


Figure 8: Plot of the linear relationship between N_{blob} and lifetime.⁵

Abstract

Dispersants are important additives in the oil industry. A type of oil-soluble dispersants consisting of a polyamine and two polyisobutylene chains will be synthesized and their efficiency for stabilizing carbon-rich particles found in engine oils will be investigated. This efficiency can be described as "associative strength", which represents the dispersant ability to self-associate in solution into reverse micelles. It will be characterized by determining the critical micelle concentration (CMC). These studies are expected to provide a correlation between the structure and the efficiency of the dispersants.

Introduction

Over time, carbonaceous deposits composed of carbon-rich particles are produced during the normal operation of the engine. The role of a dispersant is to adsorb onto the polar surface of the particles and reduce the driving force towards aggregation. As two particles coated with dispersant get close, interpenetration of the shells occurs, resulting in the non-polar layer losing disorder which is thermodynamically unfavorable. This further leads to interparticle repulsion, or in other words, stabilization of the particles.

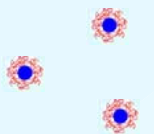


Fig. 1 CRPs coated with dispersant



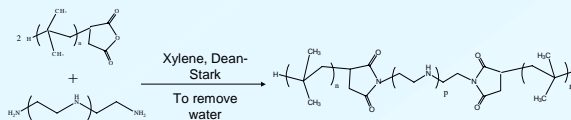
deposit formation without dispersant no deposit formation with dispersant

Fig. 2 Comparison of Intake valve of a Mercedes Benz M102E engine after 60 test hours

Proposal

In this project, a family of succinimide dispersants will be studied. They are BAB triblock copolymers synthesized by reacting polyamines with polyisobutylene terminated with one succinic anhydride at one end (PIBSA).

Scheme 1 Synthesis of the dispersants (p=0-3)



Characterization of Dispersant

The reaction with polyamines exhibiting secondary amines can generate several structures, so that the dispersant becomes a mixture of succinimide derivatives. The proportion of each derivative in the dispersant mixture can be determined by FT-IR and UV-vis absorption.

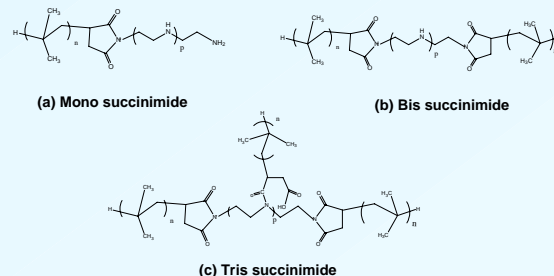
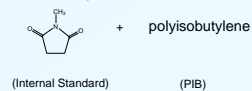


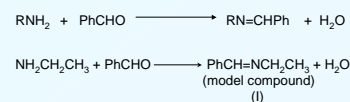
Fig. 3 Mono-, bis-, and tris- succinimide derivatives

> Characterization of succinimide content by FT-IR



The succinimide content of the dispersant can be determined by a calibration curve correlating the absorption ratio ($1717\text{cm}^{-1} / 1390\text{cm}^{-1}$) with the concentration of methyl succinimide.

> Characterization of primary amine content by UV-vis absorption



The model compound (I) will be used to determine the extinction coefficient of benzylidene.

Scheme 2 Characterization of succinimide derivatives

Characterization of the Associative Strength of the Dispersant

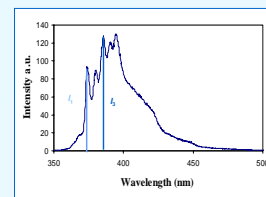


Fig. 4 Steady-state fluorescence spectrum of 1-pyrenemethanol excited at $\lambda_{\text{ex}} = 344\text{ nm}$

The ratio of the fluorescence intensity I_1/I_3 is a parameter sensitive to the polarity of the environment of the chromophore.

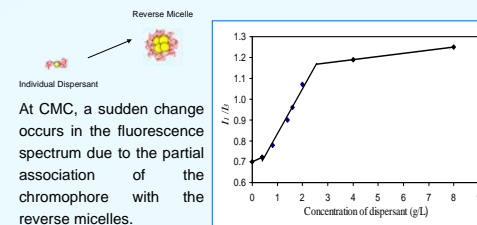


Fig. 5 Determination of the CMC of the dispersant with 1-pyrenemethanol

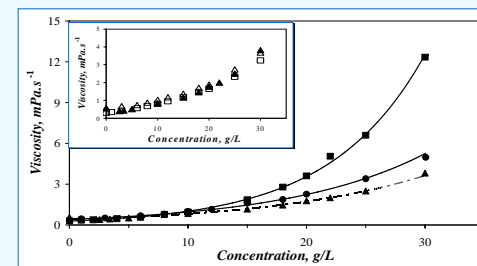


Fig. 6 Effect of aromatic compounds in oil

An increase of the content of aromatic compounds has been shown to result in a viscosity decrease in the presence of a dispersant. This is believed to be due to a decrease in the associative strength of the dispersant when aromatics are present in the oils (cf. Fig. 6). Toluene will be used as a mimic of the aromatic compounds found in oils, and the effect of its concentration on the CMC of the dispersants will be investigated.

Preliminary Results

Determination of the number of isobutylene (IB) units in PIBSA

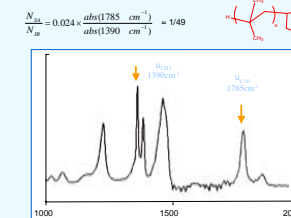


Fig. 7 Determination of PIB units by FT-IR

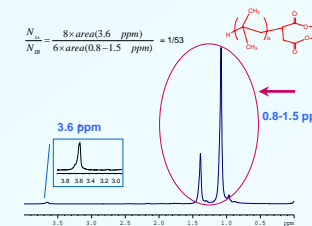


Fig. 8 Determination of PIB units by ^1H NMR through methylation

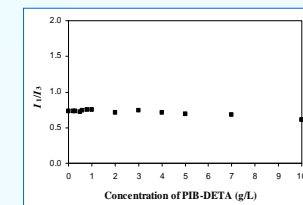


Fig. 9 CMC measurement of PIB-DETA synthesized by PIBSA and diethylenetriamine

Conclusion

- > The number of isobutylene units in polyisobutylene succinic anhydride has been calculated.
- > There is no polar microdomain generated in hexane by the dispersant PIB-DETA.

Acknowledgements

> Imperial Oil

www.basf.com/automotive-oil
Zhang M. Z., Duhamel J. Macromolecules 2005, ASAP
Mathew, A. K.; Internal Report to Imperial Oil, Nov. 17, 1999

Introduction

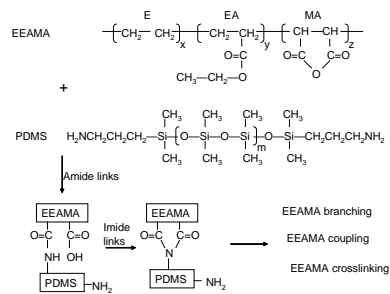
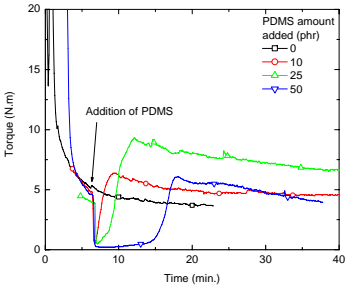
- Poly(dimethylsiloxane) (PDMS) modified polyolefin can be used as processing aids as well as a surface modifiers for polyolefin like LLDPE, HDPE.
- PDMS chemically bonded to polyolefin will avoid the bloom effects which can make the surface tacky and contaminated.

Objectives

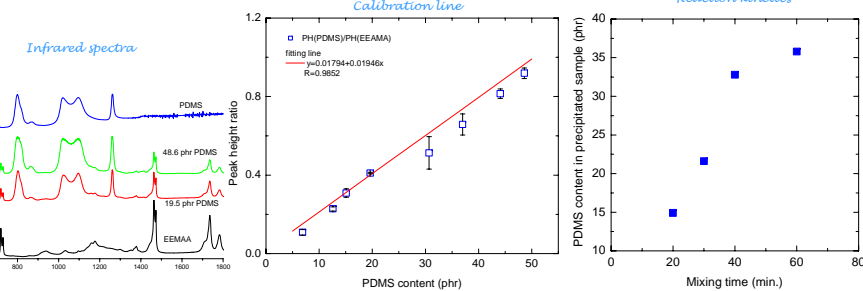
- To obtain a PDMS containing polyolefin by grafting EEAMA with an aminopropyl terminated PDMS;
- To study the reaction kinetics during the reactive processing;
- To investigate the changes in the properties (molecular weight, rheological, and surface) as a result of the grafting;
- To explore potential applications for the modified polymers.

Grafting reaction

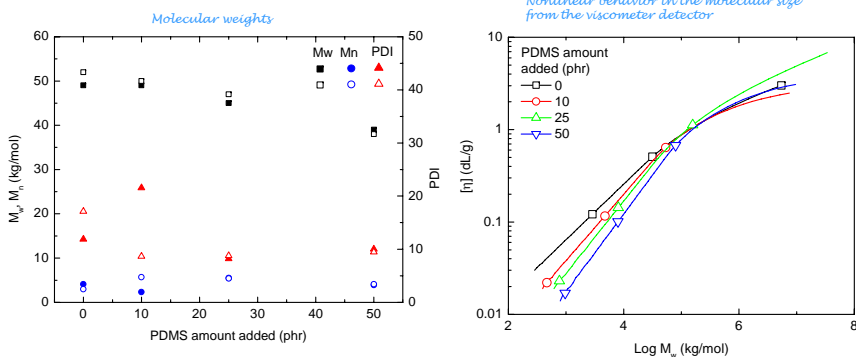
1. Torque curves and reaction mechanism



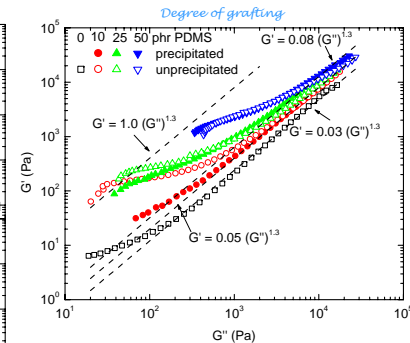
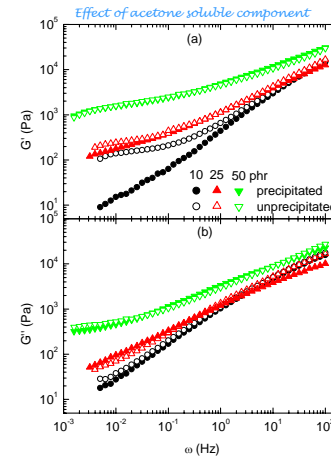
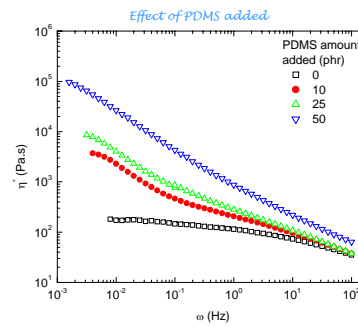
2. Acetone insoluble fraction by IR



3. GPC analysis

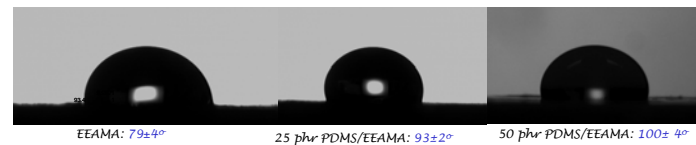


4. Rheological properties

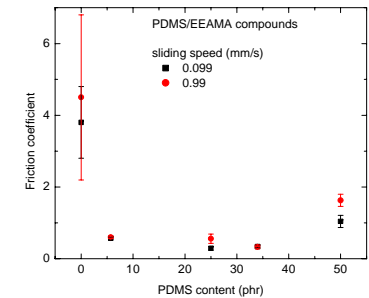


5. Surface properties

Static contact angle measurements

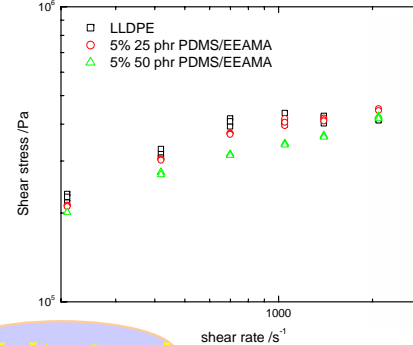


Tribological property

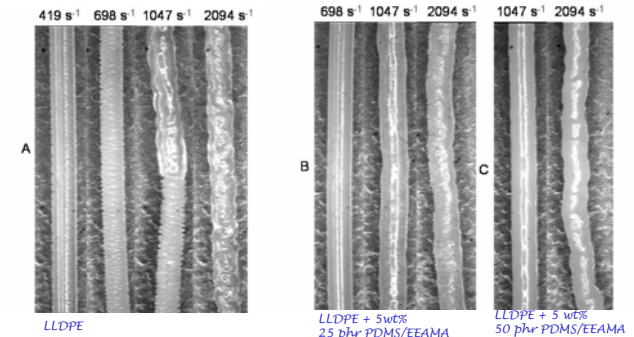


Applications

1. Shear stress reduction



2. Reduction of extrudate surface defects



Concluding Remarks

- The grafting reaction between EEAMA and amino-terminated PDMS in the melt leads to increases in torque, molecule weight, and thus viscosity and moduli;
- The PDMS modified polymer contains a majority of acetone insoluble component, in which the PDMS content increases with mixing time, and a fraction of acetone soluble component which is very elastic;
- The grafting leads to dramatic changes in surface properties like contact angle and frictional coefficient;
- The PDMS modified polyolefin is shown to be able to reduce the shear stress at the wall in a capillary die and improve the extrudate appearance of LLDPE at a concentration of 5 wt%.